A NOVEL DIELECTRIC TECHNIQUE FOR MONITORING THE LYOPHILISATION OF GLOBULAR PROTEINS

by

Phe Man Suherman
BSc, Pgrad.Dip, MSc.

A thesis in partial fulfilment of the requirements for the degree of

DOCTOR OF PHILOSOPHY

Submitted to

De Montfort University

December 2001

Acknowledgement

I would like to express my gratitude to a number of people for their contribution and assistance during my PhD studies. Firstly, to my principal supervisor, Dr. Geoff Smith, for his continual supervision and great understanding during my work. Secondly, to Dr. Peter Taylor, as associate supervisor, for reviewing the thesis and some knowledge contribution.

Financial support from SmithKlineBeecham (now GlaxoSmithKline) and De Montfort University for my PhD project is greatly appreciated. Thanks to Mr. David Merrifield from GlaxoSmithKline for some advice.

Acknowledgment is extended to Mr. Ian Fletcher (De Montfort University) for his assistance in the SEM work, to Mrs. Norma Garrington (De Montfort University) for conducting the DSC work, to Mr. Tony Woodford for fabricating some sample cells and electrodes, to Dr. Alastair Florence (Strathclyde University) for collecting the XRD data, and to Prof. Yuri Feldman (The Hebrew University of Jerusalem) for some discussions on percolation and fractal dimension.

I also would like to thank to all the staff, peers, and friends, for all uncountable minor but useful help in every situation. Finally, special thanks to my brothers and sisters, my mum and dad, for their love, support, prayer, and encouragement from across the miles.

ABSTRACT

Background. The moisture content of lyophilised proteins plays an important role in the stability and long-term storage of these substances. Residual moisture is mainly determined by the combination of formulation factors and the cycle-times of the various stages of lyophilisation. The final drying stage of the lyophilisation process, i.e. secondary drying, is a critical stage in determining the optimum residual moisture level. Some measurement techniques have been developed for *in situ* monitoring of moisture content during secondary drying. However, all these techniques involved the direct contact of a measurement probe with the freeze-dried material, which may alter the properties of the finished product. There is a challenge, therefore, to establish a non-destructive method for *in situ* monitoring of water content and the determination of the end point of the lyophilisation process.

Aim. The framework of this study was to develop a dielectric technique that is able to monitor water content of a material inside a glass vial. The technique was based on the development of a remote-electrode system, that avoids the introduction of measurement probes into the sample. In the context of this work, a remote electrode system is defined as electrodes that are separated from the sample by a non-conductive and non-dispersive medium, i.e. the glass vial used for the freeze drying process. As an initial development, this study dealt with dielectric measurements on partially hydrated globular proteins, i.e. ovalbumin, lysozyme, and pepsin.

Method. The development of the new technique is necessarily based on a detailed knowledge of the dielectric properties of water-protein interactions. The first stage of the project therefore, involved a thorough study of the low frequency dielectric properties of hydrated proteins using conventional parallel plate electrodes. The next stage involved the simulation of a simple remote electrode measurement, by placing non-conductive, non-dispersive polymer films between the sample and parallel plate electrodes. Finally, the study on dielectric measurement of hydrated proteins contained in a glass vial was undertaken with the electrodes attached to the glass vial. Other physical measurements such as FTIR, SEM, XRD, and DSC, were also employed as complementary techniques to characterise hydrated and freeze-dried protein samples.

Results. The investigation of the dielectric behaviour of selected hydrated proteins showed two independent mechanisms of proton hoppings in the bulk sample, which were distinctly identified as an anomalous low frequency dispersion and a dielectric loss peak (ε_3 dispersion). An understanding of the polarisation process underpinning the dispersion is based on the cluster model, in which the low frequency dispersion (LFD) is associated with proton hopping between clusters of water molecules (inter-cluster transport), and the ε_3 dispersion is associated with proton hopping between water molecules in the same cluster (intra-cluster transport). Protons were shown to be the charge carriers involved in both dispersions by investigating the dielectric behaviour of proteins hydrated with deuterated and normal water.

Both the LFD and ε_3 dispersion moved simultaneously toward high frequency with the increase of temperature or hydration. At a certain temperature, however, both dispersions shifted back to lower frequency. This phenomena was identified as a percolation threshold. In the hydration study, the percolation threshold was recognised as critical hydration. This critical hydration was considered due to the monolayer of water molecules network covering a single macromolecule protein, therefore creating an infinite cluster, or known as percolation threshold.

The critical hydration was also observed from both the calculation of fractal dimension (D_f) and the activation energy (ΔH) of the Arrhenius behaviour at below percolation threshold. For all selected proteins, it was found that below critical hydration level, the proton transport occurred along the surface of protein macromolecule ($D_f < 1.9$); whereas above critical hydration level, the proton transport may occur within the matrix of protein structure ($D_f > 1.9$).

With the application of the remote electrode system, it was found that the dielectric properties for the ε_3 dispersion was unaffected by the insertion of polyethylene films between the sample and the conventional parallel plate electrodes. The dielectric properties for the ε_3 dispersion was also unaffected in measurement using remote electrode system in the form of custom-made electrodes attached externally to the glass vial. Moreover, the ε_3 dispersion was still sensitive to the water content, irrespective of which remote electrode system was used. A reasonable correlation ($R^2 = 93\%$) was also observed between relaxation times (τ_3) obtained using conventional parallel plate electrodes and the remote electrodes attached to glass vial.

Conclusion. The study has revealed the mechanism and interaction of water-protein for hydrated globular proteins. The study has also shown that dielectric measurements using remote electrodes, attached to a glass vial, are applicable for the *in situ* measurement of water content in materials, for example in the determination of the end point of the lyophilisation process.

TABLE OF CONTENT

LIST OF FIGURES

LIST OF TABLES

LIST OF SYMBOLS

A_0	area of one electrode of a parallel plate capacitor (m^2)
A	pre-exponential constant for low frequency dispersion
α, β	distribution parameter (dimensionless)
C	electrical capacitance (farads, F)
C_o	empty cell capacitance (farads, F)
δ	phase shift between electric field and dielectric displacement (°)
d	the separation of the plate electrodes of a parallel plate capacitor (m), or between two charges in a dipole
D	dielectric displacement ($C.m^{-2}$), in vacuum $D = E$
D_f	fractal dimension
ΔH	activation energy ($J\ mol^{-1}$)
ΔS	entropy ($kJ\ mol^{-1}\ K^{-1}$)
e	elementary charge (Coulomb, C)
ε''	imaginary permittivity
ε'	real permittivity
ε^*	complex permittivity
ε_0	permittivity of free space ($F.m^{-1}$)
ε_r	relative permittivity (dimensionless)
ε_∞	infinite permittivity (dimensionless)
E	electric field strength ($V.m^{-1}$)
f	frequency (hertz, Hz)
G	conductance (siemens, S)
i	imaginary vector (defined as $+\sqrt{-1}$)
ϕ	phase difference between two waveforms
P	electric polarisation, the electric dipole moment per unit volume ($C.m^{-2}$)
p_1	exponential factor for low frequency dispersion
R	resistance (ohms, Ω)

σ	steady-state conductivity
τ	relaxation time (s)
V	voltage (ac or dc) (volts, V)
$\mathbf{V}_o$	peak voltage (ac) (volts, V)
ω	angular frequency $(\omega = 2 \pi f)$
W	relaxation activation energy (Joule, J)
Z	impedance (ohms, Ω

FUNDAMENTAL CONSTANT

Symbol	Quantity	Value
c	Velocity of light in free space	$2.997924590 \times 10^{8}$ m.s^{-1}
ε_0	Permittivity of free space, given by $10^{7}/4\pi c^{2}$	8.85419×10^{-12} F.m^{-1}
e	Elementary charge	1.602192×10^{-19} C
h	Planck constant	6.626196×10^{-34} J s
k	Boltzmann constant	1.38062×10^{-23} J.K^{-1}
N_o	Avogadro's number	6.022177×10^{23} mol^{-1}

1 INTRODUCTION

Proteins are being examined extensively for their potential efficacy as therapeutic agents, and numerous applications of proteins have been highlighted for routine medical treatments, e.g. insulin, gamma-globulin, and protein containing vaccines [1]. A number of these have already reached the market with many more being the subject of clinical trials.

However, the stability of protein drugs is difficult to maintain. Stability refers to the ability of protein to be processed, distributed, and used without irreversible change in primary structure, conformation, or state of aggregation [2]. The complicated structure of proteins may lead to chemical and physical instability and the ultimate degradation of a protein [3].

An aqueous protein solution is often the simplest method for formulating and handling a protein drug. However, the presence of water in a protein solution can result in physical degradation, since the solvent provides a medium for molecular movement and conformational perturbations. Water can also behave as a reactant for chemical degradation of a protein (i.e. hydrolysis). In addition, an aqueous solution is generally not resistant to large fluctuations in temperature, which could result in accidental freezing or over-heating. Both of these events could easily occur during shipping and/or storage. Moreover, various modifications of amino acid side chains can occur rapidly in aqueous protein solution. All these physico-chemical modifications may result in degradation of the protein [4,5].

Lyophilisation, or freeze-drying, is one method that may increase the stability of protein drugs[6]. In the lyophilisation process, the product is first frozen thoroughly at low temperature and atmospheric pressure. The ice which is formed, is then sublimed under a coarse vacuum, and any residual water subsequently removed at elevated temperature and reduced pressure.

Lyophilised protein is potentially more favourable than aqueous solutions since lyophilisation removes water which is the principal cause of chemical degradation in an aqueous protein solution. In addition, freeze dried proteins are generally more resistant to mechanical stress during shipping and handling.

In principle, lyophilised proteins should have the desired long-term stability over a wider range of temperature (-20 to +40 °C) and thus provide ease of handling and use of protein drugs. In practice, however, it is not a straightforward process to remove the water during lyophilisation, without damaging the protein. Some effects of lyophilisation, such as acute freezing and dehydration stresses, can cause irreversible protein denaturation and reduced storage stability of the dried solid. Another important factor in lyophilised protein which is difficult to control is moisture content. To obtain a good stability of lyophilised proteins, the end product should have an optimum moisture content. Over-drying may cause deterioration of the product, while excess moisture may cause instability of the product during the storage lifetime. Therefore, monitoring and controlling of moisture content is an important part in the freeze-drying process.

1.1 Freeze Drying Process

Freeze-drying (or lyophilisation) is a method for preservating labile materials in the dehydrated form. The lyophilisation process involves first the freezing of the substance and then evaporating the ice (*primary drying*), followed by desorption (*secondary drying*) to the level in which the solvent/water will no longer support biological growth or chemical reactions [7]. In general, the lyophilisation process is divided into three main stages, viz. freezing, primary drying, and secondary drying[8,9].

1.1.1 Freezing

The freezing stage is required to bring the material to the solid state, before primary drying commences. In this stage, the solvent is separated from the solutes. The solvent, which is

usually water, will form ice crystals, and solutes will be bound in the interstitial region between the ice crystals. In a frozen sample, there are usually ice crystals and non-ice phases comprising unfrozen water, amorphous solids, and/or crystalline additives. The freezing process may be done either in an external freezing unit or on the freeze-drying shelves.

This freezing process is critical since the internal structure of the product, the specific area of the product, the orientation, and the particle morphology are all dependent on this stage[10]. In order to obtain an optimum structure, it may be necessary to do *ad hoc* cooling cycles including intermediate rewarming periods (often called thermal treatment). It may also be necessary to add different protective agents to prevent the loss of the potency during cooling, freezing, and subsequent drying. The preliminary investigation of thermal behaviour of the material by differential thermal analysis, electric measurements, or other relevant physical methods may be necessary to achieve an appropriate freezing protocol.

1.1.2 Primary Drying

During primary drying, the bulk-freezable water is removed by sublimation. This stage is carried out at low temperatures under moderate vacuum. The heat is applied to the system to initiate sublimation of the ice crystals. Primary drying should be carried out from the solid state, i.e. at temperature below the minimum temperature of incipient melting (the eutectic temperature). During the sublimation process, the gas-ice interface occurs which can be observed from the layer of ice matrix and dry product.

Primary drying is complete when all ice has been removed. Any water remaining 'bound' to or adsorbed by the apparently dry product is removed partly by secondary drying.

1.1.3 Secondary Drying

Secondary drying is the process of desorption of moisture which still remains after primary drying. When all crystalline solvents have disappeared, the temperature can then be raised to allow the extraction of the remaining unfreezable fluids. This secondary drying process is generally performed at positive temperature and high vacuum.

Both processes of the primary and secondary drying should also be controlled by using temperature, electric or other physical methods.

1.14 Packaging and Storage

The freeze-drying process is stopped when the residual content of adsorbed solvent is low enough to be consistent with long-term preservation of the dry product at ambient temperature.

When the secondary drying process has finished, the freeze-dried material is extracted from the vacuum chamber and stored. After the freeze-drying process, the material is very sensitive to contamination. Therefore, it is important to protect the materials adequately from the outside environment.

1.2 Formulation for Freeze Drying

A formulation for freeze drying may be defined as a system containing any mixture of solvent and substances with a proper composition and condition to achieve a stability upon the removal of the solvent after freeze drying [11]. The formulation process usually involves the addition of the correct constituents, including bulking agents, stabilising agents, cryoprotectant, and lyoprotectant[12].

1.2.1 Bulking Agents

Bulking agents in a freeze drying process are used to provide support for the end product (i.e. the 'freeze dried' cake) and to prevent loss of product from the container. Some bulking agents that are usually used in the freeze-dried formulation are mannitol, glycine, dextrose, maltose, sorbitol, and glucose. Polyvinyl Pyrrolidone (PVP) has been found to be able to increase the strength of the freeze-dried cake when it is used in conjunction with another excipient.

1.2.2 Stabilising Agents

A lyophilised product has greater stability in the crystalline state than the amorphous state. Excipients can be used to induce crystallisation of the substances during the lyophilisation process. However, for protein molecules, the crystallisation of the excipient decreases stability due to the formation of oligomers[11]. For example, when mannitol is used as an excipient, it crystallises during lyophilisation and the protein molecules tend to concentrate and polymerise on the mannitol surfaces. However the protein remains in the dispersed state if the mannitol is amorphous. Some excipients, such as sucrose, do not crystallise during lyophilisation process, and thus does not cause the proteins to form oligomers.

1.2.3 Cryoprotectant and Lyoproctectant

Cryoprotectants protect the samples during the freezing process, while lyoprotectant can be defined as an excipient that enhances stability by preventing degradation of proteins during the lyophisation process. The lyoprotectant creates an environment around the protein molecules that provides a source of water molecules to prevent denaturation, which usually occurs due to the change in a configuration of the protein due to loss of bridging water in the molecule[11].

Sugars, such as trehalose, maltose, and sucrose, play a major role in maintaining the stability of proteins in solution. It has been found that sugar increases the activity and stability of enzymes.

1.3 Stability and Moisture Content in Freeze Dried Product

In general, lower moisture content gives better product quality and stability. However, this is not a common rule. Some samples may need higher residual moisture content to gain good quality and stability. Optimum moisture content is essential to achieve a stability and long-term storage of freeze-dried product. The optimum moisture content required in the end product of freeze-drying is dependent on the product properties. Some substances may need a moisture content less than 1 g/g, for example, while other substances may need certain moisture content to achieve the desired stability. Over-drying caused an aggregation of excipient free human growth hormone (hGH) [13]. Excipient free tissue type plasminogen activator (tPA) was found to aggregate at an enhanced rate if the residual water was low [14]. On the other hand, the rate of oxidation of freeze-dried haemoglobin at room temperature doubled if the residual water is increased from 2% to 8% [15].

1.4 In-Process Characterisation of Freeze-Dried Proteins

In-process characterisation of freeze-dried protein is a direct process of monitoring sample during the freeze drying stages. The characterisation may involve analysis of samples from simulation of the freeze drying stages and *in situ* measurement during the real freeze drying process. The first type of characterisation aims to investigate some freeze-drying parameters from the formulation (e.g. glass transition, eutectic temperatures, changes in exothermic and endothermic transitions) before doing the real freeze drying process. The second type of characterisation usually aims to determine the end point of the real freeze drying stages. The later characterisation usually measures the pressure or temperature change. For determination of the end point of secondary drying, the changes in temperature or pressure may be correlated to the residual moisture content.

The first type of characterisation involves: resistance measurements, freeze-drying thermal analysis, and freeze-drying microscope. The comparison between these techniques is shown in Table 1.1.

Table 1.1 *Characterisation based on the simulated freeze drying process.*

Methods	Advantages	Limitations
Resistance Measurement	Data analysis is relatively simple	The insertion of the probes in the sample may perturb the sample response
Freeze Drying Thermal Analysis	The instrument can be calibrated easily	The placement of the thermocouple in the sample may give a perturbation response
Freeze Drying Microscope	Less cost and relatively easy to use	Unwanted impact that may arise from the sample position between two glass surfaces from microscope

The second characterisation techniques that may be carried out to determine the end point of freeze-drying process are: *thermocouples, vapour pressure rise, electronic hygrometer*

1.4.1 Thermocouples

The temperature sensors, either resistance temperature detectors or thermocouples, are place in the selected vials. The product temperature versus time is then recorded. The disadvantage for this method is that the placement of the thermocouples in the selected vials may not be representative of the non-selected vials. The presence of temperature probes in a vial acts as a site for heterogeneous nucleation of ice causing a reduction in supercooling relative to the non-selected vials. The reduced supercooling results in slower freezing and faster drying rate due to the larger average size of ice crystals.

1.4.2 Vapour Pressure Test

The technique employs a thermal conductivity (thermocouple) gauge and a capacitance manometer. This system uses freeze dryers with external condenser and an isolation valve between the chamber and the condenser. When the end of drying is approached, the output of thermal conductivity gauges decreases. The isolation valve is then closed for approximately 30 seconds, which then results in an increase in chamber pressure due to the water vapour released from the product. The pressure rise, which is measured by the capacitance manometer, is related to the residual water content in the product.

1.4.3 Electronic hygrometer

The method is based on the use of an alternating voltage to a device consisting of an aluminium oxide film placed between two electrodes. The capacitance changes as water vapour is absorbed or desorbed from the aluminium oxide. The moisture content is determined from the Q value (quality factor) of the Al_2O_3 film. The Q value is obtained from the reciprocal of the energy loss. The limitation for this method is that it cannot withstand the effects of steam sterilization, so it cannot be used at for nonsterile lyophilised products.

1.5 Characterisation of Freeze-Dried Proteins

The quality of lyophilised proteins can be monitored using a number of physical measurements. To obtain a good quality of freeze-dried samples, it is important to keep monitoring and controlling the samples during the freeze-drying process. Some physical measurements that can be used to monitor the quality of lyophilised proteins are:

1. Differential Scanning Calorimetry (DSC): to detect the glass temperature (T_g) and eutectic crystallisation temperature (T_e) [16]
2. Infra red (IR) spectroscopy: to monitor protein conformation directly in frozen and dried sample, and to characterise the water content of the dried material

3. Fourier transform infrared spectroscopy (FTIR): to examine changes in secondary structure and aggregation in solid state and liquid state [17,18]
4. Nuclear Magnetic Resonance (NMR): to investigate molecular mobility[19]
5. X-ray Diffraction (XRD) to investigate the degree of crystallisation of freeze-dried pharmaceuticals [20]
6. Scanning Electron Microscopy (SEM) to examine the relationship between morphology and the freeze-drying parameters [21,22]

None of these techniques can be used *in situ*, with the exception of infra-red spectroscopy. In this study, the characterisation of freeze-dried proteins was carried out by dielectric relaxation spectroscopy (DRS) technique. Some advantages of using DRS compared to a number of other physical methods are:

- Sample preparation is relatively simple
- Varieties of sample sizes and shapes (solid compacts, powder, gels or liquids) can be measured
- Dielectric analysis can be adapted to perform *in-situ* measurements.
- The measurement can involve an extremely wide frequency range (10^{-4} - 10^{12} Hz); and therefore a number of processes on wide ranges of time can be investigated, e.g. from slow hindered motion of peptide backbones to fast vibrational motion of side chains and the fast orientation polarisation of the water dipole.
- The technique is non-invasive, since the voltages applied are relatively low; and foreign probes are not required for the measurement.
- The conditions of measurement may be varied, for example, the sample may be examined under a range of temperatures, humidities, pressures, etc, allowing direct investigation of the system.

DRS has been used widely in several areas of study, such as ceramics[23], thin films[24], polymers[25], cements[26], proteins[27,28,29,30], protein hydration[31,32,33], lyophilisation of proteins[34], and body tissues[35]. Other materials that can also be studied by dielectric

analysis are: aqueous solutions, polyelectrolytes, normal and supercooled liquids, and other solid-state materials.

1.6 Water in Biological Macromolecules

Water is a fundamental element for the origin, stability, and function of biological systems. The existence of water in biological materials may have some different features, as follows:

1.6.1 Structural Water/Bound water

Water in biological macromolecules may be present as an integral part of the structure[36]. In collagen, for example, a water molecule is hydrogen bonded to a carbonyl group, to an NH residue of one of the chains, and to a carbonyl group of another strand. The role of these water molecules is to bridge the helical chains and to stabilise the triple helical structure[37]. The removal of these water molecules may cause instability of the helical structure, therefore disrupting the internal structure. This kind of water molecules is called as structural water/bound water/internal water.

Structural water/bound water can be defined as an intrinsic part of the substance that is associated with the stability of the substance. Bound water, for example, is responsible for maintaining the folding configuration of a protein molecule. The removal of bound water may cause change in protein configuration, or protein denaturation.

The number of these water molecules is relatively small compared with the ones bound on the surface, and the orientational freedom of these water molecules is believed to be very restricted since they are a part of the internal structure of the material. As a result, this kind of water molecules is not sensitive enough to dielectric measurement. It may be identified clearly using another technique, such as electron density map from x-ray crystallographic studies.

1.6.2 Sorbed water/hydration water

Besides structural/bound water, water added to the protein (i.e. sorbed water/hydration water) also plays an important role. This water performs as a plasticiser in the protein, which is important in the development of biotechnology and industrial processes, e.g. food processing and food preservation. This kind of water has to be in an optimum amount in the sample to achieve a good performance, which determines the end point of freeze-drying process.

The behaviour of this water in the protein is still in question, whether the water is strictly adsorbed on a surface of protein or it is adsorbed to some extent into the internal structure and bound to individual protein molecules.

1.7 Gap in Knowledge

It has been mentioned earlier that moisture content in the final product of freeze-drying is very important. Some previous attempts of *in situ* characterisation during the freeze-drying process have limitations. The problem rose mainly from the contact of the electrodes or measurement probes with the sample, which created unwanted perturbation response in the sample.

This study establishes the novel technique for *in situ* monitoring of water content of proteins inside a freeze drying glass vial using low frequency dielectric measurement. The technique employed electrodes which were placed remotely from the sample, so the sample destruction due to the contact with electrodes was avoided. This technique is a primary stage for development of *in situ* monitoring of water content during a freeze-drying process.

Since the technique involved the measurement of water in the proteins, the knowledge of water-protein interaction is crucial. The understanding of water-protein interaction itself is

still an interesting study. Many studies have been done in attempt to understand the behaviour of water in proteins.

This study employing low frequency dielectric measurement with temperature dependence offers a new approach in investigating water-protein interaction in terms of percolation phenomena and fractality.

1.8 Aim

As mentioned previously, there is no instrument available yet for the *in situ* determination of the moisture content in the final freeze dried product. This work aims to perform a design/technique of *in situ* monitoring of water content in the freeze drying product using low frequency dielectric measurement to determine the end point of the lyophilisation process.

Simultaneously, this study also aims to contribute to the knowledge of water-protein interaction from the investigation of hydrated proteins using low frequency dielectric measurement. This objective is also essential prior to designing the technique of *in situ* monitoring of water content of freeze dried proteins using dielectric measurement.

1.9 Project Outline

1.9.1 Materials selection and sample preparation

Hydrated globular proteins (ovalbumin, lysozyme, and pepsin) were chosen as model materials used in this study. The general review of each protein, including the method of protein hydration, is described in Chapter 2. Low hydration level was chosen since the main idea of this work is to determine the end point of lyophilisation process, and the final freeze-drying product usually only contains a trace amount of water.

1.9.2 Principles of dielectric relaxation spectroscopy

A concise dielectric theory used to analyse and model the data from dielectric measurement in this work is composed in Chapter 3.

1.9.3 Instrument specification

A basic concept of dielectric instrument used in this study is described in Chapter 4.

1.9.5 Dielectric relaxation spectroscopy of hydrated proteins

Dielectric properties of the various hydrated proteins and the mechanisms behind the observed dielectric spectroscopy of hydrated proteins are explained in Chapter 5.

1.9.6 Temperature dependent dielectric spectroscopy on hydrated proteins

Temperature dependent study of various hydrated proteins were conducted to reveal further the mechanistic basis of each dielectric response observed. This is explained in Chapter 6.

1.9.7 In situ dielectric measurement on hydrated proteins

Chapters 5 and 6 are dealing with the basic understanding of water-protein interaction including the mechanism of the observed dielectric response. The results obtained from these sections for hydration and temperature studies are used as reference for analysing the results obtained by modification technique for *in situ* freeze drying purposes (Chapter 7).

2 PROTEINS SELECTION AND HYDRATION

2.1 Introduction

Proteins are formed when amino acids connect through loss of water from α-carboxyl and α-amino groups. A single protein molecule can comprise a few hundred to a few thousand amino acids. The amino acids in proteins are joined together by peptide bonds forming a polypeptide chain.[38].

Proteins can be classified in various ways[39, 40].

- Based on the generic structure, proteins can be classified in terms of four structural levels*: primary structure, secondary structure, tertiary structure, and quaternary structure*:

- Based on the gross structure and solubility, proteins can be classified as: *fibrous proteins* (e.g. collagen, elastin, keratin, myosin, and fibrin), *membrane proteins* (e.g. integral membrane proteins, transmembrane channels, and receptors), and *globular proteins* (albumin, soluble enzyme, O_2-carriers).

- Based on the functions, proteins can be classified into: *structural proteins* (e.g. keratin and collagen), *storage proteins* (e.g. casein and ovalbumin), *cellular transport* (e.g. hemoglobin), *hormones* (e.g. insulin), and *metabolism* as in enzymes (e.g. DNA polymerase).

Most proteins found in the aqueous, intracellular environment or in the plasma are of approximately spherical shape (globular). Unlike most fibrous proteins, they have many electrically charged groups of atoms exposed to cytoplasm and bodily fluids. This feature makes many globular proteins highly soluble[41].

Globular proteins are more likely to crystallize than membrane proteins, or fibrous proteins. As a result, the great majority of solved structures and thus studied proteins are globular proteins. This is one of the reasons of this study for choosing globular proteins as model proteins.

2.2 Selected Proteins

The globular proteins used in this study were: ovalbumin (Grade II, crude dried egg white, from Sigma), lysozyme (Fluka, Biochemika), and pepsin (Acros Organic). These proteins were chosen particularly for the reason of stability, where the conformation in a dry powder and solution is comparable. Other reasons for choosing these proteins involved the cost reason, availability, varieties of molecular structure and molecular weight.

2.2.1 Ovalbumin

Ovalbumin is an albumin that is soluble in water and can be characterised as a heat-coagulating protein. Ovalbumin is found widely in plant and animal tissues.

Ovalbumin can also be identified as a glycoprotein which comprises 60 to 65% of the total protein in egg white, and easily obtained in crystals [42]. The molecule consists of a polypeptide with up to two phosphate groups per mole and a side chain of mannose and glucosamine residues. Ovalbumin belongs to the serpin family of protease inhibitors.

A dephosphorylated form of ovalbumin found in egg-yolk may act as an amino acid store for the growing embryo. It has also been proposed that ovalbumin may play a role in the transport and storage of metal ions since a single strong binding site for several metal ions in ovalbumin has been found.

Ovalbumin is easily denatured at temperatures above 56 °C. Other factors that can also contribute to the denaturation of proteins are heavy metals, ammonium salts, alcohols, and acids.

The ovalbumin structure is illustrated in Figure 2.1. Figure 2.1 shows that the structure of ovalbumin consists of four domains. Domains A, B, and C contain both α-helices and β-strands, whereas domain D is a smaller loop of mostly α-helices.

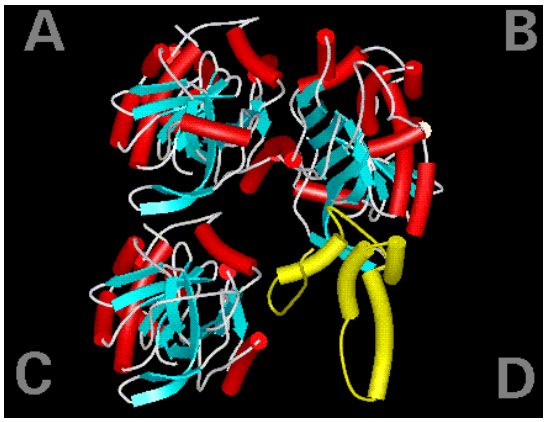

Figure 2.1 *The ovalbumin structure consisting of four domains, labelled A, B, C, and D, showing the α-helices (red and yellow tubes) and β-strands (blue sheets). Domain D contains only α-helices and is referred to as the exposed loop of ovalbumin.*[43]

2.2.2 Lysozyme

Lysozyme is an enzyme which catalyses the hydrolysis of polysaccharides, specifically hexoses consisting of alternating N-acetylglucosamine (NAG) and N-acetylmuramic acid (NAM) monomers, and hexoses of repeating NAG monomers. These hexoses are found in the cell walls of bacteria and fungi.

Lysozyme has been found in the egg whites of many birds, as well as in tears, mucus, and other body secretions of vertebrates such as humans and horses. Of all known lysozyme homologs however, the most widely studied and best-understood homolog is the hen egg white (HEW) lysozyme.

The residues that are critical to the catalytic function in the hen egg white lysozyme are: Glu35, Trp108, Asp52, and Gln57. The secondary structure of lysozyme is shown in Figure 2.2.

(a)

(b)

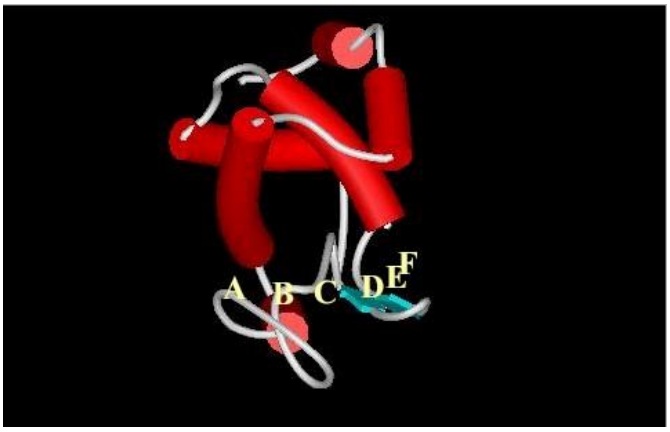

Figure 2.2 *Hen Egg White (HEW) lysozyme highlighted by secondary structure consisting of six α-helical domains (red tubes), two antiparallel β-pleated sheet domains (blue arrows), and interspersed coil (grey strings) (a) Straight on view of the active site cleft, (b) side view of the active site cleft. The binding subsites are labelled A-F and they bind substrate residues A-F, respectively.*[44]

2.2.3 Pepsin

Pepsin is a member of the aspartic proteinases. It has a role as one of three principal protein-degrading (proteolytic) enzymes in the digestive system that catalyse the hydrolysis of peptide bonds. The carbocylic side chains of two aspartic acid residues (Asp32 and Asp 215) are responsible for the catalytic activity. These two aspartate carboxyl groups typically contain a tightly bound water molecule and are the major residues in the active site of pepsin. The secondary structure of pepsin is shown in Figure 2.3.

Figure 2.3 *Element of secondary structure of pepsin, consisting of ten helices (four of these are single turns), five β-sheets (two with four strands, one with 6 strands, one with 7 strands, and one with 8 strands), and three disulfide bonds.*[45]

The comparison of main properties of the selected proteins is summarised in Table 2.1.

Table 2.1 *Various proteins properties*

	Ovalbumin	**Lysozyme**	**Pepsin**
Molecular Weight (Dalton)	45,000	14,600	34,000
Structure	• 385 amino acids • See Figure 2.1	• 129 amino acids, 26 of which are charged • 4 internal disulfide bonds • Contains 1001 non-hydrogen atoms; 958 hydrogens were added by Sybyl[1]. • see Figure 2.2	• 327 amino acids, 44 of which are charged. • Contains 2426 non-hydrogen atoms; 2255 hydrogens were added by Sybyl. • see Figure 2.3
Main Function	Used in conjugo-immuno determination, as well as drug and pharmaceutical processing	Dissolves certain bacteria by cleaving polysccharides in their cell walls so that the bacteria cell burst.	Enzymes produced by the stomach that helps digestion and protecting the epithelium
Isoelectric Point	4.63	11	N/A
Active pH range	N/A	3-8	2-4

[1] Sybyl is a comprehensive molecular modelling package which provides the tools for modelling protein structure.

2.3 General properties of globular proteins

2.3.1 Protein Stability

Thermodynamic measurements shows that native proteins are only marginally stable, with $\Delta G \sim 40$ kJ for 100 residue proteins (~ 2 hydrogen bonds). Hydrogen bonds are the most important stabilising force in secondary structure. Almost all possible hydrogen bondings in a protein can be a major influence in determining protein structure, but provide little stabilization energy because hydrogen bonding groups can also bond with water in denatured form.

2.3.2 Protein Denaturation

Loss of biological activity of proteins due to the loss of its native structure is called as denaturation. A small stabilisation energy means protein structure is readily disrupted and denatured. This occurs cooperatively (all at once). Denaturation in proteins may be complete or only partial, reversible or irreversible.

Some conditions which can denature the proteins are[46]:

- Temperature - most proteins denature with $T_M < 100°C$, depending on the hydration level.
- pH - extremes of pH change the ionisation state (and consequently the charge) of many amino acid side chains.
- detergents (e.g. SDS) - bind to the hydrophobic side chains disrupting hydrophobic interactions.
- organic solvents, such as alcohols, acetone, ether.
- high concentration of guanidinium ion and urea (5-10 M) can denature proteins by disrupting hydrophobic interactions

2.4 Protein Hydration

2.4.1 Sample preparation

Proteins were hydrated as described elsewhere[47, 48, 49]. The sample was put in a vial and placed inside a constant-humidity desiccator over saturated salt solutions for a period of one to a few days, depending on the physical state of the powder and the final hydration required. The desiccator itself was immersed in a water bath to keep the constant condition of humidity and temperature. The condition inside the desiccator was 25°C and 98% relative humidity (Figure 2.4). The temperature and humidity inside the container were measured using a LogIT (data logging system) using a humidity probe sensor.

As shown in Figure 2.4, humidity and temperature in the desiccator were constant after about 30 minutes. The vials containing the protein sample were placed in the desiccator after the humidity and temperature reached a constant condition.

The hydration level of protein was calculated by using:

$$h = \frac{\Delta m}{m_{dry}} \tag{2.1}$$

where:

h = hydration level (g water/ g protein)

Δm = $m_{hydration} - m_{dry}$ (g)

$m_{hydration}$ = mass of the sample after placing in the container for a certain time (g)

m_{dry} = mass of the dry sample (g)

The accuracy of the given hydration values in this work was estimated to be ± 0.01 g water/ g protein. Each different protein was hydrated separately. The mass of the dry sample was determined from the drying oven method as described in Section 2.4.2 below.

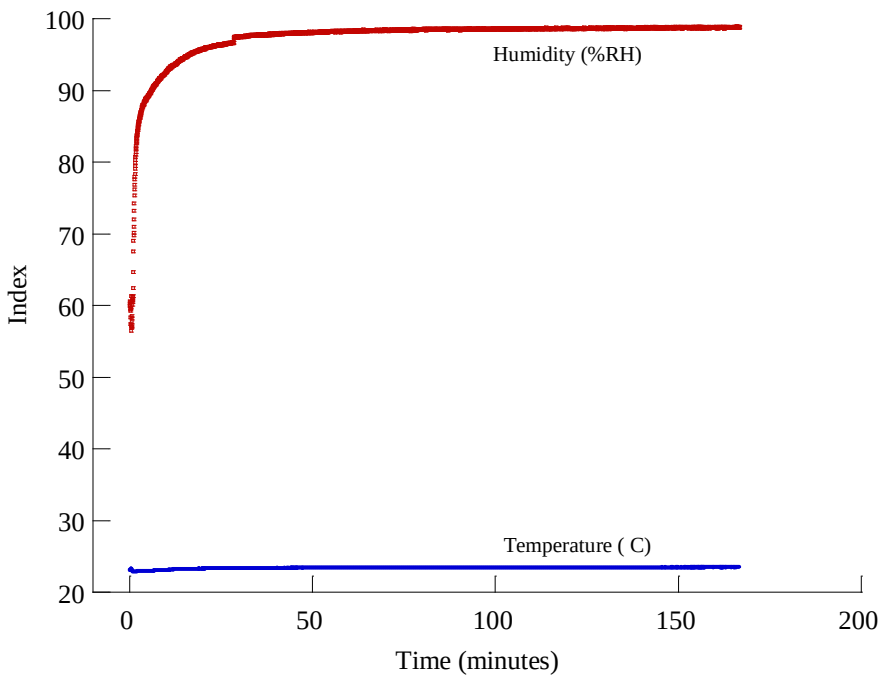

Figure 2.4 *Humidity and temperature conditions used for hydrating proteins.*

2.4.2 Validation of hydration

Each protein was expected to contain in some degree a small amount of water, which maintained the function and stability. Therefore, to obtain a true hydration level, the basal hydration of the as-received protein used in this study had to be determined. The basal water content of the as-received sample was determined by drying the hydrated proteins in a vacuum oven at less than 8 mbar and 80 °C. Drying was continued until no mass reduction was observed. The relation of total mass of hydrated sample to dissociative drying mass may be expressed as follows:

$$m(t) = m_{dry}(h\exp(-t/\tau) - K_d t + 1) \tag{2.2}$$

where:

$m(t)$	=	instantaneous total mass (g) of sample at time t
m_{dry}	=	mass (g) of sample with water desorbed
K_d	=	dissociative drying coefficient
h	=	relative moisture index or hydration level ($= \Delta m / m_{dry}$)
t	=	time (hours)
τ	=	decay time constant (hours)

Figure 2.5 shows the drying curve from the representative hydration level of each protein. The curve was fitted by equation (2.2) and the results are tabulated in Table 2.2.

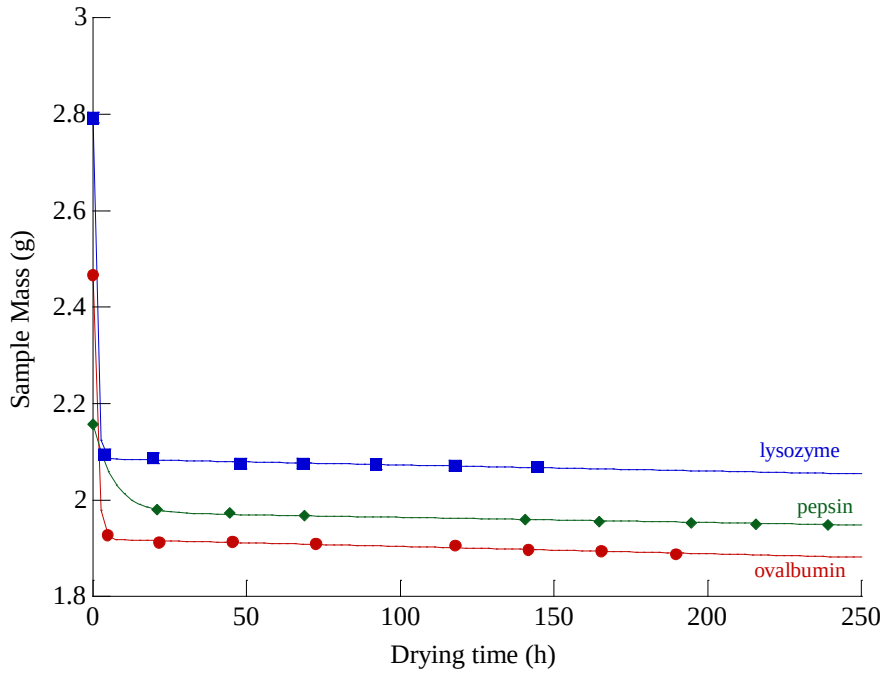

Figure 2.5 *Curve of drying time for ovalbumin, lysozyme, and pepsin. Solid lines represent the curve fitting.*

Table 2.2 *Characteristics of drying process of proteins.*

	Ovalbumin	**Lysozyme**	**Pepsin**
τ (s)	1.15 ± 0.123	0.873 ± 0.074	6.555 ± 0.761
K_d (x 10^{-3})	0.276 ± 0.038	0.178 ± 0.040	0.580 ± 0.059
M_{dry} (g)	1.919 ± 0.002	2.085 ± 0.003	1.975 ± 0.002
Moisture index (g/g)	0.285 ± 0.002	0.339 ± 0.002	0.093 ± 0.002

The mass of samples after drying (M_{dry}) as shown in Table 2.2 is the mass after removal of hydration/sorbed water. The M_{dry} shown in Table 2.2 was less than the initial weight of the proteins placed in the vial for hydration. This demonstrates that the as-received samples were not completely dry, but contain a small amount of moisture (i.e. basal hydration). This basal hydration was expected to exist in almost every protein and has a stability and functional purpose.

The moisture index shown in Table 2.2 was the true hydration level for the protein with the inclusion of basal hydration. The hydration level chosen to be representative of hydration validation was almost the highest hydration level that was employed in this study, i.e. about 0.3 g/g for lysozyme and ovalbumin, and 0.1 g/g for pepsin.

The results from Table 2.2 shows that ovalbumin and lysozyme almost have similar dissociative properties (comparable value of decay time constant τ and dissociative drying coefficient K_d). Pepsin has the highest value of value of decay time constant τ and dissociative drying coefficient K_d. In the experiment, pepsin was observed to get damp very quick and dry very slowly compared with ovalbumin and lysozyme. This explained the high value of decay time constant and dissociative drying coefficient for pepsin.

From drying mass (m_{dry}) obtained as shown in Table 2.2, the basal hydration of the proteins can be determined by using equation:

$$h(t) = h_{\infty} - \{(h_{\infty} - h_b)\exp(-t/\tau)\} \tag{2.3}$$

where:

$h(t)$ = hydration of sample (g/g) at time t

h_{∞} = saturation hydration of sample (g/g)

h_b = basal hydration (g/g)

t = time (hours)

τ = decay time constant (hours)

Figure 2.6 shows the curves of hydration versus time for ovalbumin, fitted by Equation (2.3). The results of the curve fitting for various protein hydrations are tabulated in Table 2.3.

Table 2.3 *Characteristics of hydration process for various proteins.*

	Ovalbumin	**Lysozyme**	**Pepsin**
h_{∞} (g/g)	0.391 ± 0.004	0.40 ± 0.02	0.160 ± 0.017
h_b (g/g)	0.045 ± 0.0005	0.034 ± 0.005	0.017 ± 0.001
τ (s)	84.63 ± 1.82	122.24 ± 20.74	56.37 ± 10.04

(a)

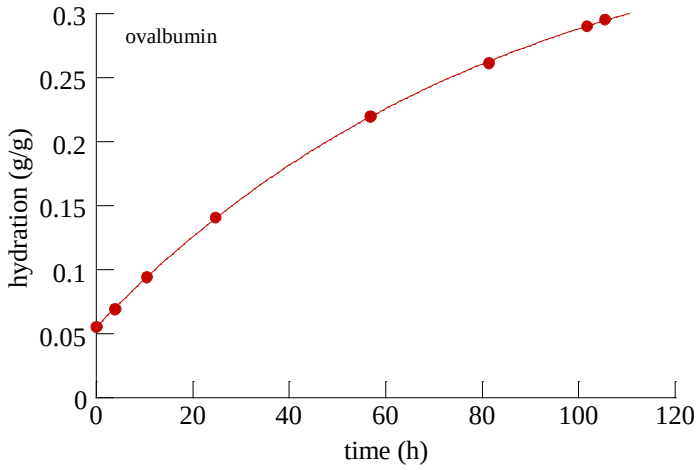

(b)

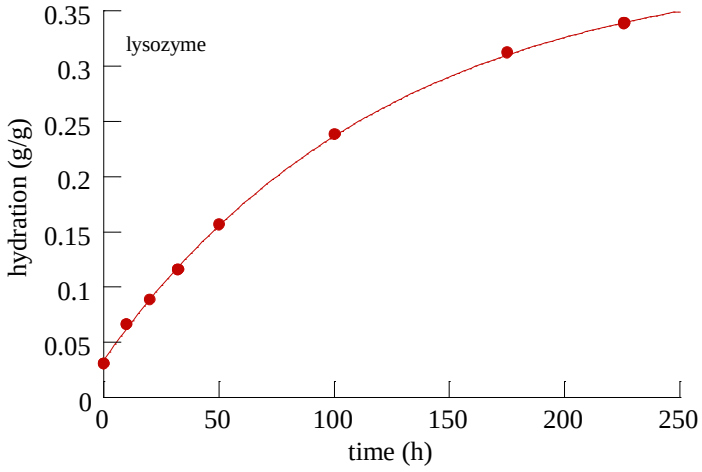

(c)

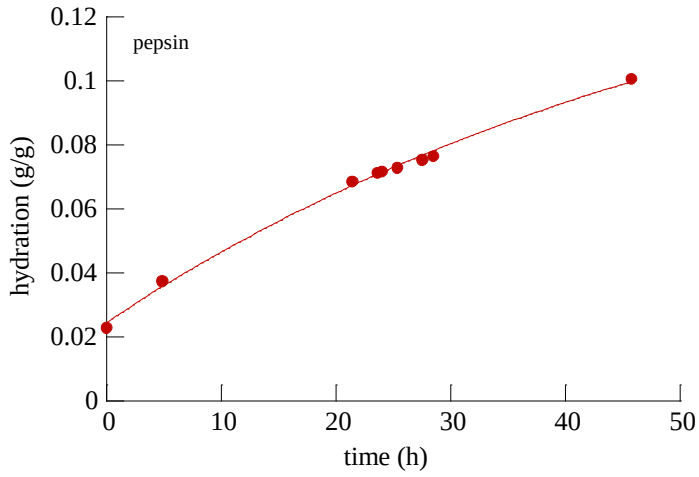

Figure 2.6 *Hydration curve versus time for (a) ovalbumin, (b) lysozyme, and (c) pepsin. Symbols represent experimental data. Solid lines represent fitting to Equation (2.3).*

The hydration curved obtained for each hydrated protein should have a sigmoidal shape which is a typical isotherm sorption curve based on the interpretation from Brunauer-Emmett-Teller (BET) theory. In term of protein hydration, below the 'knee' region, the water interacts principally with ionisable protein groups. In the plateau region, water binds to polar sites. At hydration level higher than described in the curve above, water condenses onto the weakest binding sites of the protein surface to complete the hydration processes [50].

TGA 50 Thermogravimetric Analyzer was also used to confirm the water content of the hydrated proteins in this study. For the TGA measurement, the sample (< 10 mg) was placed in a shallow dish/sample boat and positioned in a furnace with an automated recording balance. Any weight change, due to the thermal treatment of the sample, was recorded as a function of time.

Figure 2.7 shows the percentage weight loss for ovalbumin and lysozyme, obtained from TGA measurement (5 °C/min, 30 - 100 °C). In general, the plots of percentage weight loss do not show comparable results to those obtained from the drying method. The weight percentage of water loss from the TGA measurement was generally smaller compared with the results from drying method, especially for the high hydration level. This is probably due to the fact that the drying time for the TGA experiment was only ~ 20 minutes, compared to ~ 10^3 minutes for vacuum drying (depending on the hydration level and sample – see Figure 2.5). Moreover, the TGA experiment was carried out at the atmospheric pressure whereas vacuum drying was carried out was carried out at ~ 8 mbar.

The hump observed for lysozyme (0.224 g/g) at about 50 – 70 °C was suggested due to the first layer hydration of water (Figure 2.7 (b)).

(a)

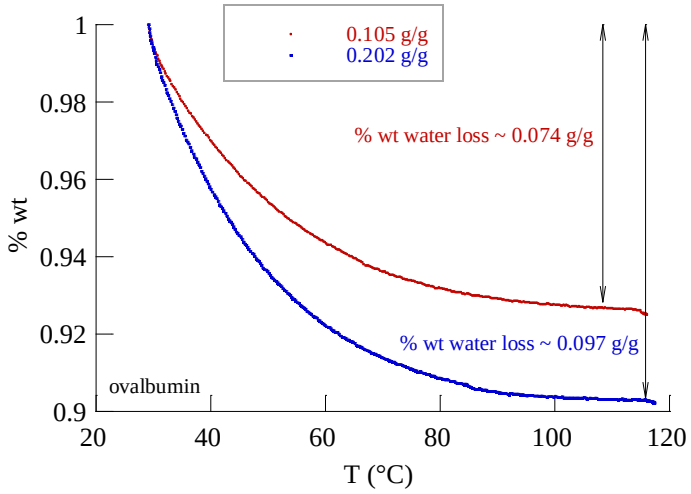

(b)

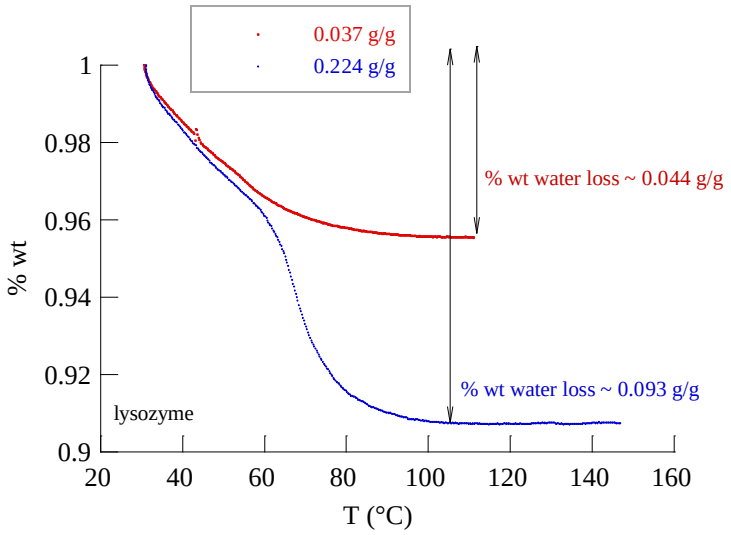

Figure 2.7 *The plots of percentage weight loss for (a) ovalbumin and (b) lysozyme obtained from TGA measurement.*

3 PRINCIPLES OF DIELECTRIC BEHAVIOUR

3.1 Introduction

This section describes a general understanding of dielectric behaviour involving the dielectric mechanism in the materials, dielectric modelling concerning the model fit used in this study, and a general theory of low frequency dispersion, which is largely used in this study.

3.2 Dielectric Mechanism

Dielectric materials are defined as materials containing dipoles, which can be either permanent or induced dipole. A *Dipole* is an entity that has charge separation but which maintains overall neutrality.

Polar or permanent dipoles occur due to the dissimilarity or an imbalance in the charge distribution of the electrons forming atoms/molecules. In the absence of an electric field, these dipoles have dipole moment, and are randomly oriented (due to Brownian motion), so no permanent polarisation exists. Under the effect of an electric field, the dipoles rotate to align with the electric field where the positive pole will tend to move in the direction of electric field and the negative end in the opposite direction.

Induced dipoles occur due to an applied electric field. In the absence of electric field, these dipoles do not have any dipole moment or only show a small dipole effect.

In general, the polarisation in the material due to an applied electric field is a dynamic process that depends on the structure and molecular properties of the material. There are five basic polarisation mechanisms that can contribute to the overall permittivity of the material. These are *electronic (induced) polarisation, orientational (dipolar) polarisation, atomic polarisation, ionic polarisation, and interfacial (space charge) polarisation*.

3.2.1 Electronic polarisation or induced polarisation

Electronic polarisation occurs in neutral atoms when an electric field acts on an individual atom. In zero field the positively charged nucleus and the negative cloud of electrons are symmetrically disposed and the atom has no dipole moment. When an electric field **E** is applied, the nucleus and the electrons move with respect to one another (Figure 3.1), creating dipole moment.

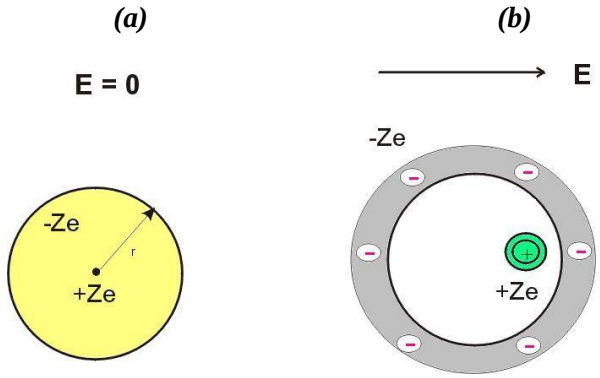

Figure 3.1 *Model of electronic polarisation (a) In the absence of electric field, the nucleus (+Ze) is in the center of spherical electron cloud (-Ze), (b) the applied field shifts the nucleus (+Ze) charge relative to the electron cloud (-Ze).*

3.2.2 Orientational polarisation or Dipolar polarisation

If the system consists of heteronuclear molecules, the disposition of the individual atoms within a molecule itself creates a permanent dipole moment. This kind of system occurs with *polar molecules*.

In zero field conditions, the permanent dipole moments are randomly oriented and the system has no net polarisation. If an electric field is applied, the electric field tends to align

the dipoles and the system takes on a net dipole moment. This process is called orientational polarisation.

3.2.3 Atomic polarisation

Besides the alignment effect on a permanent dipole, the electric field also tends to stretch the bonds between the atoms and thereby cause a change of the dipole moment of the molecule. This effect is called atomic or molecular polarisation.

3.2.4 Ionic Polarisation

A similar effect to atomic polarisation can also occur in an ionic solid (an ionic crystal). In ionic crystals, each ion pair creates an electric dipole. However, in the absence of an electric field, the lattice symmetry and the overall charge neutrality causes the dipole moments to cancel each other. An applied electric field can displace the ions from their equilibrium positions by the force of the electric field. The positive ion sub-lattice is shifted relative to the negative ion sub-lattice and creates a dipole moment in a crystal (Figure 3.2). This process is called ionic polarisation.

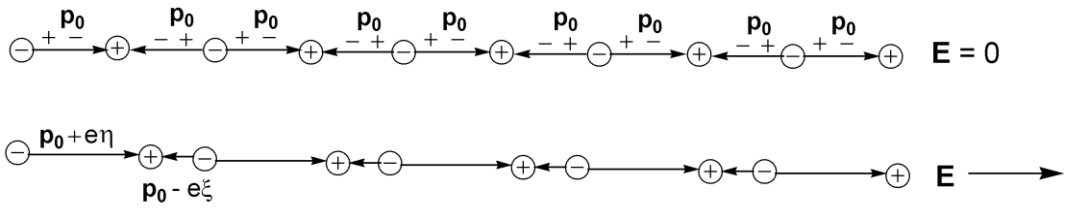

Figure 3.2 *Model of an ionic polarisation. The applied electric field E causes the cations move to the right by an amount of η creating dipole moment of $p_0 + e\eta$, while the anions move to the left by an amount of ξ creating the dipole moment of $p_0 - e\xi$ (ref. [51]).*

3.2.5 Interfacial or space charge polarisation (Maxwell-Wagner polarisation)

Electronic, atomic, ionic, and orientation polarisation occur when charges are locally bound in atoms, molecules, or structures of solids or liquids. Besides the locally bound charges, under a low frequency electric field, charge carriers may also exist and migrate over a distance through the material. When the motion of these migrating charges is impeded, interfacial or space charge polarisation occurs. The charges can become trapped within the interfaces of a material. Motion may also be impeded when charges cannot be freely discharged or replaced at the electrodes. The field distortion caused by the accumulation of these charges increases the overall capacitance of a material which appears as an apparent increase in real permittivity.

All these dielectric mechanisms produce a polarisation which is proportional to the applied electric field **E**. The dielectric response occurring in the materials is actually the summation of all the possible polarisation in materials. Figure 3.3 shows the schematic frequency response of dielectric mechanisms.

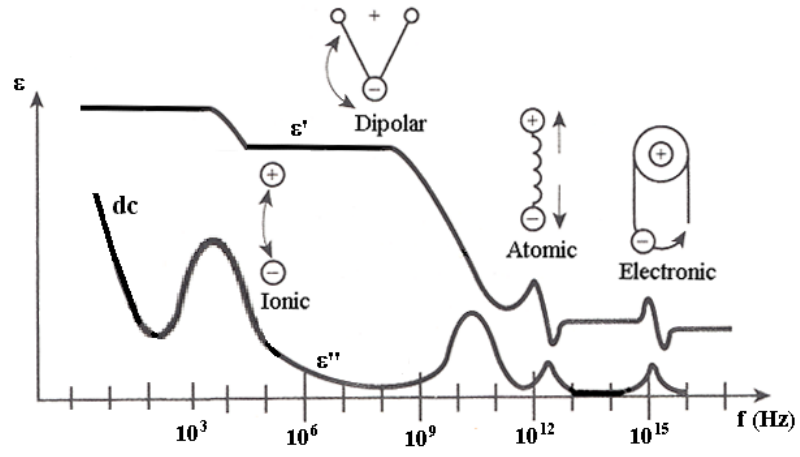

Figure 3.3 *Frequency response of dielectric mechanisms (taken from ref.[52], with some modifications.*

3.3 Dielectric Theory

When a static electric field $\mathbf{E}$ is applied to a dielectric material, the dipoles within that sample will experience a finite displacement. This displacement leads to a polarisation $\mathbf{P}$ in the direction of applied field, which can be expressed as:

$$\mathbf{P} = N\langle\boldsymbol{\mu}\rangle \tag{3.1}$$

where:

N = number of dipoles per unit volume

$\langle\boldsymbol{\mu}\rangle$ = mean dipole moment.

Dipole moment ($\boldsymbol{\mu}$) is defined as the product of the elementary charge (e) and the distance between two charges ($\mathbf{r}$)

$$\boldsymbol{\mu} = e.\mathbf{r} \tag{3.2}$$

The polarisation $\mathbf{P}$ of the system is defined as the dipole moment per unit volume. If any non-linearity of the system is neglected then the polarisation $\mathbf{P}$ can also be expressed in terms of the field strength, $\mathbf{E}$, and the electric susceptibility of the material, χ_e:

$$\mathbf{P} = \varepsilon_0 \chi_e \mathbf{E} \tag{3.3}$$

where:

ε_0 = permittivity of free space

The relative permittivity, ε, is defined as:

$$\varepsilon = 1 + \chi_e \tag{3.4}$$

and therefore the polarisation $\mathbf{P}$ can also be expressed as:

$$\mathbf{P} = \varepsilon_0(\varepsilon - 1)\mathbf{E} \tag{3.5}$$

$$\mathbf{P} = \varepsilon_0 \varepsilon \mathbf{E} - \varepsilon_0 \mathbf{E} \tag{3.5a}$$

The first term in Equation (3.5a) is defined as a dielectric displacement $\mathbf{D}$:

$$\mathbf{D} = \varepsilon_0 \varepsilon \mathbf{E} \tag{3.6}$$

The alignment of the dipoles itself creates an additional electrical field. Therefore, the actual field in the proximity of dipolar molecules is in fact larger than the applied field. This new field is referred to as the internal field. In the assumption of isotropic media, the magnitude of the internal field $\mathbf{F}$ is given by[37]:

$$\mathbf{F} = \mathbf{E} + \frac{1}{3\varepsilon_0}\mathbf{P} \tag{3.7}$$

This internal field $\mathbf{F}$ is the field that is felt by the individual molecules, so the torque is created by $\mathbf{F}$ rather than $\mathbf{E}$. Therefore the mean dipole $\langle \boldsymbol{\mu} \rangle$ should be proportional to the total field $\mathbf{F}$, as expressed by:

$$\langle \boldsymbol{\mu} \rangle = \alpha \mathbf{F} \tag{3.8}$$

where:

α = polarisability or the dipole moment of a molecule per unit polarizing field.

Combining Equations (3.1), (3.7) and (3.8) gives:

$$\mathbf{P} = N\alpha(\mathbf{E} + \frac{1}{3\varepsilon_0}\mathbf{P}) \tag{3.9}$$

Since $\mathbf{P} = \varepsilon_0(\varepsilon - 1)\mathbf{E}$ then Equation (3.9) can be rewritten as:

$$\alpha = \frac{3\varepsilon_0}{N}\frac{(\varepsilon - 1)}{(\varepsilon + 2)} \tag{3.10}$$

This equation is known as the Clausius-Mossotti equation.

3.4 Dielectric Modelling

As mentioned before, the dielectric properties of materials are determined by the polarisability of the material when an electric field is applied. If the applied electric field is an alternating electric field, instead of a static electric field, there will be a phase shift between the electric field $\mathbf{E}$ and the polarisation $\mathbf{P}$.

When a static electric field is applied, any dipoles in the dielectric material will reorientate with the field and return to the original state when the electric field is removed. When an alternating electric field is applied, the response of the sample will vary with the applied frequency. Such dependence on frequency is called as dispersion.

The alternating electric field is usually expressed in term of a complex function:

$$\mathbf{E}^* = \mathbf{E}_0 e^{i\omega t} \tag{3.11}$$

where:

ω = angular frequency

$\mathbf{E}_0$ = amplitude of electric field

The analogy from Equation (3.11) may be expressed for the dielectric displacement $\mathbf{D}$:

$$\mathbf{D}^* = \mathbf{D}_0 e^{i(\omega t - \delta)} \tag{3.12}$$

where:

δ = the phase shift between the applied electric field and the displacement.

Equation (3.6) shows that the dielectric permittivity ε may be obtained from the ratio between the dielectric displacement $\mathbf{D}$ and electric field $\mathbf{E}$. The ratio between Equations (3.11) and (3.12) therefore gives a complex dielectric permittivity ε^*:

$$\varepsilon^* = |\varepsilon| e^{-i\delta} \tag{3.13}$$

where $|\varepsilon| = \frac{\mathbf{D_0}}{\mathbf{E_0}}$.

The complex dielectric permittivity ε^* can also be expressed in terms of real and imaginary parts:

$$\varepsilon^* = \varepsilon' - i\varepsilon'' \tag{3.14}$$

where:

ε' = the real component of the permittivity, which relates to the energy stored by the material; the capacitive/storage properties of the system. Energy may be exchanged between the field and the material in a bi-directional (loss less) manner.

ε'' = the imaginary component of the permittivity, comprising dielectric loss and ohmic conductivity, which relates to the energy loss. Energy may be permanently lost from the field, and absorbed by the material as heat.

3.4.1 Debye Model

When an alternating electric field $\mathbf{E}^*$ is applied to a system consisting a group of dipoles, the total polarisation of the system can be described as:

$$\mathbf{P}_t^* = \mathbf{P}_o^* + \mathbf{P}_\infty^* \tag{3.15}$$

where:

$\mathbf{P}_t^*$ = total polarisation

$\mathbf{P}_o^*$ = orientational polarisation

$\mathbf{P}_\infty^*$ = the sum of the atomic and electronic polarisations.

From Equation (3.5), $\mathbf{P}_t^*$ and $\mathbf{P}_\infty^*$ can be expressed as:

$$\mathbf{P}_t^* = \varepsilon_0(\varepsilon_s - 1)\mathbf{E}^* \tag{3.16}$$

$$\mathbf{P}_{\infty}^{*} = \varepsilon_0(\varepsilon_{\infty} - 1)\mathbf{E}^{*} \tag{3.17}$$

Equations (3.16) and (3.17) give the orientational polarisation $\mathbf{P}_o^*$:

$$\mathbf{P}_{o}^{*} = \varepsilon_0(\varepsilon_s - \varepsilon_{\infty})\mathbf{E}^{*} \tag{3.18}$$

Orientational polarisation ($\mathbf{P}_o^*$) is a very slow process compared with atomic and electronic polarisation ($\mathbf{P}_{\infty}^*$) and lags behind the rise of the electrical field. If $\mathbf{P}_o^*(t)$ is defined as the orientational polarisation during the transient time, its time derivative defines the rate increase in polarisation with time, which is proportional to the number of unpolarised dipoles:

$$\frac{d\mathbf{P}_o^*(t)}{dt} = \frac{1}{\tau}\left(\mathbf{P}_o^* - \mathbf{P}_o^*(t)\right) \tag{3.19}$$

where:

τ = relaxation time

$1/\tau$ = rate constant

By substituting Equation (3.18) to (3.19):

$$\frac{d\mathbf{P}_o^*(t)}{dt} = \frac{1}{\tau}\left(\varepsilon_0(\varepsilon_s - \varepsilon_{\infty})\mathbf{E}_0 e^{\mathrm{i}\omega t} - \mathbf{P}_o^*(t)\right) \tag{3.20}$$

The solution of Equation (3.20) is:

$$\mathbf{P}_o^*(t) = Ce^{-t/\tau} + \varepsilon_0 \frac{\varepsilon_s - \varepsilon_{\infty}}{1 + \mathrm{i}\omega\tau}\mathbf{E}_0 e^{\mathrm{i}\omega t} \tag{3.21}$$

The first term in Equation (3.21) will diminish to zero when time increases.

From Equation (3.15):

$$\mathbf{P}_t^* = \mathbf{P}_o^* + \mathbf{P}_{\infty}^* \tag{3.22}$$

$$\mathbf{P}_t^* = \left(\varepsilon_0 (\varepsilon_\infty - 1) + \varepsilon_0 \frac{\varepsilon_s - \varepsilon_\infty}{1 + \mathrm{i}\omega\tau} \right) \mathbf{E}_0 e^{\mathrm{i}\omega t} \tag{3.23}$$

From Equation (3.5a), the dielectric displacement $\mathbf{D}^*$ may now be expressed as:

$$\mathbf{D}^* = \left(\varepsilon_\infty + \frac{\varepsilon_s - \varepsilon_\infty}{1 + \mathrm{i}\omega\tau} \right) \varepsilon_0 \mathbf{E}_0 e^{\mathrm{i}\omega t} \tag{3.24}$$

From Equation (3.6), the complex dielectric permittivity is therefore obtained:

$$\varepsilon^* = \left(\varepsilon_\infty + \frac{\varepsilon_s - \varepsilon_\infty}{1 + \mathrm{i}\omega\tau} \right) \tag{3.25}$$

Equation (3.25) is well known as Debye model, which is often expressed[53]:

$$\varepsilon^* = \varepsilon_\infty + \frac{\Delta\varepsilon}{1 + \mathrm{i}\omega\tau} \tag{3.26}$$

where:

$\Delta\varepsilon$ = $\varepsilon_s - \varepsilon_\infty$

= relative permittivity increment (relaxation strength), which relates to the number of polarisable molecules and the extent of molecular-dipole polarisation in the applied field

ε_∞ = high frequency real relative permittivity (relative permittivity at $\omega \to \infty$)

ε_s = static field real relative permittivity (relative permittivity at $\omega \to 0$)

τ = relaxation time of the orienting dipoles; which is a characteristic of the material as it gives time constant of the dipolar reorientation process

In the presence of an ionic dc-conductivity (σ_{dc}), Equation (3.26) can be expressed as:

$$\varepsilon^* = \varepsilon_\infty + \frac{\Delta\varepsilon}{1 + \mathrm{i}\omega\tau} - \mathrm{i}\frac{\sigma_{dc}}{\varepsilon_0 \omega} \tag{3.27}$$

The real and imaginary part of permittivity from Equation (3.26) can be expressed respectively as:

$$\varepsilon' = \varepsilon_{\infty} + \frac{\Delta\varepsilon}{1+(\omega\tau)^2} \tag{3.28}$$

$$\varepsilon'' = \frac{\omega\tau\Delta\varepsilon}{1+(\omega\tau)^2} \tag{3.29}$$

Figure 3.4 shows the plot of real and imaginary permittivity over a range of frequencies, describing a Debye model. At low frequency (i.e. frequencies below the relaxation/characteristic frequency), the real part of permittivity is effectively constant ($\varepsilon' = \varepsilon_s$), and the mean orientation of the dipoles will change direction in phase with the oscillating field. In this range of frequency, the polarisation of the system is fully developed. However as the frequency increases, the phase lag develops between the mean dipole alignment and the electric field, and the permittivity begins to decrease.

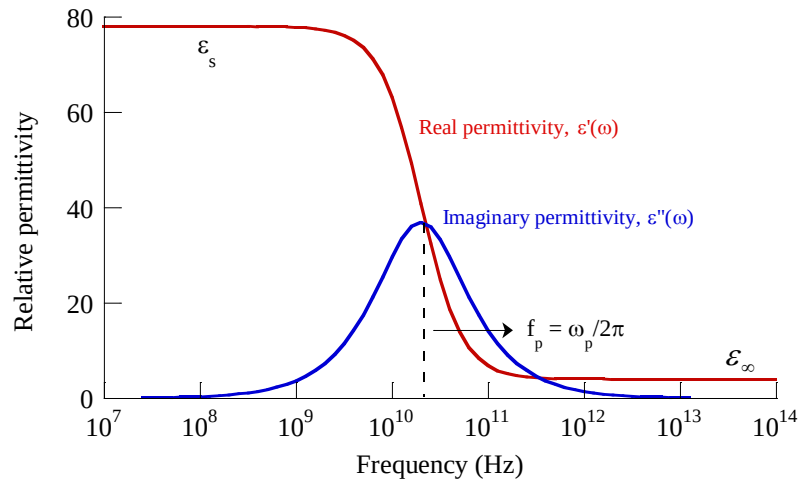

Figure 3.4 *Real and imaginary permittivity of water, showing a Debye model.*

At the characteristic frequency, ω_p, ($f_p = \omega_p / 2\pi$), the real part of permittivity is decreasing at a maximum rate and therefore the rate of energy absorption by the system is at a maximum, and therefore the imaginary part of permittivity shows a peak at a characteristic frequency, ω_p (peak loss frequency). The characteristic frequency is related to the relaxation time by expression:

$$\omega_p = 1/\tau \tag{3.30}$$

At very high frequencies (frequencies above the characteristic frequency), the changes in field direction are so rapid that the dipoles are unable to reorientate with that field because of their inertia and viscous damping. Therefore, the total polarisation of the system falls. It is described by the decrease in ε' to ε_∞.

The relaxation time can also be related to the dimensions of the relaxing molecule. Early Debye theory shows a simple expression for the relaxation time for a non-interacting population of spheres of radius *a* in a medium of viscosity η and temperature *T*, as:

$$\tau = \frac{4\pi a^3 \eta}{kT} \tag{3.31}$$

3.4.2 Modification of the Debye Model

The Debye model (as expressed in Equation (3.26)) is derived by assuming that the rate of rise and/or decay of polarisation is characterised by a single exponential function, with one time constant. It means that Debye model should only be valid for conditions of uniform and isotropic molecules, as in the gas state. If the size of the molecules is not uniform or if the shape is not spherical, then it is likely that the Debye model will no longer be applicable.

A deviation from the Debye model usually occurs for macromolecular systems which may have cooperative and isolated movements of side-chain molecular groups. The deviation

from the Debye model is usually interpreted in terms of a distribution or cooperation of relaxation times. Experimental results show that the behaviour of most dielectric materials departs from the Debye model to some degree.

In attempt to give a better empirical fit in dielectric spectra, some modifications of the Debye model have been suggested and used extensively in the literature. A simple way to differentiate Debye model from non-Debye models is by looking at the permittivity plots in the complex plane. The complex plane for the Debye model is a symmetrical behaviour and a perfect semi circle (Figure 3.5 (a)). For non-Debye models, the semi-circle is depressed or/and tilted as shown in Figure 3.5 (b), (c), and (d).

When the circular arc of Debye model is symmetrical, but tilted from the real axis by the angle of $\alpha(\pi/2)$ with $(0<\alpha\leq 1)$, the modification is called as Cole-Cole model (Figure 3.5 (b)), which can be expressed as[54] :

$$\varepsilon^*(\omega)=\varepsilon_\infty+\frac{\Delta\varepsilon}{1+(\mathrm{i}\omega\tau)^{(1-\alpha)}} \tag{3.32}$$

This α parameter, therefore, does not have any direct physical significance. It is only an empirical factor to describe or quantify the deviation of experimental data from the Debye response.

However, the Cole-Cole model is only adequate for correcting small deviations of the dielectric plot from the Debye response. For more extreme forms of non-Debye behaviour, Davidson and Cole[55] proposed another modification, as given by:

$$\varepsilon^*(\omega)=\varepsilon_\infty+\frac{\Delta\varepsilon}{(1+\mathrm{i}\omega\tau)^{\beta}} \tag{3.33}$$

The parameter β $(0<\beta\leq 1)$ relates to the angle of tilt of the tangent to the plot at the intersection with the ε' axis, given by $\beta\pi/2$, and causes an asymmetrical shape of the circular arc of Debye (Figure 3.5 (c)). This parameter β also does not have any direct physical significance.

There are still many dielectric materials that cannot be represented by either the Cole-Cole model or the Davidson-Cole model. A more general modification was therefore introduced by Havriliak and Negami [56] (Equation 3.34):

$$\varepsilon^*(\omega) = \varepsilon_\infty + \frac{\Delta\varepsilon}{(1+(\mathrm{i}\omega\tau)^{(1-\alpha)})^{\beta}} \tag{3.34}$$

The Havriliak-Negami model is actually a combination of the Cole-Cole and Cole-Davidson models. It can be seen that if $\alpha = 0$ and $\beta = 1$, the Havriliak-Negami expression equates to the Debye model. If $\beta = 1$, the expression equates to the Cole-Cole model, and if $\alpha = 0$, the expression equates to the Cole-Davidson model. In the complex plane, the Havriliak-Negami model is a circular arc of Debye which is tilted in the angle of $(1-\alpha)\beta\pi/2$ (Figure 3.5 (d)).

The plot comparison of complex planes from Debye, Cole-Cole, Cole-Davidson, and Havriliak-Negami models is shown in Figure 3.5.

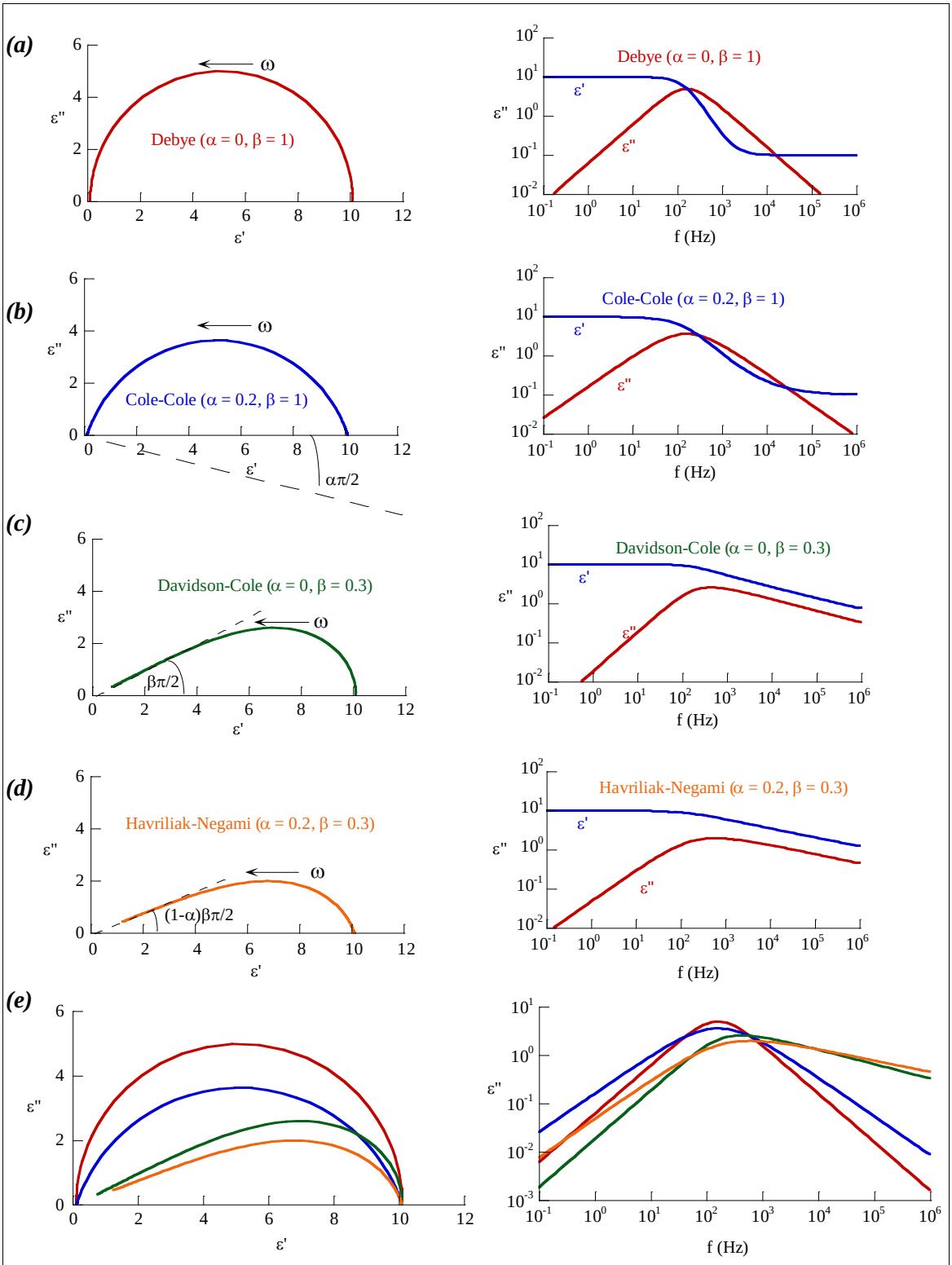

Figure 3.5 *Comparison of Debye and non-Debye models in the complex plane and Bode plots (a) Debye, (b) Cole-Cole (c) Davidson-Cole, (d) Havriliak-Negami, (e) mixture of Debye and all non-Debye models.*

3.5 Low Frequency Dispersion

As has been described previously, induced and permanent dipoles involve the polarisation of two component charge systems that are very strongly coupled together, and cannot be dissociated into separate charges by a normal force. Besides these inseparable charges, some systems may contain completely free charges, such as electrons in metals or holes in crystalline semiconductors. These charges can move freely without any constraint and may give rise to a dc-conductivity.

Some other systems have an intermediate behaviour between dipoles and free charges, which are often mentioned as *hopping charge carriers*. These charge carriers reside in localised sites and may experience hopping transitions to some preferred neighbouring localised sites with a distance of one or many atomic spacing away. These charge carriers have much higher mass which makes them impossible to propagate in the "free bands". This hopping motion is considered as the only possible form of transport for all forms of ionic conductors. Examples of these systems are amorphous and disordered non-metallic solids. The probability of hopping transition may be determined by the distance between the two sites and the potential barrier that has to be overcome. If the localised sites form a continuous connected network, the charges may be able to pass through the entire system and therefore give rise to a dc-conductivity. In the case where the system has a self-similarity, the formation of continuous network may be explained in term of percolation phenomena (see Appendix A3).

The dielectric behaviour caused by the hopping of charge carriers is usually observed at very low frequency. Free charge carriers (e.g. electrons and holes) which move in conduction and valence bands, are characterised by mean free paths between collisions that extend over many interatomic spaces. The dielectric behaviour of these free charge carriers is only observed at the high frequency range of 10 – 100 GHz. This confirms the

perception that at low frequency, dielectric mechanism is dominated by the response from localised charge carriers, i.e. the hopping transition, not a free charge carrier.

When the mechanism of charge hopping occurs in the sample, dielectric response gives an excessive increase in both real and imaginary permittivities. This is due to free moving charge carriers between the electrodes which in turn give rise to large polarisabilites. The enormous rise in both real and imaginary permittivities is known as *low frequency dispersion* (LFD) [57,58] .

The LFD phenomenon has been generally recognized to occur in numerous amounts of samples, such as hydrated samples[59], tissues[60], porous samples[61], semiconducting samples[62,63], layered compounds[64], humid silica surface[65, 66], some organic compounds[67] and ceramics[68]. For a long time it was thought to be a process of Maxwell-Wagner effect or simple dc-conduction effect.

3.5.1 Frequency Domain Response

In terms of frequency domain, low frequency dispersion (LFD) is an anomaly of dielectric properties at low frequency, in which no dielectric loss peak observed. The real and imaginary permittivities in LFD are rise steeply as frequency decreases, following a 'universal' fractional power law of frequency[57, 69, 70, 71]. The LFD generally consists of two parts: the low frequency part ($\omega < \omega_c$) and high frequency part ($\omega > \omega_c$), where ω_c is the characteristic frequency representing the intersection point between the real and imaginary permittivities (Figure 3.6). In log-log plots, the real and imaginary permittivities are parallel before and after crossing ω_c. This characteristic frequency, ω_c, is analogous with the frequency of the loss peak in a dipolar system.

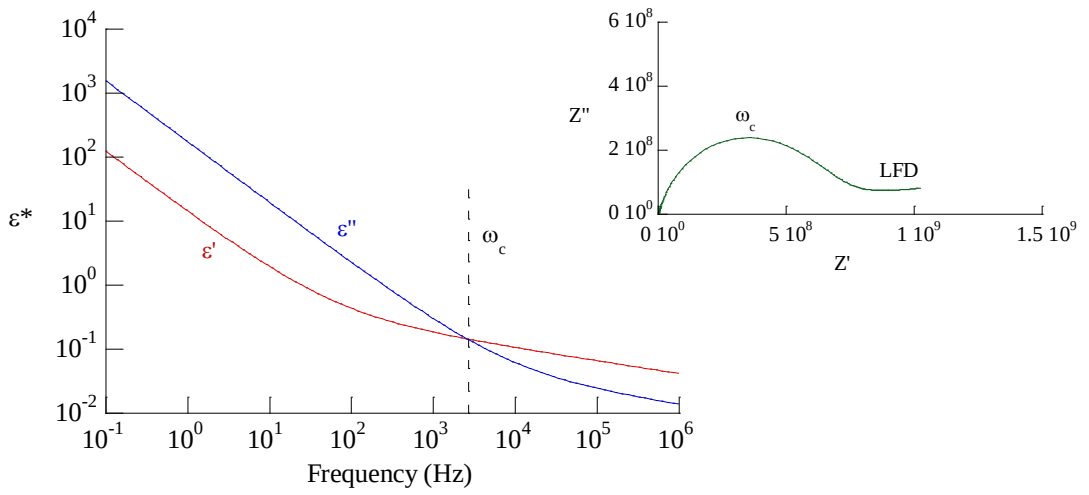

Figure 3.6 *A typical spectra of low frequency dispersion (LFD).*

The general expression for LFD consists of two fractional power laws of frequency:

$$\varepsilon^*(\omega) = A_1(\mathrm{i}\omega)^{-p} + B_1(\mathrm{i}\omega)^{n-1} \tag{3.35}$$

where A_1 and B_1 are pre-exponential factor for low frequency part ($\omega < \omega_c$) and high frequency part ($\omega > \omega_c$), respectively. The exponent p for low frequency part and the exponent n for high frequency part are close to one. Figure 3.6 shows the schematic of LFD feature for p = 0.95 and n = 0.8.

Based on the characteristic frequency, ω_c, Equation (3.35) may also be expressed as:

$$\varepsilon^* = A_2\left(\frac{\mathrm{i}\omega}{\omega_c}\right)^{-p} + B_2\left(\frac{\mathrm{i}\omega}{\omega_c}\right)^{n-1} \tag{3.36}$$

Both Equations (3.35) and (3.36) are actually approximations of the LFD when the frequency is much less or much greater than characteristic frequency, for first and second part of the equations, respectively. The true equations are in the form of hypergeometric function, in which the dielectric permittivity is expressed in the form [71]:

$$\varepsilon^*(\omega) = \varepsilon(0) F\left(\frac{\omega}{\omega_c}\right) \tag{3.37}$$

where:

$\varepsilon(0)$ = the magnitude of dispersion, i.e. the dielectric increment for the single process of relaxation.

$F\left(\frac{\omega}{\omega_c}\right)$ = spectral shape function, normalised to the characteristic frequency ω_c

From the cluster model of relaxation, for *bound dipolar charge*, the spectral shape function is expressed as:

$$F\left(\frac{\omega}{\omega_p}\right) = F_0^{-1}\left(1+\frac{\mathrm{i}\omega}{\omega_p}\right)^{n-1} {}_2F_1\left[1-n, 1-m; 2-n; \frac{1}{1+i\omega/\omega_p}\right] \tag{3.38}$$

where ω_p is the frequency of dielectric loss peak, n and m are correlation coefficients for specific intra-cluster and inter-cluster relaxation mechanisms, and having value between 0 and 1. F_0 is the normalising parameter:

$$F_0 = \frac{\Gamma(2-n)\Gamma(m)}{\Gamma(1+m-n)} \tag{3.39}$$

$\Gamma()$ is a gamma function and ${}_2F_1(,;;)$ is a gaussian hypergeometric function.

When the binding between dipolar charges is weak and when the charges can only move effectively within a limited distance (*quasi-free charges*), the spectral shape function has a form of:

$$F\left(\frac{\omega}{\omega_c}\right) = F'^{-1}_0\left(1+\frac{\mathrm{i}\omega}{\omega_c}\right)^{n-1} {}_2F_1\left(1-n, 1+p; 2-n; \frac{1}{1+\mathrm{i}\omega/\omega_c}\right) \tag{3.40}$$

where p is the fractional correlation index for the transport of the quasi-free charge between clusters, and F'^{-1}_0 is the equivalent normalising constant:

$$F'^{-1}_{0} = \Gamma(2-n)\Gamma(1-p)\left(\frac{p+n-1}{p\Gamma(2-n-p)}\right) \tag{3.41}$$

One example of quasi-free charges is quasi-free ions in the fast ion conductors.

In the asymptotic behaviour at $\omega << \omega_p$ and $\omega >> \omega_p$ (for bound dipolar charge); $\omega << \omega_c$ and $\omega >> \omega_c$ (for weakly bound dipolar charge/charge hopping), Equation (3.38) for *bound dipolar charge carrier* may be expressed as:

$$\varepsilon(0) - \varepsilon(\omega) \propto \left(\frac{\mathrm{i}\omega}{\omega_p}\right)^m \qquad \omega << \omega_p \tag{3.42}$$

$$\varepsilon^*(\omega) \propto \varepsilon(0)\left(\frac{\mathrm{i}\omega}{\omega_p}\right)^{n-1} \qquad \omega >> \omega_p \tag{3.43}$$

and for *quasi-free charge carrier* Equation (3.40) may be expressed as:

$$\varepsilon(\omega) \propto \left(\frac{\mathrm{i}\omega}{\omega_c}\right)^{-p} \qquad \omega << \omega_c \tag{3.44}$$

$$\varepsilon^*(\omega) \propto \varepsilon(0)\left(\frac{\mathrm{i}\omega}{\omega_c}\right)^{n-1} \qquad \omega >> \omega_c \tag{3.45}$$

Equations (3.44) and (3.45) are equivalent to the first and second terms in Equation (3.36). For simplicity and agreement with the software used for the fitting of LFD response in this study, Equations (3.44) and (3.45) may be rewritten as:

$$\varepsilon^*(\omega) = A(\mathrm{i}\omega)^{-p} \qquad \omega << \omega_c \tag{3.44a}$$

$$\varepsilon^*(\omega) = B(\mathrm{i}\omega)^{n-1} \qquad \omega >> \omega_c \tag{3.45a}$$

The pre-exponential factors A and B involve the cell capacitance and characteristic frequency, ω_c (see Appendix A2).

The relationship between real and imaginary parts from Equation (3.42), (3.43) and (3.44) can be expressed as follows, respectively:

$$\frac{\varepsilon''(\omega)}{\varepsilon'(\omega)} = \cot(n\pi/2) \qquad \omega >> \omega_p \tag{3.46}$$

$$\frac{\varepsilon''(\omega)}{\varepsilon(0)-\varepsilon'(\omega)} = \tan\left(\frac{m\pi}{2}\right) \qquad \omega << \omega_p \tag{3.47}$$

$$\frac{\varepsilon''(\omega)}{\varepsilon'(\omega)} = \tan\left(\frac{p\pi}{2}\right) \qquad \omega << \omega_c \tag{3.48}$$

Based on the 'p' value from Equation (3.44), the dispersion observed may be due to the 'hopping charge carrier' between localised levels ($0.6 < p < 1$) or 'lattice responses' ($p \to 0$)[57].

This LFD effect needs to be distinguished from a dc-conductivity effect and Maxwell-Wagner effect (interfacial polarisation effect). For a dc-conductivity effect at low frequency:

- the real permittivity is frequency independent:

$$\varepsilon' \neq \varepsilon'(\omega) \tag{3.49}$$

- 'p' value is 1 for

$$\varepsilon''_{dc}(\omega) \propto \frac{\sigma_{dc}}{\omega} \tag{3.50}$$

where σ_{dc} is dc-conductivity.

For Maxwell-Wagner effect (interfacial electrode polarisation effect) at low frequency,

$$\varepsilon'(\omega) \propto \omega^{-2} \tag{3.51}$$

$$\varepsilon''(\omega) \propto \omega^{-1} \tag{3.52}$$

3.5.2 Time Domain Response

The time domain response is measured following the application of a step-function voltage to the sample. The expression for the time domain response of an LFD process is obtained by converting the power laws of frequency in the low and high frequency regimes, into time response using a Fourier transform, viz. [72].

$$\omega^{n-1} \rightarrow t^{-n} \qquad \text{for } t \ll \tau \qquad 0 < n < 1 \tag{3.54}$$

$$\omega^{-p} \rightarrow t^{-(1-p)} \qquad \text{for } t \gg \tau \qquad 0 < p < 1 \tag{3.55}$$

The fractional power law of time for LFD in time domain response may be expressed as:

$$i(t) = A_1 t^{-n} + A_2 t^{-(1-p)} \tag{3.56}$$

The plot of the time domain response corresponding to LFD behaviour is shown in Figure 3.7. The high frequency part, i.e. the short-time behaviour is represented by the steep gradient of the curve (corresponding to the exponent $-n$), while the long time behaviour is represented by shallow gradient of the curve (corresponding to the exponent $-(1-p)$).

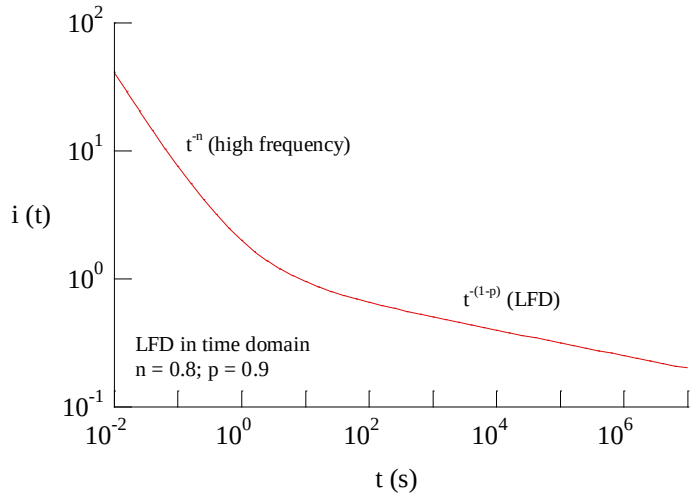

Figure 3.7 *Low frequency dispersion in the expression of time domain response.*

3.5.3 Mechanism of the low frequency dispersion

The LFD responses usually occur in dielectric materials with large densities of low-mobility charge carriers. As has been mentioned before, LFD corresponds to the hopping charge carriers which can be ionic[68] or electronic[63]. The charge carrier may exist as an intrinsic or extrinsic property of the material. The intrinsic charge carriers in material may occur due to the presence of some impurities, as in semiconductors or ionic glasses. The extrinsic charge carrier may occur due to the addition of mobile charge element through special treatment, such as exposure to humidity[73]. In practice, it is difficult to differentiate the presence of either intrinsic or extrinsic property. The addition of moisture, for example, may combine with the intrinsic property of the material.

Based on the experimental evidence, Jonscher recommended a division of the LFD mechanism into three phenomena i.e. (a) volume transport, (b) transport across interfaces, and (c) transport along interfaces (Figure 3.8)[69]. The LFD observed are suggested due to the dominance of any of these three phenomena.

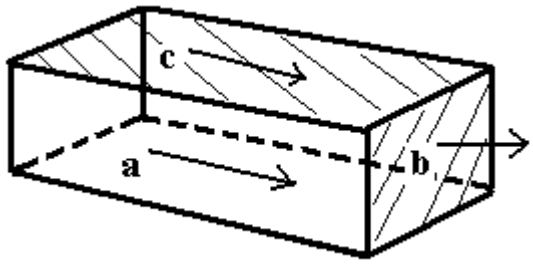

Figure 3.8 *Diagram of LFD mechanism, representing (a) volume transport, (b) transport across interfaces, and (c) transport along interfaces.*

The mechanism of "volume transport" and "transport across interfaces" may be distinguished experimentally in several ways, such as varying the interface with the same bulk material, measuring the potential distribution along the thickness of the sample, and varying the thickness of the bulk material.

Usually the LFD mechanism for volume transport will have a perfectly parallel real and imaginary part of the relative permittivity. The LFD mechanism for transport across interfaces is analogous with the interfacial electrode polarisation or known as Maxwell-Wagner polarisation.

Jonscher (1991) also suggested an electrochemical model as the nature of the LFD phenomena[69]. The energy loss arising from the reserve of electrochemical reaction may be large enough to supply the polarisation energy, leading to a strongly dispersive LFD.

3.6 Fractality and Dielectric Response

The fractional power law relating frequency and permittivity as shown in Section 3.5 above is usually represented by a constant phase angle (CPA)[74] or constant phase element (CPE)[75], which is expressed as:

$$Z(\omega) = \frac{1}{A(\mathrm{i}\omega)^{n_z}} \tag{3.57}$$

with a unit symbol : 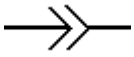

The exponent parameter n_z in Equation (3.57) corresponds to the exponent parameter p in Equation (3.44a). Derivation of these parameters is shown in Appendix A2.

The justification of this constant phase angle response is based upon a presumed self-similarity in the system or in its relaxation dynamics[76]. This self-similarity can be modelled as a circuit construction of resistors and capacitors (fractal circuit)[77] which can be used to represent the macroscopic behaviour of heterogeneous system.

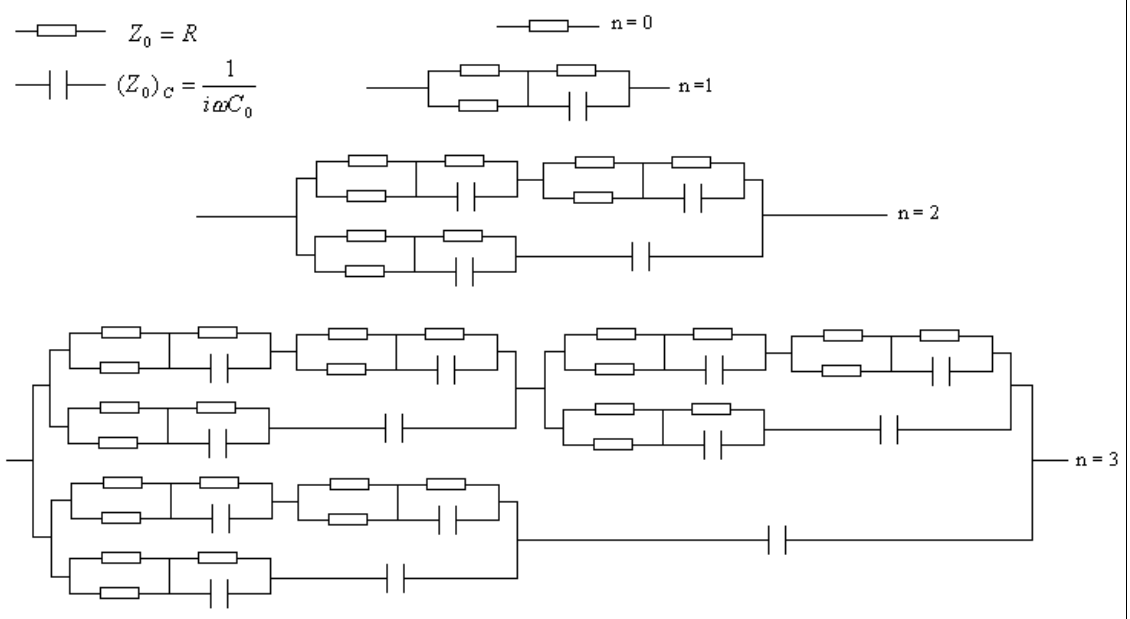

Figure 3.9 *Circuit construction of self-similar hierarchy for n = 0 – 3, consisting of resistors and capacitors.*

The type of hierarchy shown in Figure 3.9 can give a constant phase angle response with the exponent parameter n dependent on the electrical composition or the degree of self-similar scaling. The exponent parameter n can be expressed in the form of:[78]

$$n = 1 - \frac{d_f}{d_w} < 1 \tag{3.58}$$

where:

d_f = fractal dimension of the self-similar hierarchy and is purely geometrical origin

d_w = size scale of the electrical hierarchy R that has relaxed in time t, which can be expressed as:

$$t \propto R^{d_w} \tag{3.59}$$

As mentioned earlier, polarisation is defined as a separation of opposite charge carriers by the electrical field, and this polarisation can be related to the relaxation of the system. In terms of charge transport, relaxation in polarisation may be seen as the exploration of the system by a mobile charge seeking a counter charge for recombination[79]. Based on the fractal circuit, the charge carrier is free to move in the parts of circuit represented by the conductance elements, but the movement is blocked by the capacitance elements. As a result, the charge carrier may explore some 'dead ends' and go to some parts of the circuit more than once.

The behaviour of exploring the system by charge carrier is considered to be related to the 'random walk' model. In 'random walk' system, a particle on a lattice can transport to the bonds which represent the conductance elements. In this case:

d_w = "walk" dimension of the system

$R(t)^{d_w}$ = number of steps along the bonds while exploring the region of the system with a scale of $R(t)$.

$R(t)^{d_f}$ = volume of the system explored which is related to the number of different conductance elements visited in time t

The relaxation rate $\Phi(t)$ is defined as proportional to the volume explored per step[80]:

$$\Phi(t) \propto \frac{R(t)^{d_f}}{R(t)^{d_w}} \tag{3.60}$$

From Equations (3.58) and (3.59), it was obtained that:

$$\Phi(t) \propto R(t)^{d_f - d_w} \propto R(t)^{-nd_w} \propto t^{-n} \tag{3.61}$$

The Fourier transform of $\Phi(t)$ from Equation (3.61) gives the frequency dependence of susceptibility $\chi(\omega)$ with a fractional power law of frequency.

$$\chi(\omega) = \int_0^\infty \Phi(t) e^{-i\omega t} dt \tag{3.62}$$

$$\chi(\omega) \propto (i\omega)^{n-1} \tag{3.63}$$

4 INSTRUMENT SPECIFICATION

4.1 Introduction

Dielectric spectroscopy is a powerful technique to study the molecular dynamic and charge transport of the system. Nowadays, dielectric spectroscopy can cover a wide-range of frequency (10^{-6} – 10^{12} Hz) by using different measurement techniques, i.e. frequency response analysis (10^{-6} – 10^{8} Hz), impedance analysis (10^{2} – 10^{7} Hz), radio frequency (RF)- reflectometry (10^{6} – 10^{9} Hz), and network analysis (10^{7} – 10^{12} Hz)[81, 82, 83].

This study is concerned with the low to intermediate frequency range measurement, i.e. between 10^{-1} – 10^{6} Hz. This chapter covers the specification of the frequency response analyser used in this work including the dielectric interface used to improve the measurement quality. The sample cell design, which plays an important role in obtaining accurate results, is also described briefly.

4.2 FRA (Frequency Response Analyser)

The Frequency Response Analyser (FRA) applies a sinusoidal signal of angular frequency ω to the sample, and then takes a direct vectorial measurement from the ratio of the alternating current i and alternating voltage V.

Figure 4.1 shows the basic set-up of frequency response analyser technique. The sinusoidal signal was produced digitally by the *Generator* in the FRA, in the form of varying voltage signal of given frequency and amplitude for period of time ($u(\omega,t) = \mathrm{U}\sin(\omega t)$). The resistor R converts the sample current $I_s(\omega)$ into a voltage $y(\omega,t)$. The output signal $y(t)$ is a sinusoidal wave with different magnitude Y and phase ϕ at the frequency ω of the input signal (Figure 4.2).

Therefore:

$$\frac{Y}{U} = \left|G(\mathrm{i}\omega)\right| \text{ = gain at } \omega \tag{4.1}$$

$$\phi = \angle G(\mathrm{i}\omega) \text{ = phase at } \omega \tag{4.2}$$

By sequentially measuring the gain $G(\mathrm{i}\omega)$ and phase ϕ at various frequencies, a dielectric response can be obtained in the selected frequency range.

The complex impedance of the sample from the frequency response analyser (FRA) technique may also be obtained from:

$$Z_s(\omega) = \frac{\Delta V}{I_s(\omega)} = \frac{u(\omega) - y(\omega)}{\frac{y(\omega)}{R}} \tag{4.3}$$

$$Z_s(\omega) = R\left(\frac{u(\omega) - y(\omega)}{y(\omega)}\right) \tag{4.4}$$

The input and output/response obtained from the FRA technique as shown in Figure 4.2 can be measured directly from an oscilloscope trace. However the results are not accurate enough since in practice, the factors such as noise, harmonic distortion, and non-linearity are involved in the measurement.

In commercial FRA as used in this study (i.e. *Solartron 1255 FRA*), the FRA is equipped by a *Correlator*. Harmonic distortion and all non-linearities are rejected by the correlation process, while the noise is rejected by averaging the signal over a number of cycles[84].

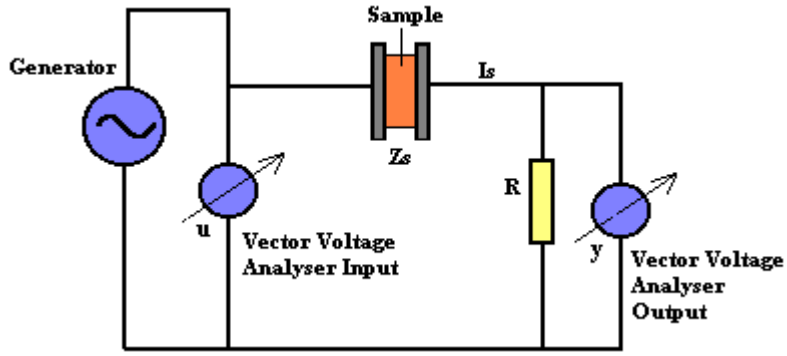

Figure 4.1 *Schematic diagram of basic circuit from frequency response analyser.*

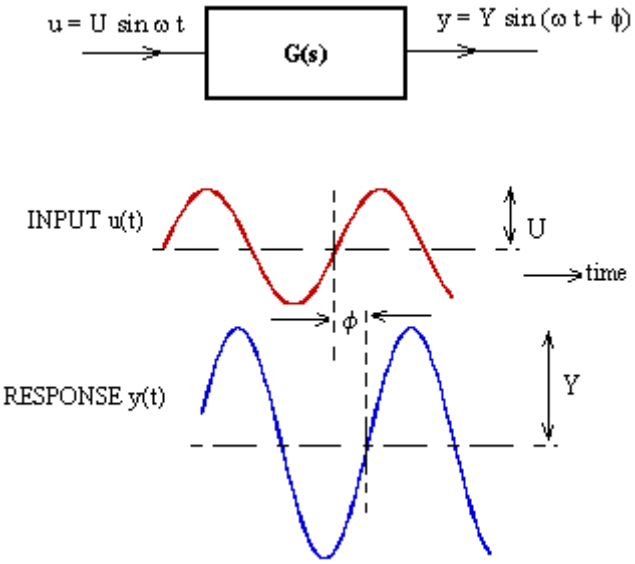

Figure 4.2 *Sine-wave input and output for Frequency Response Analyser (G(s)).*

4.2.1 Correlator

The correlation process in FRA may be described as follows[4].

The output waveform $y(t)$ from the sample has the form:

$$y(t) = y_0 + y_1 \sin(\omega t + \theta_1) + y_2 \sin(2\omega t + \theta_2) + ... + \text{noise} \tag{4.5}$$

where:

y_o = DC offset

y_1 = the return signal which is going to be analysed since it has the same frequency as the generator waveform.

$y_2, y_3, ...noise$ = harmonic distortion component

The output waveform $y(t)$ is then Fourier-analysed by multiplication the output signal $y(t)$ by the sine and cosine of the input signal $u(\omega,t)$ at frequency ω. The multiplication results are then integrated and averaged over a period T. As the averaging time increases, the contribution of the unwanted frequency components in $y(t)$ is negligible. The integrator produces the real $R(T)$ and imaginary $I(T)$ parts, which is a constant value depending only on the gain and phase of the system at frequency ω.

The outputs of the $R(T)$ and $I(T)$ may be expressed as follows:

$$R(T) = \frac{U}{T}|G(i\omega)|\int_0^T \sin\omega t \sin(\omega t + \phi)dt \tag{4.6}$$

$$I(T) = \frac{U}{T}|G(i\omega)|\int_0^T \cos\omega t \sin(\omega t + \phi)dt \tag{4.7}$$

If: $T = \frac{N\pi}{\omega}$, N = 1, 2, 3…, Equations (4.6) and (4.7) become, respectively:

$$R\left(\frac{N\pi}{\omega}\right) = \frac{U}{2}|G(\mathrm{i}\omega)|\cos\phi \tag{4.8}$$

$$I\left(\frac{N\pi}{\omega}\right) = \frac{U}{2}\left|G(\mathrm{i}\omega)\right|\sin\phi \tag{4.9}$$

This process of multiplication and integration is known as "Correlation". The correlation process rejects all the spurious components ($y_o, y_2, y_3, ...noise$) leaving only the non-vanishing R and I components, which are required for the analysis. R is the *real* (*in-phase*) component and I is the *imaginary* (*quadrature*) component. From these results (in-phase and imaginary components), the magnitude $\left|G(i\omega)\right|$ and phase-shift (ϕ) of the measured signal can be obtained:

$$G(\omega) = \sqrt{(R(\omega))^2 + (I(\omega))^2} \tag{4.10}$$

$$\phi_1 = \frac{I}{R} \tag{4.11}$$

From the magnitude ($\left|G(i\omega)\right|$) and phase-shift (ϕ), the nature of the test sample can be known. For example, a pure resistor will give zero phase-shift between the measured voltage and current waveforms, whereas a pure capacitor gives 90 degrees phase shift.

4.2.2 Dielectric Interface

For the purpose of measurement at very low frequencies with high impedance samples, the resistor R shown in Figure 4.1 is replaced by a current to voltage converter with variable gain. This part is included in the interface between the sample and FRA. The interface used in this study is *Solartron 1296 Dielectric Interface*.

In a dielectric interface, the gain of the current to voltage converter is improved by the measuring resistors and capacitors that can be switched to suit the varying magnitude of the impedance of the sample, according to the frequency of the measurement. The system is usually controlled by a computer after a number of measurement parameters are entered.

The FRA alone is unable to give accurate results for samples with low conductivity, low loss, or high impedance. The combination of FRA and dielectric interface with reference

capacitors has a capability of measurement of impedance in the range of 100 Ω - 100 TΩ, capacitance of 1 pF – 0.1 F, and phase angles tan δ of 10^{-4} – 10^{3}. The reference modes provided for Solartron 1296 Dielectric Interface consists of *normal*, *internal*, and *external* mode. For a quick measurement, it can use normal mode, while for measurement of dispersive materials, the internal or external reference capacitors may be used, depending on the needs.

The FRA (*Solartron 1255 FRA*) used in this study is connected to a dielectric interface (*Solartron 1296 Dielectric Interface*), and controlled by a computer via a GPIB (IEEE 488)[2] interface bus and a software Solartron version 3.1 (Figure 4.3).

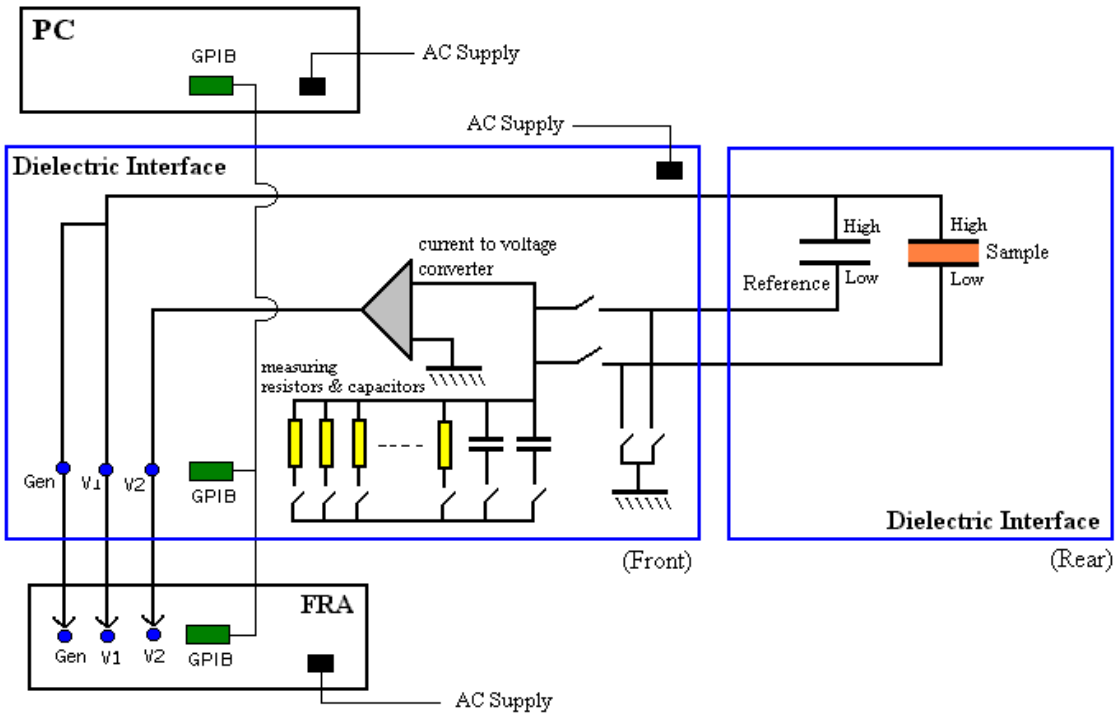

Figure 4.3 *Connection of FRA and Dielectric Interface 1296*

2 GPIB = General Purpose Interface Bus; IEEE = Institute of Electrical and Electronic Engineers

4.3 Temperature Controller

The instrumental specification mentioned above is for isothermal measurement. When the temperature study is carried out, the sample is placed in the cryostat in which the temperature of sample can be controlled.

The cryostat used in this study was Spectrostat^{DN} connected to the Oxford temperature controller ITC^{503}. The temperature controller was linked to the Dielectric Interface, so the operation of the system involving the frequency sweep and temperature control was carried out via a personal computer employing Solartron software version 3.1 (1997).

The heating in the cryostat was provided by applying a current to a heater coil from the temperature controller. The temperature was controlled via sensors set up in the cryostat (see Figure 4.4). For temperature below room temperature, the cooling was carried out using liquid N_2 filled to the outer vacuum chamber of the cryostat. The software controls the whole system so that the measurement only starts when the temperature reaches an equilibrium.

The rate of heating and cooling can be adjusted by manually controlling the rate release of the liquid N_2 vapour. Figure 4.5 shows a photograph of the measurement system involving frequency response analyser (Solartron 1255 FRA), dielectric interface (Solartron 1296 Dielectric Interface), and the cryostat (Spectrostat^{DN}). The temperature controller is not shown in the figure. The orange balloon was filled with Helium gas which function to give a better conduction from liquid N_2 to the sensor and samples.

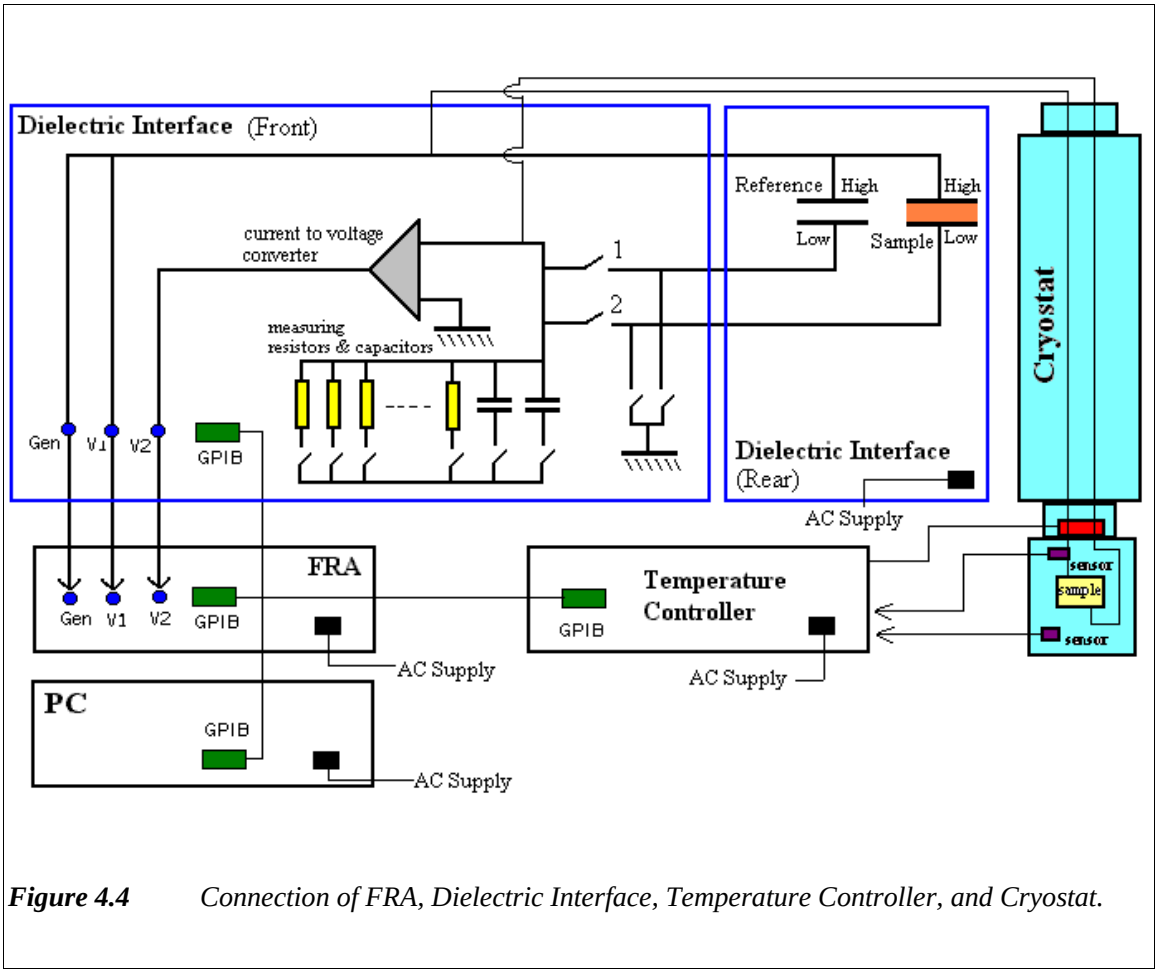

Figure 4.4 *Connection of FRA, Dielectric Interface, Temperature Controller, and Cryostat.*

(a) ***(b)***

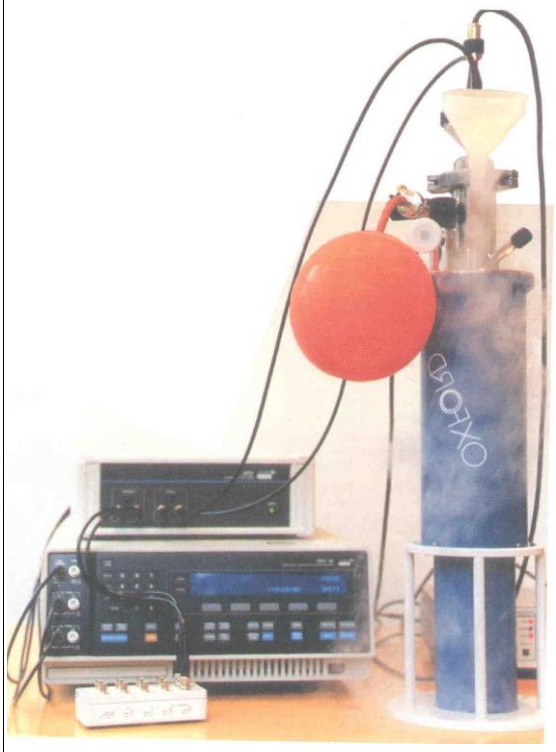

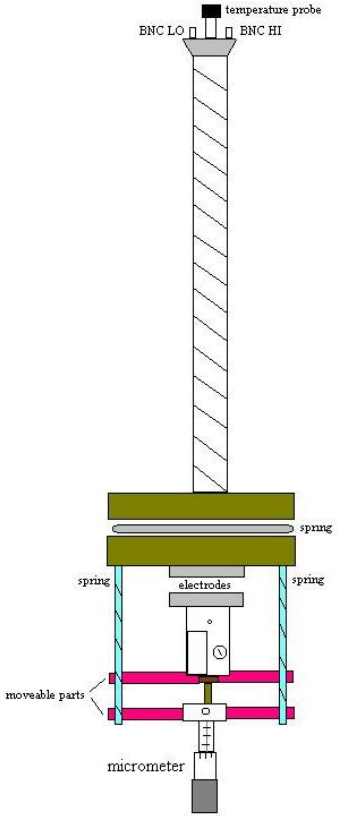

Figure 4.5 *(a) Photograph of Solartron FRA 1255, Solartron 1296 Dielectric Interface, and cryostat, (b) schematic of the cryostat rod as a sample holder.*

4.4 Sample Cells

The sample cell used in this study was a prototype sample cell from Solartron (12962 Solartron sample holder – see Figure 4.6). The sample cell has two different geometrical parallel plates:

1. Liquid-sample cell (diameter ϕ = 20 mm) with a guard ring on one of the electrodes connected to 'LO', and surrounded by a cylinder of PTFE. This sample cell is suitable for liquid samples or powder samples, since the sample can be contained by the PTFE cylinder (see "parallel plate cells (1)" in Figure 4.6 (a)).

2. Solid-sample cell (diameter ϕ = 40 mm) with a guard ring on the electrode connected to the 'LO' terminal of the dielectric interface. This sample cell is suitable for the measurement of bulk sample/sheet materials, where the sample is sandwiched between the electrodes (see "parallel plate cells (2)" in Figure 4.6 (b)).

This study employed a liquid-sample cell since the work is related with powder samples. The solid sample cell was utilised for calibration purposes.

Sample cell for temperature study has a similar geometry as liquid sample cell for isothermal measurement, with diameter ϕ = 25 mm. There is no guard ring in the sample cell for temperature study, since the guard ring has been set up at the fixed electrode in the cryostat.

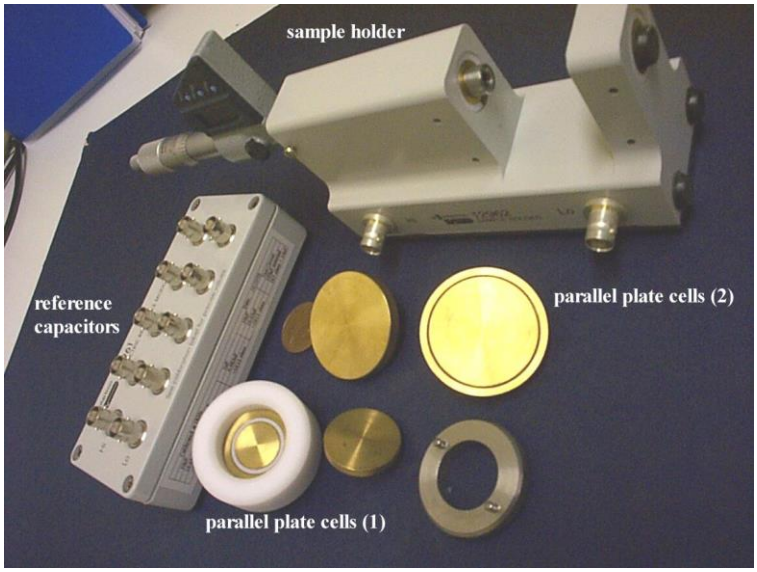

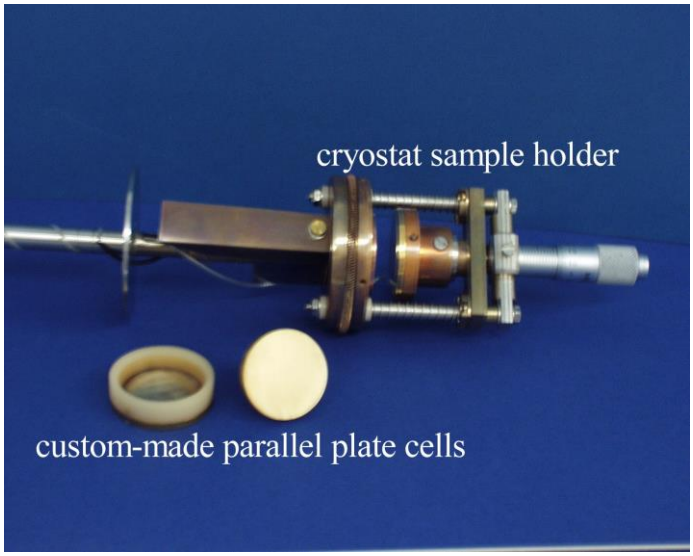

Figure 4.6 *Sample cells for (a) isothermal dielectric measurement (b) temperature study*

5 ISOTHERMAL STUDY OF HYDRATED PROTEINS

5.1 Introduction

This chapter describes a study of the dielectric properties of selected hydrated proteins, measured using a conventional parallel plate electrode system. The main aim of this part of the study was to understand the intrinsic dielectric properties of the selected proteins (as a function of water content and protein structure) and understand the polarisation mechanisms behind the observed dielectric responses.

Three model proteins, i.e. ovalbumin, lysozyme, and pepsin, were studied as a function of hydration. In attempt to eliminate the interfacial electrode polarisation, the use of remote electrodes, i.e. electrodes that are separated from the sample by non-conductive and non-dispersive medium, were investigated. The use of remote electrodes was not only useful to remove the interfacial electrode polarisation, but also it may be applied further for *in situ* determination of water content during freeze drying by employing the dielectric measurement technique. This application will be discussed in Chapter 7.

5.2 Isothermal dielectric properties of hydrated proteins

5.2.1 Introduction

This section covers the experimental results obtained from dielectric measurement on hydrated spray dried proteins (i.e. ovalbumin, lysozyme, and pepsin). The main interest covers the study of hydrated proteins measured isothermally at ambient temperature. The spray-dried proteins used are specified in Section 2.2 and the method of hydration is also described in Section 2.4.

5.2.2 Method

5.2.2.1 Dielectric Measurement

The frequency dependent dielectric response of each sample (at ~ 25 °C) was measured between 0.1 Hz – 10 MHz, using a Solartron 1296 dielectric interface connected to a Solartron 1255 frequency response analyser (see Chapter 4 for specification of the instrument). The voltage (3 V_{rms}) was applied to the sample, giving an output of amplitude and phase shift of the resulting current. These output parameters were then converted to dielectric parameters (e.g. impedances, capacitances, permittivities) using Solartron Impedance Measurement Software version 3.1. The curve fitting to complex functions was undertaken using commercial software (Zview™).

The measurement employed "internal reference", so the instrument selected automatically the capacitance that was comparable to the samples. As mentioned in Section 4.2, FRA has capability to remove the noise and all non-linear response by signal integration which averages the signal over a whole number of cycles. This process narrows the measurement bandwidth and therefore increases the signal to noise ratio. To get a more accurate result, a greater number of cycles need to be averaged, with the compensation of longer time of measurement. In this study, the integration period chosen is Auto Integration (V1, Long) with maximum period of 10 cycles. This means that the signal in the measurement is averaged until the standard deviation reaches a target value with the maximum period of 10 cycles to avoid excessive measurement times.

5.2.2.2 Sample cell for dielectric measurement

The sample cell used in this study is a prototype sample cell from Solartron (12962 Solartron sample holder – see Figure 5.1). The sample cell consists of parallel plates: (diameter ϕ = 20 mm) with a guard ring on one of the electrodes connected to the low voltage 'LO', and surrounded by a cylinder of PTFE.

Samples of hydrated proteins (thickness 3 –3.5 mm) were placed between two circular brass electrodes, each with surface area of 3.14 x 10^{-4} m^2. For measurement using 'remote' parallel plate electrodes, thin sheets of polyethylene film (d = 0.025 mm) were placed between each brass electrode and the sample to create a remote electrode system (Figure 5.1).

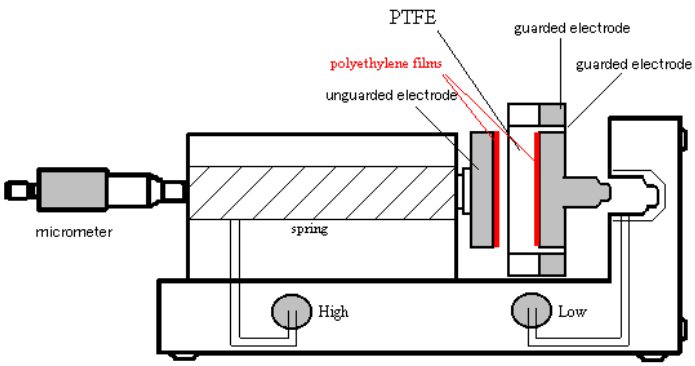

Figure 5.1 *Solartron 12962 sample holder, with a PTFE sample cell.*

5.2.2.3 Other complementary techniques

Besides dielectric measurement, hydrated protein samples were also characterised using other complementary techniques: FTIR (Fourier Transform Infra Red), SEM (Scanning Electron Microscopy), Differential Scanning Calorimetry (DSC), and X-ray Powder Diffractometer (XRD). The FTIR technique is expected to give information of the hydrated protein state, such as denaturation, aggregation, conformation, etc. SEM can reveal the morphology of the sample powder, while DSC may give the information of glass transition temperature and other thermo-properties of the samples.

5.2.2.3.1 FTIR

FTIR measurement was carried out using a Shimadzu FTIR, with standard detector, in the range of 4000 – 500 cm^{-1} and spectral resolution 2 cm^{-1}. Approximately 0.5 - 1 mg of freeze dried ovalbumin was mixed and ground with KBr, placed into a die and uniaxially pressed (~ 8 N m^{-2}) to form a thin pellet. The pellet was then mounted in the IR sample cell. Before the measurement of the sample was carried out, the IR spectrum of a KBr blank was also taken as a reference. This method of sample processing (i.e. mixing the protein sample with KBr and pressing into a pellet) does not affect the properties of the protein sample. This has been investigated by Prestrelski, et. al. by collecting spectra of protein powder using an attenuated total reflectance sampling device that did not require mixing and pressing with KBr[85].

5.2.2.3.2 SEM

A sample of protein powder was sprinkled onto an aluminium stub and gold coated in a sputter coater (Edwards 5150B) to a thickness of ~ 10 μm. This gold coating is to prevent the highlighting effect on the SEM images and to improve the quality of secondary electron imaging. The SEM analysis was carried out using a Leica S430 with a beam accelerator voltage of 7.5 kV and current 10 pA. Secondary electron imaging was employed in order to examine the morphology of the sample.

5.2.2.3.3 DSC

Samples of approximately 5 – 10 mg were routinely placed in the DSC pan and weighed using a Sartorius balance 4401. The sample pan was then sealed and placed in the sample holder of the instrument (Perkin Elmer DSC-4). A reference pan was positioned in the reference holder. Before the measurement was carried out, the temperature of the system was cooled down to –50 °C using liquid nitrogen. DSC thermograms were then recorded from –50 °C to + 150 °C. The temperature range was chosen to match approximately the temperature range used in the dielectric work.

5.2.2.3.4 XRD

XRD spectra were collected using a Bruker D8 Advance X-ray powder diffractometer with a capillary geometry (Debye-Scherrer). Protein powder samples were loaded into a 0.7 mm borosilicate glass capillary. The data collection was operated under 40 mA current and 50 kV voltage. The type of anode-tube used was Cu anode, with a primary monochromator i.e. monochromatic $CuK_{\alpha 1}$ radiation (λ = 1.54056 Å). The size of divergent (monochomator) slit used was 1 mm. A position sensitive detector was employed with the following settings for all spectra: 0.0145° (2θ) step size and 2.0 s count time per step over the range 5-50° (2θ).

5.2.3 Results

Figures 5.2, 5.3, and 5.4 showed typical dielectric spectra (real and imaginary permittivities) for hydrated ovalbumin, lysozyme, and pepsin, respectively. Each spectrum is clearly characterised by two relaxations:

(i) low frequency part ($\omega < \omega_c$)

(ii) high frequency part ($\omega > \omega_c$)

where ω_c is the characteristic frequency representing the intersection frequency of the real and imaginary permittivities.

The low frequency part ($\omega < \omega_c$) of the spectrum is characterised by a significant increase in both real and imaginary permittivities, while the high frequency part ($\omega > \omega_c$) is characterised by a dielectric loss peak, which was designated as ε_3 dispersion.

All the dielectric spectra of hydrated proteins were well fitted to a parallel circuit comprising an LFD element, a Davidson-Cole (D-C) element and an instantaneous

permittivity ε_∞ (Figure 5.2 (c), Figure 5.3 (c), and Figure 5.4 (c)), which can be expressed by Equation (5.1).

$$\varepsilon^*(\omega) = A(\mathrm{i}\omega)^{-p} + \frac{\Delta\varepsilon_3}{(1+\mathrm{i}\omega\tau_3)^{\beta_3}} + \varepsilon_\infty \tag{5.1}$$

The LFD element ($A(\mathrm{i}\omega)^{-p}$) models the universal fractional power law response of the low frequency part ($\omega < \omega_c$), as expressed in Equation (3.44a); the instantaneous permittivity, ε_∞, represents the permittivity at $\omega \to \infty$, and the remainder (the Davidson-Cole element – Equation (3.33)) models the high frequency part, i.e. ε_3 dispersion ($\omega > \omega_c$).

The universal power law of frequency as expressed in Equation (3.44a) is comparable with the constant phase element in the Zview software. The agreement between the universal power law of frequency as expressed in Equation (3.44a) and the constant phase element from Zview is shown in Appendix A2.

The curve fitting result from the LFD gave the value of pre-exponential factor A and exponent p, while the fitting result from ε_3 dispersion gave the value of relaxation time τ_3, relaxation strength $\Delta\varepsilon_3$, infinite permittiviy ε_∞, and distribution parameter β_3. The pre-exponential factor A shown in this study involved the cell capacitance, characteristic frequency ω_c, and the A_2 value from Equation (3.36)). The expression of the pre-exponential value A is show in Equation (A2.10).

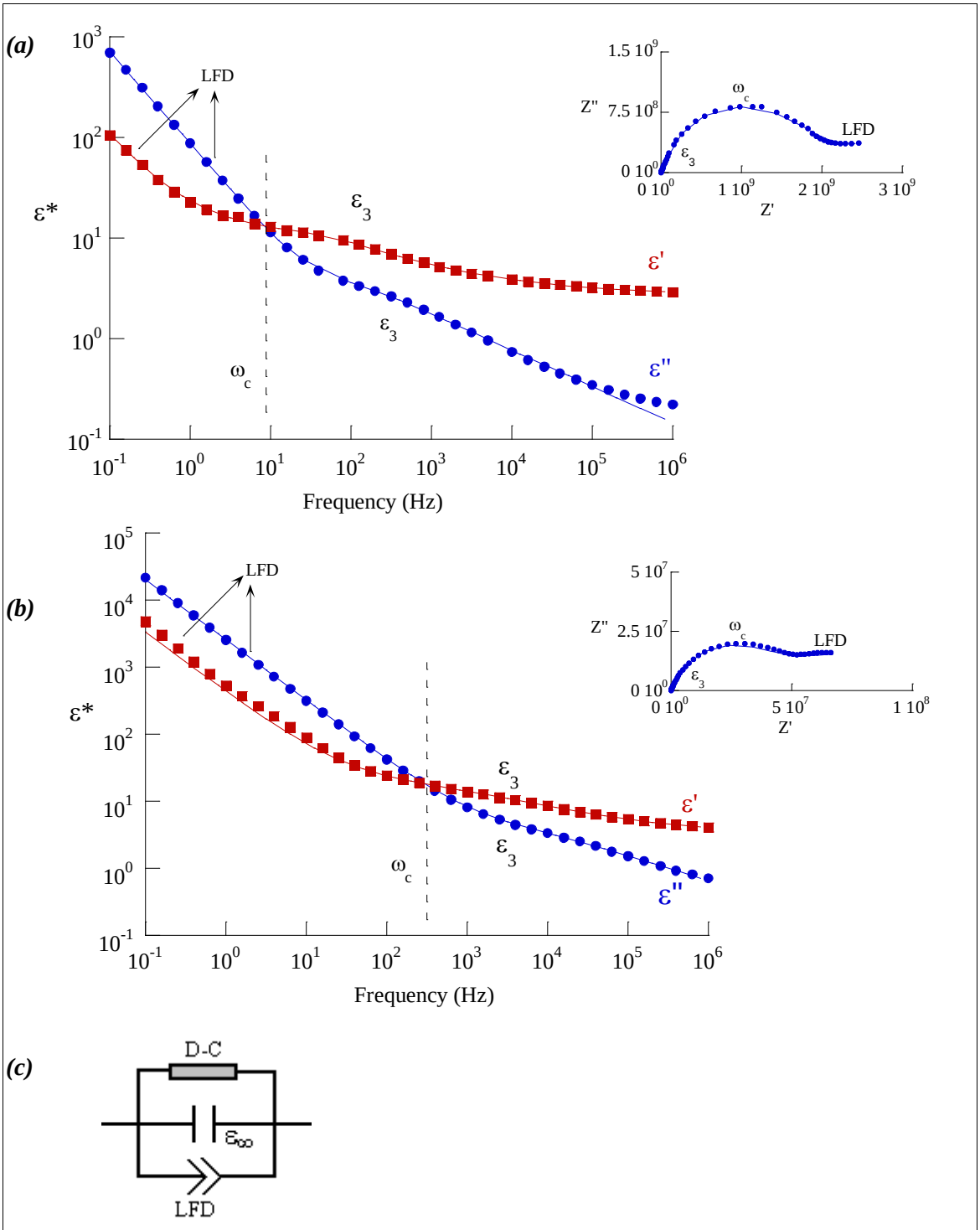

Figure 5.2 *Real and imaginary permittivities of hydrated ovalbumin without the use of remote electrodes, showing LFD and ε_3 dispersion (a) 0.07 g/g, (b) 0.11 g/g. Symbols represent experimental data, solid lines represent curve fitting. Only 50% of the experimental points are shown, to highlight the fitting lines. The inset shows the Cole-Cole plots of impedance. (c) Circuit model used for the fitting.*

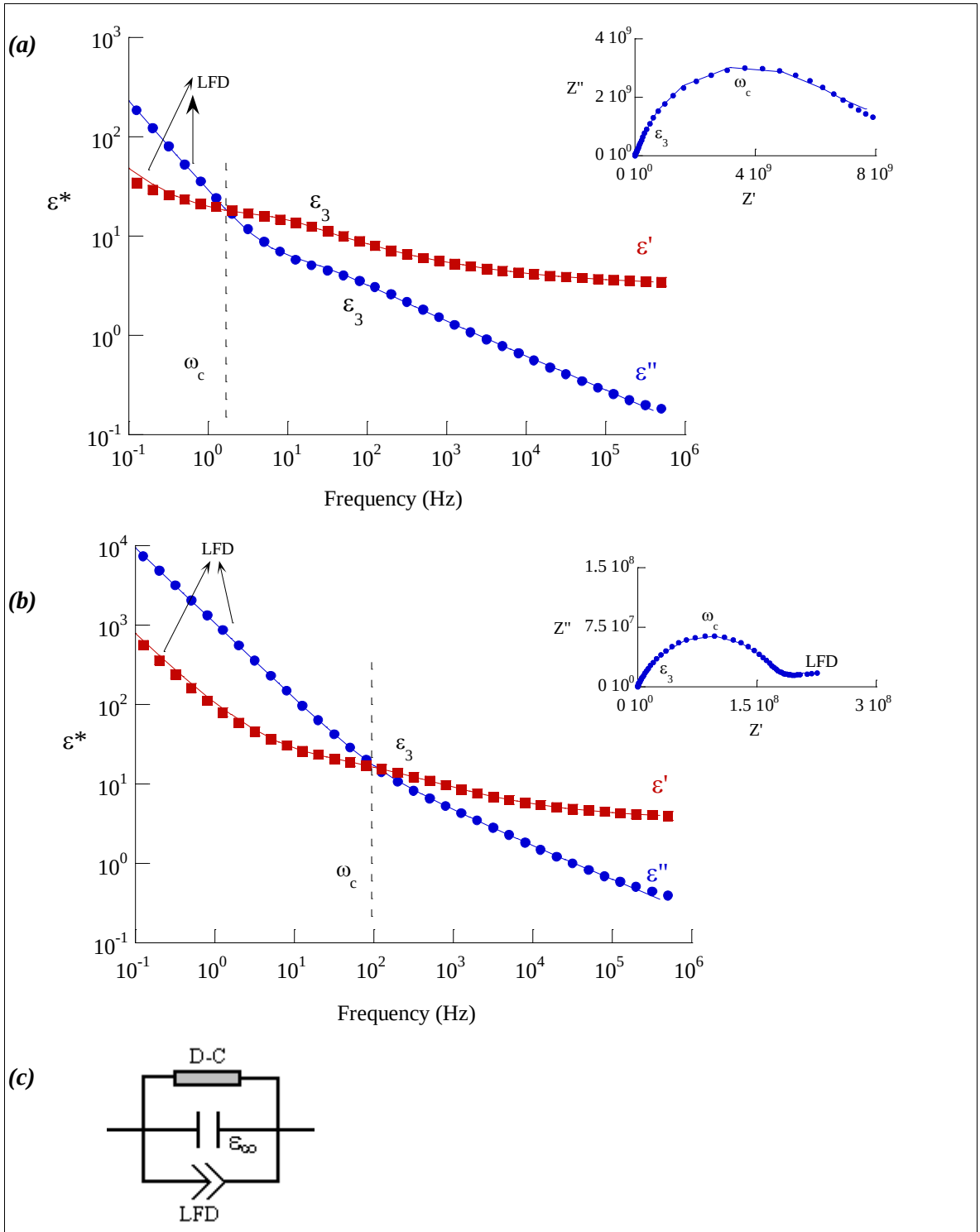

Figure 5.3 *Real and imaginary permittivities of hydrated lysozyme without the use of remote electrodes, showing LFD and ε_3 dispersion (a) 0.054 g/g, (b) 0.096 g/g. Symbols represent experimental data, solid lines represent curve fitting. Only 50% of experimental points are shown, to highlight the fitting lines. The inset shows the Cole-Cole plots of impedance. (c) Circuit model used for the fitting..*

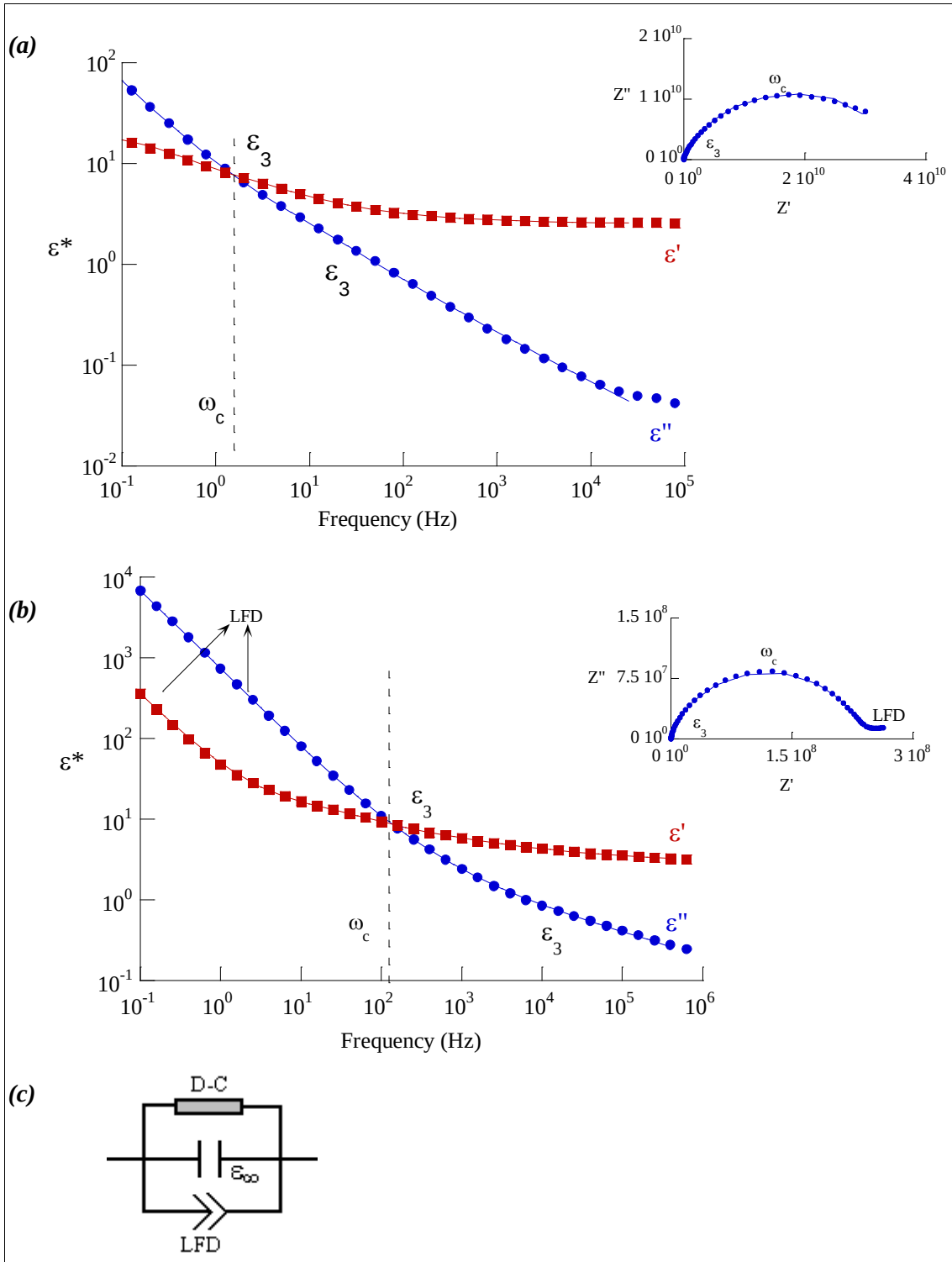

Figure 5.4 *Real and imaginary permittivities of hydrated pepsin without the use of remote electrodes, showing LFD and ε_3 dispersions (a) 0.019 g/g, (b) 0.037 g/g. Symbols represent experimental data, solid lines represent curve fitting. Only 50% of experimental points were shown, to highlight the fitting lines The inset shows the Cole-Cole plots of impedance. (c) Circuit model used for the fitting.*

5.2.3.1 LFD response

The significant increase in real and imaginary permittivities over the low frequency part of the spectrum was thought to show *LFD (low frequency dispersion)* behaviour. Some literatures referred to this low frequency dispersion as a *quasi-dc* process[59, 71, 74]. This LFD response or quasi-dc process is evidenced from the parallelism of the real and imaginary permittivities at $\omega < \omega_c$ (Figure 5.2, Figure 5.3, and Figure 5.4). As mentioned in section 3.5.1, the LFD response is often confused with the interfacial electrode polarisation (a Maxwell-Wagner effect) and/or dc-conductivity. As shown in Figure 5.2, Figure 5.3, and Figure 5.4, the real and imaginary permittivities do not satisfy Equations (3.49), (3.50) and (3.51), (3.52) for dc-conductivity and Maxwell-Wagner effect, respectively. For dc-conductivity, the real permittivity should be independent of frequency, and for the Maxwell-Wagner effect, the high frequency part should have a gradient of about –2 and –1 for real and imaginary part, respectively (Figure 5.5). Instead, this low frequency part satisfied the power law equation for LFD behaviour.

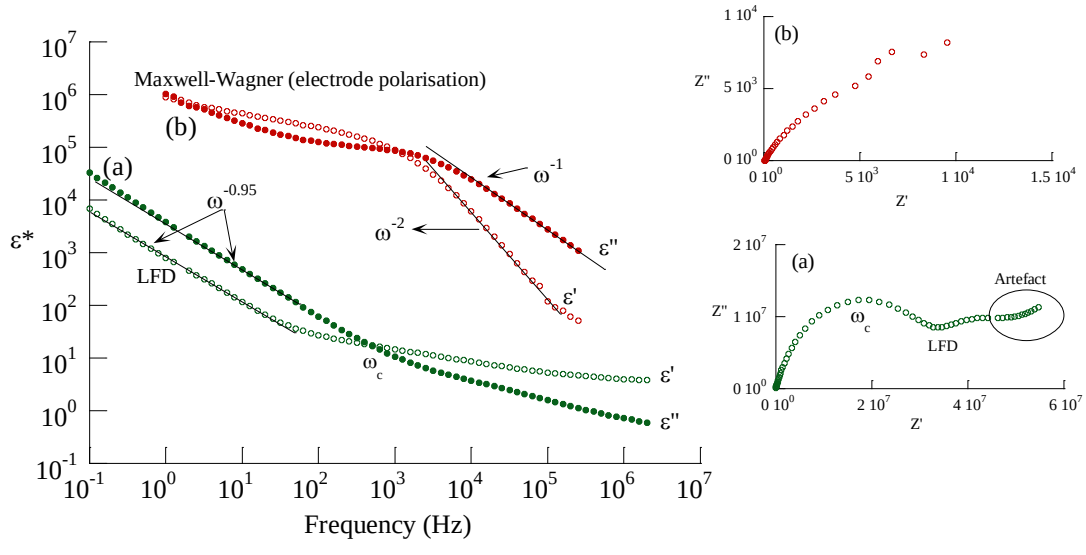

Figure 5.5 *Comparison of LFD behaviour and Maxwell-Wagner process (a) 0.1 g/g ovalbumin, (b) gelatin sample. Parallel lines show LFD behaviour. Insets show Cole-Cole impedance plots.*

5.2.3.2 ε_3 Dispersion

The high frequency dispersion ($\omega > \omega_c$) observed (i.e. ε_3 dispersion), was a weak relaxation, which was only observed at low hydration level. Unlike the LFD process, the ε_3 dispersion was easier to distinguish at low hydration levels. When the hydration level increases, the ε_3 dispersion was obscured, which may be due to the shifting to the higher frequency which beyond the experimental window, or suppressed under LFD part. This ε_3 dispersion was fitted well by a Davidson-Cole expression (Equation 3.33).

Compared with ovalbumin and lysozyme, the appearance of the ε_3 dispersion for pepsin is more obscure. Different structure, morphology, bonding, and crystalline state for pepsin compared with ovalbumin and lysozyme, may be the reason of this difference. This will be discussed in Section 5.4.6.

5.2.3.3 Hydration Study

The features of the LFD and the ε_3 dispersions were further confirmed from the hydration study. Figure 5.6, Figure 5.7, and Figure 5.8 showed the real and imaginary permittivities for various hydration levels of ovalbumin, lysozyme, and pepsin, respectively. The figures showed that the entire dielectric spectrum (involving the LFD and the ε_3 dispersion) shifted simultaneously to higher frequencies, as the hydration level was increased.

For all spectra for each protein, the LFD is not observed at the lowest hydration level. LFD is not observed for ovalbumin at 0.05 g/g, lysozyme at 0.037 g/g, and pepsin at 0.019 g/g. The LFD at low hydration level occurred at frequency lower than experimental window, therefore the LFD is not fully observed at relative low hydration level. With the increase of hydration level, the LFD part shifted to higher frequency hence the LFD is gradually perceived. The ε_3 dispersion, on the other hand, is more obscured at the higher hydration levels.

For lysozyme, at lower hydration (0.034 g/g) and (0.037 g/g), there is another weak dispersion observed at a frequency higher than frequency at which ε_3 dispersion was found (Figure 5.7 (b)). For the subsequent notation, this new dispersion was labelled as the ε_4 dispersion. This dispersion is confirmed in the temperature study (see Section 6.6). From the temperature study (reported in Chapter 6), it will be shown that ovalbumin also has an ε_4 dispersion.

(a)

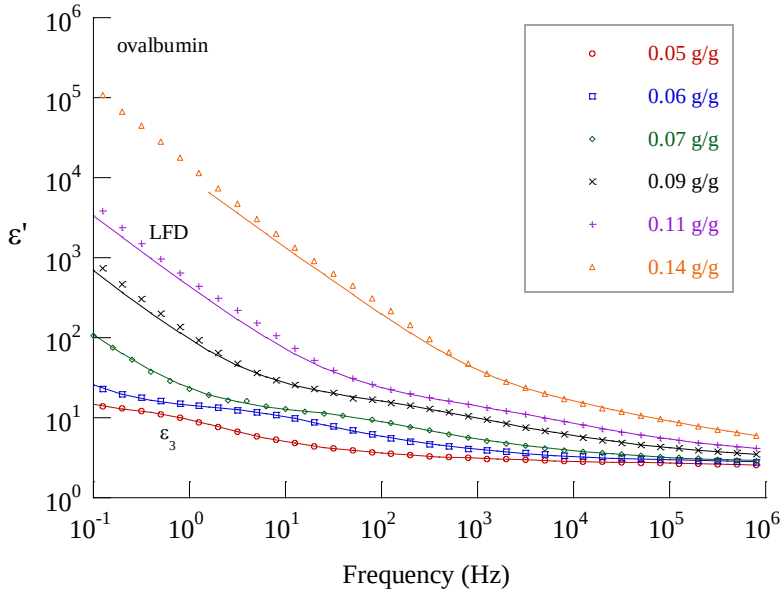

(b)

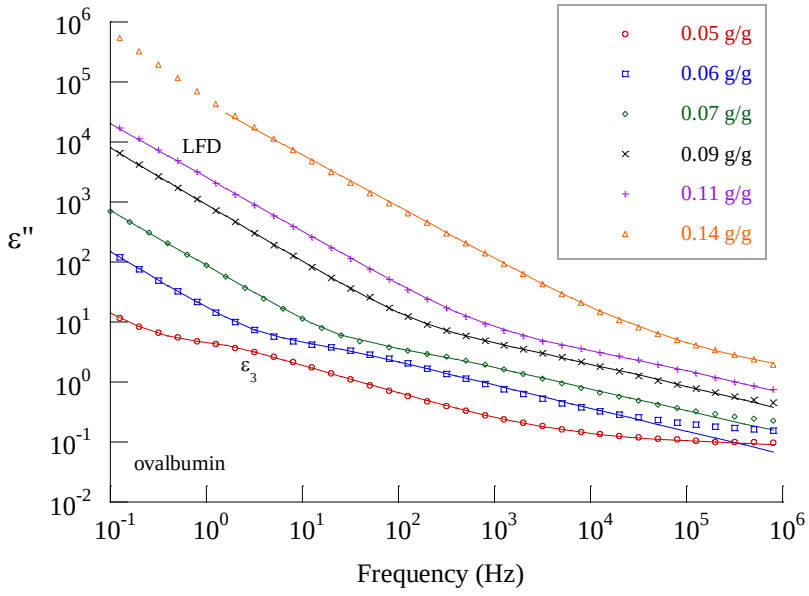

Figure 5.6 *(a) Real and (b) imaginary permittivities of various hydrated ovalbumin without the use of remote electrodes. Symbols represent experimental data, solid lines represent curve fitting. Only 50% of experimental data is shown.*

(a)

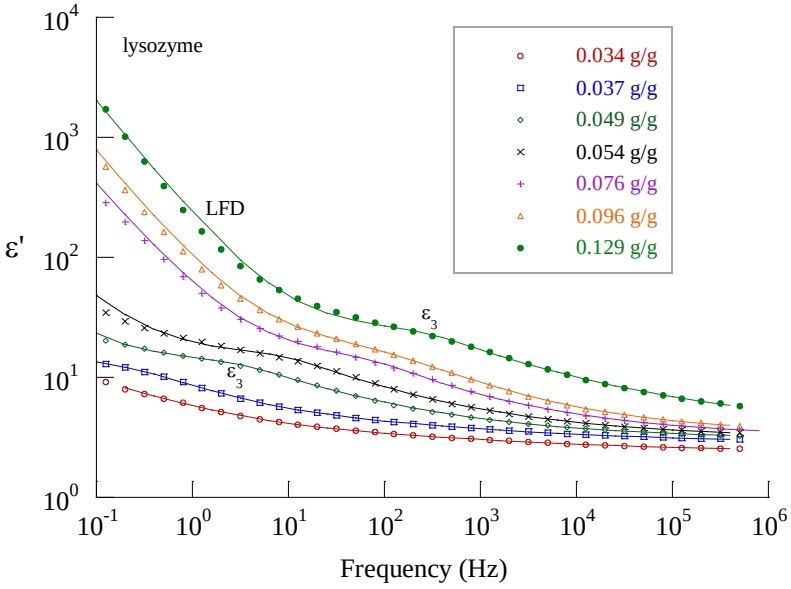

(b)

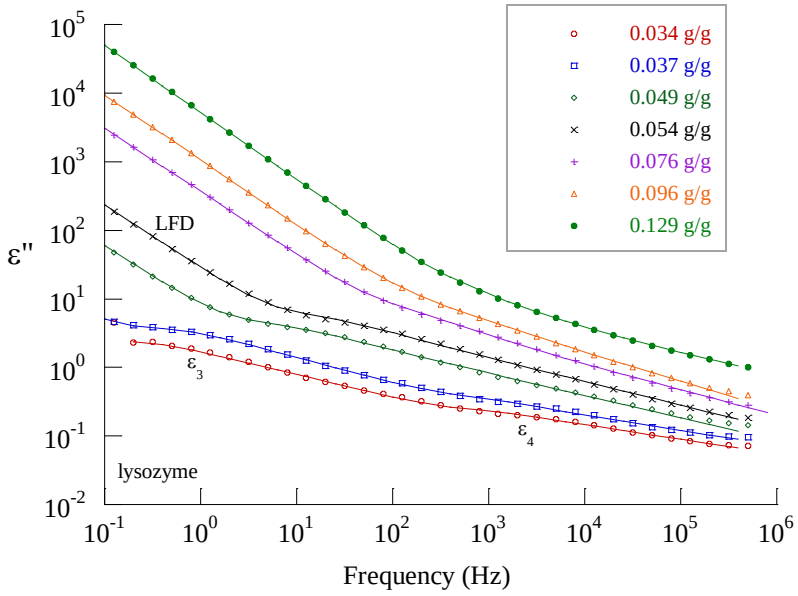

Figure 5.7 *(a) Real and (b) imaginary permittivities of various hydrated lysozyme without the use of remote electrodes. Symbols represent experimental data, solid lines represent curve fitting. Only 50% of experimental data is shown.*

(a)

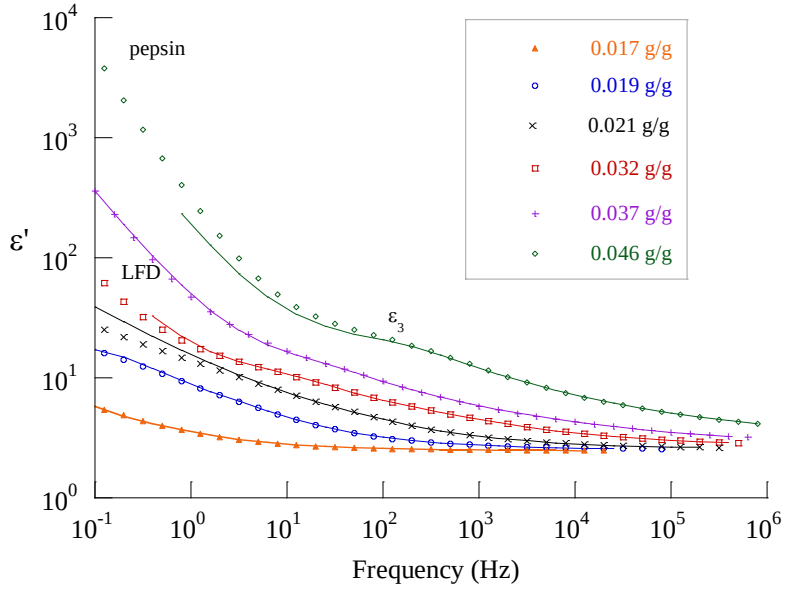

(b)

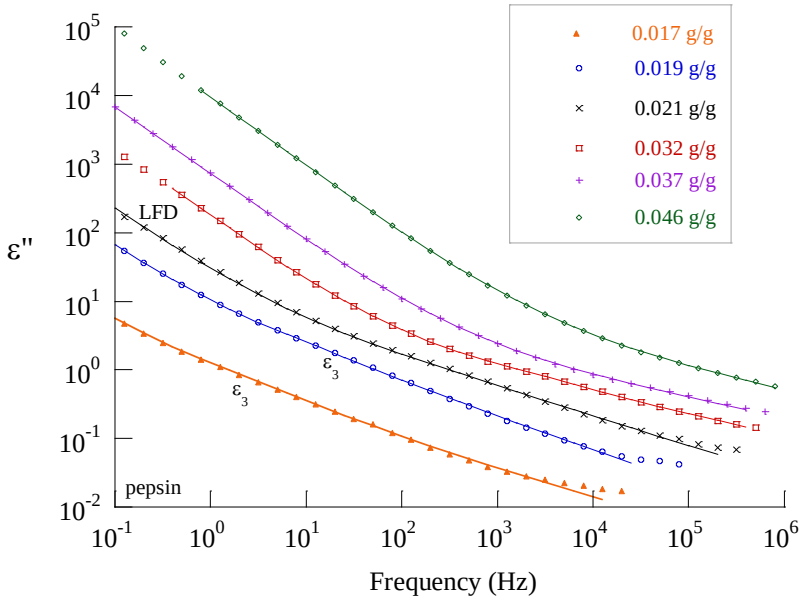

Figure 5.8 *(a) Real and (b) imaginary permittivities of various hydrated pepsin without the use of remote electrodes. Symbols represent experimental data, solid lines represent curve fitting. Only 50% of experimental data is shown.*

When the hydration level gets much higher, the LFD process was not perfectly a straight line in the log-log plot of permittivities, as representative of power law. At high hydration, the LFD plot bulged slightly, and therefore gave a poor fit for low frequency. This distorted LFD process at high hydration level was believed to be due to artefacts that may involve the interaction between conducting sample and electrodes (i.e. electrode polarisation).

The artefact causing the bulge at the LFD region for high hydrated proteins is probably difficult to observe in the real or imaginary permittivity plot. However, by investigating a Cole-Cole impedance plot in a complex plane, the artefact is clearly seen (see Figure 5.9).

Figure 5.9 shows bode plots of permittivities and Cole-Cole impedance plots for high hydration ovalbumin (0.153 g/g) and pepsin (0.046 g/g). The bode plot shows that the LFD part for hydrated ovalbumin (0.153 g/g) shows only a slight bulge at very low frequency (< 10 Hz). This bulge, as an artefact, can be seen more clearly in the Cole-Cole impedance plots, which is described by a sharp turn in the straight line (see inset in Figure 5.9 (a)). Because of this artefact, the curve fit only achieved up to frequency ~ 100 Hz as the lowest point.

A similar feature was also observed for high hydration pepsin (0.046 g/g). The bode plot for permittivites does not show a clear artefact. However, the Cole-Cole impedance plot shows clearly an artefact, which is revealed as a sharp turning of straight line. Again, because of this artefact, the curve fit was only attempted up to frequency ~ 10 Hz.

(a)

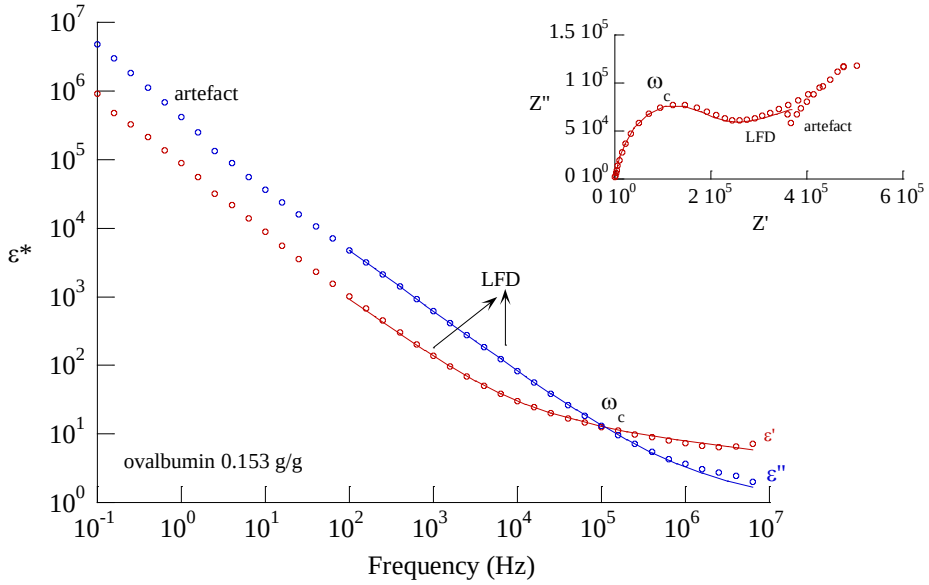

(b)

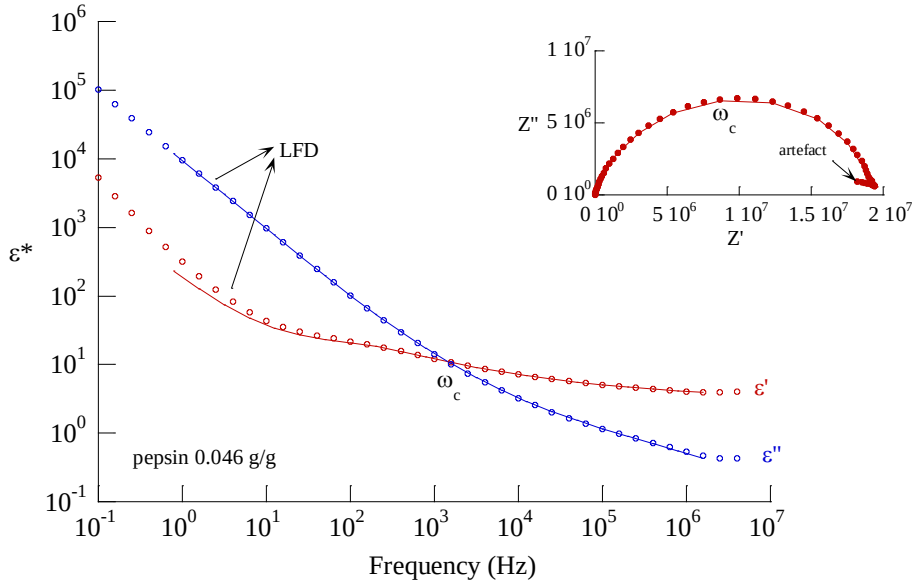

Figure 5.9 *Real and imaginary permittivities of (a) hydrated ovalbumin 0.15 g/g, (b) hydrated pepsin 0.046 g/g, showing artefact at low frequency which is not observed clearly in the bode graph of permittivites. Insets show Cole-Cole impedance plots. Symbols represent experimental data, solid lines represent fitting. Only 50% of experimental data are shown.*

Figure 5.10, Figure 5.11, and Figure 5.12 show the relaxation time τ_3, pre-exponential factor *A*, and exponential parameter *p*, over various hydration ranges for ovalbumin, lysozyme, and pepsin, respectively. These values are obtained from the fitting results. A distinct transition was observed for relaxation time τ_3, pre-exponential factor *A*, and exponential parameter *p* for ovalbumin and lysozyme. The graph of relaxation times for pepsin does not show any clear transition. The transition hydration for pepsin, however, is shown clearly in the graphs of pre-exponential factor *A* and exponential parameter *p*.

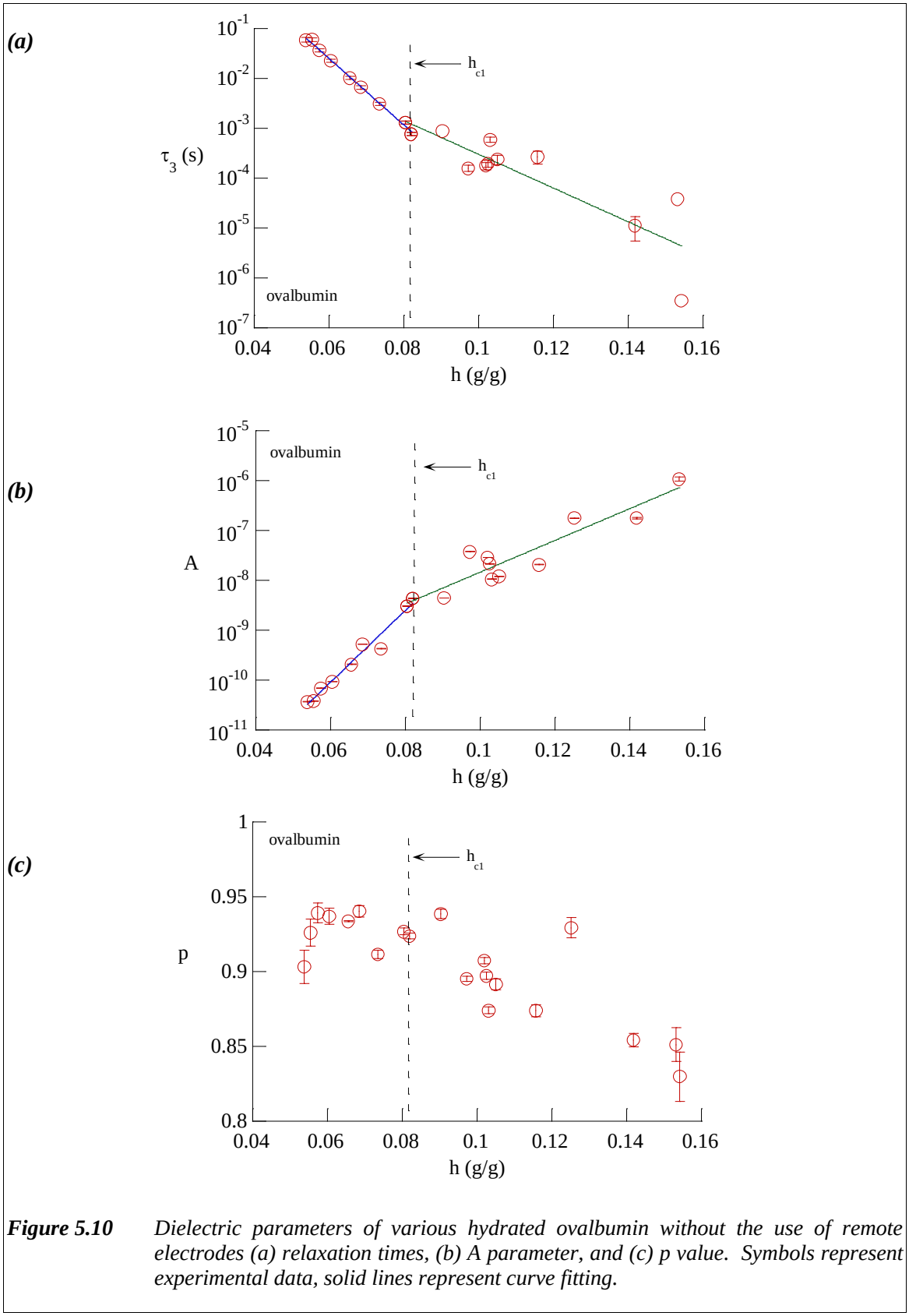

Figure 5.10 *Dielectric parameters of various hydrated ovalbumin without the use of remote electrodes (a) relaxation times, (b) A parameter, and (c) p value. Symbols represent experimental data, solid lines represent curve fitting.*

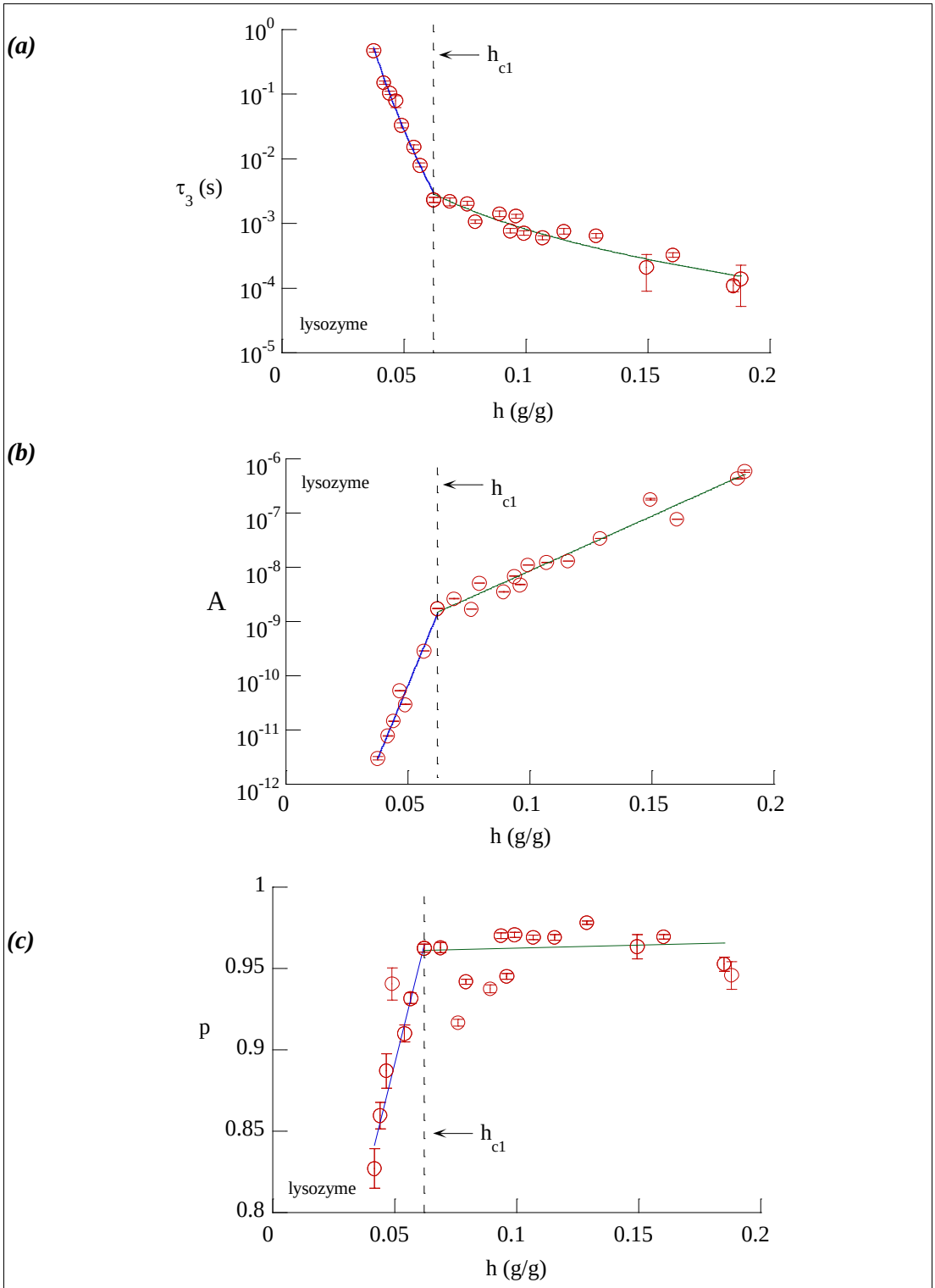

Figure 5.11 *Dielectric parameters of various hydrated lysozyme without the use of remote electrodes (a) relaxation times, (b) A parameter, and (c) p value. Symbols represent experimental data, solid lines represent curve fitting.*

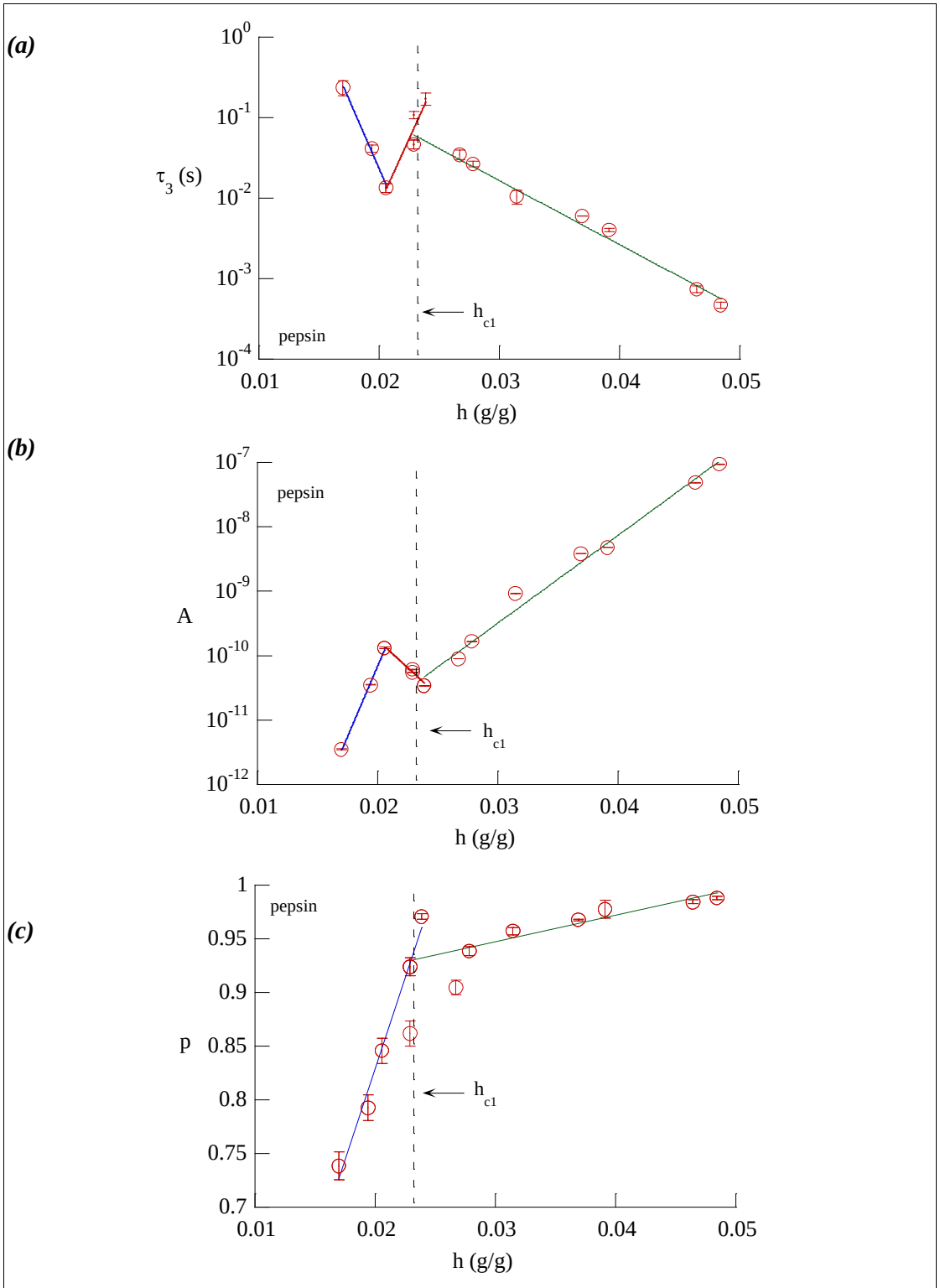

Figure 5.12 *Dielectric parameters of various hydrated pepsin without the use of remote electrodes (a) relaxation times, (b) A parameter, and (c) p value. Symbols represent experimental data, solid lines represent curve fitting.*

The transition hydration observed is different for each protein. Table 5.1 shows the hydration level at which the transition is observed for each protein. This transition hydration observed at relaxation times τ_3, pre-exponential factor *A*, and exponential parameter *p*, is called the first critical hydration level (h_{c_1}). In Section 5.3.2.2, it will be shown that there is another transition hydration observed at dielectric parameters obtained from the result of fitting curves to the ε_3 dispersion.

Table 5.1 *Transition hydration level observed at relaxation times τ_3 and pre-exponential factor A.*

Protein	**First critical hydration level h_{c_1} (g/g)**
Ovalbumin	0.08
Lysozyme	0.06
Pepsin	0.023

Table 5.2 shows the equation used to fit relaxation time τ_3 and pre-exponential factor *A* over various hydration range as shown in Figure 5.10, Figure 5.11, and Figure 5.12 for each protein. The pre-exponential factor *A* may be related to the conductivity, which is usually fitted by exponential function for various hydration ranges.

Table 5.2 *Equation for fitting relaxation times τ_3 and pre-exponent parameter A over the hydration range.*

	$< h_{c_1}$	$> h_{c_1}$
Ovalbumin	$\tau_{<h_c} = 6.75x10^{-15} h^{-10.27}$; R^2 = 97 %	$\tau_{>h_c} = 1.78x10^{-11} h^{-7.21}$; R^2 = 75%
	$A_{<h_c} = 4.37x10^{-15} e^{165.82h}$; R^2 = 98 %	$A_{>h_c} = 5.30x10^{-11} e^{51.25}$; R^2 = 99 %
Lysozyme	$\tau_{<h_c} = 1.21x10^{-15} h^{-10.27}$; R^2 = 99 %	$\tau_{>h_c} = 1.83x10^{-6} h^{-2.65}$; R^2 = 88 %
	$A_{<h_c} = 2.40x10^{-16} e^{251.05h}$; R^2 = 99 %	$A_{>h_c} = 8.23x10^{-11} e^{46.49}$; R^2 = 96%
Pepsin	$\tau_{<h_c} = 2.27x10^{-27} h^{-14.71}$; R^2 = 99 %	$\tau_{>h_c} = 4.25x10^{-12} h^{-6.26}$; R^2 = 87 %
	$A_{<h_c} = 1.25x10^{-19} e^{1007.2h}$; R^2 = 99.8 %	$A_{>h_c} = 2.6x10^{-14} e^{314.01h}$; R^2 = 99 %

Figure 5.13 shows the static permittivity ε_s over various hydration levels for each protein. As shown in Figure 5.13, for ovalbumin, ε_s increased rapidly after the first critical hydration (h_{c_1}). The rate of increase of ε_s at $h > h_{c_1}$ is higher than at $h < h_{c_1}$. The behaviour of lysozyme and pepsin was slightly different compared with ovalbumin, in that ε_s seemed to increase rapidly after another critical hydration level (which is called as h_{c_2}). This second transition hydration level is approximately double that of the first transition hydration level (h_{c_1}) (see Table 5.1 and Table 5.3), and is notably absent in the other dielectric parameters of τ_3, A, and p (see Figure 5.10, Figure 5.11, and Figure 5.12).

Table 5.3 *Second transition hydration level as observed in dielectric properties (ε_s, $\Delta\varepsilon_3$, and β_3) of each protein*.*

Protein	Second critical hydration level h_{c_2} (g/g)
Ovalbumin	N/A
Lysozyme	0.1
Pepsin	0.037

* see Figure 5.13 (b), Figure 5.22, and Figure 5.23

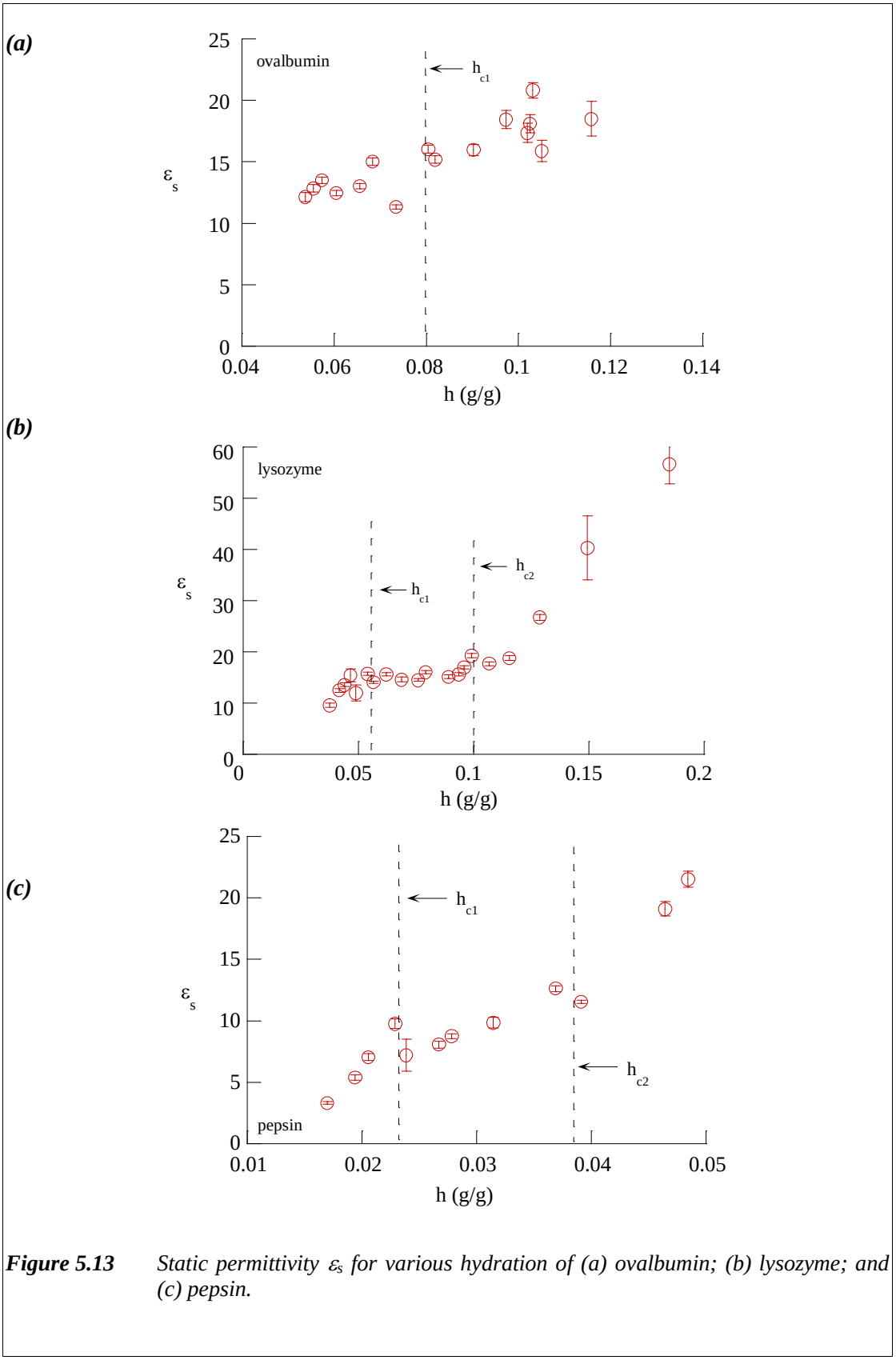

Figure 5.13 *Static permittivity ε_s for various hydration of (a) ovalbumin; (b) lysozyme; and (c) pepsin.*

5.2.3.4 Deuteration Study

In the previous section, it was shown that the dielectric spectra of each hydrated protein were especially sensitive to water content. Hence, the underlying mechanism of each dispersion observed is most probably due to charge transfer process in the hydration surfaces of the proteins. Moreover, it is assumed that these charge transport processes are associated primarily with the release of protons from water molecules. To confirm that the proton is the principle charge responsible for the dielectric properties of each sample, the protein sample was deuterated.

Figure 5.14 shows the comparison of relaxation times τ_3 of hydrated and deuterated proteins as a function of the degree of hydration level, in which the deuteration level was corrected to the hydration level by normalizing to the molecular weight. The data was fitted well by using a power function of hydration:

$$\tau = Ah^b \tag{5.2}$$

where:

τ = relaxation times

A = constant

b = relaxation times rate

h = hydration level

The logarithmic form of equation (5.2) is expressed as:

$$\log\tau = \log A + b\log h \tag{5.3}$$

Table 5.4 shows the fitting result from relaxation times of hydrated and deuterated samples for each proteins.

Table 5.4 *Relaxation times τ_3 of hydrated and deuterated proteins including the ratio of relaxation times rate between hydrated and deuterated proteins.*

	hydrated	**deuterated**	$\left(\frac{\log A_{hydrated}}{\log A_{deuterated}}\right)$	$\left(\frac{b_{hydrated}}{b_{deuterated}}\right)$
Ovalbumin	$\tau_{hyd.} = 6.75x10^{-15} h^{-10.27}$; R^2 = 97 %	$\tau_{deut.} = 5.54x10^{-14} h^{-7.21}$; R^2 = 96 %	1.06	1.42
Lysozyme	$\tau_{hyd.} = 1.21x0^{-15} h^{-10.27}$; R^2 = 99 %	$\tau_{deut.} = 6.32x10^{-11} h^{-7.25}$; R^2 = 99 %	1.46	1.42
Pepsin	$\tau_{hyd.} = 8.75x10^{-12} h^{-6.05}$; R^2 = 92 %	$\tau_{deut.} = 2.18x10^{-11} h^{-5.84}$; R^2 = 89 %	1.04	1.04

If the proton is the mobile charge responsible for the ε_3 dispersions in hydrated proteins, then the relaxation times of deuterated protein should be higher than hydrated protein because the mass of total protons in D_2O is twice that in H_2O. Figure 5.14 shows that the relaxation times τ_3 for deuterated proteins, are longer than hydrated protein, confirming that proton is the charge responsible for the ε_3 dispersion.

The conclusion of proton as charge transport causing dispersion in hydrated protein is also supported by the ratio calculation of relaxation times rate between hydrated and deuterated proteins. Since the total mass of proton in D_2O is twice than in H_2O, the relaxation times rate for hydrated protein should be approximately $\sqrt{2}$ times higher than for deuterated protein, if mobile protons are the reason of causing dispersion. The ratio calculation of relaxation times between hydrated and deuterated is around $\sqrt{2}$, which also confirmed that protons are principally responsible for charge transport in the hydrated proteins (Table 5.4).

The relaxation times, τ_3, of hydrated and deuterated protein intersect at a hydration level which corresponds to the basal hydration, i.e. the hydration level of the as-received sample. The basal hydration found from the intersection point for each hydrated protein is comparable with the basal hydration obtained from drying the sample in the oven (see Table 2.3, Section 2.4.2).

Table 5.4 and Figure 5.14 show that pepsin has different features compared with ovalbumin and lysozyme. This is probably due to the physical and chemical properties of starting material of pepsin, that is significantly different from ovalbumin and lysozyme, as discussed in Section 5.4.6 and summarised in Table 8.2.

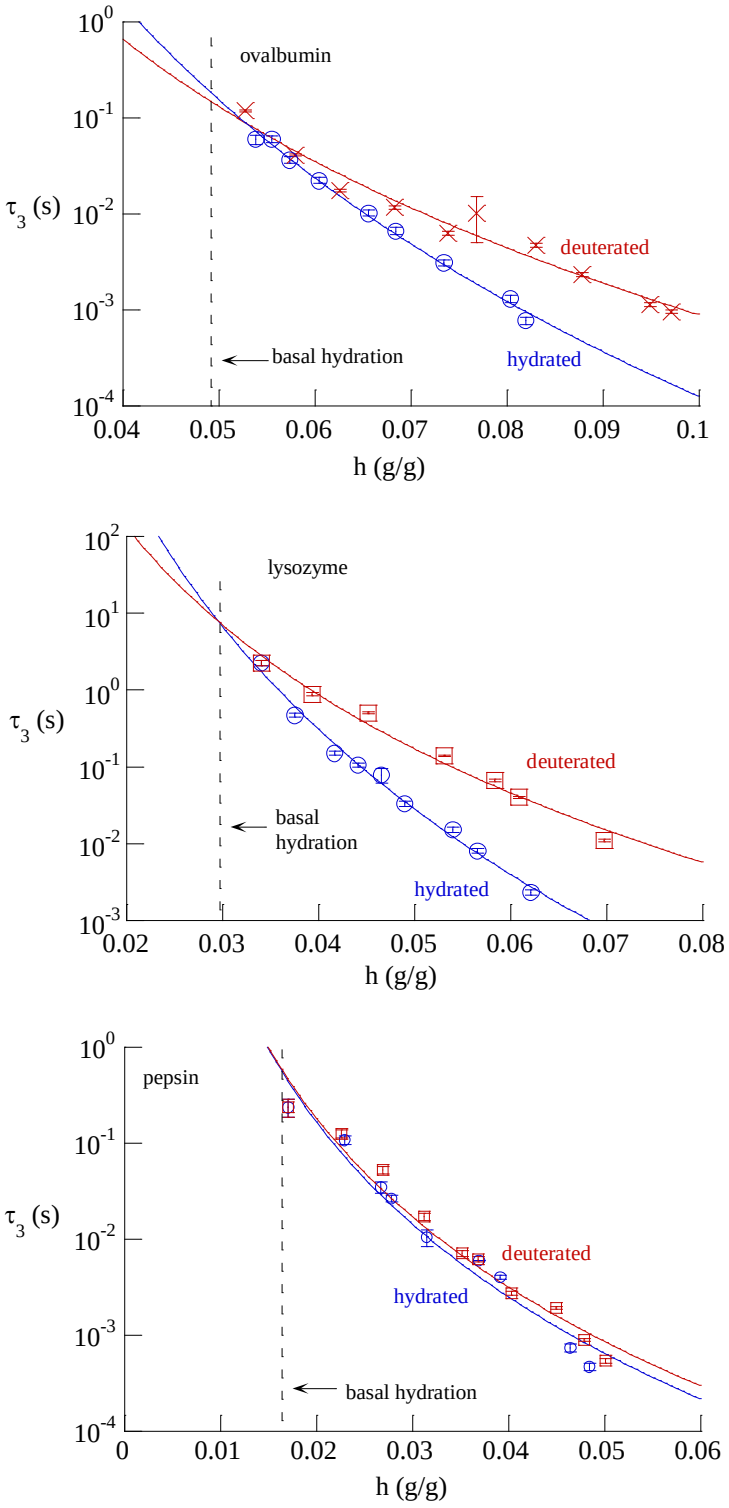

Figure 5.14 *Comparison of relaxation times τ_3 of hydrated and deuterated (a) ovalbumin, (b) lysozyme, and (c) pepsin. Symbols represent experimental data, solid lines represent curve fitting.*

5.3 Use of Remote Electrodes

5.3.1 Introduction

The term 'remote electrode' is used in this study for electrodes that are separated from the sample by a non-conductive and non-dispersive medium. One reason for using remote electrodes is to eliminate the effect of electrode polarisation that often occurs for highly conducting materials, especially for biological and pharmaceutical materials. The material used for remote electrodes has to be as thin as possible to minimise the impedance and to avoid any unwanted additional dielectric properties. However, the principle reason for the use of remote electrodes in this study was to research the development of an *in situ* dielectric measurement system to be used to monitor the freeze drying process, and to determine the water content of final freeze dried product. Measurements using remote electrodes on a freeze drying glass vial are discussed in Chapter 7.

The experimental method for dielectric measurement using remote electrodes was similar to that described in Section 5.2.2. The only difference in the method was that polyethylene films were inserted between the electrodes and sample (Figure 5.1).

5.3.2 Results

5.3.2.1 Effect of remote electrodes

In this study, polyethylene films of thickness 0.025 mm and dielectric permittivity 2, were employed as spacers between the sample and electrodes, to create a remote electrode system (Figure 5.1).

Figure 5.15, Figure 5.16, and Figure 5.17 show the effect of the use of polyethylene films for various hydrated ovalbumin, lysozyme, and pepsin, respectively.

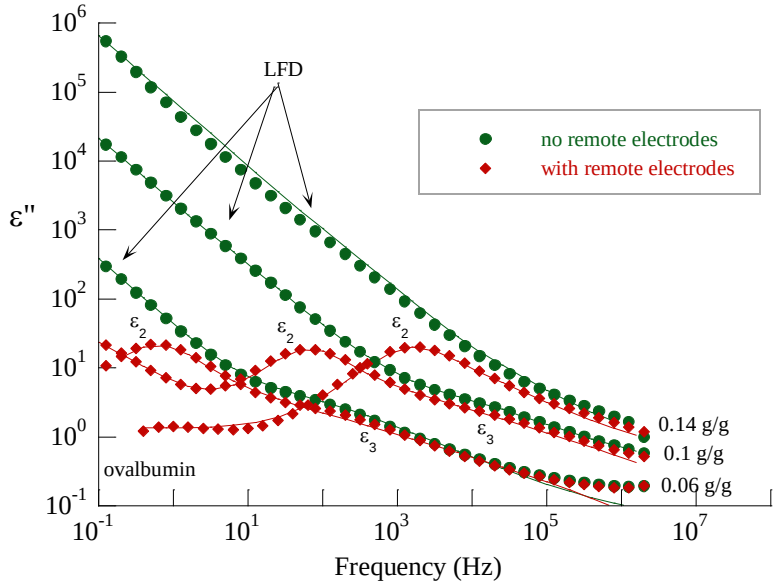

Figure 5.15 *Imaginary permittivity of ovalbumin, obtained from measurement with and without remote electrodes. Symbols represent experimental data, solid lines represent the fitting result. Only 50% of experimental data point is shown.*

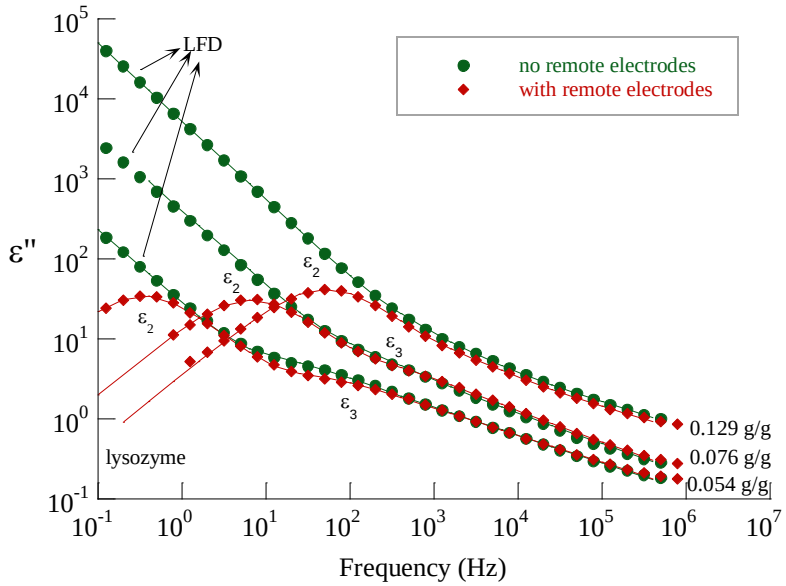

Figure 5.16 *Imaginary permittivity of lysozyme, obtained from measurement with and without remote electrodes. Symbols represent experimental data, solid lines represent the fitting result. Only 50% of experimental data point is shown.*

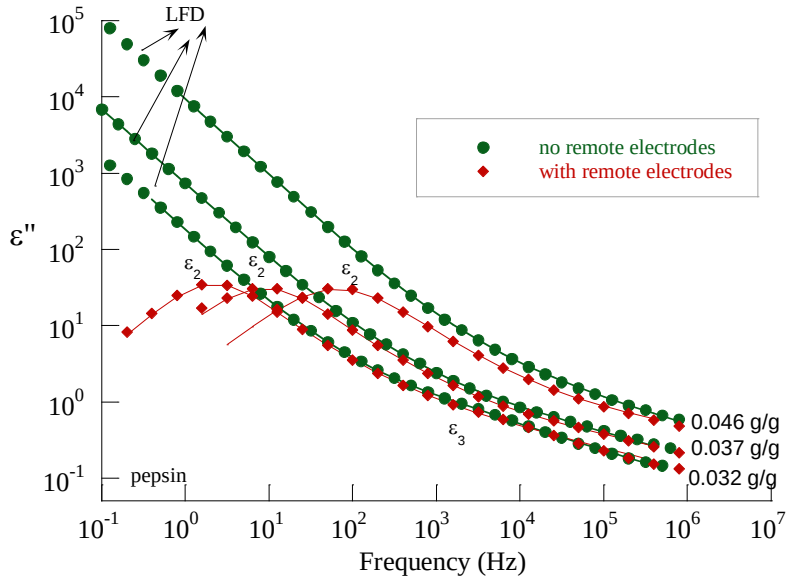

Figure 5.17 *Imaginary permittivity of pepsin, obtained from measurement with and without remote electrodes. Symbols represent experimental data, solid lines represent the fitting result. Only 50% of experimental data point is shown.*

As shown in Figure 5.15, Figure 5.16, and Figure 5.17, the insertion of polyethylene films created a new dispersion, designated as the ε_2 dispersion, which transform the shape of the LFD process. The ε_3 dispersion however is still observed in a similar way as without the use of polyethylene films. With increasing hydration, both the ε_2 and ε_3 dispersions shifted towards higher frequencies.

The ε_2 dispersion is assumed to be associated with a Maxwell-Wagner process that originates from the composite impedance of the LFD (a sample property) and the polyethylene film. The proposed Maxwell-Wagner process, as a cause of ε_2 dispersion, is confirmed by the circuit model used to fit the dielectric response (Figure 5.18). The main circuit is similar to that shown in Figure 5.2 (c), Figure 5.3 (c), and Figure 5.4 (c), i.e. an LFD, a Davidson-Cole element, and an infinite permittivity in parallel. Since a polyethylene film has been inserted between the sample and electrodes, then the fitting

circuit can be considered as a series connection of the sample properties with a capacitor (ε_b) representing the electrical capacitance of the polyethylene spacers (Figure 5.18).

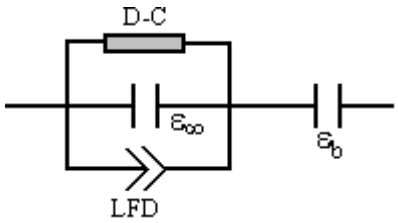

Figure 5.18 *Circuit modelling for fitting the dielectric response of the samples measured using remote electrodes.*

The permittivity from circuit in Figure 5.18 may be expressed as:

$$\left[\varepsilon^*(\omega)\right]^{-1} = \left[A(\mathrm{i}\omega)^{-p} + \frac{\Delta\varepsilon_3}{(1+\mathrm{i}\omega\tau_3)^{\beta_3}} + \varepsilon_\infty \right]^{-1} + \left(\varepsilon_b\right)^{-1} \qquad (5.4)$$

As has been verified, the ε_2 dispersion was attributed to a Maxwell Wagner process associated with the heterogeneous dielectric mixture at the boundary of the analysed system, i.e. the polyethylene/sample interface. Considering the non-dispersive and inert nature of the polyethylene spacers, it is possible to infer that changes in the ε_2 dispersion will also depend primarily on changes to the LFD, i.e. from the hydrogen-bonded network within the protein water system. This is supported by the observation that the relaxation time for the Maxwell Wagner process shows a strong dependence on water content (Figure 5.15, Figure 5.16, and Figure 5.17).

Figure 5.19, Figure 5.20, Figure 5.21 show various hydration levels of ovalbumin, lysozyme, and pepsin, measured with the use of remote electrodes. The figures show that, the ε_2 dispersion (like ε_3 dispersion) was also strongly dependent on hydration level, by shifting towards higher frequency with the increase in hydration level.

(a)

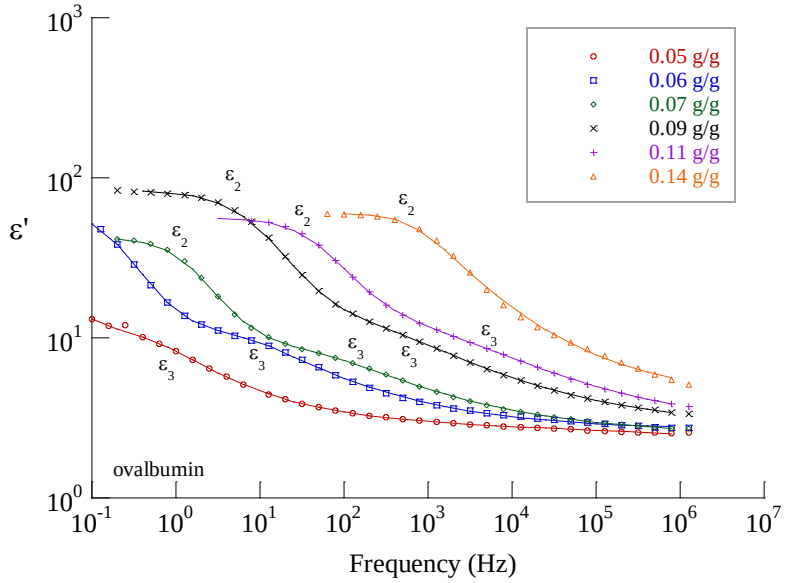

(b)

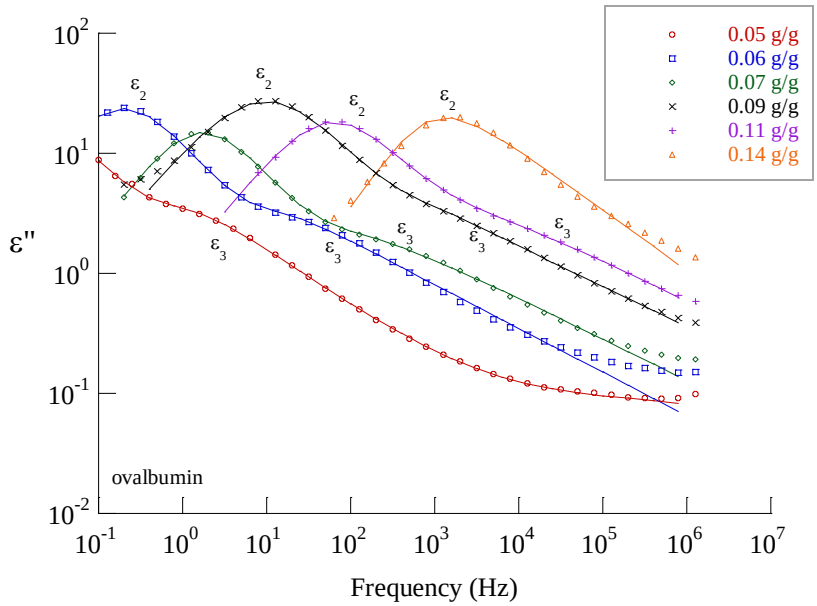

Figure 5.19 *(a) Real and (b) imaginary permittivities of various hydrated ovalbumin with the use of polyethylene films. Symbols represent experimental data, solid lines represent curve fitting. Only 50% of experimental data point is shown.*

(a)

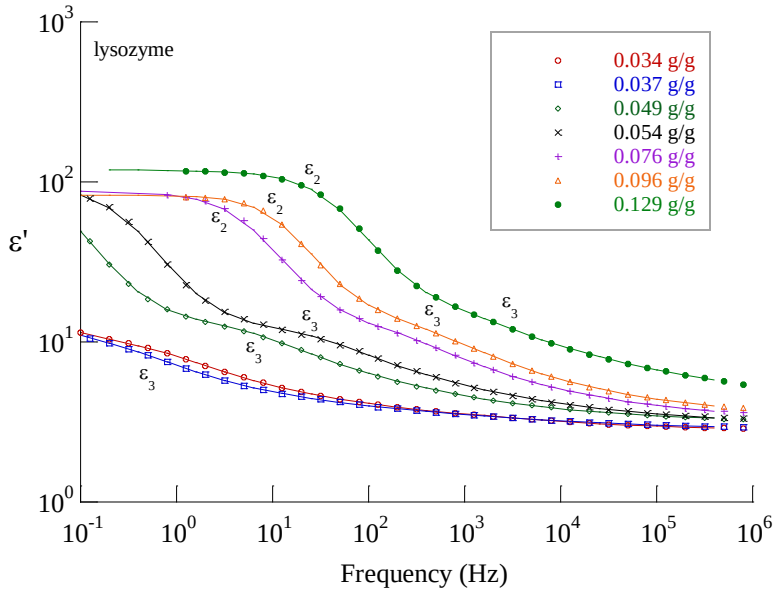

(b)

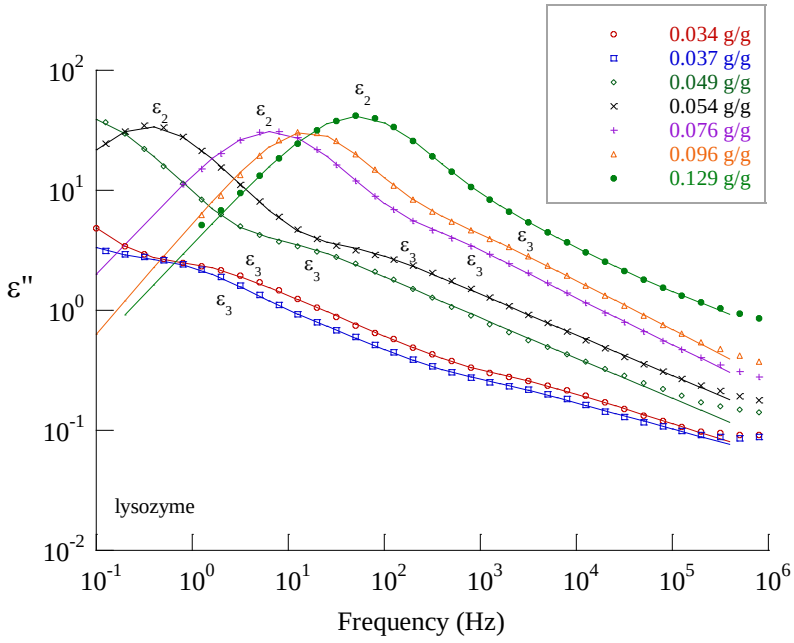

Figure 5.20 *(a) Real and (b) imaginary permittivities of various hydrated lysozyme with the use of polyethylene films. Symbols represent experimental data, solid lines represent curve fitting. Only 50% of experimental data point is shown.*

(a)

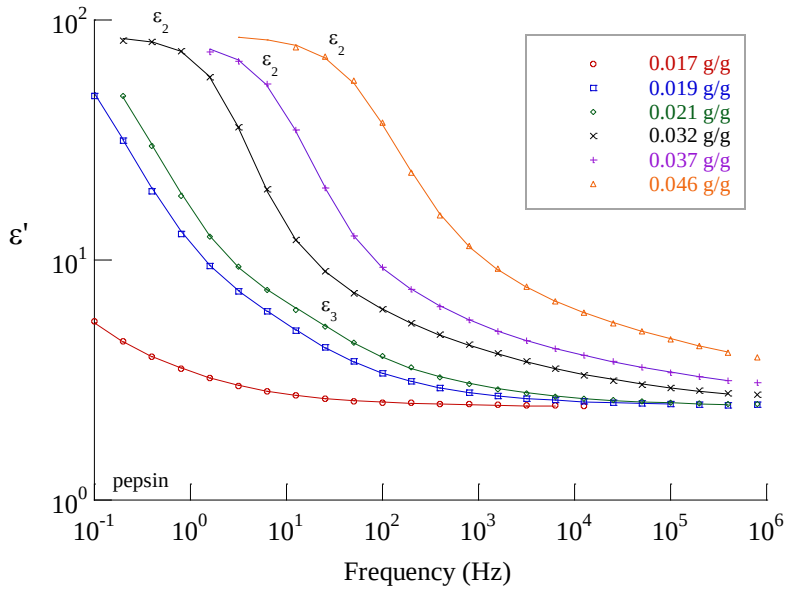

(b)

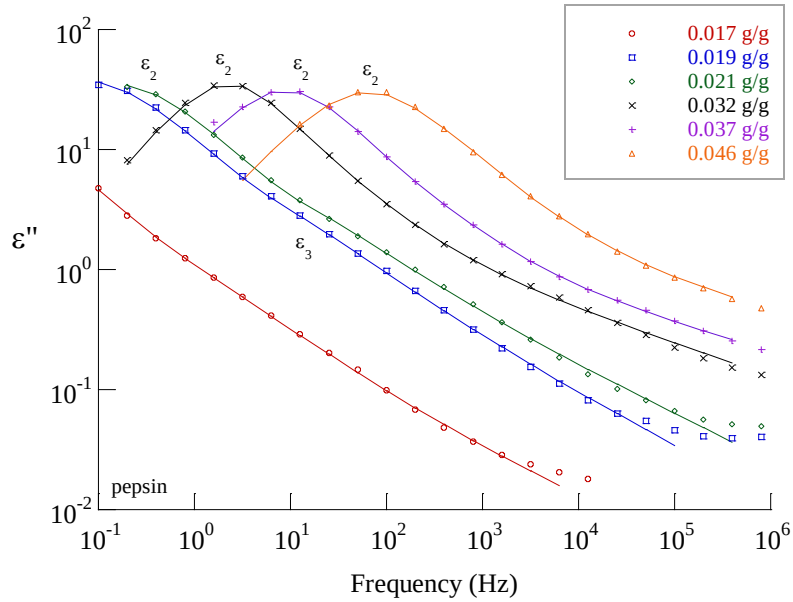

Figure 5.21 *(a) Real and (b) imaginary permittivities of various hydrated pepsin with the use of polyethylene films. Symbols represent experimental data, solid lines represent curve fitting. Only 50% of experimental data point is shown.*

5.3.2.2 Comparison between the response with and without remote electrodes.

Figure 5.22, Figure 5.23, and Figure 5.24, show dielectric parameters β, $\Delta\varepsilon_3$, and ε_∞ for each hydrated protein obtained from the fitting of the ε_3 dispersion with the Davidson Cole model. The figures also show the comparison between the measurement with and without polyethylene films. The figures show that dielectric parameters obtained from measurement without polyethylene films were comparable to those obtained from measurement with polyethylene films. However, at higher hydration level, the values of $\Delta\varepsilon_3$ obtained from these measurements revealed differences. The values for $\Delta\varepsilon_3$ obtained from the measurement with remote electrodes tend to be lower than those without remote electrodes. These differences may be due to the fact that ε_3 dispersion was more obscure with the higher hydration, resulting inaccuracy in the fitting.

Transition hydration was also observed in the dielectric parameters $\Delta\varepsilon_3$ and β_3 for each protein, while ε_∞ was almost independent of hydration level. For lysozyme, similar as observed for ε_s (Figure 5.13 (b)), besides the transition hydration at h_{c1} ~ 0.06 g/g, there is another transition hydration observed at h_{c2} ~ 0.1 g/g. This second transition was not observed in LFD parameters (i.e. pre-exponent factor *A* and exponent parameter *p*) as shown in Figure 5.11. It was also not revealed in the relaxation time τ_3 from ε_3 dispersion. Pepsin showed the second transition hydration only at β parameter. The second transition hydration for pepsin is h_{c2} ~ 0.037 g/g and was not observed either in relaxation time τ_3, pre-exponential factor *A*, or exponent parameter *p* (Figure 5.12). Unlike lysozyme and pepsin, ovalbumin did not show any second transition hydration.

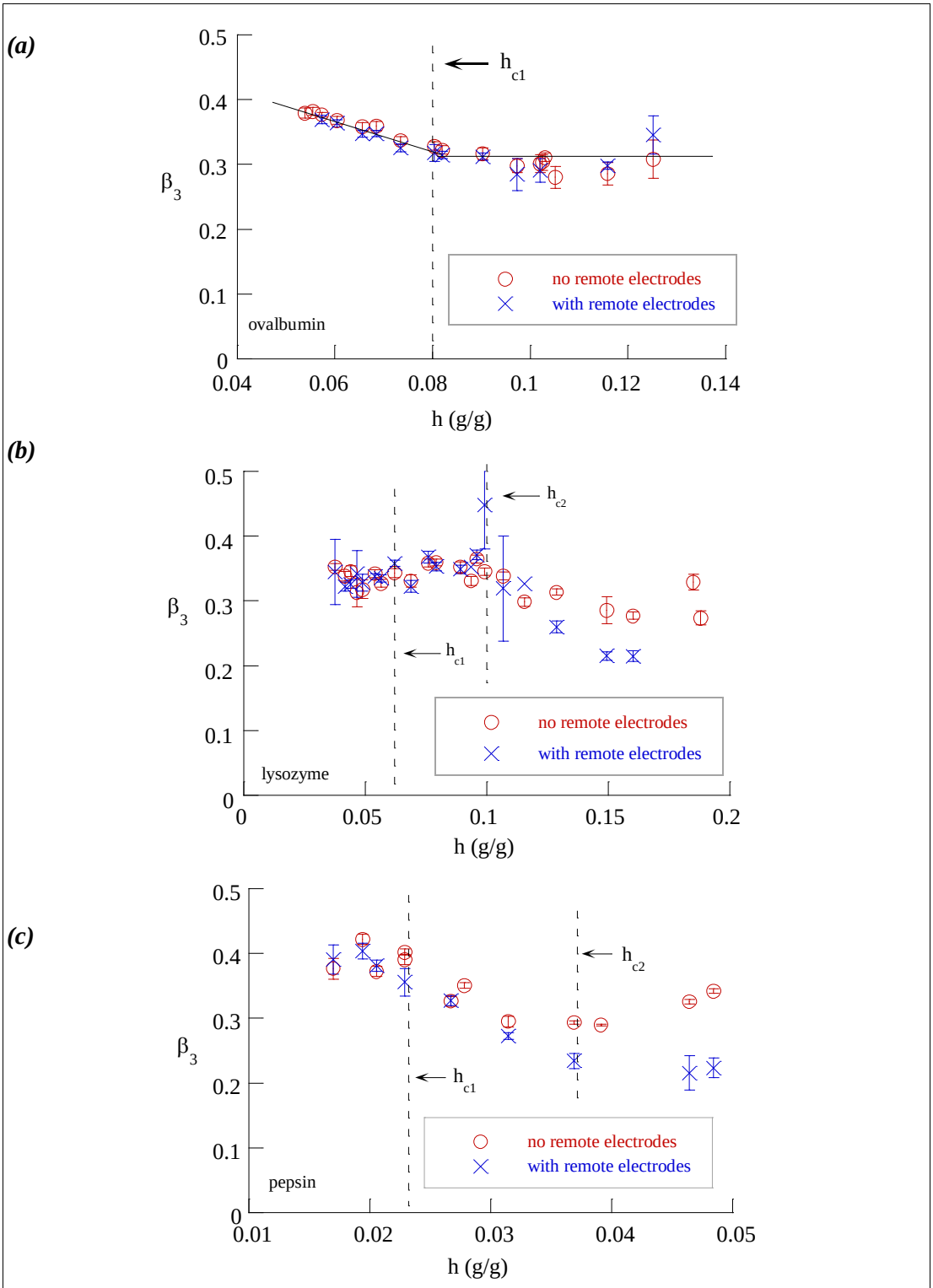

Figure 5.22 *β parameter for various hydrated (a) ovalbumin, (b) lysozyme, and (c) pepsin, obtained from measurement with and without the use of remote electrodes. Solid lines represent the tendency of the data*

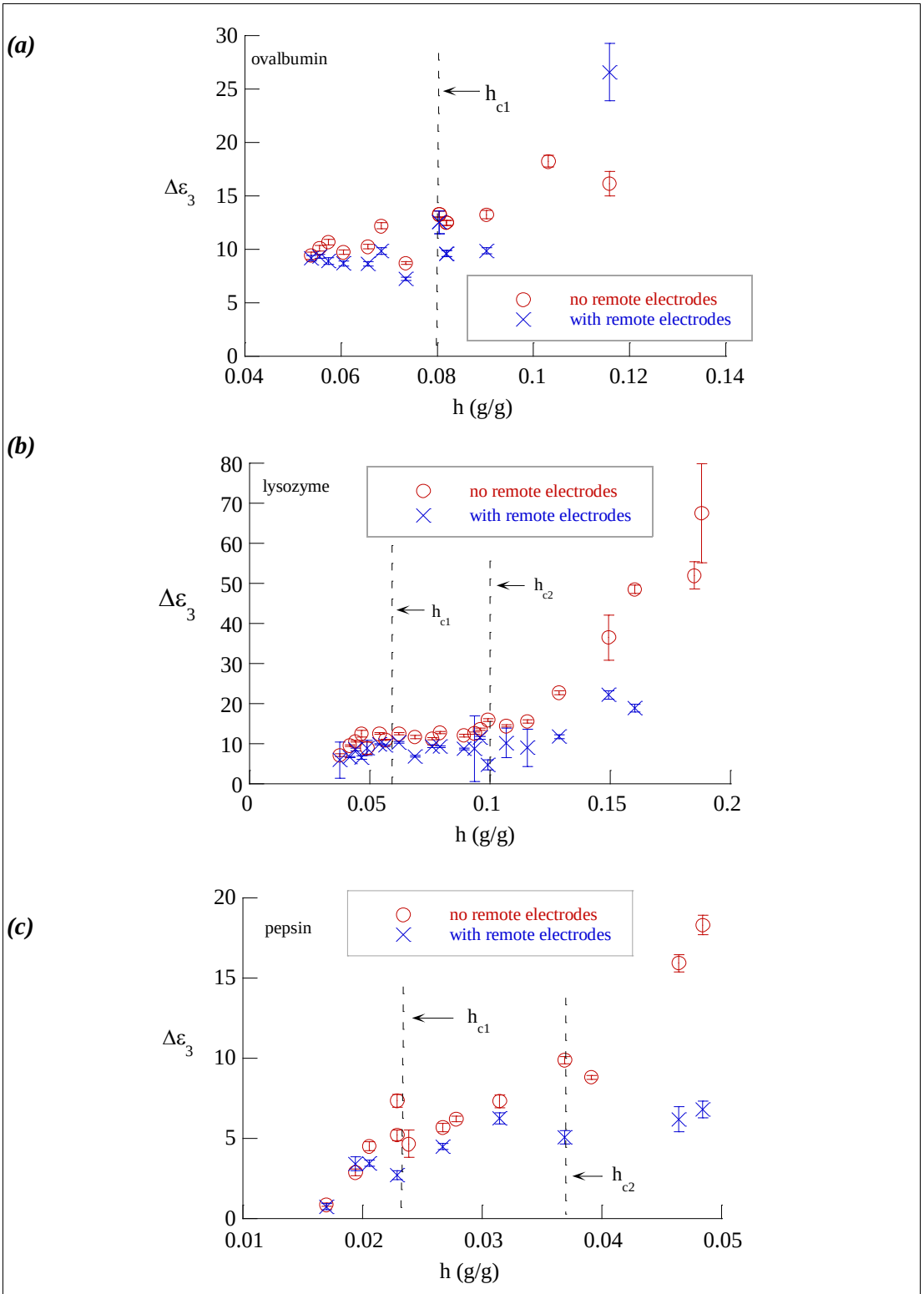

Figure 5.23 *Relaxation strength $\Delta\varepsilon_3$ for various hydrated (a) ovalbumin, (b) lysozyme, and (c) pepsin, obtained from measurement with and without the use of remote electrodes.*

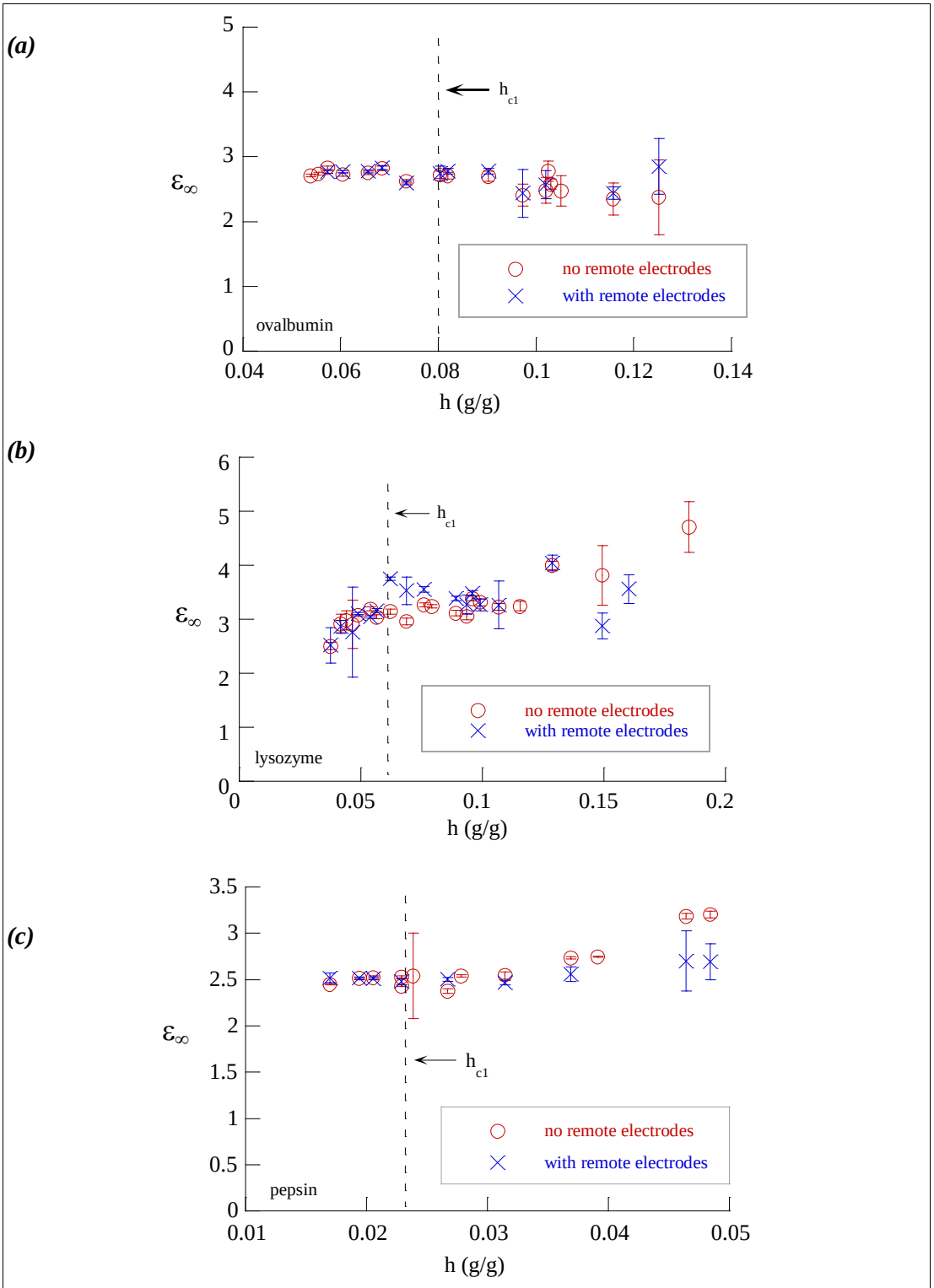

Figure 5.24 *Infinite permittivity ε_∞ for various hydrated (a) ovalbumin, (b) lysozyme, and (c) pepsin, obtained from measurement with and without the use of remote electrodes.*

Figure 5.22, Figure 5.23, and Figure 5.24 shows that ε_3 dispersion from measurement with and without polyethylene films are comparable. The independence of ε_3 dispersion on the use of remote electrodes is also shown in the correlation of relaxation times τ_3 between measurement using parallel plate electrodes with and without polyethylene films (Figure 5.25).

The correlation of relaxation time τ_3 between measurement with and without polyethylene films was fitted by a power function to obtain a linear line. The correlation is defined good if the line passes the intersection point $(\log A \to 0)$ with gradient 45° $(m = 1)$ and coefficient variation R^2 is 1. Table 5.5 shows the fitting result from the correlation between measurement with and without remote electrodes.

Table 5.5 *Fitting result from correlation between measurement with and without the use of remote electrodes.*

	Intersection Point, log A	Gradient m	Correlation R^2 (%)
Ovalbumin	-0.004	1.09	99
Lysozyme	-0.081	1.11	97
Pepsin	-0.086	1.16	98

(a)

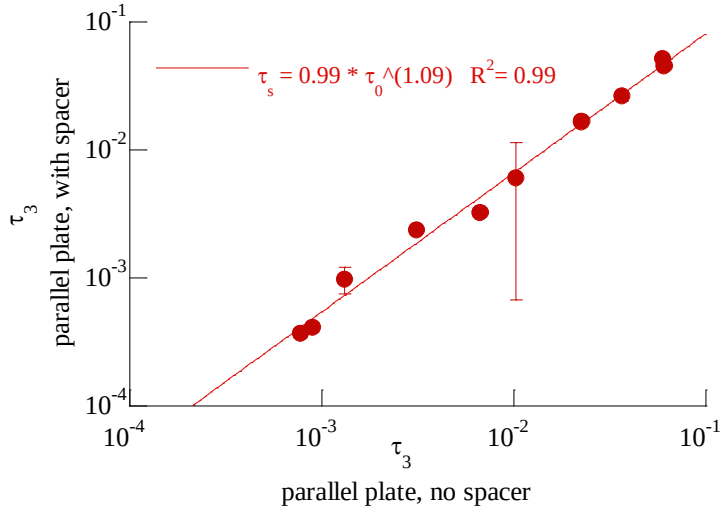

(b)

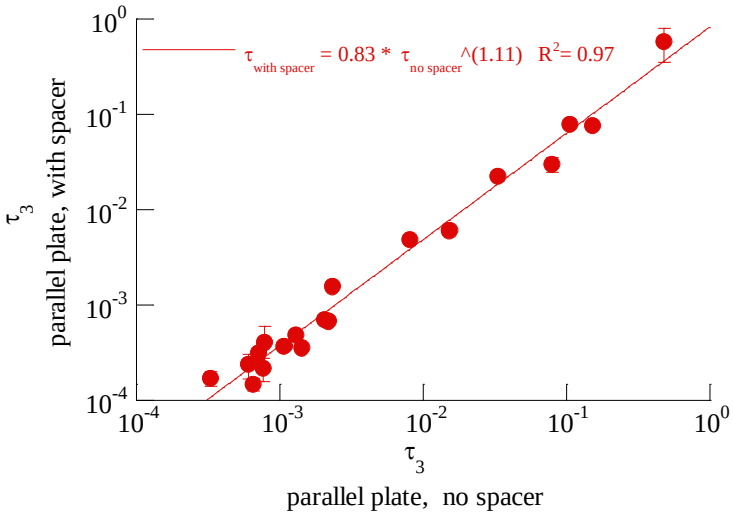

(c)

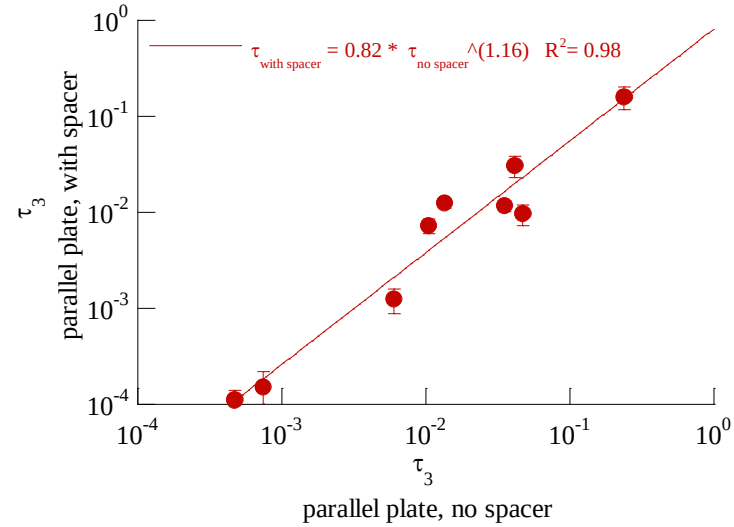

Figure 5.25 *Relaxation times of various hydrated (a) ovalbumin. (b) lysozyme, and (c) pepsin, comparing the results from measurement with and without spacer.*

5.3.2.3 Deuteration Study

The ε_2 dispersion may also be used to understand the characteristics of the LFD response from the sample. It has been shown in Section 5.2.3.4 via a deuteration study on the sample, that proton transport is the principle underlying charge transport process responsible for the ε_3 dispersion, based on the observation that the relaxation times τ_3 of ε_3 dispersion from hydrated sample is lower than deuterated sample. The LFD itself is not characterised by a mean of relaxation times, nevertheless it is possible to establish that proton transport is responsible for the LFD process via the relaxation time τ_2 of the ε_2 dispersion. This can be realised since ε_2 dispersion also fits a simple Davidson-Cole model. In this case, the dielectric response from measurements using remote electrodes was modelled by a parallel circuit of two Davidson-Cole elements, representing ε_2 and ε_3 dispersions (Figure 5.26). From this circuit model, the relaxation time τ_2 of ε_2 dispersion can be obtained.

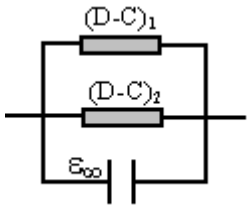

Figure 5.26 *Fitting model consisting 2 Davidson-Cole elements in parallel for measurement with the use of remote electrodes.*

The expression for the permittivity for the circuit shown in Figure 5.26 is:

$$\varepsilon^*(\omega) = \frac{\Delta\varepsilon_3}{(1 + i\omega\tau_3)^{\beta_3}} + \frac{\Delta\varepsilon_2}{(1 + i\omega\tau_2)^{\beta_2}} + \varepsilon_\infty \qquad (5.5)$$

The subscripts '2' and '3' in Equation (5.5) denote ε_2 and ε_3 dispersions, respectively. The relaxation times τ_3 obtained from both equations (5.4) and (5.5) are comparable.

Figure 5.27 show the relaxation times τ_2 for hydrated and deuterated samples, as a function of hydration level, in which the deuteration level was corrected to the hydration level by normalizing to the molecular weight. As with the relaxation times τ_3, the figure shows that the ε_2 dispersion of hydrated proteins has smaller relaxation times compared with deuterated proteins. The data was also fitted well by using a power function of hydration as in Equation (5.2). Table 5.6 shows the fitting result from relaxation times τ_2 of hydrated and deuterated proteins.

Table 5.6 *Relaxation times τ_2 of hydrated and deuterated proteins including the ratio of relaxation times rate between hydrated and deuterated proteins.*

	hydrated	**deuterated**	$\left(\frac{\log A_{hydrated}}{\log A_{deuterated}}\right)$	$\left(\frac{b_{hydrated}}{b_{deuterated}}\right)$
Ovalbumin	$\tau_{hyd.} = 1.71x10^{-14} h^{-11..32}$; R^2 = 94 %	$\tau_{deut.} = 1.94x10^{-10} h^{-8.04}$; R^2 = 97 %	1.42	1.40
Lysozyme	$\tau_{hyd.} = 8.42x10^{-14} h^{-10.11}$; R^2 = 97 %	$\tau_{deut.} = 3.08x10^{-11} h^{-9.03}$; R^2 = 84 %	1.42	1.12
Pepsin	$\tau_{hyd.} = 5.69x10^{-19} h^{-11.05}$; R^2 = 95 %	$\tau_{deut.} = 8.03x10^{-14} h^{-8.12}$; R^2 = 95 %	1.39	1.36

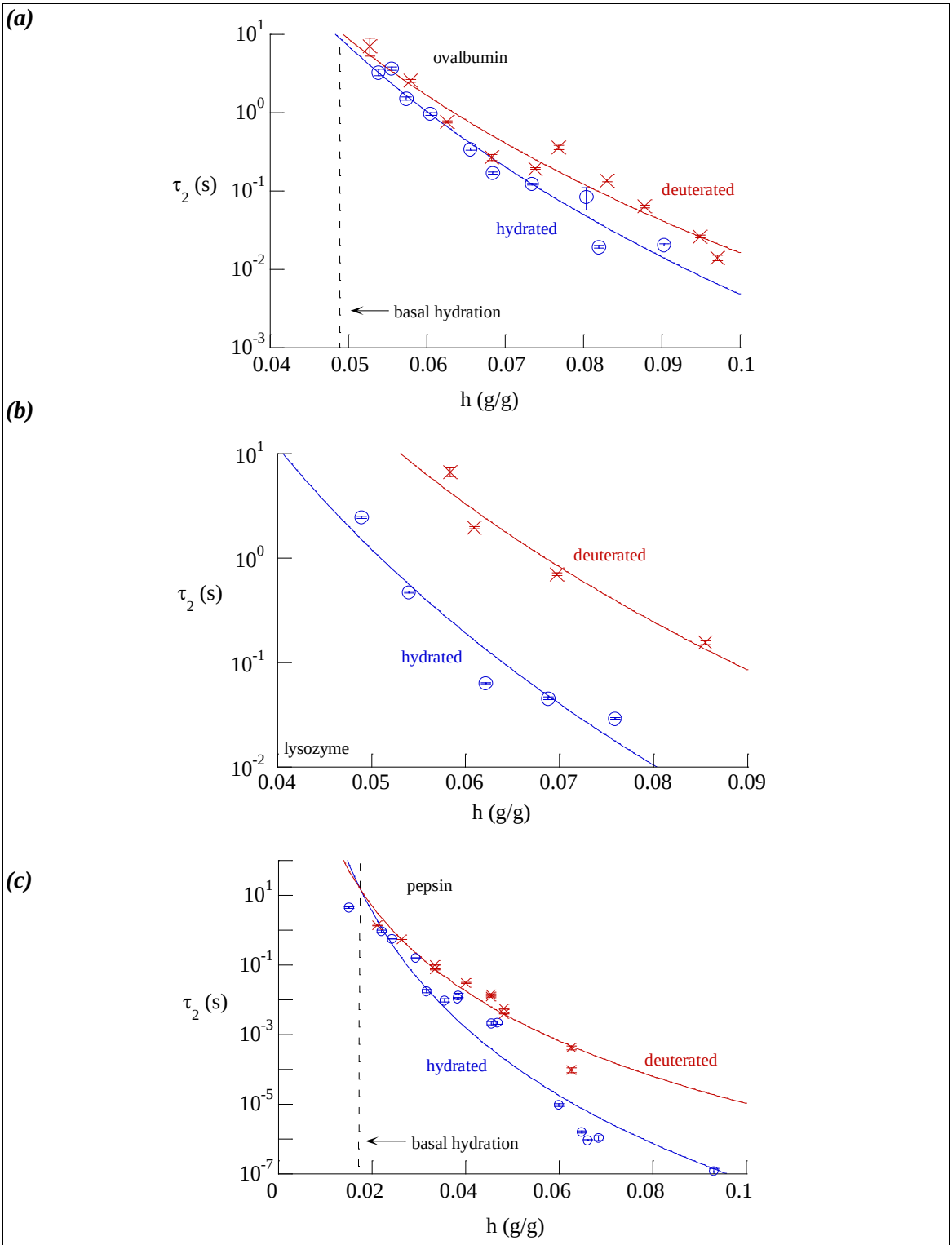

Figure 5.27 *Comparison of relaxation times τ_3 of hydrated and deuterated (a) ovalbumin, (b) lysozyme, and (c) pepsin. Symbols represent experimental data, solid lines represent curve fitting.*

Similar as explained in Section 5.2.3.4, if the charge transport responsible for the LFD response (or the ε_2 dispersion) is proton, then the relaxation times of deuterated protein should be higher than hydrated protein because the mass of total protons in D_2O is twice that in H_2O. Figure 5.27 show that the relaxation times τ_2 for deuterated proteins, are higher than hydrated protein, confirming that proton is the charge responsible for the LFD response (or ε_2 dispersion).

Since the total mass of proton in D_2O is twice than in H_2O, the relaxation times rate for hydrated protein should be approximately $\sqrt{2}$ times higher than for deuterated protein, if mobile protons are the reason of causing dispersion. The ratio of relaxation times for hydrated and deuterated protein as shown in Table 5.6, confirmed that protons are principally responsible for charge transport in the hydrated proteins.

It also has been explained in Section 5.2.3.4, that the intersection point between the relaxation times, τ_2, of hydrated and deuterated ovalbumin corresponds to the basal hydration, i.e. the hydration level of the as-received sample. This basal hydration is comparable with the basal hydration obtained from drying the sample in the oven (see Table 2.3, Section 2.4.2).

5.4 Discussion

5.4.1 LFD and ε_3 dispersion

An LFD process was observed in each hydrated protein used in this study. The origin of the LFD process is attributed to a 'many body' interaction within the material[71, 86]. LFD processes have been observed in a number of materials possessing structural similarity, i.e. those having one-dimensional channels (e.g. Hollandite crystals) or those with interior surfaces containing a number of binding sites which are occupied by ions or adsorbed molecules[71]. The adsorbate structure associated with LFD response develops an array of localised groups of cluster. In the case of hydrated proteins used in this study, the LFD process is due to water molecules, that are adsorbed onto binding sites on the protein surface. The charged and polar groups are the primary binding sites in the protein. The adsorbed water molecules are then hydrogen bonded to a series of water molecules network, thus forming localised groups or cluster. The size of the cluster is defined by the range over which the motion of charge carriers can still be correlated [59]. The assumption of water molecules adsorbed on protein surface is strengthened by the observation and determination of fractal dimension in the hydrated proteins (see Section 6.5).

The water that contributes to the dielectric responses observed in this study may be categorised as a water of hydration, or sorbed water. The water of hydration (or sorbed water) is loosely attached to the binding sites of protein, but it is not entirely 'free'. When an electric field (in the frequency ranges 0.1 Hz – 1 MHz) is applied, dielectric susceptibility in the material is caused through the transport of charge. The process of charge transport in the form of LFD has been considered earlier in Section 3.5. Since the sample dielectric properties are highly dependent on water content, then the most probable charge transport mechanism may be associated with protons, that are originated from clusters of water molecules. The idea of protons as charge carriers responsible for the

dispersion observed in hydrated proteins was also confirmed from deuteration study (Sections 5.2.3.4 and 5.3.2.3). This proton transport is considered can take place in the cluster itself or between different clusters.

The time constant describing the rate of these induced polarisations is dependent not only on the size of the induced dipole (i.e. cluster), but also the number or frequency of the charge transfer events between nearest neighbour water dipoles. In general, the movement of protons within a cluster can be thought of as short range, and therefore the process can be observed to relax at reasonably high frequency. As the concentration of the water in the system is increased, the number or frequency of cluster polarisations increases and therefore the time constant decreases. This explains why the relaxation time shifts to bigger values with the higher water content.

The size of the cluster dipoles increases with increased water content. An understanding of the relationships between cluster size and water content, however, can only be observed from a study of the temperature dependence of the ε_3 relaxation time (see Chapter 6).

At high frequency ($\omega > \omega_c$), the intra-cluster proton transport generates a cluster polarisation. The fluctuation in distribution of cluster polarisation in the protein may be limited to the domain size of protein, which creates ε_4 dispersion; or it may be limited to the size of a single macromolecule, which creates ε_3 dispersion. The appearance of loss peak of the ε_3 and ε_4 dispersions is due to the limited size of distribution of cluster polarisation. A single macromolecule may consist of more than one domain. The distribution of cluster polarisation for the ε_3 distribution is therefore bigger than that of the ε_4 dispersion. This is the reason of higher relaxation times of ε_4 dispersion compared with ε_3 dispersion.

At lower frequencies ($\omega < \omega_c$), a new stochastic event becomes even more probable, and this is the transfer of charge between groups of clusters. The transfer of charge between a number of clusters is not limited to the cluster size, and so a giant dipole is created that grows in size as the time period of observation increases (i.e. as the experimental frequency

of the applied oscillating field decreases). This mode of proton transport depends on the long range order in the system and may be described in terms of percolation phenomena (see Section 5.4.4). The transition from predominantly intra-cluster transport (i.e. at high frequency) to both intra- and inter-cluster transport is marked by the intersection frequency ω_c.

The movement of proton between water molecules, which occurs within the hydrogen bonding connected between water molecules can be illustrated as in Figure 5.28 [87]. When water was added to protein, the first interaction was the ionisation of side-chains. This produced proton redistribution in the protein system which resulted in proton transport as explained above. With the increase of hydration level, the cluster of water molecules grew and the surface backbone and non-ionisable side chain start to be involved.

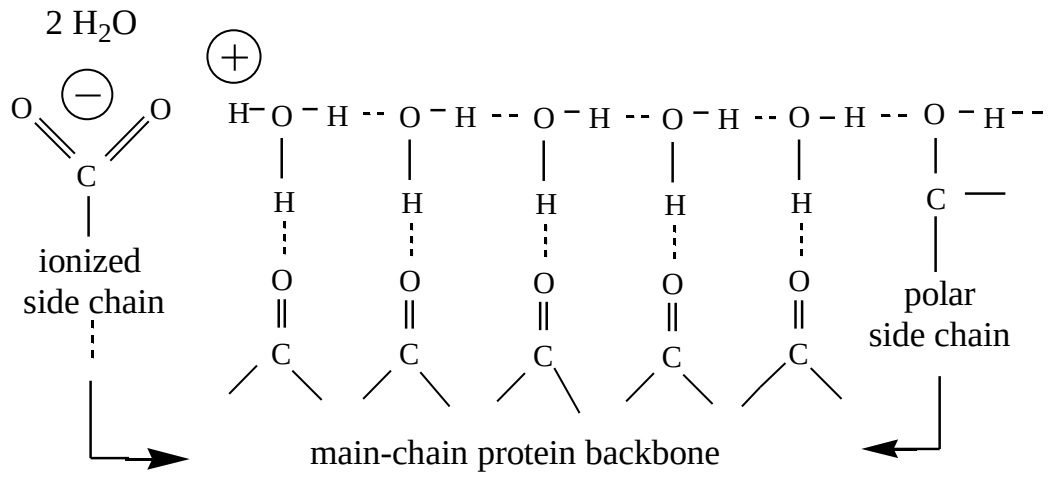

Figure 5.28 *Hydrogen bonded water to protein molecules as a bridge for proton transport in hydrated protein.*

Since the dielectric response is mainly due to proton transport related to the cluster of water molecules, then dielectric response for each hydrated protein has a similar pattern. However, each protein has a different surface and interior structure and therefore sorbed water molecules will be attached to different binding sites in each protein. As a result, each protein has different value of dielectric parameters (e.g. τ, A, p, $\Delta\varepsilon$, β, and ε_∞) as has been shown earlier.

5.4.2 Rationale of fitting model

In general, the LFD for proteins has a feature as shown in Figure 3.6 (Section 3.5.1), in which it consists of two power laws representing low frequency ($\omega < \omega_c$) and high frequency part ($\omega > \omega_c$). In this study, however, the high frequency part is dominated by a loss peak, named as the ε_3 dispersion. In some cases (i.e. at very low hydration level or at low temperature (Section 6.6)), another loss peak at higher frequency than that of ε_3 dispersion, was observed. This dispersion is termed as ε_4 dispersion. The high frequency part of LFD may be observed at higher frequencies than those used in this study.

In the fitting process, therefore, only one power law of frequency is used (i.e. one constant phase element) to fit the low frequency part of LFD. The high frequency part is fitted by a Davidson-Cole element, and not with another power law of frequency. In the case of the lowest hydration level of the sample studied, there was a very low-loss dielectric response observed at high frequency, which cannot be fitted by an infinite frequency permittivity (see Figure 5.2(a)). This part probably originated from the high frequency part of LFD (i.e. the second power law of frequency). Another possibility is that this low-loss dielectric at high frequency is a part of low frequency arm of the ε_4 dispersion.

The loss peak of the ε_3 dispersion is fitted well with a Davidson-Cole expression. The use of the Davidson-Cole model gave the smallest error in all dielectric parameters, and gave better fitting results compared with the Havriliak-Negami or Cole-Cole model. This is not surprising since the low frequency arm of the ε_3 dispersion is largely hidden below the LFD

response. It follows that compensation between the parameters in the LFD response and those in the Havriliak-Negami expression will give rise to large uncertainties in the fit parameters.

The distribution parameter β represents the slope of high frequency part of Davidson-Cole element. As shown in Figure 5.22, distribution parameter β decreased with the increase of hydration level. With the increase of hydration level, LFD became more dominant and probably cover the ε_3 dispersion, which consequently results in smaller distribution parameter β.

The fitting used in the data is also able to show whether the dispersion observed is a bulk property of the sample or merely an interfacial effect. The good fit of the data to the model consisting of LFD and Davidson-Cole elements in parallel showed that the LFD observed in the hydrated ovalbumin is a bulk property of the sample. If the LFD observed is an interfacial phenomenon or Maxwell-Wagner effect, it would be likely to be in a serial circuit with the Davidson-Cole model. The independence of the LFD relative permittivity on the compaction and thickness variation of the sample also confirmed that the LFD process reflected a volume/bulk property of the sample (see Figure 5.29).

The charge transport mechanism for the LFD process fulfilling power law function of frequency (Equation 3.44a) may also be considered from the dependence of the exponent parameter p. If the exponent value p characterizing the response was between $0.6 < p < 1$, then the precise mechanism was said to be due to charge carrier hopping[57]. The exponent value p, obtained from the fitting a universal power law element to data from measurements on each hydrated protein, was in the range of $0.95 < p < 0.7$ (Figure 5.10(c), Figure 5.11(c), and Figure 5.12(c)). Therefore, it can be said that the LFD observed on hydrated protein was probably due to charge hopping. Since this LFD is greatly affected by water content, it is probable that the exact mechanisms of charge hopping correspond to proton transfer within the hydrogen-bonded water-protein system. The mechanism of proton transfer is confirmed from the deuteration study.

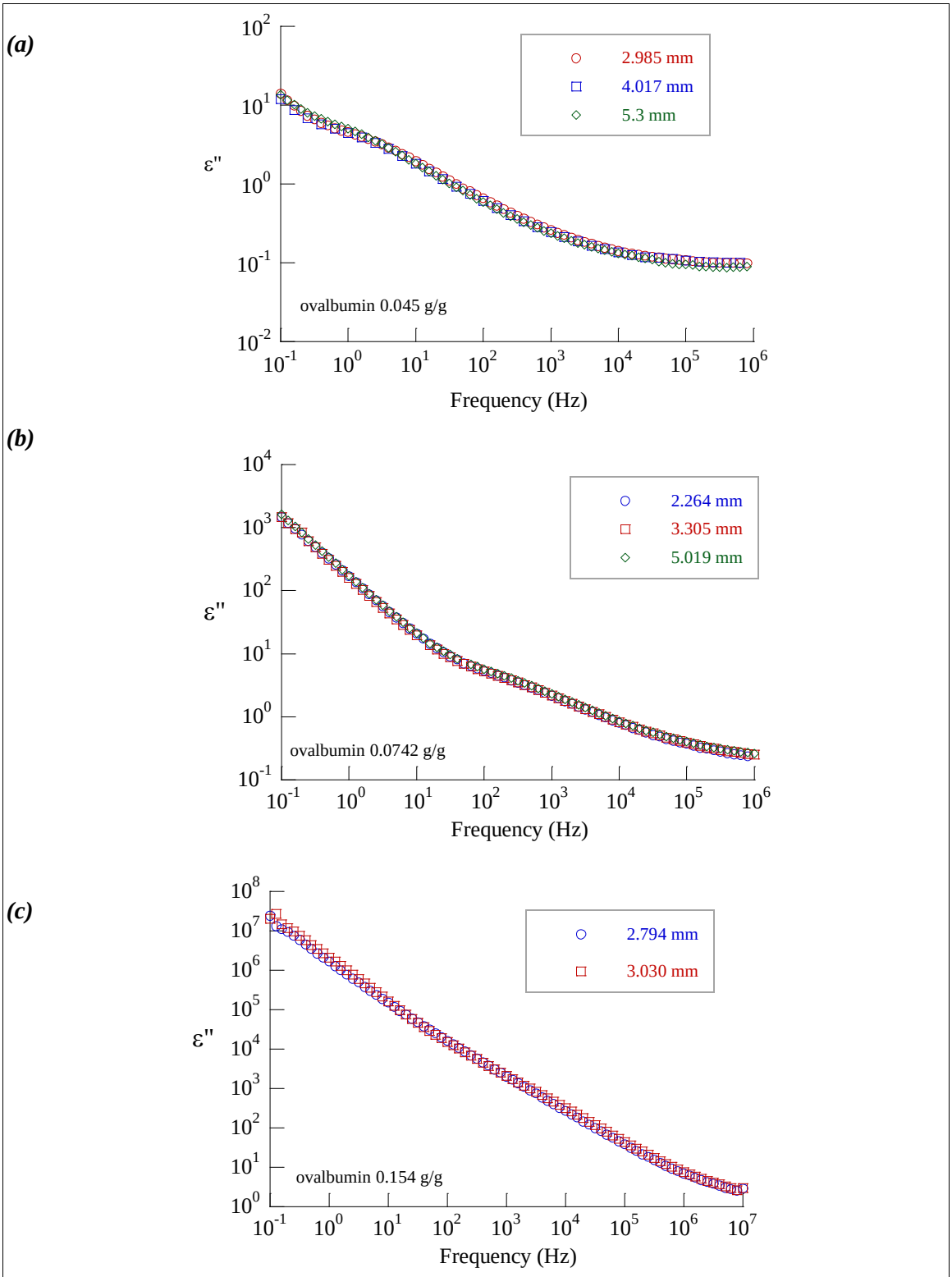

Figure 5.29 *Imaginary permittivity ovalbumin (a) 0.045 g/g, (b) 0.0742 g/g, (c) 0.154 g/g, for various thickness.*

5.4.3 Critical Hydration

The transition hydration level as observed in dielectric parameters of $\tau, A, p, \Delta\varepsilon, \beta,$ and ε_s. may be due to changes in water-water and water-protein interaction. Since each protein in this study showed a similar behaviour, it may be said that the critical hydration level is a fundamental feature of the sorption water on protein powder. The critical hydration level on hydrated proteins is also observed in IR spectra for lysozyme, which was found at about 0.05 - 0.1 g/g[88]. Other studies of hydrated proteins using IR, calorimetric, and ESR showed that there are some common stages of hydration level in protein, i.e. at hydration level of about 0 - 0.07 g/g, 0.07 - 0.15 g/g, 0.15 – 0.25 g/g, 0.25 - 0.38 g/g, and 0.38 g/g - full hydration [89, 90]. All these previous studies confirm the presence of critical hydration levels as obtained in this study, i.e. first critical hydration level and second critical hydration level (Table 5.1 and Table 5.3).

The first transition hydration (h_{c1}) observed in dielectric parameters from LFD and ε_3 dispersion (as shown in Figure 5.10, Figure 5.11, Figure 5.12, and Figure 5.13) may be due to the first hydration stage for globular proteins. As stated before, some literatures state the stages of hydration protein, in which the first hydration stage is at about hydration level of 0 - 0.07 g/g [89,90]. This first hydration stage is thought to be due to the saturation of charged surface groups on the protein[88]. The water mobility within this hydration level is considered to be low and enzymatic activity negligible. The transition hydration at the first hydration level is considered due to the transition in the properties of surface water, from disordered to ordered or from dispersed to clustered state[89].

In this study, the first critical hydration (h_{c1}) found was assumed due to a similar transition as occurring in the first hydration stage of globular proteins. The first critical hydration (h_{c1}) in this study may be assumed as the formation of infinite cluster of water molecule in a single macromolecule.

The description of hydrated proteins, based on the cluster model to illustrate the formation of infinite cluster in a single macromolecule is shown in Figure 5.30. At low hydration h_1 and high frequency ($\omega > \omega_c$), cluster of water molecules (cluster polarisation) are dispersed throughout the surface of each macromolecule. When the hydration level was increased (h_2), more cluster polarisations were present in the system, and the distribution of cluster polarisation is bigger. When more water was added, the number of water molecules forming a cluster increased. At certain point, i.e. at first critical hydration level (h_{c1}), the group of cluster polarisation in the macromolecules formed infinite cluster. At this stage, long-range connectivity was formed, and thus percolation started to occur. This level was also associated to a percolation threshold.

The formation of an infinite cluster (or the onset of percolation phenomenon) in hydrated proteins was also observed from the difference in the rate of relaxation times as a function of the hydration level. At $h < h_{c_1}$, the relaxation times decreased faster than at $h > h_{c_1}$. This rate of relaxation times upon hydration level may be expressed in term of exponent value for the power function of hydration level from relaxation times. As shown in Table 5.2 the exponent value for relaxation times at $h < h_{c_1}$ is higher than at $h > h_{c_1}$.

When hydration level was further increased ($h > h_{c1}$), the water molecules filled the available empty sites in the single macromolecule, until the surface of macromolecule was fully covered (i.e. at h_{c2}). The size of the infinite cluster itself did not change during the hydration level $h_{c1} < h < h_{c2}$, since the cluster size has reached the maximum (which was determined by the size of a single macromolecule). This explains that the dielectric parameters ($\varepsilon_s, \Delta\varepsilon$) for pepsin and lysozyme increased up to h_{c1}, but then remain constant in the hydration range of $h_{c1} < h < h_{c2}$ (see Figure 5.13 and Figure 5.23). The critical hydration level h_{c2} in this study, is therefore considered as the hydration level where water molecules covered the whole surface of a single macromolecule (formation of water monolayer in a single macromolecule). For ovalbumin, h_{c2} was not observed. It was possible that when the infinite cluster formed at h_{c1} for ovalbumin, water molecules have

already covered the surface of single macromolecule, and no more available site for added water molecule.

At further higher hydration level ($h > h_{c2}$), since the single macromolecule surface has already covered by water molecules, the added water molecules now reside on the top of water monolayer. This explains the gradual change of fractal dimension D_f from 2-dimension to 3 dimension in the hydration range $h_{c1} < h < h_{c2}$ (see Figure 6.28, Section 6.5).

Careri assumed that critical hydration occurring in the globular protein is universal, i.e. involving several stages as mentioned earlier. The results from this study, however, show that the critical hydration for each hydrated protein is different. It can be argued that Careri only did the study for lysozyme and assumed that the results are similar for all globular proteins. Therefore, it may be said, that the hydration stages are observed for each hydrated proteins, but the value of critical hydration for each stage may vary, depending on the protein itself. This is due to the interaction of water with the interior protein surface itself, even though it is considered as a loose interaction.

As have been shown earlier the critical hydration was observed in all dielectric parameters. Distribution parameter β, for example, was derived empirically and stated as having no physical meaning (see Section 3.4.2). However, in this study, distribution parameter β also revealed critical hydrations that may also be related to a change of ionisation state and enzymatic activity on hydrated proteins. The results from this study showed that this parameter may also be able to contribute to the physical meaning of the samples.

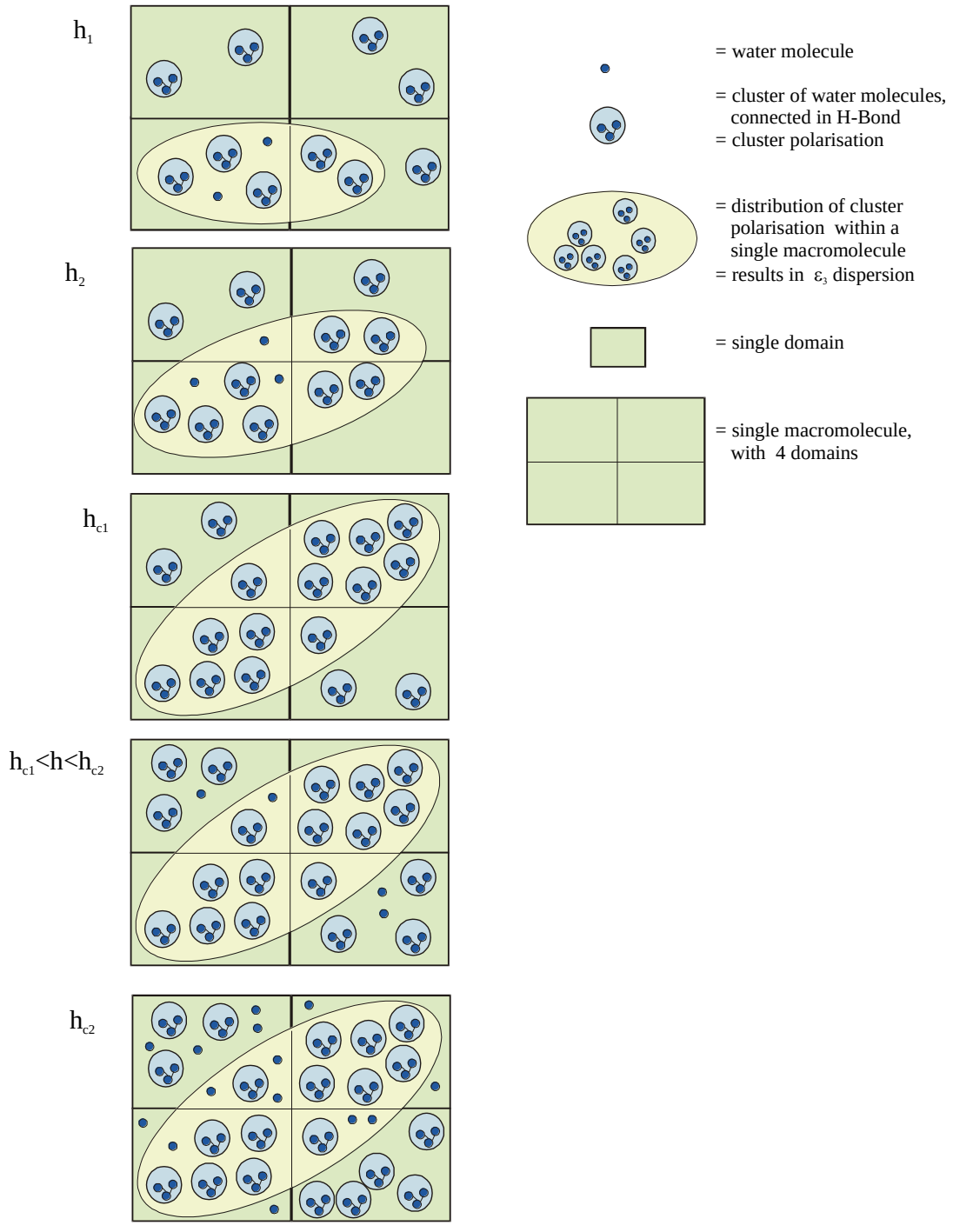

Figure 5.30 *Cluster model showing a group of cluster molecules (cluster polarisation) at various hydration ($h_1 < h_2 < ... < h_{c1} ... < h_{c2}$) in a single macromolecule. An infinite cluster is formed at hydration level h_{c1}, which is the onset of percolation threshold. Water molecules cover the surface of single macromolecule at h_{c2}.*

The cluster model above illustrates the mechanism of cluster polarisation and the fluctuation of its distribution at high frequency (i.e. at $\omega > \omega_c$) in a single macromolecule (Figure 5.30). At low frequency, i.e. where $\omega < \omega_c$, the protons have enough time to shift to a nearest neighbour cluster. As has been mentioned earlier, the hopping of proton transport between the clusters (inter-cluster) is the one responsible for LFD response. This can be illustrated in Figure 5.31. The cluster (light-blue circles) consists of few water molecules connected with hydrogen bonding (blue dots).

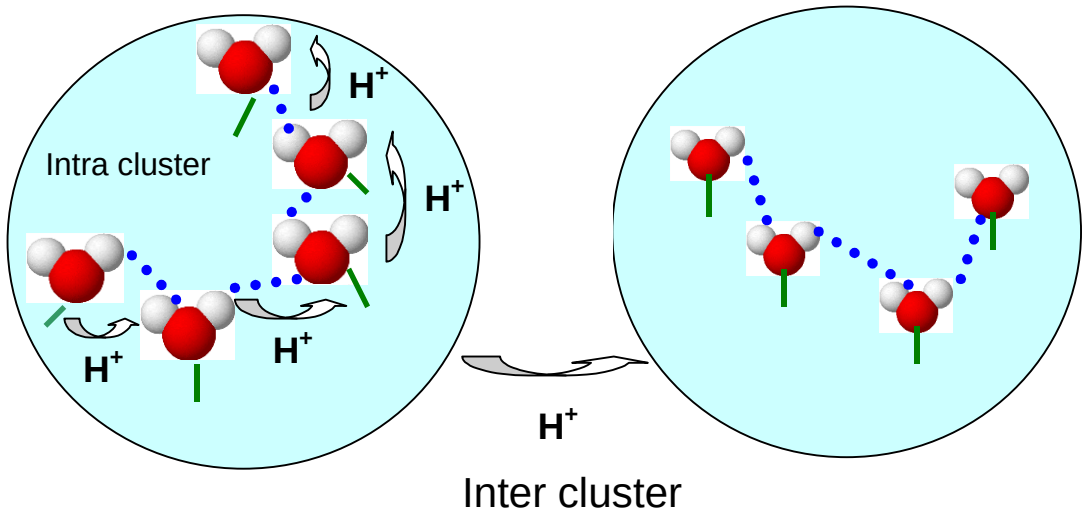

Figure 5.31 *A feature representation from Figure 5.30 above for one cluster consisting a number of water molecules. This also portrays the proton transport inter and intra cluster of water molecules. Red balls represent oxygen atoms, grey balls represent hydrogen atoms, blue dots represent hydrogen bonding O-H---O, green lines represent bonding to the proteins, big light blue circles represent a cluster.*

5.4.4 Percolation in hydrated proteins

The mechanism for the LFD process observed in hydrated protein may also be explained in the context of percolation. Some reasons for this come from the fact that the LFD observed in hydrated proteins in this study has a power function of frequency and an abrupt increase observed in static permittivity ε_s.

Charge transport in percolation systems are characterised by a conductivity that has a power law dependence on frequency. The complex permittivity of hydrated proteins at low frequency ($\omega < \omega_c$) was seen to fulfil the power law of frequency. Since the imaginary permittivity is linearly directed to the conductivity of the sample, then one can infer that the mechanism of the LFD in the hydrated proteins is based on a percolation process.

The abrupt increase of static permittivity after critical hydration (Figure 5.13) also supports the idea of percolation phenomenon in hydrated proteins. As shown in Equation (A3.12) the static permittivity ε_s of a percolation system for frequency dependent charge transport is a power function of occupied sites. In the case of hydrated proteins, the water molecules are considered as occupied sites.

Percolation theory (Appendix A3) also implies the existence of the percolation transition/percolation threshold, p_c, in which all the sites belong to the infinite clusters. This phenomenon may also represent the long-range connectivity among the elements of a system which suddenly appears at a critical concentration of carriers[91]. Associated to the hydrated proteins, the critical hydration may correspond to the percolation transition/percolation threshold.

As mentioned before in the percolation theory (Appendix A3), the sample consisting of a network of conductor (occupied sites) and insulator (empty sites) elements shows an abrupt increase in sample's conductivity as a function of composition or concentration, which is known as a percolation phenomenon. It has been confirmed above that hydrated proteins

satisfied the phenomenon of percolation. In this case, the hydration level in the proteins may be related to the composition/concentration of the water molecules in the sample. The water molecules here may represent the conductor parts (occupied sites) in the sample. The occupant of the water molecules are all elements forming the water molecules, i.e. hydrogen and oxygen atoms. The one that causes a current flow is charge element. From the nature of water molecule and the bonding between water and protein molecules, the most probable charge hopping from one site of water molecules to the others is proton. Proton as the charge hopping in hydrated proteins has also been verified in previous section by deuterating the proteins. Table 5.7 shows the correspondence of hydrated proteins with percolation phenomenon. This percolation phenomenon may also be described by an illustration as in Figure 5.30 and Figure 5.31.

Table 5.7 *Analogy of percolation in hydrated proteins*

Percolation Theory	**Hydrated Proteins**
Occupied sites	Water molecules
Empty sites	Protein
Cluster (occupied and empty sites)	Group of water molecules
Connected bonds	Hydrogen bond
Flowing element	Proton

5.4.5 Use of remote electrodes

Most of biological samples including hydrated proteins used in this study are very high conducting materials since the samples involve a number amount of water or other conducting organic materials. The contact between electrodes and sample may cause an electrochemical reaction at the electrode-sample interface that makes the electrode to

polarise and generate an electrical double layer (i.e. an interfacial capacitance). The technique of low frequency dielectric measurement (< 10 MHz) for most of biological samples is thus suffering from the electrode polarisation effect.

In this study of hydrated proteins, the LFD process itself may consist of electrode polarisation at low frequency. However the LFD process may be much more dominant than electrode polarisation effect, thus the electrode polarisation process may be covered by the LFD.

When the hydration level is getting higher the electrode polarisation effect started to appear and merged with the LFD process, resulting in the bulge appearance at the log-log plot of real and imaginary permittivities at low frequency as has been shown earlier.

The electrode polarisation effect may be entirely eliminated due to the use of remote electrodes. However, in the case of the presence of LFD, the dispersion observed from the use of remote electrodes (i.e. ε_2 dispersion) is arisen from the combination of LFD and the spacer itself. The LFD is not simply removed by the use of remote electrodes.

Besides eliminating the electrode polarisation effect, the advantage of using remote electrodes, especially for biological samples, is that ε_2 dispersion may be used as a representative for LFD. With the use of remote electrodes, the bulk properties of the sample itself are unchanged and therefore the essential properties of the sample are still observable. This has been evidenced from the results of dielectric parameters obtained from both ε_2 and ε_3 dispersions. Another advantage of using remote electrodes is explored more detail in Chapter 7 for *in situ* measurement of water content to determine the end point of freeze drying process, which is expected to contribute a novel technique on the application of pharmaceutical technology.

5.4.6 Comparison with other complimentary techniques

From the comparison of each hydrated proteins observed in this study pepsin has slightly different behaviour compared with ovalbumin and lysozyme. ε_3 dispersion observed in pepsin is more obscure compared with ovalbumin and lysozyme (Figure 5.32 and some Figures shown earlier in the result section). The value of critical hydration for pepsin is also significantly different from ovalbumin and lysozyme.

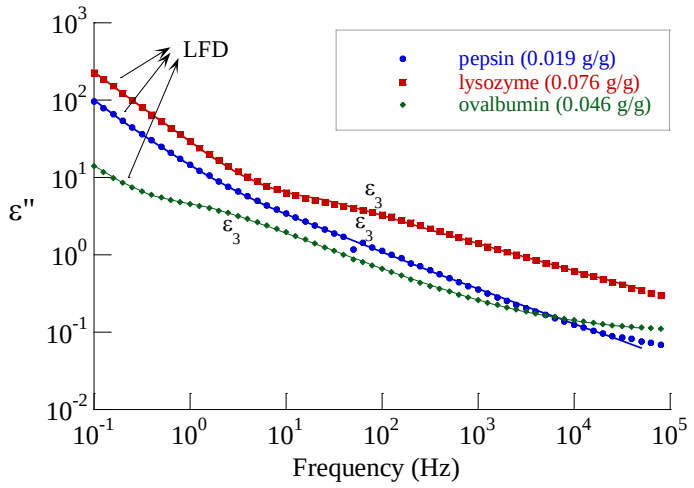

Figure 5.32 *Imaginary permittivity for ovalbumin, lysozyme, and pepsin.*

This difference may also be observed in the SEM micrograph comparing the particle shape of ovalbumin, lysozyme, and pepsin (Figure 5.33). Both ovalbumin and lysozyme show a nice spherical shape as typical particle shape for spray drying materials, whereas pepsin shows an unordinary lumped shape.

It is not clear whether pepsin sample used in this sample has undergone a denaturation due to the storage or other things like sample preparation, crystallinity state, etc.

The FTIR spectroscopy in Figure 5.34 shows that pepsin behaved differently compared with ovalbumin and lysozyme. Unlike ovalbumin and lysozyme, the peak showing the chemical bonding in FTIR for pepsin was broken in several peaks which show the denaturation state of pepsin.

XRD pattern for each protein shows that pepsin is a crystalline (i.e. crystalline alpha-lactose monohydrate) whereas ovalbumin and lysozyme are amorphous (Figure 5.35).

All these differences may be the answer of pepsin being performed differently compared with ovalbumin and lysozyme.

(a)

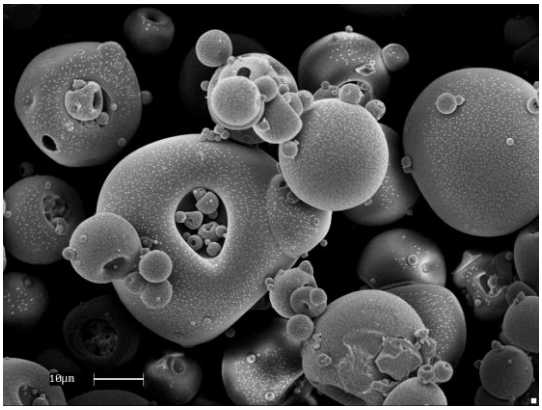

(b)

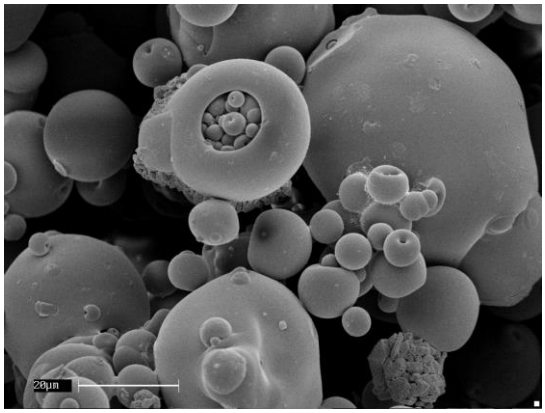

(c)

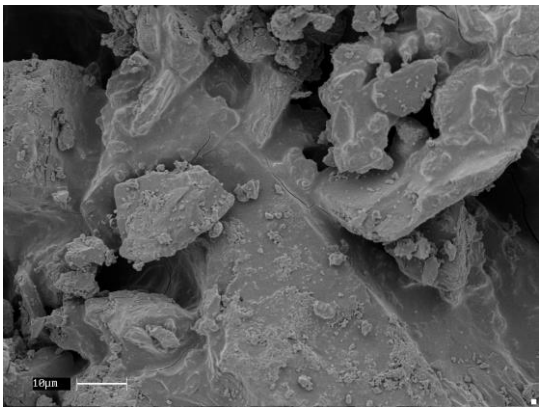

Figure 5.33 *SEM images for (a) ovalbumin 0.16 g/g; (b) lysozyme (0.092 g/g); and (c) pepsin (0.005 g/g).*

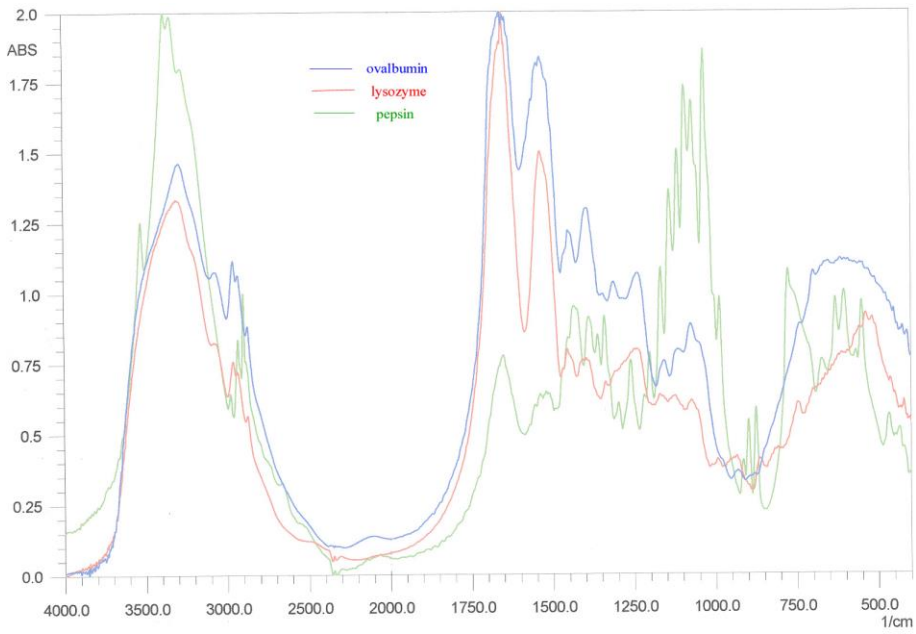

Figure 5.34 *FTIR spectra from ovalbumin, lysozyme, and pepsin.*

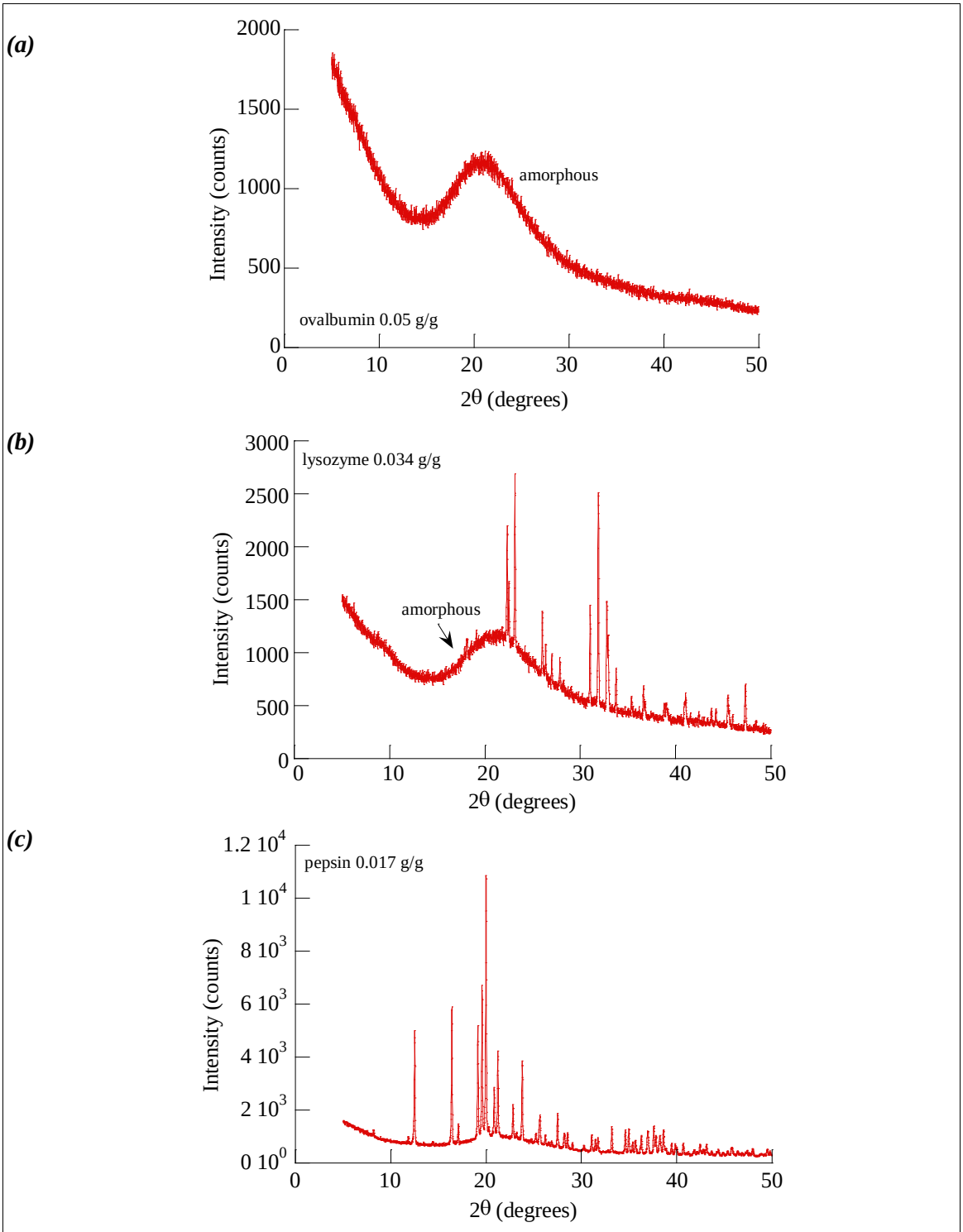

Figure 5.35 *XRD patterns for (a) ovalbumin; (b) lysozyme; and (c) pepsin.*

5.5 Summary

Hydration study has shown that LFD and ε_3 dispersion are the main features of dielectric spectroscopy on each globular protein (ovalbumin, lysozyme, and pepsin), and are strongly dependent on water content in the sample. Both the LFD and the ε_3 dispersion shifted toward higher frequency with the increase of hydration. Based on the cluster model, the origin of the LFD was due to charge transport between clusters (inter-cluster) of water molecules, thus creating a long-range order transport, which gave rise an enormous polarisation. The ε_3 dispersion was considered to be due to fluctuation in distribution of cluster polarisation (which is due to the charge transport within the cluster itself (i.e. intra-cluster charge transport)). The proton transport in hydrated protein was assisted by water molecules interacted with the ionisable side chain on the surface of single macromolecule of protein. The proton transport was also evidenced from the deuterated study.

At the low hydration of lysozyme (< 0.054 g/g), a very weak dispersion at higher frequency than that of ε_3 dispersion was observed, which is named as ε_4 dispersion. The ε_4 dispersion was observed further with the temperature study (see Section 6.6). Briefly discussion about the mechanism of ε_4 dispersion is given in Sections 6.7.5 and 8.1.1.

The critical hydration levels observed in the hydrated proteins may be associated with the percolation phenomenon in a single macromolecule of protein (i.e. by the formation of infinite cluster of water molecules) and may also be related to first water monolayer on a single macromolecule.

The use of remote electrodes for dielectric measurement on hydrated proteins did not affect the appearance of ε_3 dispersion. A new dispersion, i.e. ε_2 dispersion, was observed due to

the combination of LFD process and the spacers from remote electrodes. Both of LFD and ε_3 dispersion are therefore believed as bulk properties of the samples.

6 TEMPERATURE STUDY ON HYDRATED PROTEINS

6.1 Introduction

The main objectives of investigating the temperature dependent dielectric properties of hydrated proteins were:

- to elucidate the mechanism of dispersions observed in these materials
- to verify the existence of dispersions that were not revealed in the ambient temperature hydration study
- to investigate further the water-protein interaction
- to examine the stability of hydrated protein powders
- to investigate the dielectric response of hydrated proteins during a certain temperature range which can be applied for *in situ* dielectric measurement on freeze-drying.

This chapter includes the method of temperature dependent dielectric measurement and the response of hydrated protein powders as a function of temperature*. Parameters such as the percolation threshold, the activation energy for charge transport, and the fractal dimension are determined and discussed. The validation of temperature studies involving the validation of sample cell and the possible properties change of each protein due to the liquid N_2 treatment are also discussed.

* Some part of this work has now been accepted for publication in the Journal of non-crystalline solids (see Appendix A7.1).

6.2 Method

The temperature dependent dielectric response of each hydrated protein was measured using an Oxford temperature controller ITC^{503} and Spectrostat^{DN} cryostat, connected to Solartron 1296 dielectric interface and Solartron 1255 frequency response analyser (Figure 4.5). The measurements were carried out after cooling the samples down to ~ 253 K, followed by heating up to ~ 400 K with a step of 5 K. The sample cell used for this temperature study consists of two circular brass electrodes, each with surface area of 4.91 x 10^{-4} m^2, embedded with a PET cylinder (Figure 4.6 (b)).

6.2.1 Validation for custom parallel plate cell for cryostat

Temperature studies were carried out using a custom made sample cell, designed for temperature dielectric measurement in the Oxford cryostat (Figure 4.6 (b)). Validation of this sample cell was implemented by comparison of measurements on the empty cell and the commercial Solartron sample cell (used for isothermal hydration study in Chapter 5).

Figure 6.1 shows the comparison of the Solarton empty cell and the empty cell of the custom-made parallel plate for the Oxford cryostat. There were some similarities and differences between commercial Solartron sample cell and custom-made parallel plate cell for the cryostat.

The imaginary permittivity of the Solartron empty cell and the empty custom-made parallel plate cell (for the Oxford cryostat) both showed artefacts at high frequency (i.e. between 0.1 – 10 MHz). This high frequency artefact is manifest as an apparent increase in the capacitance of the cell. This artefact is consistent with the induction effects arising from the instrument set-up, especially from the cables connected to sample cell. The instrument set-up for the cryostat requires long cables to connect the sample cell to the dielectric instrument. This is the reason of the more pronounced induction effect observed for custom made parallel plate cells used in the cryostat compared with the Solartron sample

cells for isothermal measurement. The high frequency artefact associated with lead inductance is less obvious with measurements on samples with relatively high permittivities. In this study, all fits to measurement data were limited to the range in which this artefact was insignificant.

Real permittivity for air measurement using custom-made parallel plate cell is slightly higher than 1 (Figure 6.1). This may be due to the design of the cell itself or other measurement residuals from the instrument set-up (e.g. cables, other conducting elements) that contributed to a stray capacitance. The effect of the stray capacitance is negligible when the permittivity of the sample is relatively high, as was the case from the hydrated proteins in this study. The stray capacitance itself may also be corrected by a simple subtraction routine (see Appendix A1).

Figure 6.1 shows that custom made liquid cell for cryostat suffered more from the artefact effect than commercial Solartron liquid cell. However, when the measurement of the sample was employed, there was no significant difference between the result from measurements using commercial Solartron liquid cell or custom made liquid cell for cryostat (Figure 6.2). The slight difference observed may just be due to the temperature for Solartron liquid cell since the ambient temperature may fluctuate slightly according to the environment temperature.

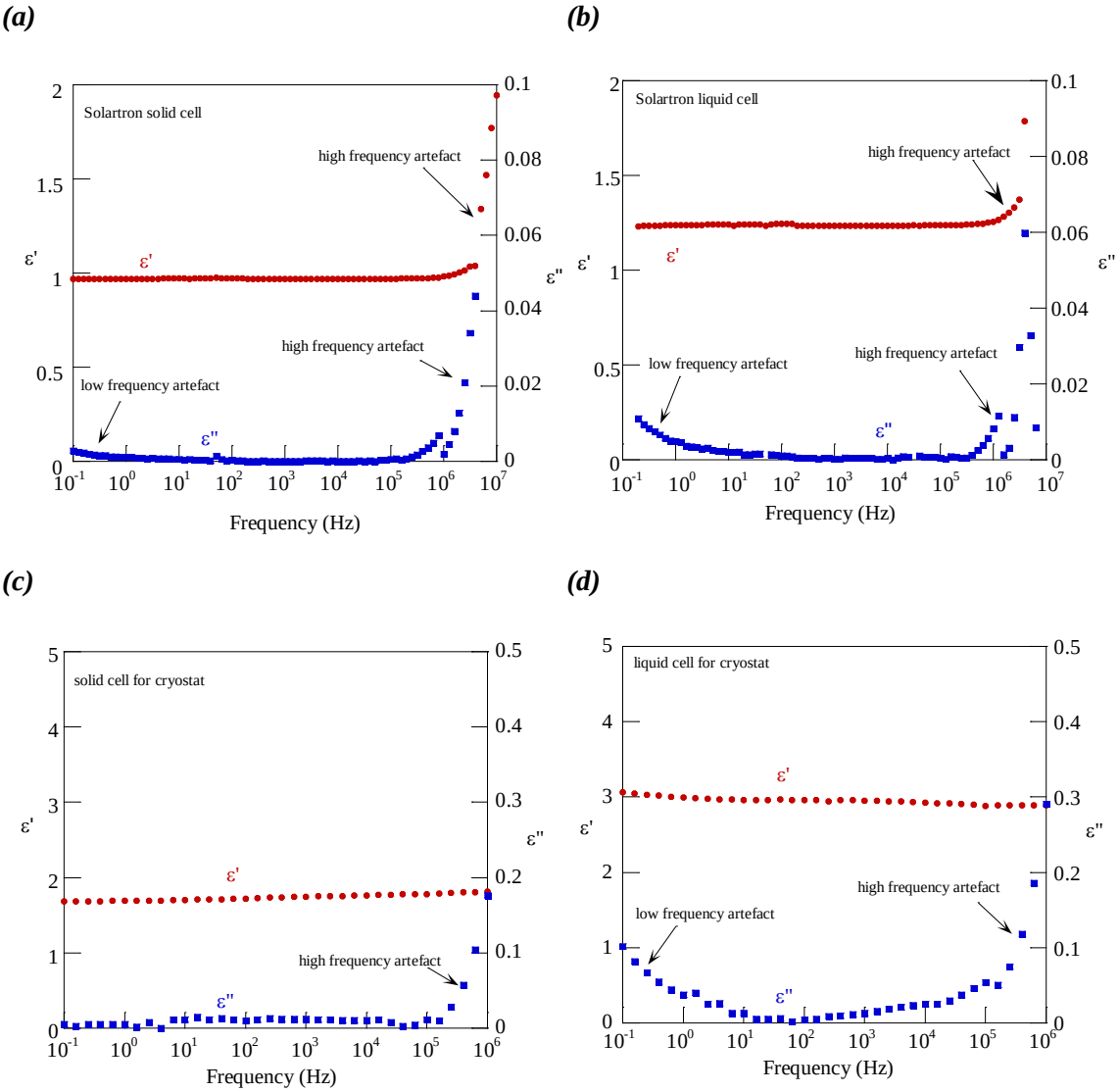

Figure 6.1 *Real and imaginary permittivities of empty sample cell from (a) Solid cell for Solartron, (b) Liquid cell for Solartron, (c) Solid cell for cryostat, and (d) Liquid cell for cryostat (see Section 4.4 for details).*

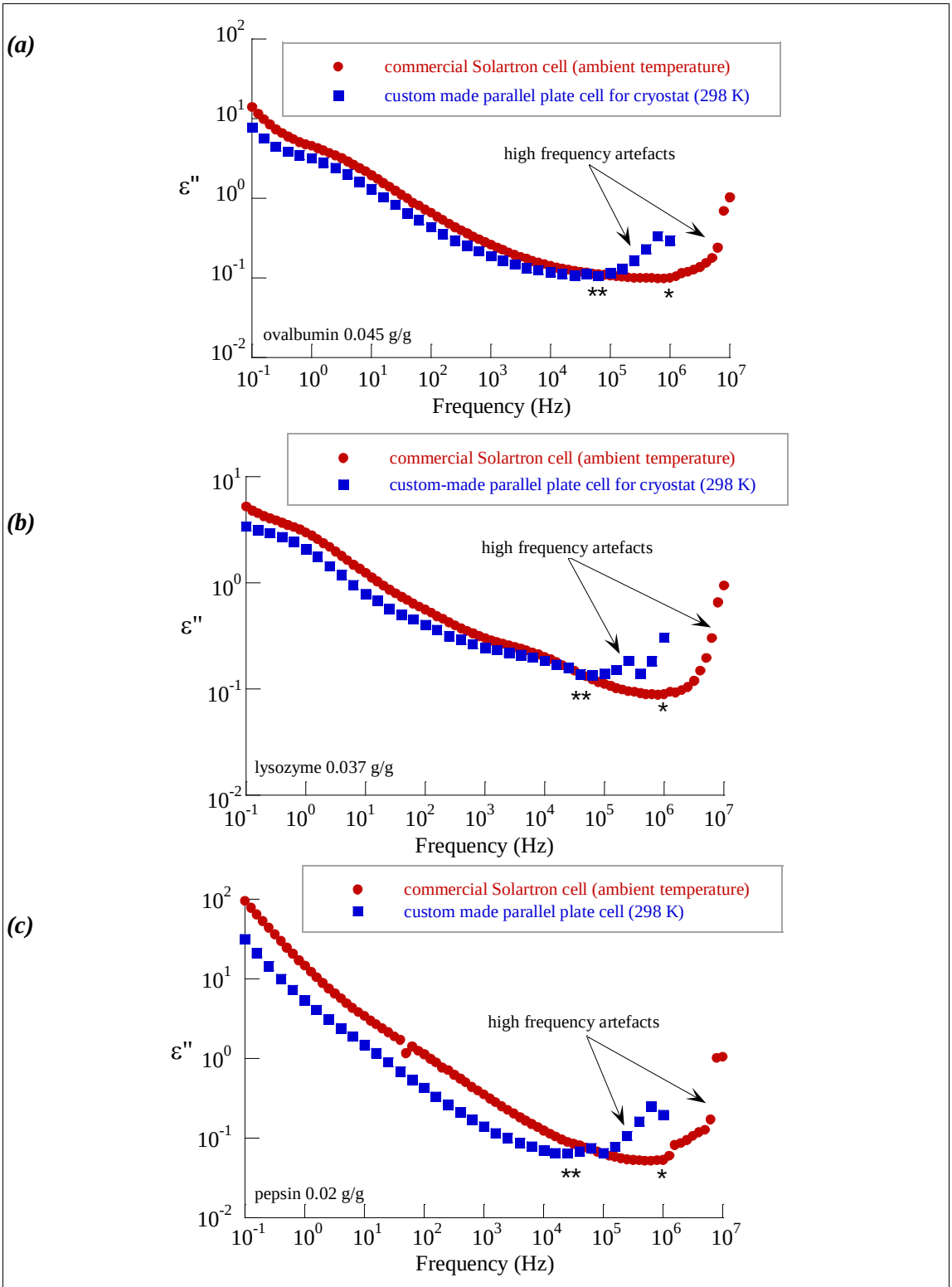

Figure 6.2 *Comparison of imaginary permittivites using commercial Solartron liquid cell and custom made liquid cell for cryostat; (a) ovalbumin; (b) lysozyme (c) pepsin. * and ** are the onsets of the high frequency artefacts for Solartron and custom made cell, respectively.*

6.2.2 Validation for measurement before and after liquid N_2 treatment

Proteins are very complex materials, whose structure and function is highly temperature dependent. A quick temperature reduction of a protein may cause a temperature shock that results in a change in a protein structure. Dielectric measurements on proteins before and after freeze thawing with liquid N_2 were compared to check that the large variant of temperature did not affect the structure and dielectric properties of each protein. Moreover, the use of step-wise heating and cooling rate was also employed to prevent undesired temperature shock on the proteins. To prevent the undesired structure change during measurement, the duration of the measurement was minimised by choosing an appropriate frequency range and a number of measurement points. The temperature range and number of steps per decade were chosen based on the optimum number of data point for analysis and consideration of the nature of the sample itself. A low minimum frequency or too many data points translates to a long measurement period that may induce undesired structural changes of the protein during measurement.

Figure 6.3 shows the dielectric permittivity of each hydrated proteins as a comparison for measurement before and after cooling with liquid N_2.

(a)

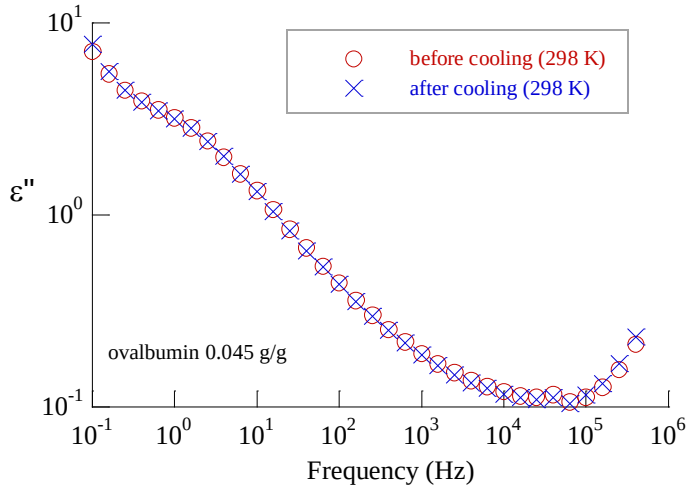

(b)

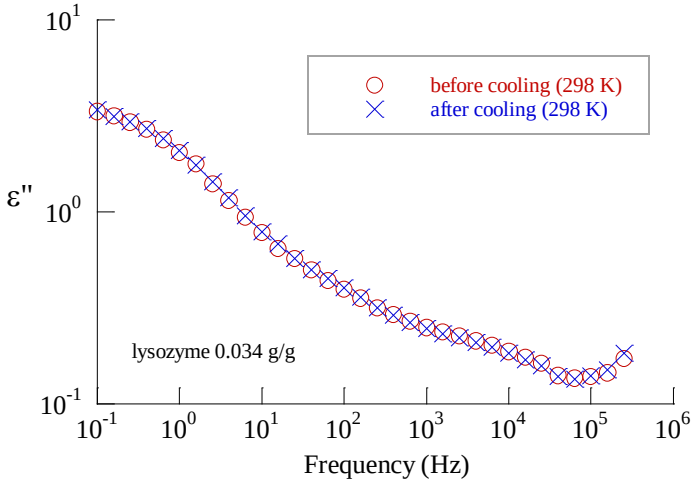

(c)

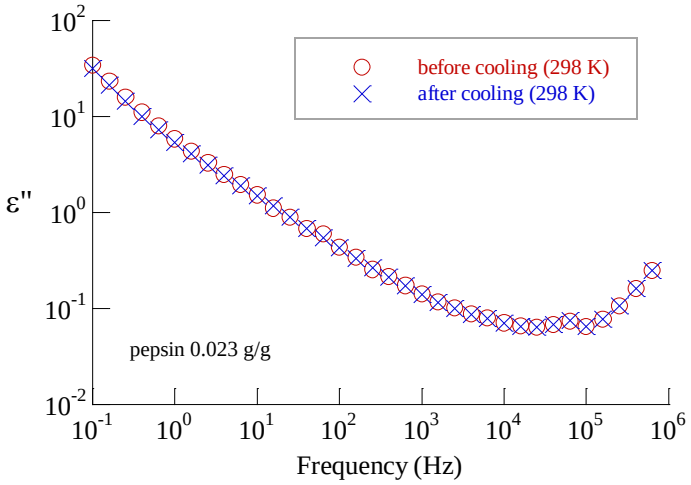

Figure 6.3 *Imaginary permittivity for various hydrated proteins before and after cooling with liquid N_2 for: (a) ovalbumin, (b) lysozyme, (c) pepsin.*

6.3 Percolation Threshold

It has been shown and discussed in previous chapter (Chapter 5) that the dielectric properties of globular proteins revealed two dispersions called LFD and ε_3 dispersion, which are, respectively, due to a proton transport over long range (inter-cluster) and short range (intra-cluster) scales. The latter is possibly at the scale of the individual macromolecule of protein. This section shows the effect of temperature on LFD and ε_3 dispersion for each hydrated proteins (ovalbumin, lysozyme, and pepsin). The main dielectric parameters, i.e. pre-exponential parameter, *A*, and relaxation time, τ_3, representing LFD and ε_3 dispersions, respectively, were highlighted in this temperature study.

6.3.1 Ovalbumin

Figure 6.4 shows a typical temperature study of hydrated ovalbumin (0.047 g/g). Both the LFD and ε_3 dispersion moved toward higher frequencies with the increasing temperature.

For ovalbumin (0.047 g/g), at temperatures below 268 K and in the frequency range 0.1 Hz – 10 MHz, only the tail of the ε_3 dispersion was observed and the LFD was not observed (Figure 6.4 (a)). With the subsequent increase in temperature, the ε_3 dispersion was appeared progressively within the experimental frequency window and the LFD started to emerge at ~ 293 K.

The temperature dependent shift in both the LFD and ε_3 dispersion toward high frequency was reversed at a certain temperature and both the LFD and ε_3 dispersion then shifted toward lower frequency (Figure 6.4 (b)). The permittivity also reversed at this temperature point. The temperature at which the relaxation time begins to increase and the permittivity begins to decrease is called the percolation threshold. This percolation threshold was also

observed in hydration study of proteins, as discussed in Section 5.4.4. A brief theory of percolation is explained in Appendix A3.

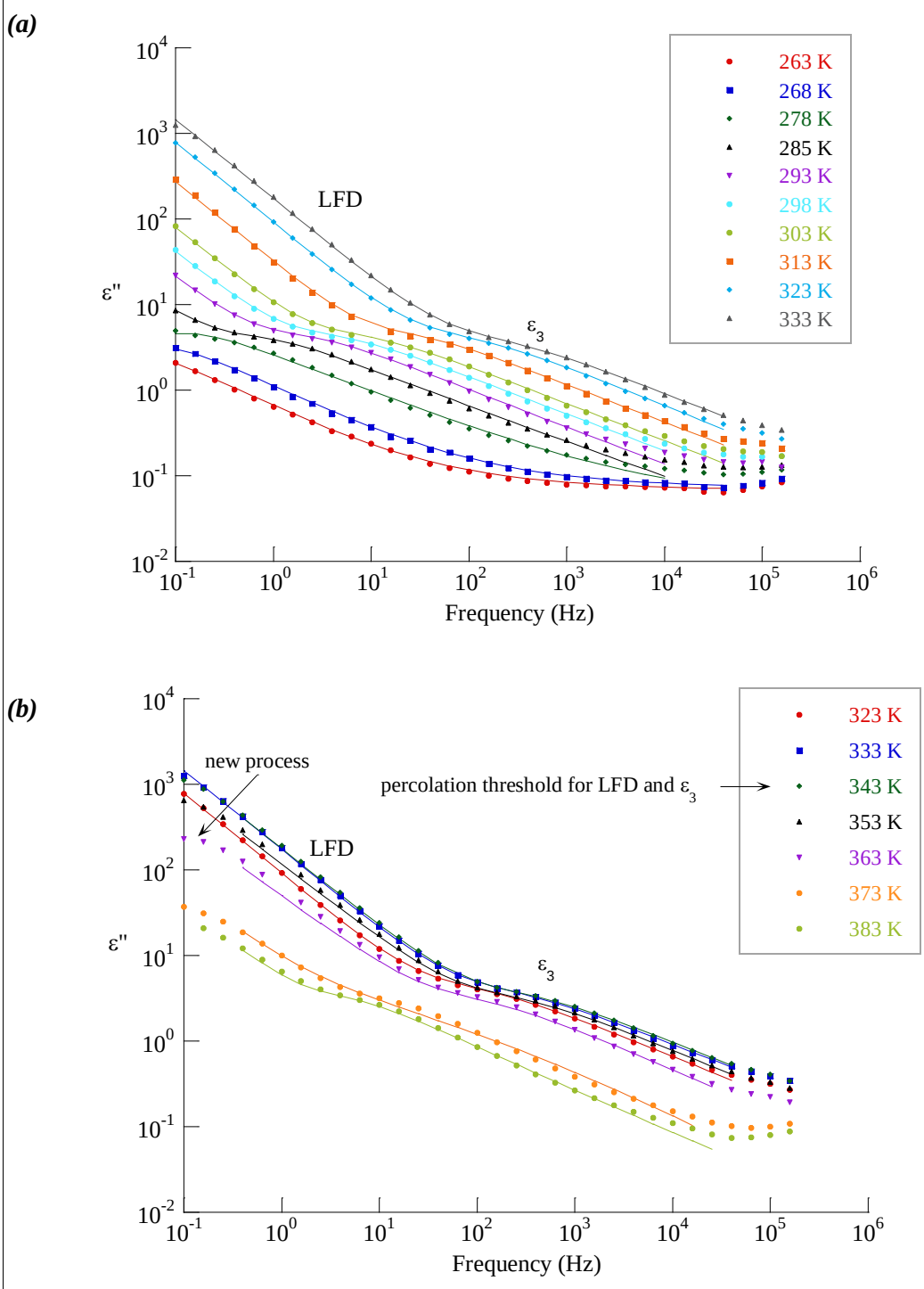

Figure 6.4 *Imaginary permittivity of hydrated ovalbumin (0.047 g/g) for various temperatures (a) 263 – 333 K, (b) 323 – 383 K. Symbols represent experimental data, solid lines represent curve fitting.*

At the percolation threshold, the LFD process is accompanied by a new process (Figure 6.4 (b)). This additional process is manifest as a slightly curve of LFD process at low frequency, instead of continual straight line from power law of frequency. The polarisation mechanism responsible for this additional process is not yet clear since there is no suitable fitting model for this process, especially for the real permittivity. In this study, the fitting model at which percolation threshold occurred, was limited to ~ 0.5 Hz.

It was not clear whether the new process observed at very low frequency at the percolation threshold, was simply an artefact (possibly due to electrode polarisation), or a new process associated with the stochastic system at the percolation threshold. When temperature was kept increase, at certain temperature point, the LFD and ε_3 dispersion seemed to emerge again. Figure 6.5 shows the re-appearance of LFD and ε_3 dispersion at 383 K.

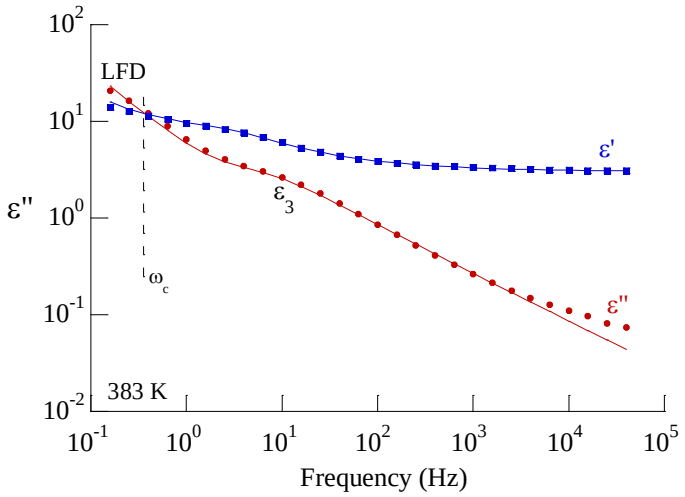

Figure 6.5 *Real and imaginary permittivities of hydrated ovalbumin (0.047 g/g) at 383 K, which shows the presence of new LFD and ε_3 dispersion after percolation threshold. Symbols represent experimental data, solid lines represent curve fitting.*

6.3.2 Lysozyme

Hydrated lysozyme has almost the same behaviour as hydrated ovalbumin. Figure 6.6 shows the temperature dependence of permittivity for hydrated lysozyme 0.082 g/g. As shown in Figure 6.6 (a), the LFD was outside the experimental frequency window below 248 K and only the tail of ε_3 dispersion was observed. Section 5.2.2.3 mentioned briefly the ε_4 dispersion. This ε_4 dispersion was observed vaguely between 238 – 268 K. More about ε_4 dispersion will be discussed in Section 6.6.

The percolation threshold for the LFD of lysozyme (0.082 g/g) occurred at 318 K, while the percolation threshold for ε_3 dispersion occurred at 323 K (Figure 6.6 (b)). At the percolation threshold, the LFD process was also accompanied by another new process at low frequency, that was manifest as a slight curve in the straight line of the LFD process (Figure 6.6 (b)). This was similar to that observed for ovalbumin.

When the temperature was increased beyond the percolation threshold, another new process was observed in the middle frequencies between the LFD and the ε_3 dispersion. This unknown process is named, in this work, as a transition process (Figure 6.6 (b)). This transition process started to appear at ~ 328 K and disappeared promptly after reaching ~348 K. At temperature above 348 K, another LFD and dispersion were observed again, with the pattern almost similar as the process before percolation threshold (Figure 6.7(a)). From the shape of the permittivity plots, it can be inferred that the new LFD and dispersion are probably originated from the former processes of the LFD and ε_3 dispersion observed below the percolation threshold. It seems that when the temperature is increased after percolation threshold, the process is repeated in the same way as before percolation threshold. The observed LFD after percolation threshold is verified by a parallel real and imaginary permittivity plots (see Figure 6.7(b)).

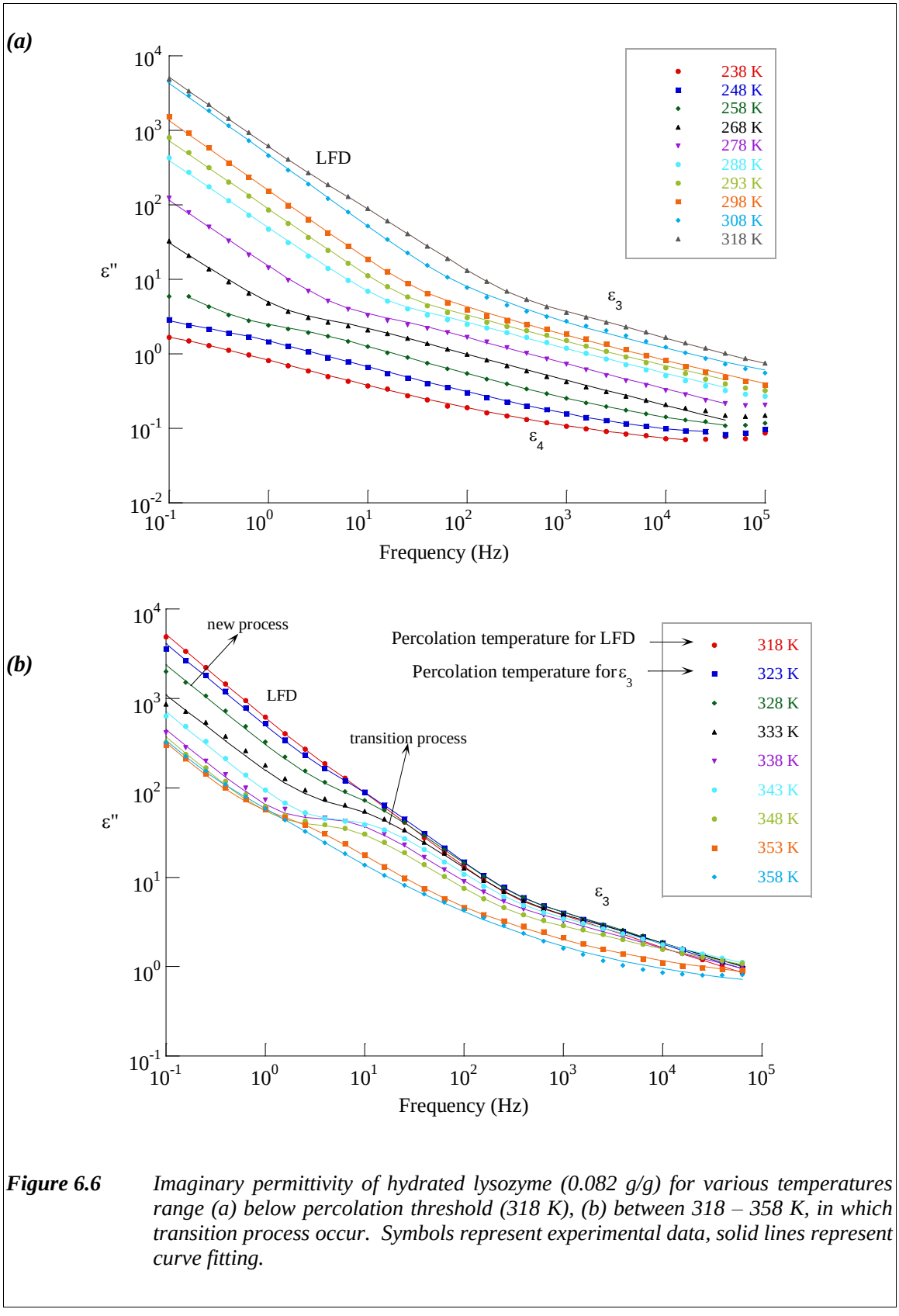

Figure 6.6 *Imaginary permittivity of hydrated lysozyme (0.082 g/g) for various temperatures range (a) below percolation threshold (318 K), (b) between 318 – 358 K, in which transition process occur. Symbols represent experimental data, solid lines represent curve fitting.*

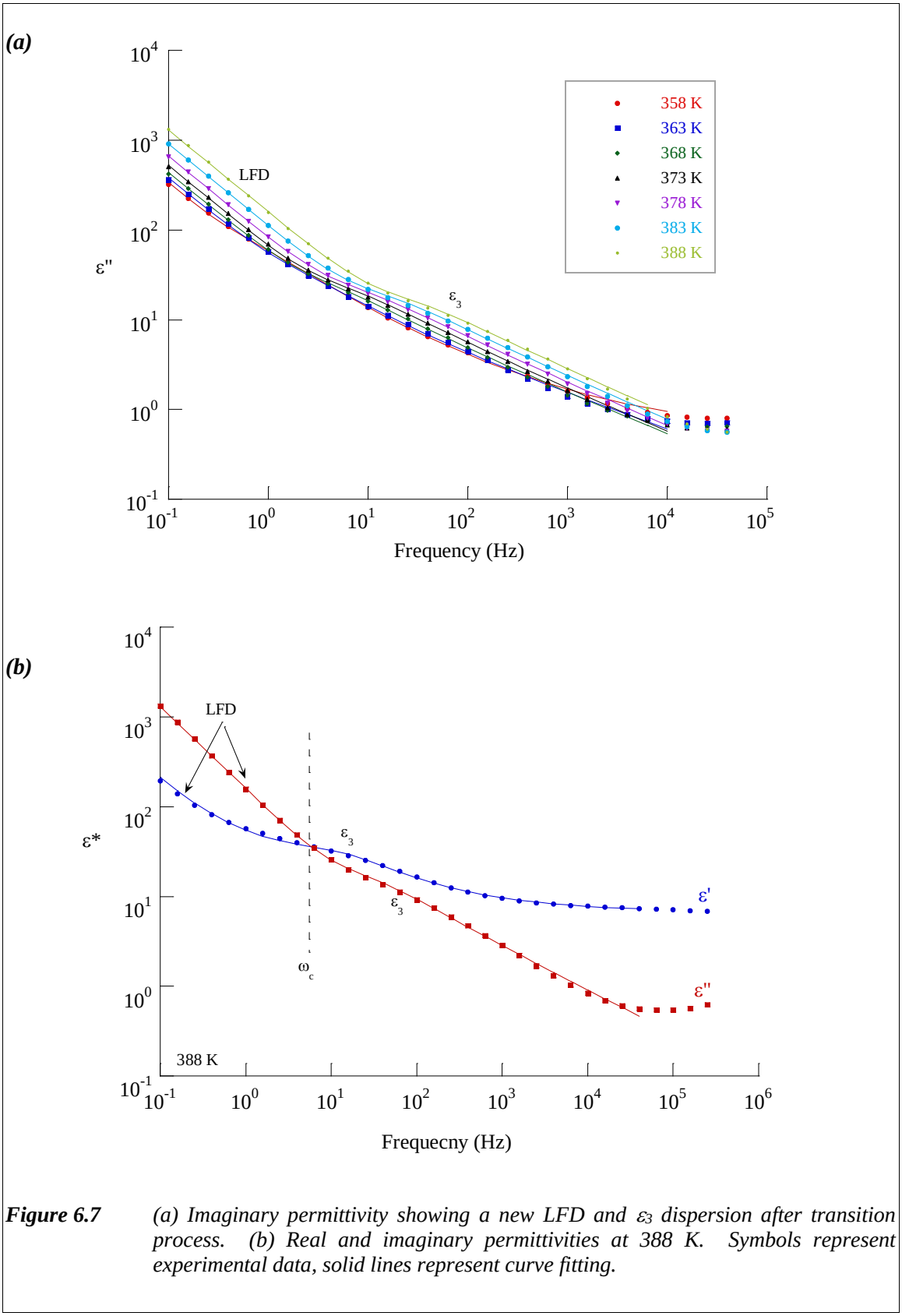

Figure 6.7 *(a) Imaginary permittivity showing a new LFD and ε_3 dispersion after transition process. (b) Real and imaginary permittivities at 388 K. Symbols represent experimental data, solid lines represent curve fitting.*

6.3.3 Pepsin

As was discussed earlier, the ε_3 dispersion for pepsin was not clearly observed (Section 5.2.3.3). Even with the temperature study, the ε_3 dispersion was still not clearly revealed (Figure 6.8). Nevertheless, the entire temperature dependence of permittivity is similar with ovalbumin and lysozyme, i.e. the LFD and ε_3 dispersion moved toward higher frequency with increasing temperature.

Figure 6.8 (a) shows a typical temperature dependence of permittivity for hydrated pepsin (0.039 g/g). The data on low hydrated pepsin below 273 K was characterised by a large degree of noise. For this reason, the presentation of dielectric spectra for hydrated pepsin was limited to above 273 K.

As shown in Figure 6.8 (b), the percolation threshold for pepsin (0.039 g/g) was reached closed to 328 K. There was no significant difference in the percolation threshold temperature observed in the LFD and ε_3 dispersions. Both the LFD and ε_3 dispersions moved to lower frequency after reaching 328 K and the strength of the LFD and ε_3 dispersions decreased.

Similar to ovalbumin, there was no transition process observed in hydrated pepsin. After reaching the percolation threshold, both the strength of the LFD and ε_3 dispersions were decreasing up to 363 K. New LFD and ε_3 dispersion were observed at higher temperatures. As shown in Figure 6.8 (c), from 368 K, the permittivity from both new LFD and ε_3 dispersion increased and moved towards high frequency.

(a)

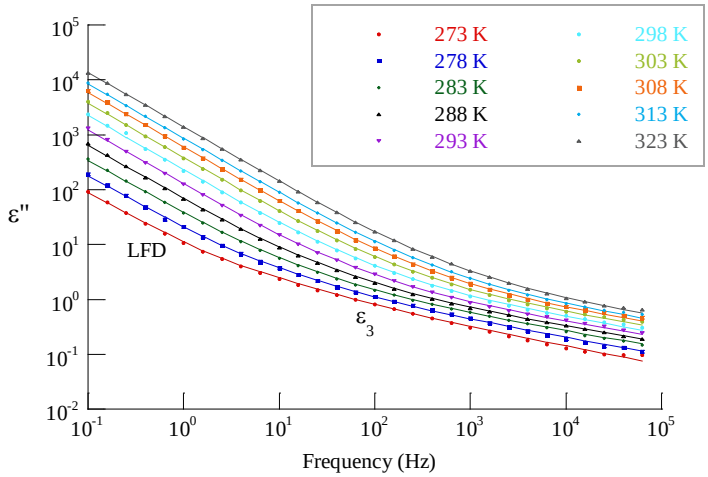

(b)

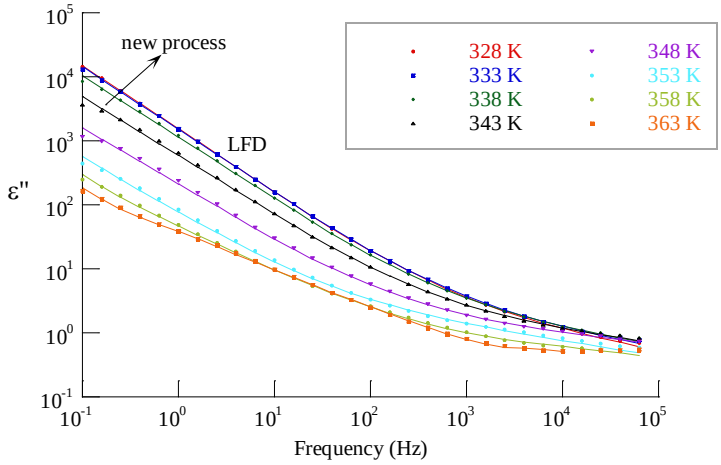

(c)

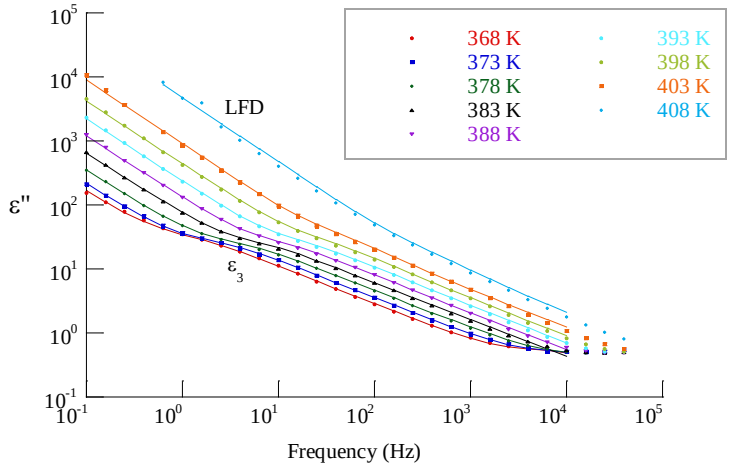

Figure 6.8 *Imaginary permittivity of hydrated pepsin (0.039 g/g) for various temperatures range(a) below percolation threshold (323 K), (b) between 329 – 363 K, (c) between 368 – 408 K. Symbols represent experimental data, solid lines represent curve fitting.*

6.3.4 Relaxation times and pre-exponential factor

Some information from the temperature studies on hydrated proteins may be ascertained more readily from 3-dimensional graphs of permittivity against both temperature and frequency. Figure 6.9 – 6.13 show 3-dimensional graphs of real and imaginary permitivitties versus temperature for different hydration levels of ovalbumin, lysozyme, and pepsin. The figures show clearly the percolation threshold which is identified as the peak of the 3-dimensional graph.

Figures 6.9 – 6.13 showed that, as the hydration level increases, the peak of percolation threshold is less sharp. For higher hydration levels, the peak of the percolation threshold is flattened, except for pepsin. The 3-dimensional graph for pepsin at a low hydration level showed a flattened peak for percolation threshold (Figure 6.12(a)), but the peak became sharper with an increase in hydration (Figure 6.12 (c) and Figure 6.13).

When the hydration level increased, the samples became more 'conducting'. Thus, the accumulation of charge between the sample and the electrodes became more pronounced. The impedance also increased with the higher hydration level. The impedance might be too high for the instrument specification, resulting noise over the low frequency range. The rigorous electrochemical reaction between the samples and the electrodes as mentioned before may also cause the noise at low frequency range. This noise was shown as irregular sharp edges in the 3-dimensional graph at low frequency range for high hydration samples (Figure 6.10 (b), Figure 6.11 (c), and Figure 6.13 (b))

In the 3-dimensional graph, it was also observed a little hump at around 270 - 280 K for ovalbumin (0.047 g/g) and lysozyme (0.037 g/g) (Figure 6.9 (a) and Figure 6.11(a)). This hump was less obvious as the hydration level increases, either because the process occurred at lower temperatures than the experimental window or the process was obscured under LFD process. For lysozyme, this small hump was observed again as the hydration was increased further (Figure 6.11 (c)). This small hump observed on 3-dimensional graph at

just below the room temperature was suggested to be due to the formation of a proton glass. In dielectric study, the proton glass can be identified from a very broad distribution of relaxation times at around the freezing temperature T_f. The freezing temperature itself is defined as the temperature at which the maximum imaginary permittivity occurs at the lowest available frequency[92]. The 3-dimensional graph shows the maximum imaginary permittivity at the lowest frequency, indicated by the small shoulder (see Figure 6.9 (a) and Figure 6.11 (a)). This shoulder was located at ~ 270 K for ovalbumin (0.047 g/g) and ~ 280 K for lysozyme (0.037 g/g). The broad distribution of relaxation times was also shown in Figure 6.4 (a) and Figure 6.6 (a).

The exception again was observed for pepsin. This proton glass was not clearly observed on pepsin. A vague hump observed at pepsin 0.053 and 0.062 g/g (Figure 6.13 (a) and (b)) may be considered as proton glass.

(a) 0.047 g/g

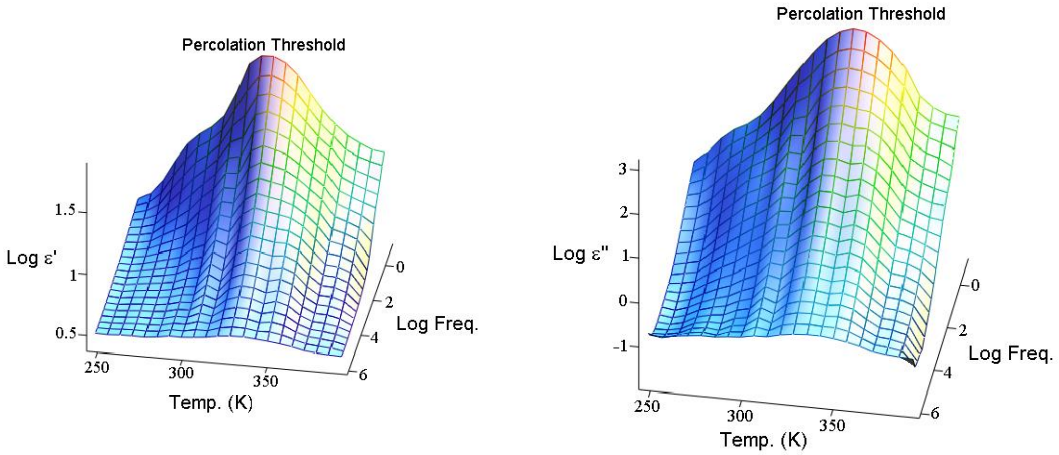

(b) 0.088 g/g

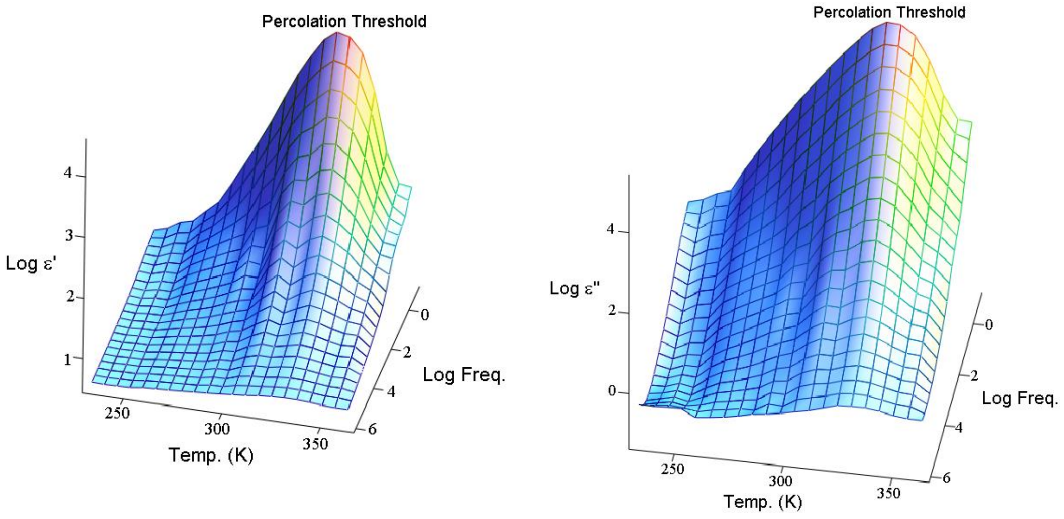

Figure 6.9 *Three dimensional graph of real permittivity ovalbumin obtained from temperature study (a) 0.047 g/g, (b) 0.088 g/g*

(a) 0.202 g/g

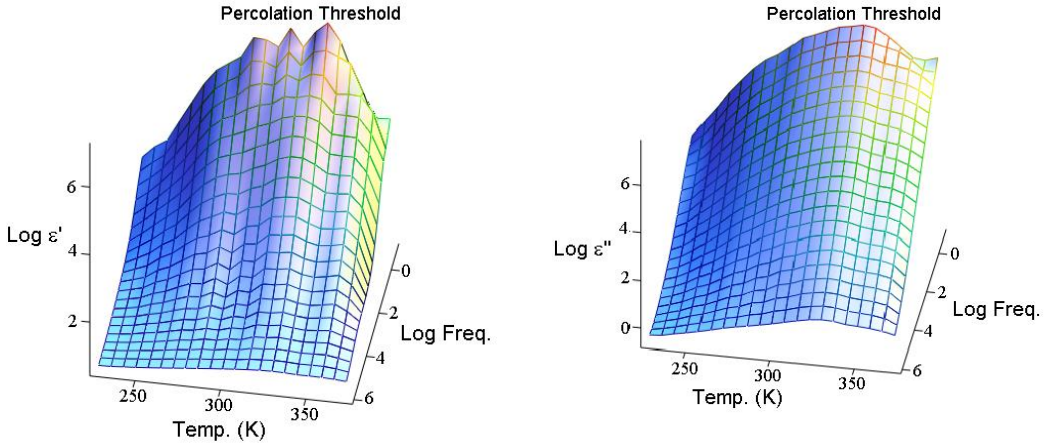

(b) 0.264 g/g

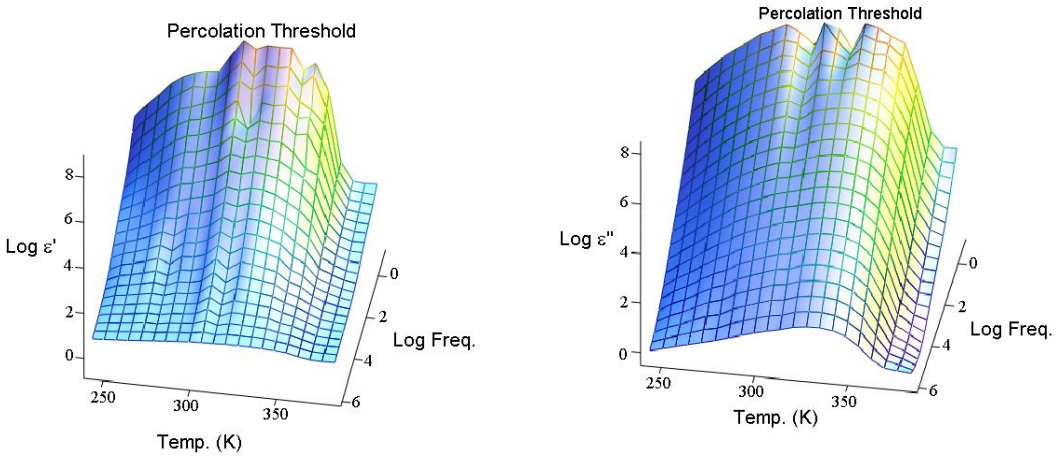

Figure 6.10 *Three dimension graph of real and imaginary permittivities for ovalbumin obtained from temperature study (c) 0.202 g/g, (d) 0.264 g/g.*

(a) 0.037 g/g

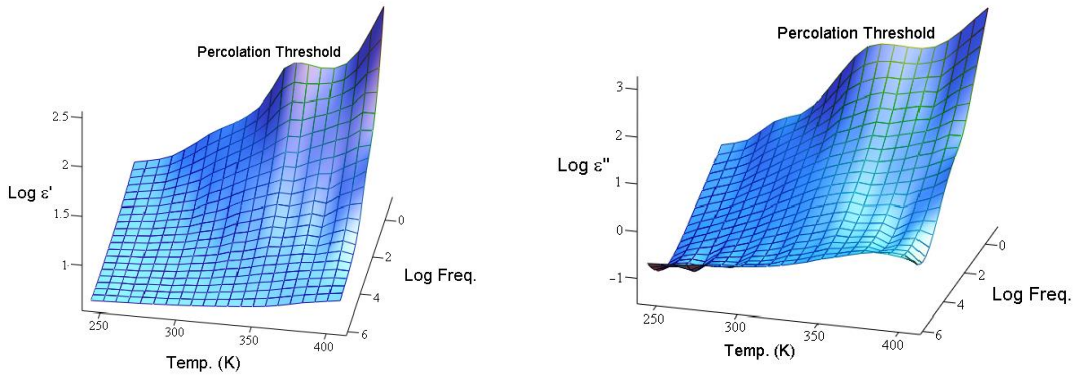

(b) 0.082 g/g

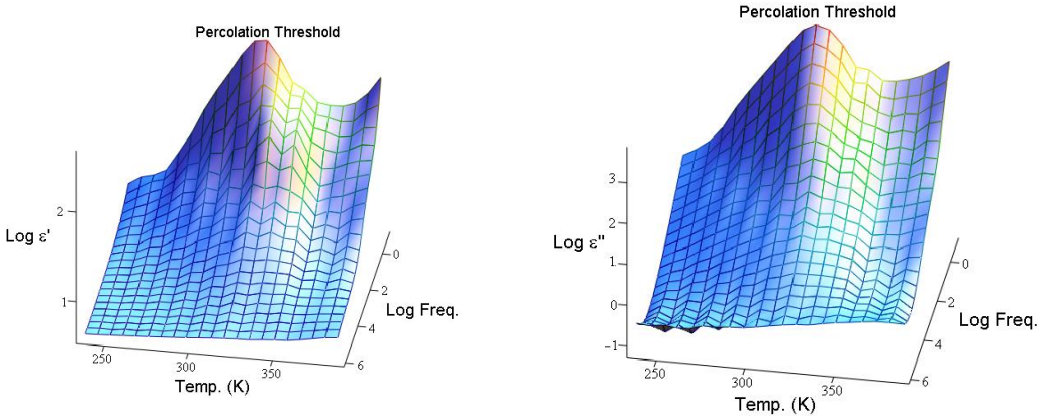

(c) 0.224 g/g

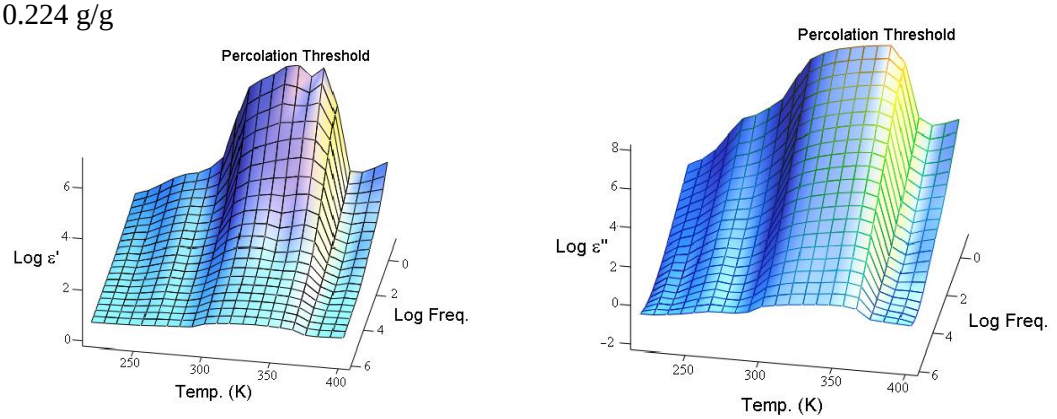

Figure 6.11 *Three dimension graph of real and imaginary permittivities for lysozyme obtained from temperature study (a) 0.037 g/g, (b) 0.082 g/g, and (c) 0.224 g/g.*

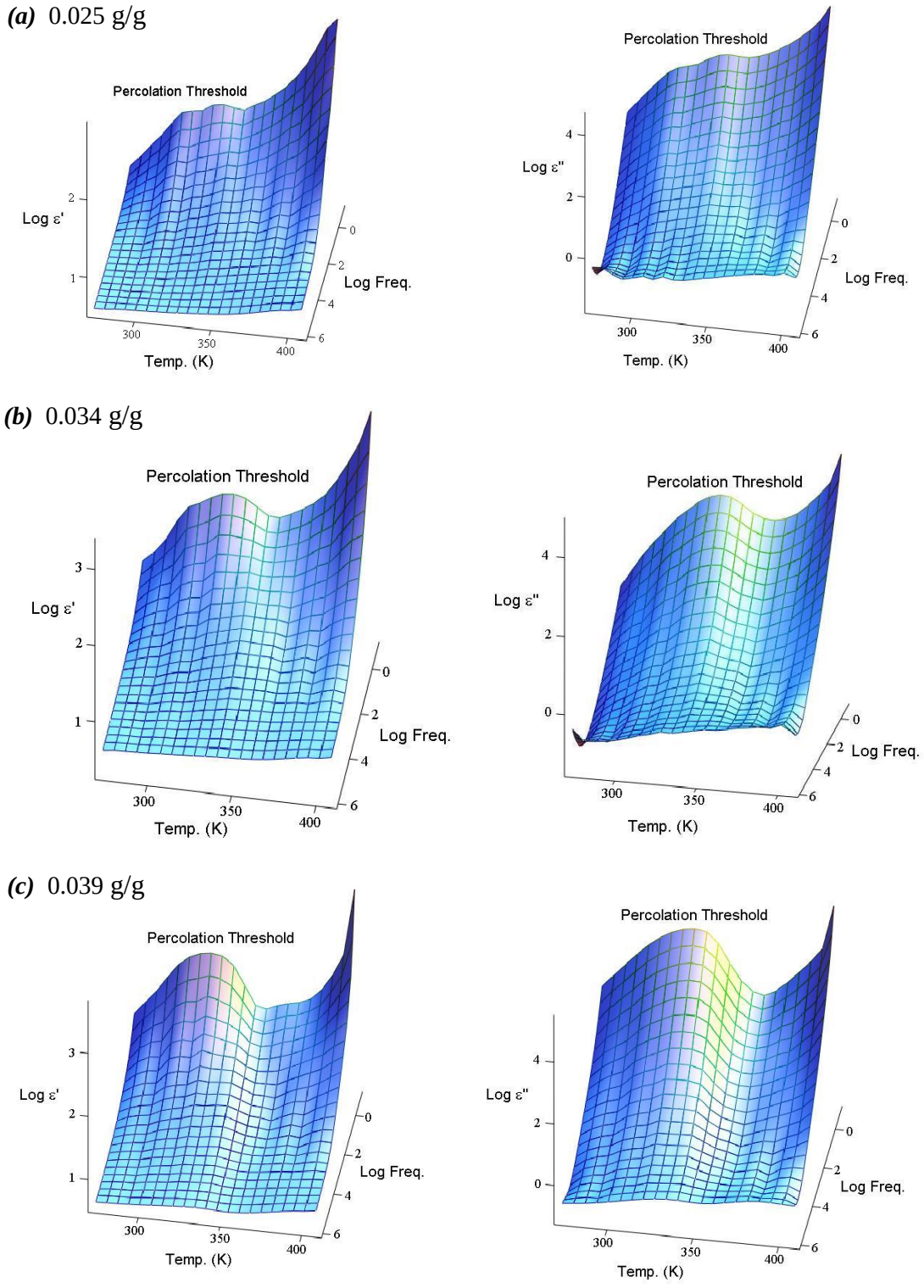

Figure 6.12 *Three dimension graph of real and imaginary permittivities for pepsin obtained from temperature study (a) 0.025 g/g, (b) 0.034 g/g; (c) 0.039 g/g.*

(a) 0.053 g/g

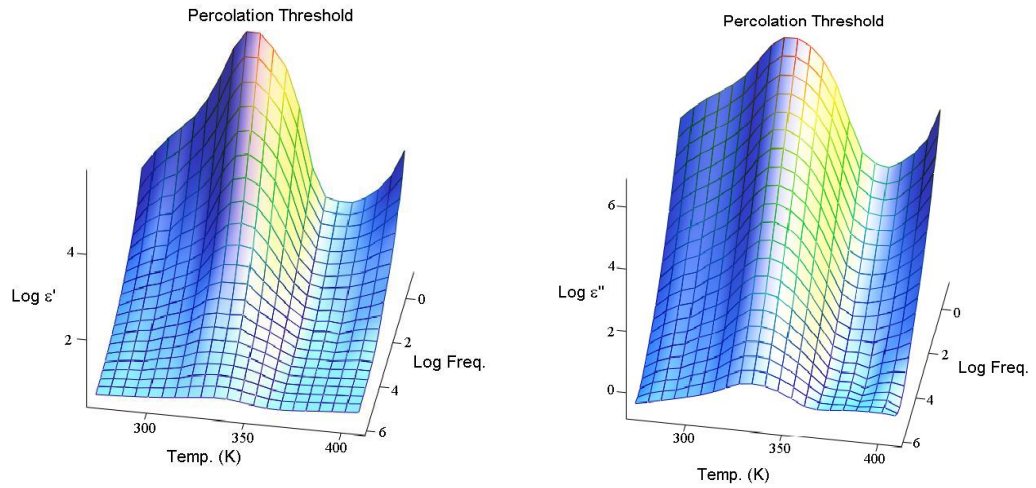

(b) 0.062 g/g

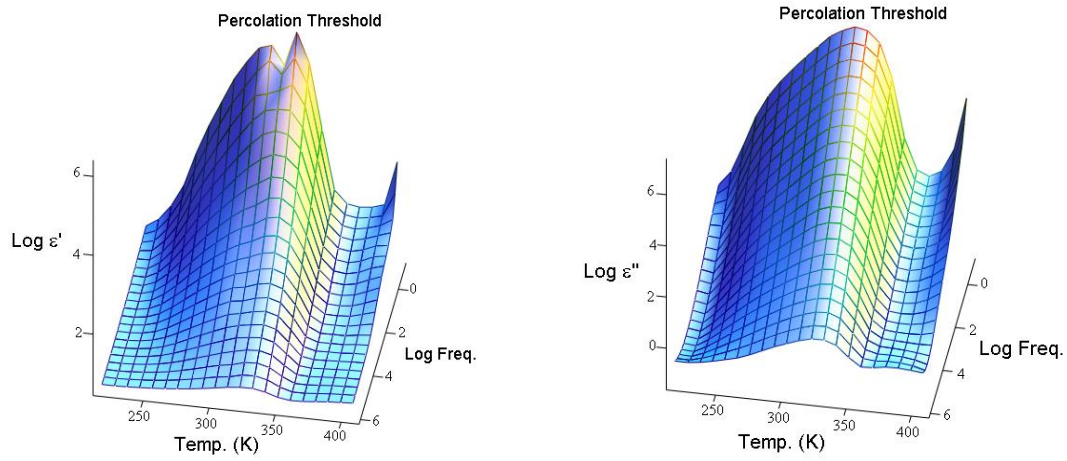

Figure 6.13 *Three dimension graph of real and imaginary permittivities for pepsin obtained from temperature study (a) 0.053 g/g, (b) 0.062 g/g.*

Each complex spectrum for each temperature point was fitted using the circuit model described in Section 5.2.3, i.e. a parallel circuit comprising a constant phase element for the LFD process, and a Davidson-Cole element for ε_3 dispersion located at the higher frequency end of the LFD. From the fitting of dielectric data for each temperature point, dielectric parameters of the sample can be plotted versus temperature.

The main parameters that characterise the properties of the LFD and ε_3 dispersions are the pre-exponential factor *A* and the relaxation times τ_3, respectively. Figure 6.14 – 6.16 show the dependence of relaxation times τ_3 and pre-exponential factor *A* on temperature for various hydration levels of ovalbumin, lysozyme, and pepsin. The percolation threshold of each protein is shown clearly by a maximum in pre-exponential factor *A* of the LFD and a minimum in the relaxation time τ_3 of the ε_3 dispersion .

The fitting result of temperature dependences of relaxation times τ_3 and pre-exponential factor *A* can also be related to the features in 3-dimensional graph. This is also another way to verify the model used for the fitting. Relaxation time is obtained from the frequency in which the peak of the ε_3 dispersion occurred. Relaxation time can be seen as a saddle projection on the sample surface in a 3-dimensional graph. It can also be seen that the pre-exponential factor *A* is actually a projection of LFD at the lowest frequency of experimental window (see inset in Figure 6.14 (b), Figure 6.15 (b), and Figure 6.16 (b)).

The peak from both relaxation times τ_3 and pre-exponential factor *A* is the indication of percolation threshold. At higher hydration level, the percolation threshold moved to a lower temperature. With the increase of hydration level, the peak of percolation threshold became less sharp.

Besides a clear indication of percolation threshold, the temperature dependence of relaxation times τ_3 and pre-exponential factor *A* (Figure 6.14 – 6.16) also showed some detail features, such as: Arrhenius behaviour at below percolation threshold (Section 6.4.1.1), Arrhenius behaviour above percolation threshold, which is only observed clearly

at pepsin and lysozyme (Section 6.4.1.2), and a possibility of VTF (Vogel-Tamman-Fulcher) curvature, which was overlapped with the curvature of percolation threshold (see Section 6.4.2). The sharp point observed at the onset of the high temperature Arrhenius was probably due to phase transition where protein starts to refold.

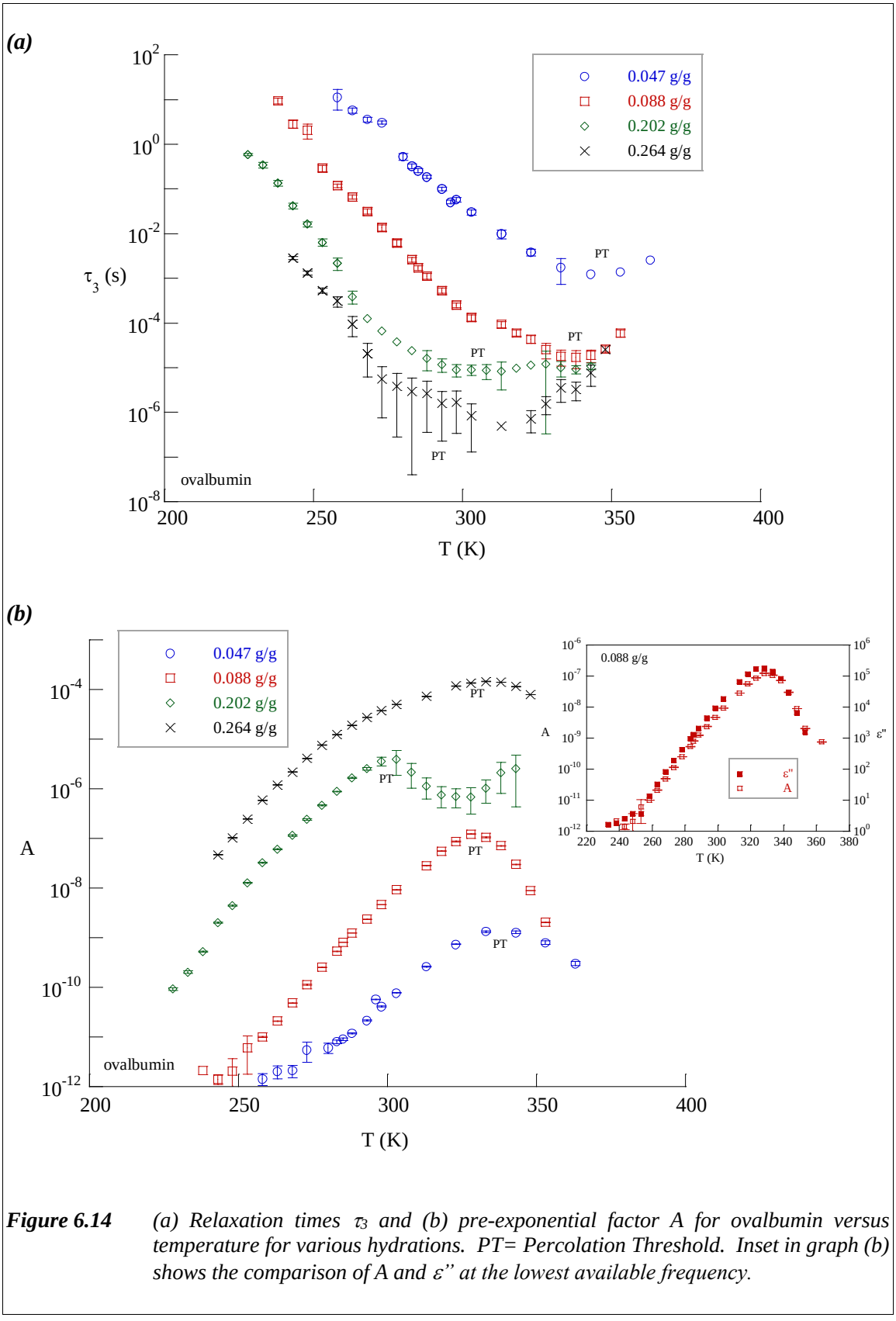

Figure 6.14 *(a) Relaxation times τ_3 and (b) pre-exponential factor A for ovalbumin versus temperature for various hydrations. PT= Percolation Threshold. Inset in graph (b) shows the comparison of A and ε'' at the lowest available frequency.*

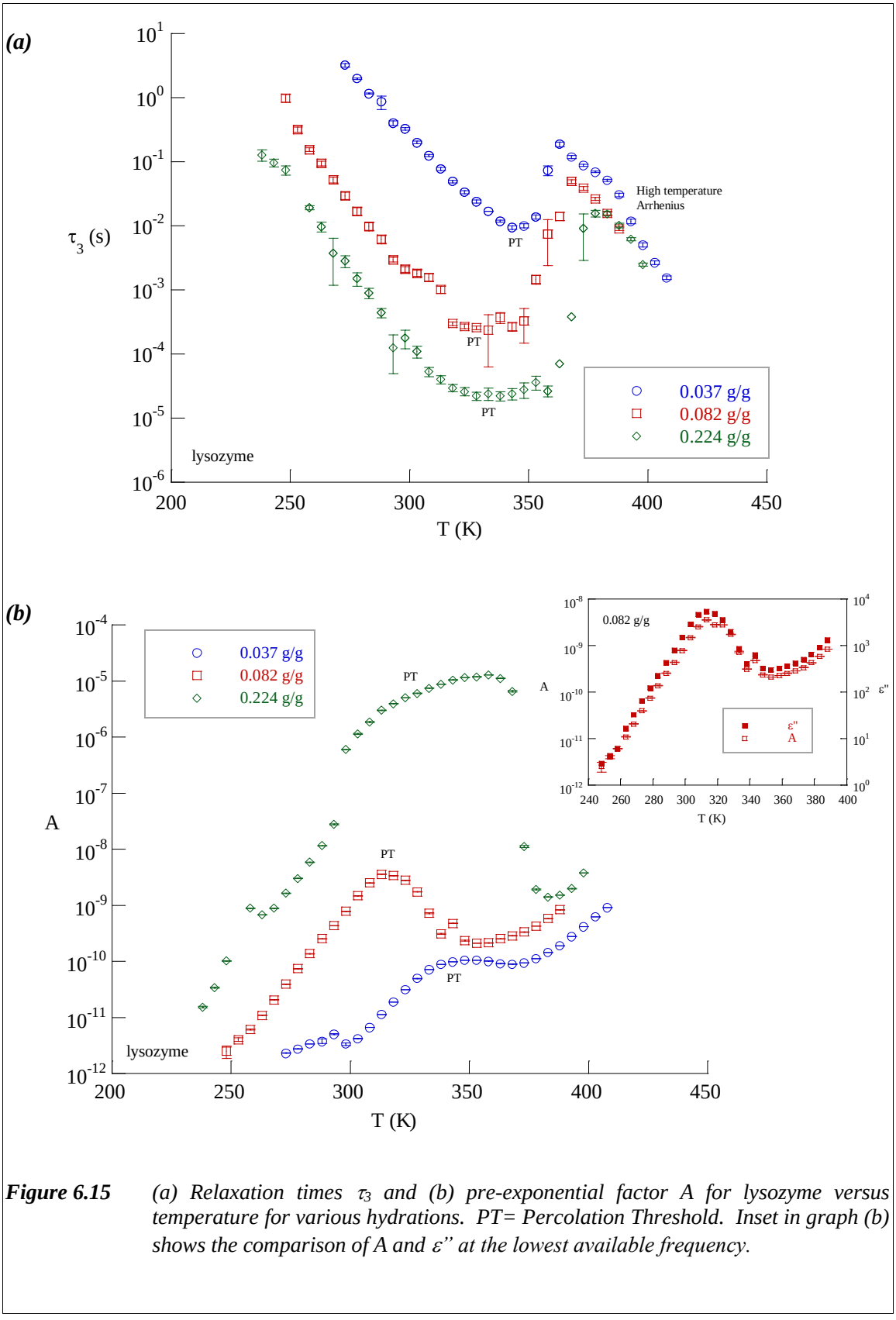

Figure 6.15 *(a) Relaxation times τ_3 and (b) pre-exponential factor A for lysozyme versus temperature for various hydrations. PT= Percolation Threshold. Inset in graph (b) shows the comparison of A and ε'' at the lowest available frequency.*

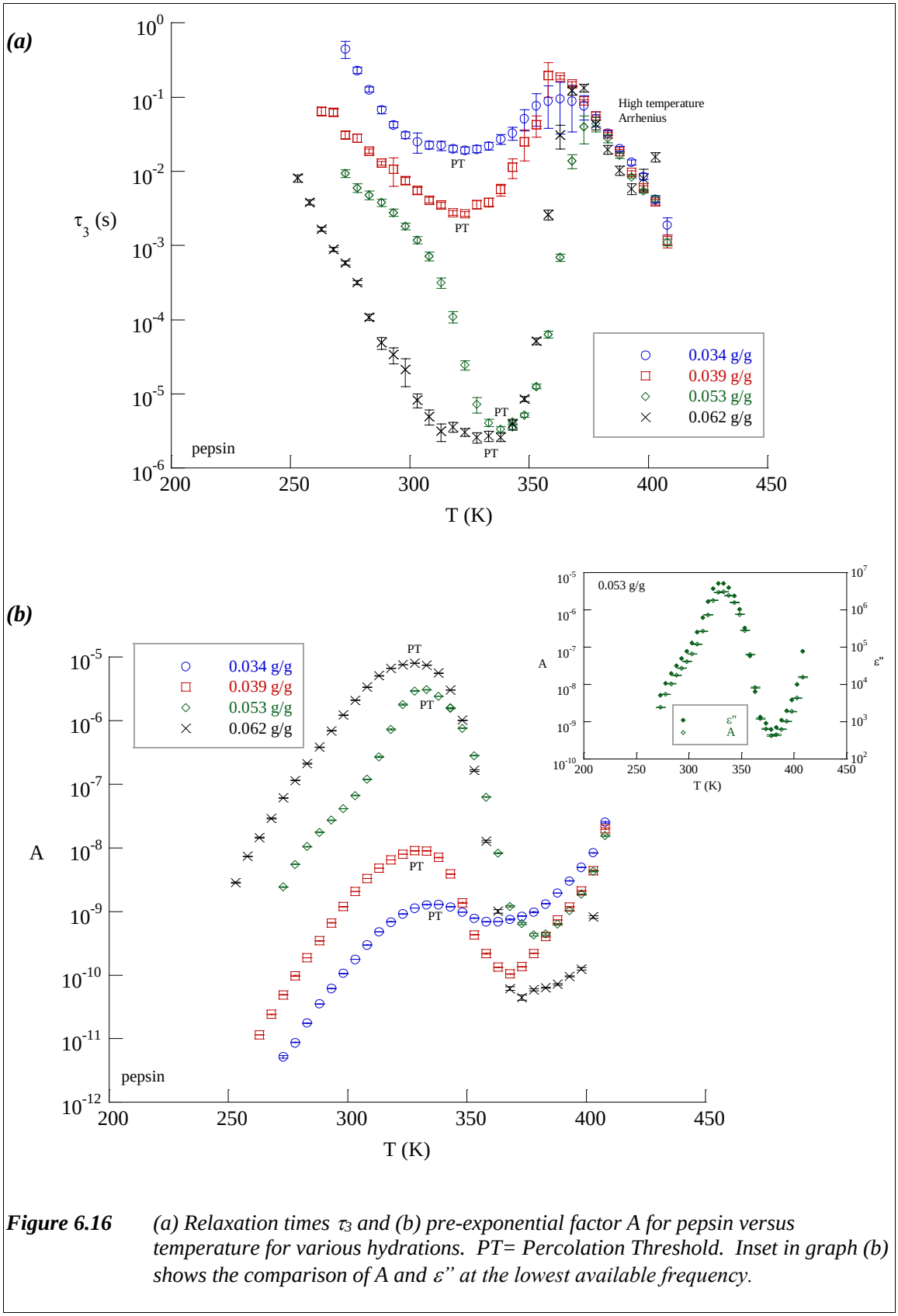

Figure 6.16 *(a) Relaxation times τ_3 and (b) pre-exponential factor A for pepsin versus temperature for various hydrations. PT= Percolation Threshold. Inset in graph (b) shows the comparison of A and ε" at the lowest available frequency.*

6.3.5 Reversible and Irreversible process

A reversibility of dielectric properties of hydrated protein before and after temperature treatment was also investigated. The aims were to examine whether the dielectric properties of proteins change during the temperature study, to investigate the mechanism behind the percolation threshold and its relation to the protein structure, and also to explore the stability of hydrated protein in relation with temperature.

The results show that dielectric properties of hydrated protein are reversible when heated up to percolation threshold temperature, but irreversible when heated far beyond the percolation threshold temperature. Figure 6.17 shows the relaxation time τ_3 and pre-exponential factor A, before and after temperature study, for ovalbumin 0.047 g/g. The figure shows that the relaxation times τ_3 are comparable before and after temperature measurement up to the percolation threshold (Figure 6.17 (a)). The similar observation was also found for the pre-exponential factor A, although slight differences are observed at temperature around the percolation threshold, where the A values after temperature measurement were slight lower than those before temperature measurement (Figure 6.17 (b)). The percolation threshold temperature observed in this hydrated ovalbumin 0.047g/g was ~ 343 K.

The inset in Figure 6.17 (a) shows the imaginary permittivity of ovalbumin (0.047 g/g) at 298 K, before and after temperature studies. Three plots of the imaginary permittivity overlapped when the temperature measurement was carried out just up to the percolation threshold temperature (1st measurement, 2nd measurement, and 3rd measurement). After the temperature measurement far beyond the percolation threshold temperature, the plot from 4th measurement shows a difference, i.e. shifted to a lower frequency. The pattern of the plot itself did not change, i.e. consists of the LFD and the ε_3 dispersion. The shift toward lower frequency after measurement beyond the percolation threshold temperature may indicate partial water loss from the sample after temperature measurement. The fact that

the plot from 4th measurement still showed the presence of the LFD and the ε_3 dispersion, indicates that the sample did not loss all the water, even though the measurement has been carried out until 393 K.

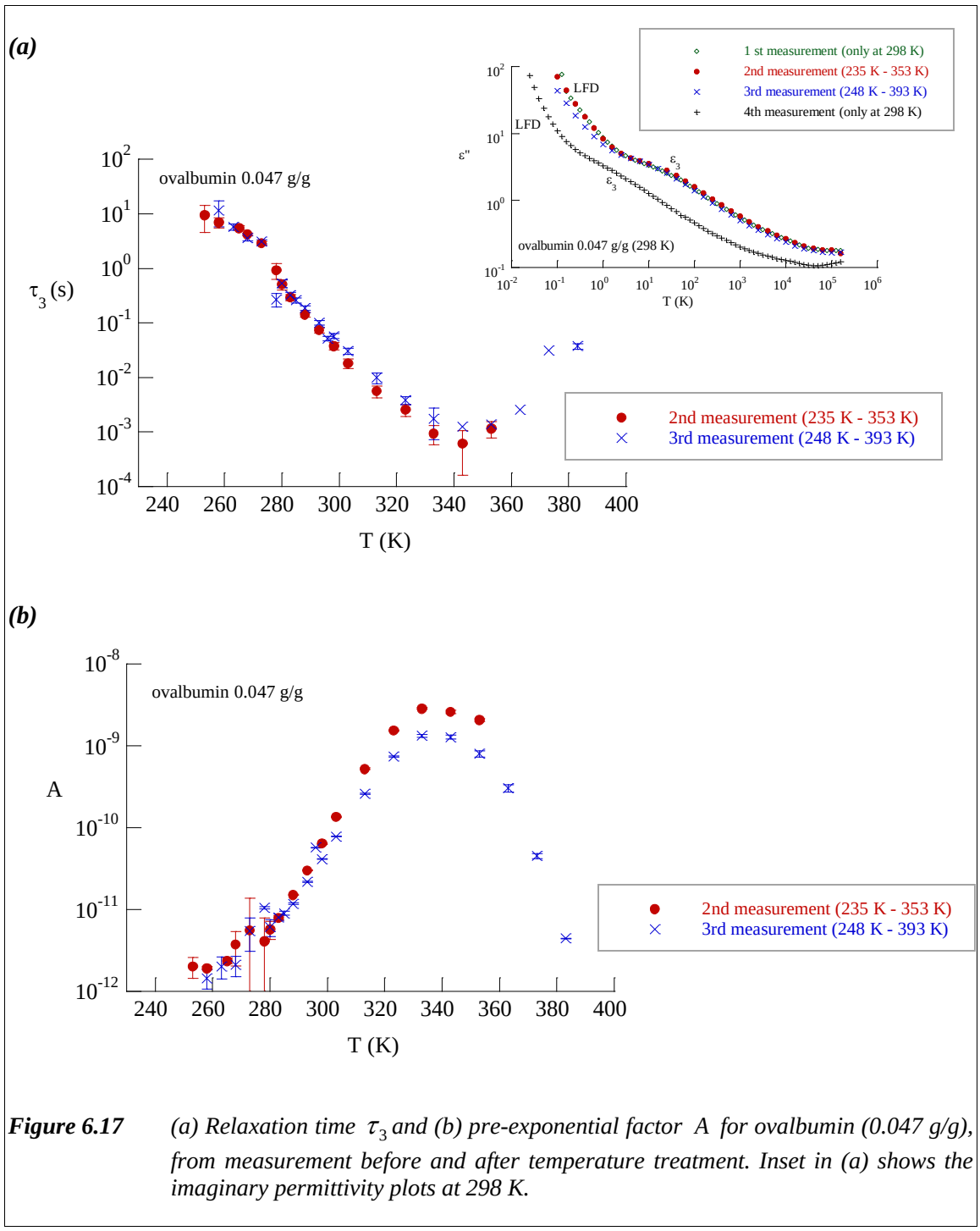

Figure 6.17 *(a) Relaxation time τ_3 and (b) pre-exponential factor A for ovalbumin (0.047 g/g), from measurement before and after temperature treatment. Inset in (a) shows the imaginary permittivity plots at 298 K.*

6.4 Arrhenius and VTF behaviour

Relaxation time as a main parameter in describing dielectric properties of material, may be related to the energy activation of the system via a temperature dependent study. This was generally expressed by Arrhenius behaviour as will be explained in this section.

6.4.1 Activated behaviour

The general empirical equation for relaxation times related to the absolute temperature may be expressed as [93]:

$$\tau \propto T^{-n} \exp(\Delta H / RT) \tag{6.1}$$

where:

τ	=	relaxation time (s)			
ΔH	=	activation energy (J mol^{-1})			
R	=	universal gas constant (8.314 J mol^{-1} K^{-1})			
T	=	absolute temperature (K)			
n	=	exponential constant;	n	= 0	for Arrhenius
			n	= 0.5	for Bauer
			n	= 1	for Eyring equation

The relaxation time is proportional to the inverse of the frequency of jump between two alternative states. Based on this activated states, the variation of relaxation times with temperature may be expressed as:

$$\tau = \frac{h}{kT} \exp\left(\frac{\Delta F}{RT}\right) \tag{6.2}$$

where:

h	=	Planck constant (6.626 x 10^{-34} J s)
k	=	Boltzmann constant (1.38 x 10^{-23} J K^{-1})

ΔF = the difference between the free energy of the activated state and the ground state

Since $\Delta F = \Delta H - \Delta S$, equation (6.2) can be expressed as:

$$\tau = \frac{h}{kT}\exp\left(\frac{-\Delta S}{R}\right)\exp\left(\frac{\Delta H}{RT}\right) \tag{6.3}$$

where:

ΔS = entropy of the activation, which is related to the ratio of the number of available sites between the activated states and inactivated states (ground state).

ΔH = enthalpy of the activation, which is related to the barrier height between two alternative states

Equation (6.3) is also known as Eyring behaviour. By taking the natural logarithmic, Equation (6.3) may also be expressed as:

$$\ln(\tau T) = \ln\left(\frac{h}{k}\right) - \frac{\Delta S}{R} + \frac{\Delta H}{RT} \tag{6.4}$$

Equation (6.1) shows that for Arrhenius behaviour, n = 0:

$$\tau = A\exp\left(\frac{\Delta H}{RT}\right) \tag{6.4a}$$

The relationship between logarithmic relaxation times with the inverse temperature in Arrhenius behaviour is linear ($\ln\tau \propto T^{-1}$). Correspondence with this, the Eyring expression in Equation (6.4) also shows the linear relationship between $\log(\tau T)$ and the inverse temperature ($\ln\tau T \propto T^{-1}$). To distinguish between Arrhenius and Eyring behaviours, Equation (6.4) may also be expressed as:

$$\tau = \frac{h}{kT}\exp\left(\frac{-\Delta S^*}{R}\right)\exp\left(\frac{\Delta H^*}{RT}\right) \tag{6.4b}$$

where ΔS^* and ΔH^* are the entropy and enthalpy activations for Eyring behaviour. The entropy activation for Arrhenius behaviour may be determined by using equation:

$$A = \nu_0^{-1} \exp\left(\frac{-\Delta S}{R}\right) \tag{6.4c}$$

where ν_0 is the lattice quantum vibration (~ 10^{12} Hz). The difference in enthalpy activation between Eyring and Arrhenius behaviours may be not too significant, while the entropy activation between these behaviours may differ significantly. The relations of enthalpy and entropy activations between Eyring and Arrhenius behaviours are shown in Appendix A4.

6.4.1.1 Arrhenius behaviour at below percolation threshold

The graphs of logarithmic relaxation times with temperature have been shown previously in Figure 6.14, Figure 6.15, and Figure 6.16 for some representative hydration levels for hydrated ovalbumin, lysozyme, and pepsin, respectively. Figure 6.18 shows the plot of data range fulfilling Arrhenius behaviour below percolation threshold. By taking the gradient of the curve $\ln(\tau)$ versus $(1000/T)$, the enthalpy or activation energy (ΔH) of the system can be determined. The entropy of the system was calculated from Equation (6.4c). Figure 6.19 shows the enthalpy and entropy of various hydration levels of ovalbumin, lysozyme, and pepsin. The features of activation energy (ΔH) for various hydration levels as shown in Figure 6.19, also highlight the existence of transition at hydration level, which is coincident with the critical hydration levels discussed earlier in Chapter 5 (see Section 5.4.3). For each protein, ΔH increased rapidly up to h_{c1}, and then gradually increased between h_{c1} and h_{c2}, and almost constant at above h_{c2}.

(a)

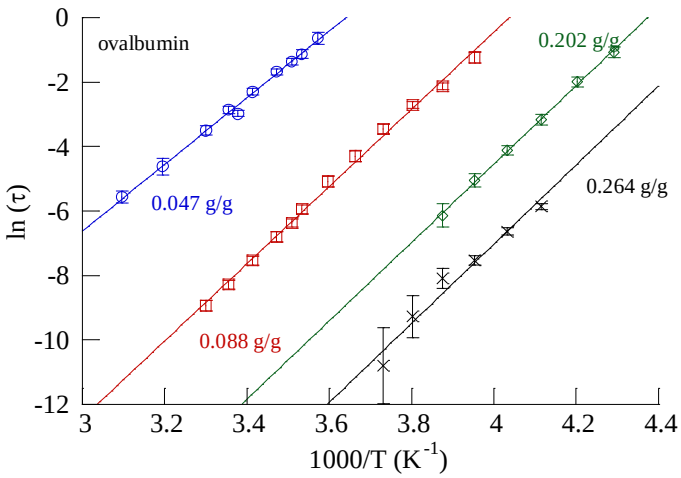

(b)

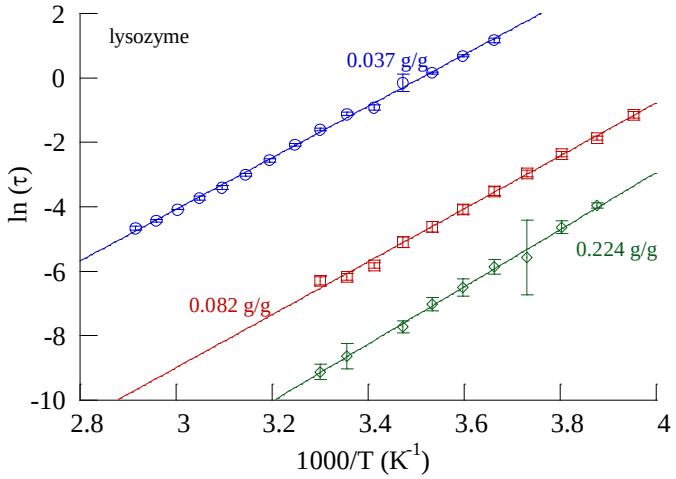

(c)

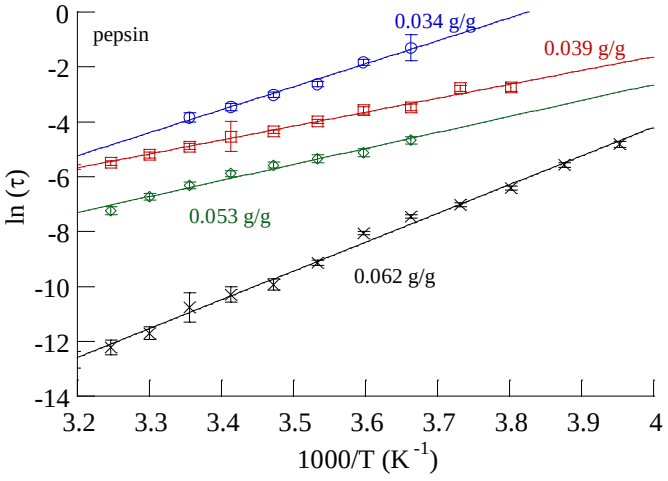

Figure 6.18 *Arrhenius behaviour shown in the specific temperature ranges for (a) ovalbumin, (b) lysozyme, and (c) pepsin.*

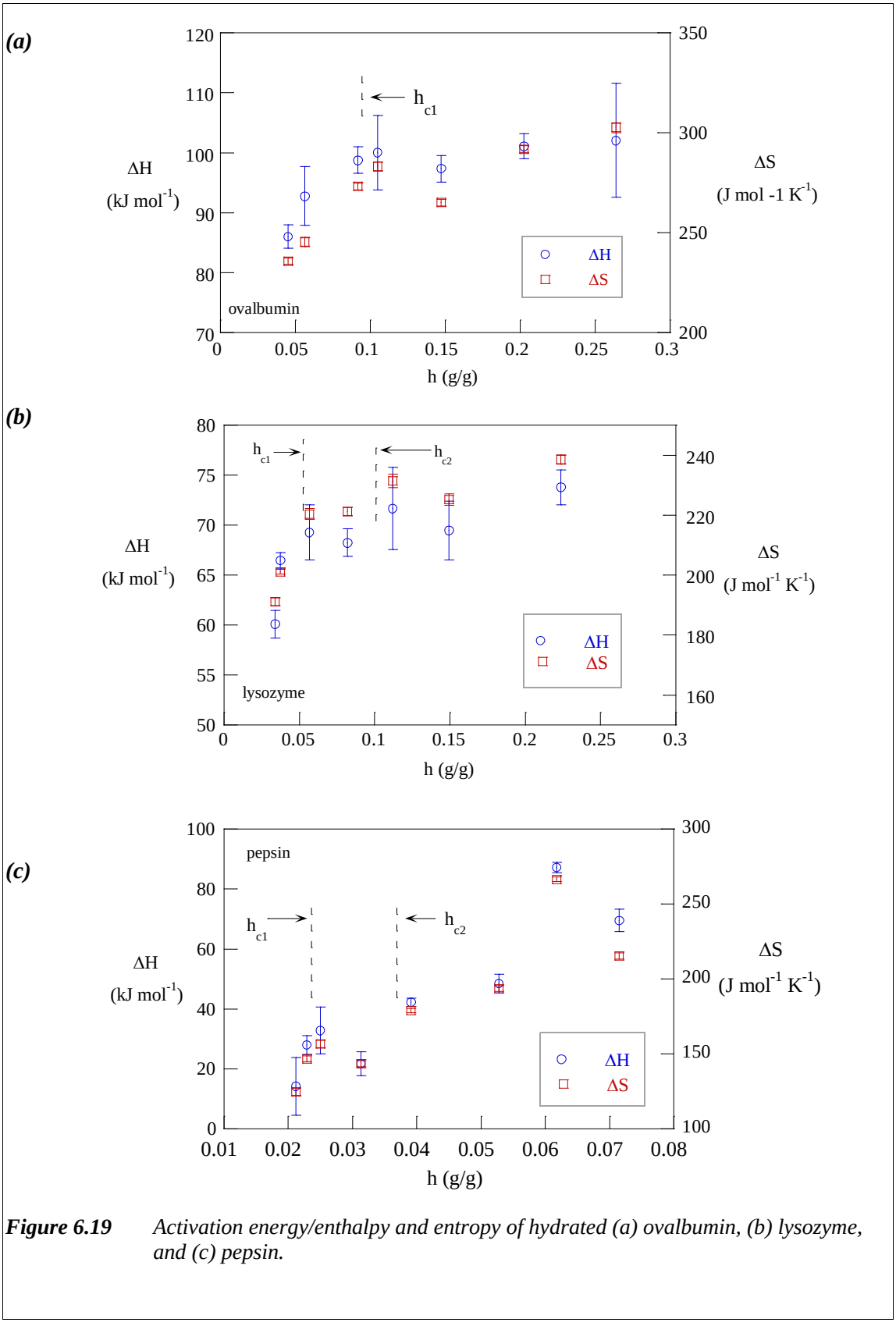

Figure 6.19 *Activation energy/enthalpy and entropy of hydrated (a) ovalbumin, (b) lysozyme, and (c) pepsin.*

6.4.1.2 Arrhenius behaviour above percolation threshold

Besides Arrhenius plot at below percolation threshold, lysozyme and pepsin showed another Arrhenius behaviour at high temperature after percolation threshold (Figure 6.15 and Figure 6.16 (a)). For ovalbumin, this high temperature Arrhenius was not observed. It was probably located at higher temperature than experimental window. Particularly for pepsin, the high temperature Arrhenius was observed more clearly compared with lysozyme.

Figure 6.20 shows the high temperature Arrhenius plots for lysozyme and pepsin for various hydration levels. It is interesting that all these high temperature Arrhenius plots are crossed over approximately in one temperature point, i.e. ~ 395 K for lysozyme and ~ 380 K for pepsin. This temperature point may correspond to the total loss of sorbed water in the sample.

The enthalpy and entropy of various hydrated lysozyme and pepsin obtained from the high temperature Arrhenius plot is shown in Figure 6.21. The data points of ΔH and ΔS for high temperature Arrhenius are scattered for both lysozyme and pepsin. In the range of error bars, the data appears to be constant over various hydration levels.

(a)

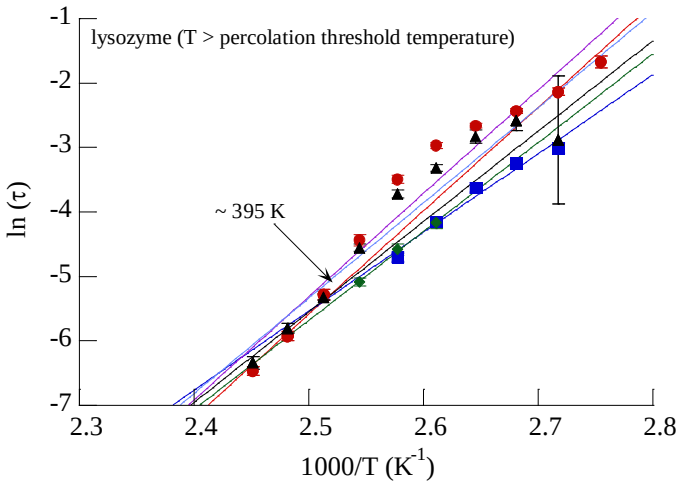

(b)

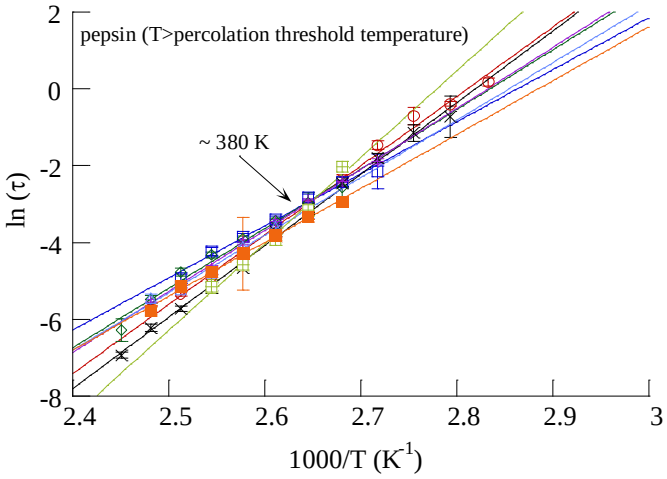

Figure 6.20 *High temperature Arrhenius plots for various hydration levels for (a) lysozyme, (b) pepsin.*

(a)

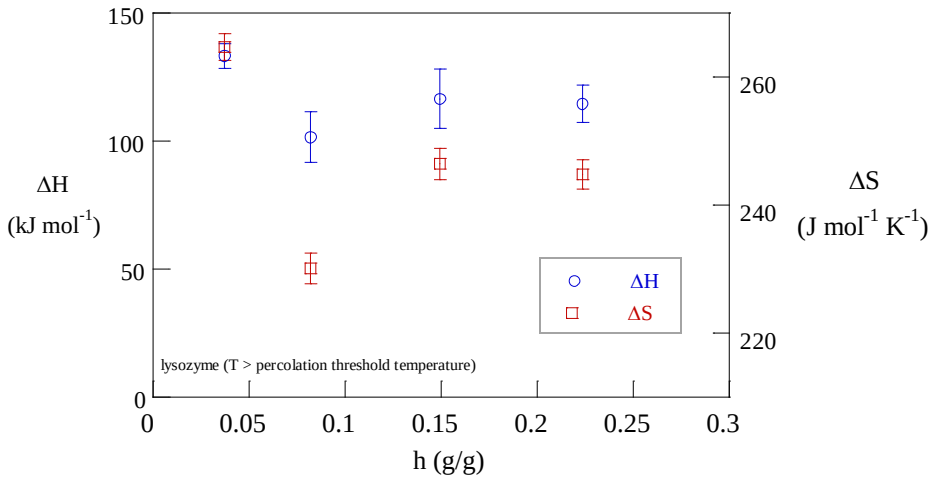

(b)

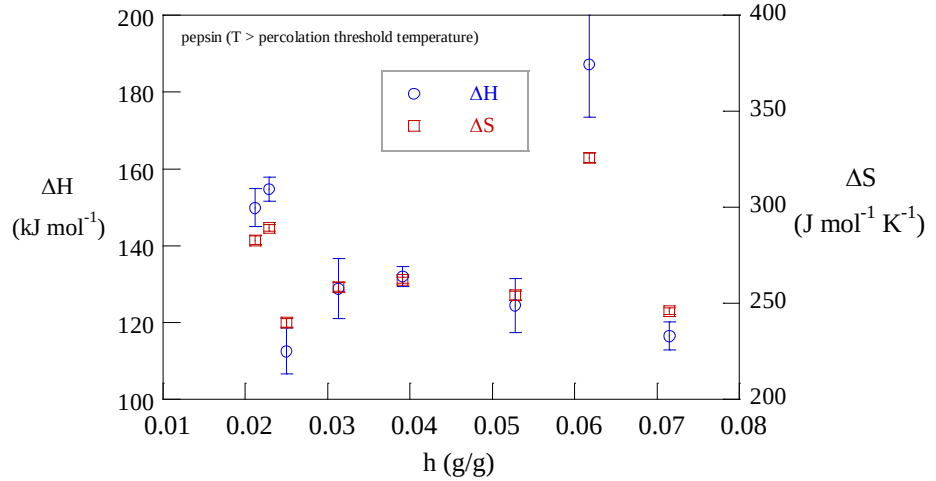

Figure 6.21 *Activation energy/enthalpy and entropy of (a) lysozyme, (b) pepsin obtained above percolation threshold.*

6.4.2 VTF (Vogel-Tamman-Fulcher)

In some cases, the temperature dependence of the relaxation times (ln τ versus T^{-1}) shows a curvature instead of linearity. This dependence can be described by the Vogel-Tamman-Fulcher-Hesse equation, which is usually called as VTF equation[94, 95]:

$$\tau(T) = 2\pi f_0 \exp\left(\frac{A_{VTF}}{T - T_{VTF}}\right) \tag{6.5}$$

where:

f_0 = pre-exponential frequency, which is in the order of lattice vibration frequency ($f_0 \approx 10^{10} - 10^{13}$ Hz)

T_{VTF} = ideal glass transition temperature generally 30 – 70 K below T_g or VTF characteristic temperature of the material, sometimes is identified as a true second-order transition corresponding to the vanishing of the excess entropy[96, 97]

A_{VTF} = constant VTF parameter, related either to an activation energy or to thermal expansion coefficient of the free volume.

Sometimes A is expressed as

$$A_{VTF} = DT_{VTF} \tag{6.6}$$

where:

D = strength parameter, which is a measure of the fragility of the hydrogen-bonded glass former.

For ovalbumin and lysozyme, the VTF behaviour was found at higher hydration level. However, for pepsin, the VTF behaviour was observed at lower hydration (Figure 6.12 (a) and Figure 6.16 (a)). Figure 6.14 and Figure 6.15 show that at higher hydration, the peak of percolation threshold for ovalbumin (0.202 g/g and 0.264 g/g) and lysozyme (0.224 g/g)

is no longer sharp, but forming a curvature. This curvature at higher hydration can be fitted by VTF model, which is later shown in Section 6.4.4. The flattened peak of percolation threshold is shown clearly in 3-dimensional graph (Figure 6.10 and Figure 6.11 (c)).

6.4.3 Arrhenius verification

Determination of either Arrhenius, Eyring, or VTF behaviour from the curve of log relaxation times versus inverse temperature should be verified further. The limited range of temperature may give a straight line which is actually a part of very wide curvature. So, probably what is thought as an Arrhenius behaviour is actually a VTF or Eyring behaviour (see Appendix A4). The verification of Arrhenius behaviour can be carried out by using a derivative of log relaxation time over inverse temperature ($\frac{d\ln(\tau)}{d(1/T)}$)[98]. The derivation of this derivative function for Arrhenius, Eyring, and VTF verification is shown in Appendix A4. Based on Equation (A4.4), the derivative of log relaxation times with inverse temperature should give a straight line, independent on the temperature:

$$\frac{d\ln(\tau)}{d(1/T)} = \frac{\Delta H}{R} \tag{6.7}$$

A representative description for verification of Arrhenius behaviour for hydrated ovalbumin, lysozyme, and pepsin is shown in Figure 6.22, Figure 6.23, and Figure 6.24, respectively.

From the curve of ln τ vs. T^{-1}, the Arrhenius behaviour for hydrated ovalbumin (0.088 g/g) appeared in the range of inverse temperature between ~ 0.033 – 0.044 K^{-1} (Figure 6.22 (b)). In the same range of inverse temperature, the derivative of log relaxation times over inverse temperature gave a straight line, independent of temperature (Equation 6.8):

$$\left(\frac{d\ln(\tau)}{d(1/T)}\right)_{\text{ovalbumin (0.088 g/g)}} = \left(\frac{\Delta H}{R}\right)_{\text{ovalbumin (0.088 g/g)}} = 11797.24 \tag{6.8}$$

The activation energy can also be calculated from Equation (6.8):

$$(\Delta H)_{\text{ovalbumin (0.088 g/g)}} = 11797.24x\text{R} \tag{6.9}$$

$$(\Delta H)_{\text{ovlabumin (0.088 g/g)}} \approx 98 \text{ kJ.mol}^{-1} \tag{6.10}$$

If the response is either Eyring or VTF, then Figure 6.22 (c) and (d) should show the linear dependence of temperature (for Eyring) and linear dependence of inverse temperature (for VTF), following Equation (A4.11) and Equation (A4.15), respectively.

For hydrated lysozyme (0.037 g/g) the Arrhenius behaviour appeared in the range of inverse temperature between ~ 0.029 – 0.037 K^{-1} (Figure 6.23 (b)). In the same range of inverse temperature, the derivative of log relaxation times with inverse temperature gave a straight line, independent on the temperature:

$$\left(\frac{d\ln(\tau)}{d(1/T)}\right)_{\text{lysozyme (0.037 g/g)}} = \left(\frac{\Delta H}{R}\right)_{\text{lysozyme (0.037 g/g)}} = 7880.18 \tag{6.11}$$

The activation energy calculated from Equation (6.11):

$$(\Delta H)_{\text{lysozyme(0.037 g/g)}} = 7880.18x\text{R} \tag{6.12}$$

$$(\Delta H)_{\text{lysozyme(0.037 g/g)}} \approx 65.5 \text{ kJ mol}^{-1} \tag{6.13}$$

High temperature Arrhenius for lysozyme (0.037 g/g) in the inverse temperature range between ~ 0.025 – 0.027 K^{-1}, only involves few points, and therefore it may not be really accurate.

Again, if the response is either Eyring or VTF, then Figure 6.23 (c) and (d) should show the linear dependence of temperature (for Eyring) and linear dependence of inverse temperature (for VTF), following Equation (A4.11) and Equation (A4.15), respectively.

Unlike ovalbumin and lysozyme, hydrated pepsin (0.053 g/g) clearly showed two Arrhenius behaviours, i.e. at low and high temperature (Figure 6.24 (b)). Low temperature Arrhenius plot for pepsin were observed in the range of inverse temperature between ~

0.032 – 0.038 K^{-1}, while the high temperature Arrhenius plot were found in the range of inverse temperature between 0.025 – 0.027 K^{-1}.

For Arrhenius plot at low temperature:

$$\left(\frac{d\ln(\tau)}{d(1/T)}\right)_{\text{pepsin (0.053g/g) LT}} = \left(\frac{\Delta H}{R}\right)_{\text{pepsin (0.053g/g) LT}} = 5345.62 \tag{6.14}$$

$$(\Delta H)_{\text{pepsin (0.053g/g) LT}} = 5345.62x\text{R} \tag{6.15}$$

$$(\Delta H)_{\text{pepsin (0.053g/g) LT}} \approx 44.4\ \text{kJ mol}^{-1} \tag{6.16}$$

For Arrhenius plot at high temperature:

$$\left(\frac{d\ln(\tau)}{d(1/T)}\right)_{\text{pepsin (0.053g/g) HT}} = \left(\frac{\Delta H}{R}\right)_{\text{pepsin (0.053g/g) HT}} = 14930.88 \tag{6.17}$$

$$(\Delta H)_{\text{pepsin (0.053g/g) HT}} = 14930.88x\text{R} \tag{6.18}$$

$$(\Delta H)_{\text{pepsin (0.053g/g) HT}} \approx 124\ \text{kJ mol}^{-1} \tag{6.19}$$

Similar as explained above, if the response is either Eyring or VTF, then Figure 6.24 (c) and (d) should show the linear dependence of temperature (for Eyring) and linear dependence of inverse temperature (for VTF), following Equation (A4.11) and Equation (A4.15), respectively.

All the activation energy (ΔH) calculated above is comparable with the activation energy shown in Figure 6.19 and Figure 6.21.

(a)

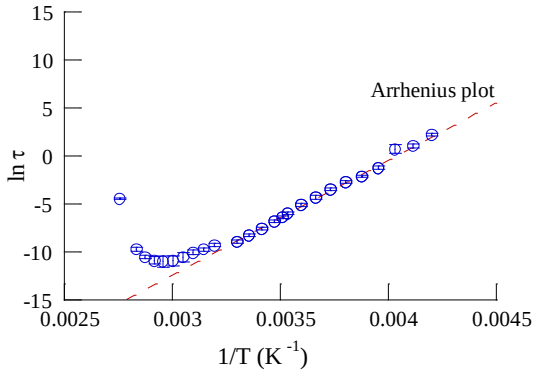

(b)

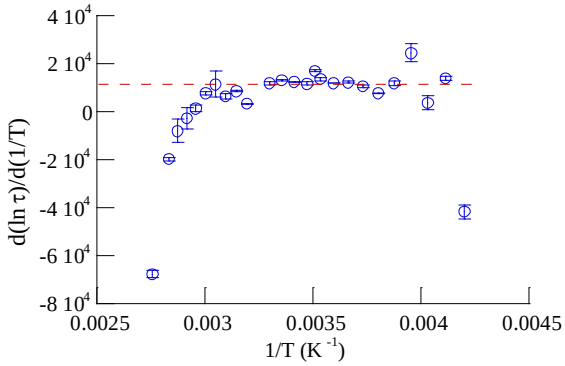

(c)

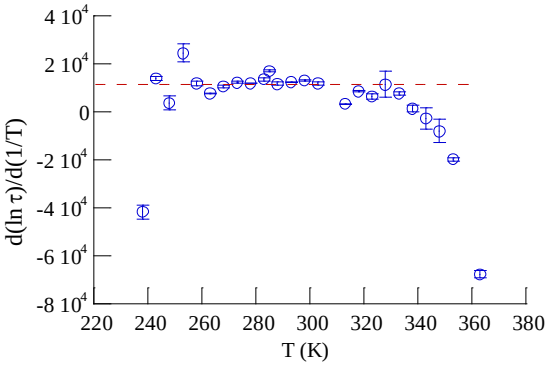

(d)

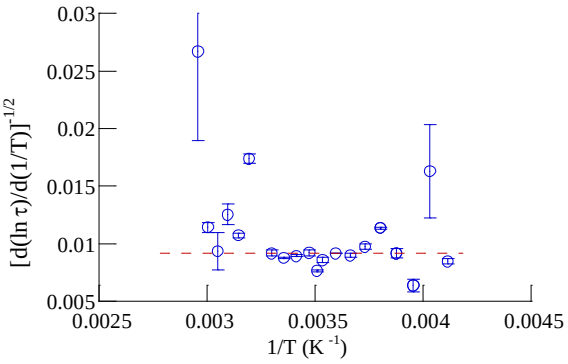

Figure 6.22 *(a) Relaxation times of ovalbumin (0.088 g/g) over various temperatures and the derivtive plots for (b) Arrhenius, (c) Eyring, and (d) VTF behaviour.*

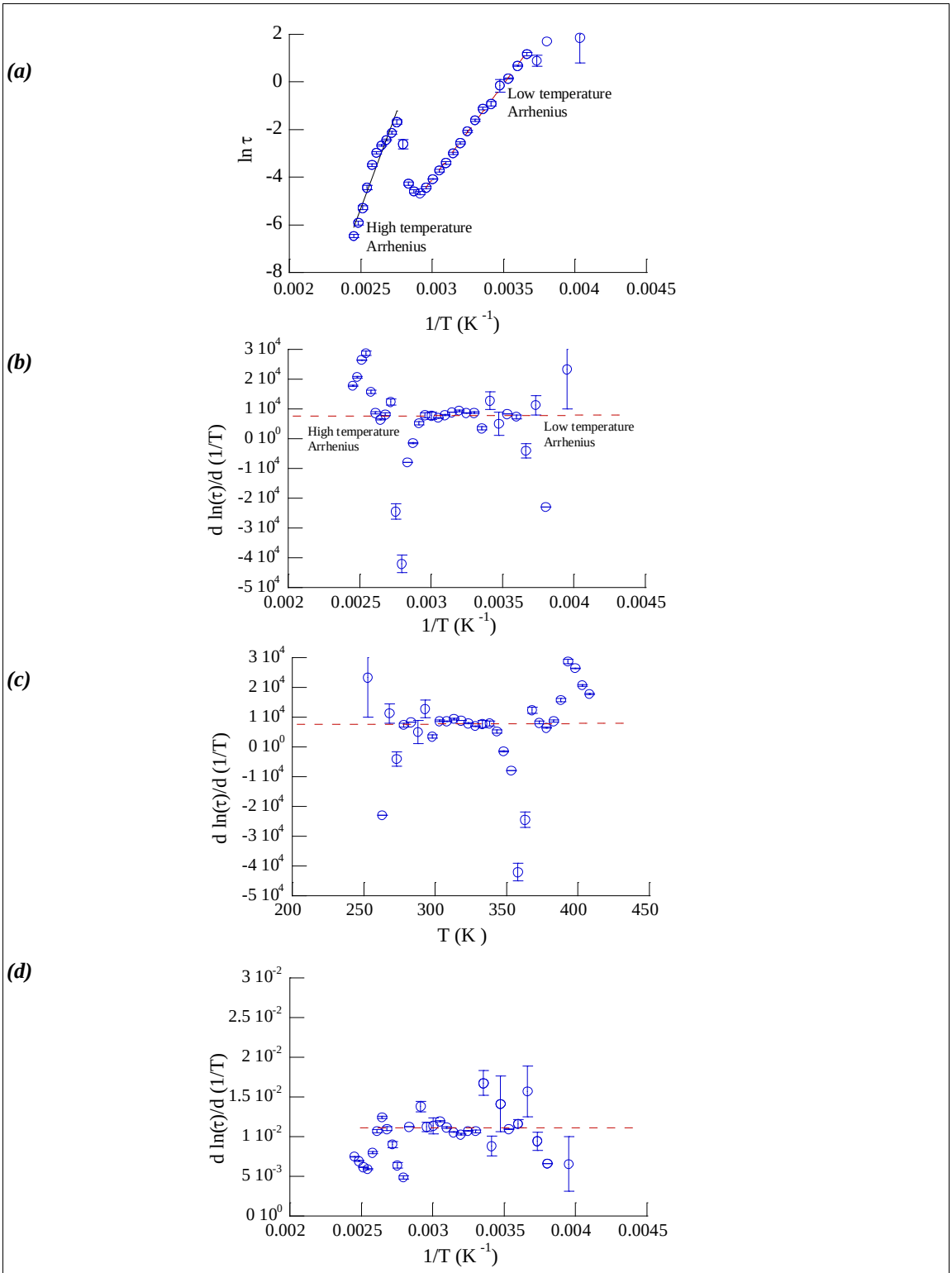

Figure 6.23 *(a) Relaxation times of lysozyme (0.037 g/g) over various temperatures and the derivative plots for (b) Arrhenius, (c) Eyring, and (d) VTF behaviour.*

(a)

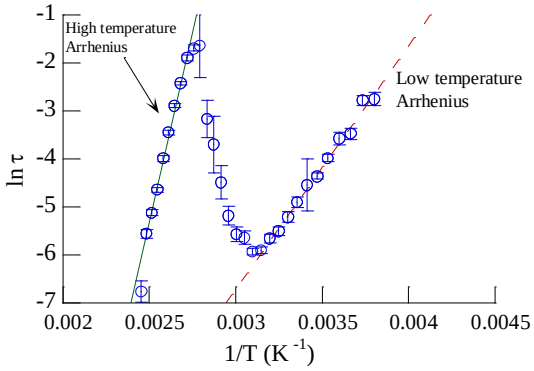

(b)

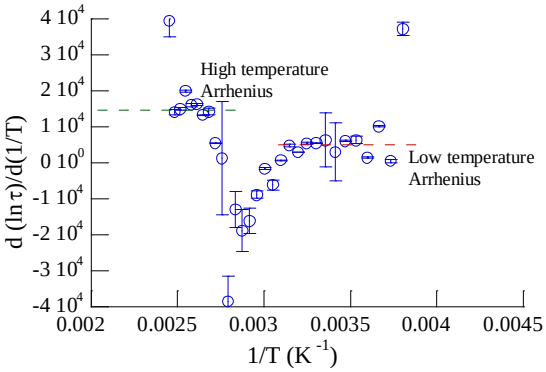

(c)

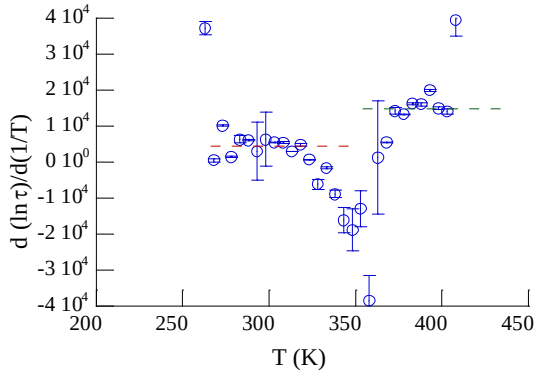

(d)

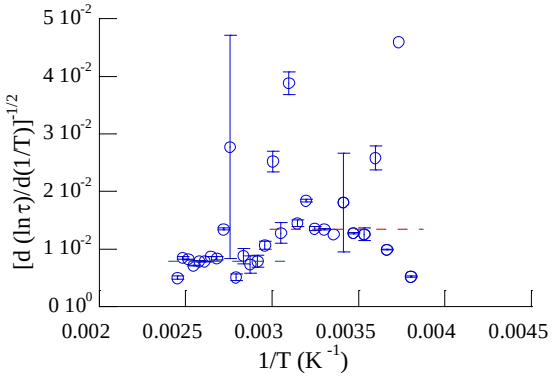

Figure 6.24 *(a) Relaxation times of pepsin (0.039 g/g) over various temperatures and the derivative plots for (b) Arrhenius, (c) Eyring, and (d) VTF behaviour.*

6.4.4 VTF verification

As shown before the dependence of relaxation times on temperature for hydrated proteins show Arrhenius behaviour and it has also been verified further by a derivative procedure (Figure 6.25). When the hydration level of proteins was getting higher, the dependence of log relaxation times on inverse temperature revealed both the linearity and curvature (Figure 6.14 (a), Figure 6.15 (a), and Figure 6.16 (a)). The linearity from Arrhenius behaviour was partly substituted by a curvature near the temperature point of percolation threshold. The percolation threshold for higher hydration level is not sharp anymore but forming a curvature. This curvature of log relaxation times versus inverse absolute temperature can be fitted with VTF expression.

The VTF behaviour is then verified further by using a derivative of log relaxation times over inverse temperature (Equation 6.20).

$$\left(\frac{d\ln\tau}{d(\frac{1}{T})}\right)^{-1/2} = (A_{VTF})^{-1/2} - (A_{VTF})^{-1/2} T_{VTF}\left(\frac{1}{T}\right) \qquad (6.20)$$

Appendix A4 describes the derivation of Equation (6.20). From the gradient and axis-intersection point of curve $\left[d\ln\tau / d(1/T)\right]^{-1/2}$ versus $1/T$, the VTF temperature, T_{VTF}, can be determined.

The verification of VTF behaviour for ovalbumin, lysozyme, and pepsin, is shown in Figure 6.25, Figure 6.26, and Figure 6.27, respectively.

6.4.4.1 Ovalbumin

Figure 6.25 shows the VTF verification for ovalbumin (0.202 g/g). Figure 6.25 (a) shows that the graph of log relaxation times versus temperature for ovalbumin (0.202 g/g) involved a mixture of Arrhenius and VTF behaviours. The Arrhenius behaviour was performed briefly at temperature below 258 K, while the VTF behaviour was revealed at temperature range between 258 – 313 K. The curvature from VTF behaviour in this temperature range (i.e. 258 – 313 K) was slightly curled up after reaching temperature 313 K, which was caused by the percolation threshold. The curvature of log relaxation times of ovalbumin (0.202 g/g) in the range of 258 – 313 K is therefore believed as a mixture of VTF behaviour and percolation threshold. Fitting results from both Arrhenius and VTF plots are shown in Table 6.1.

Derivative of logarithmic relaxation times over inverse temperature is shown in Figure 6.25 (b). A slight straight line, independent of temperature, is shown in the range of inverse temperature 0.0388 - 0.042 K^{-1}. This corresponded with the brief Arrhenius plot below 258 K. The points of derivative function is fairly scattered due to the small number points attribute to the Arrhenius plot. Table 6.1 shows the value of derivative results of Arrhenius plot (i.e. activation energy, ΔH, and pre-exponential factor A_{VTF}) compared with the results from actual fitting. Figure 6.25 (c) shows the verification for VTF behaviour based on Equation (6.5). In the range of inverse temperature 0.0295 – 0.0385 K^{-1}, the graph performed a straight line with gradient $A_{VTF}T_{VTF} \approx -18.91$ and intersects at the ordinate-axis at value of $A_{VTF} \approx 0.079$. The value for characteristic VTF temperature T_{VTF} is then able to determine (see Table 6.1). Since VTF temperature of material is usually 30 – 70 K below glass transition temperature, the glass transition T_g was then obtained by adding approximately 30 –70 K to the VTF temperature.

Table 6.1 *Fitting result and verification from derivative function of Arrhenius and VTF behaviours from hydrated ovalbumin (0.202 g/g)*

	Arrhenius	VTF		
	ΔH (kJ mol^{-1})	A_{VTF}	T_{VTF} (K)	T_g (K)
Fitting	102.67 ± 4.32	109.61 ± 30.35	243.09 ± 0.75	273 - 313
Derrivative	101.6	161.85 ± 13.35	253.26 ± 14.51	283 - 323

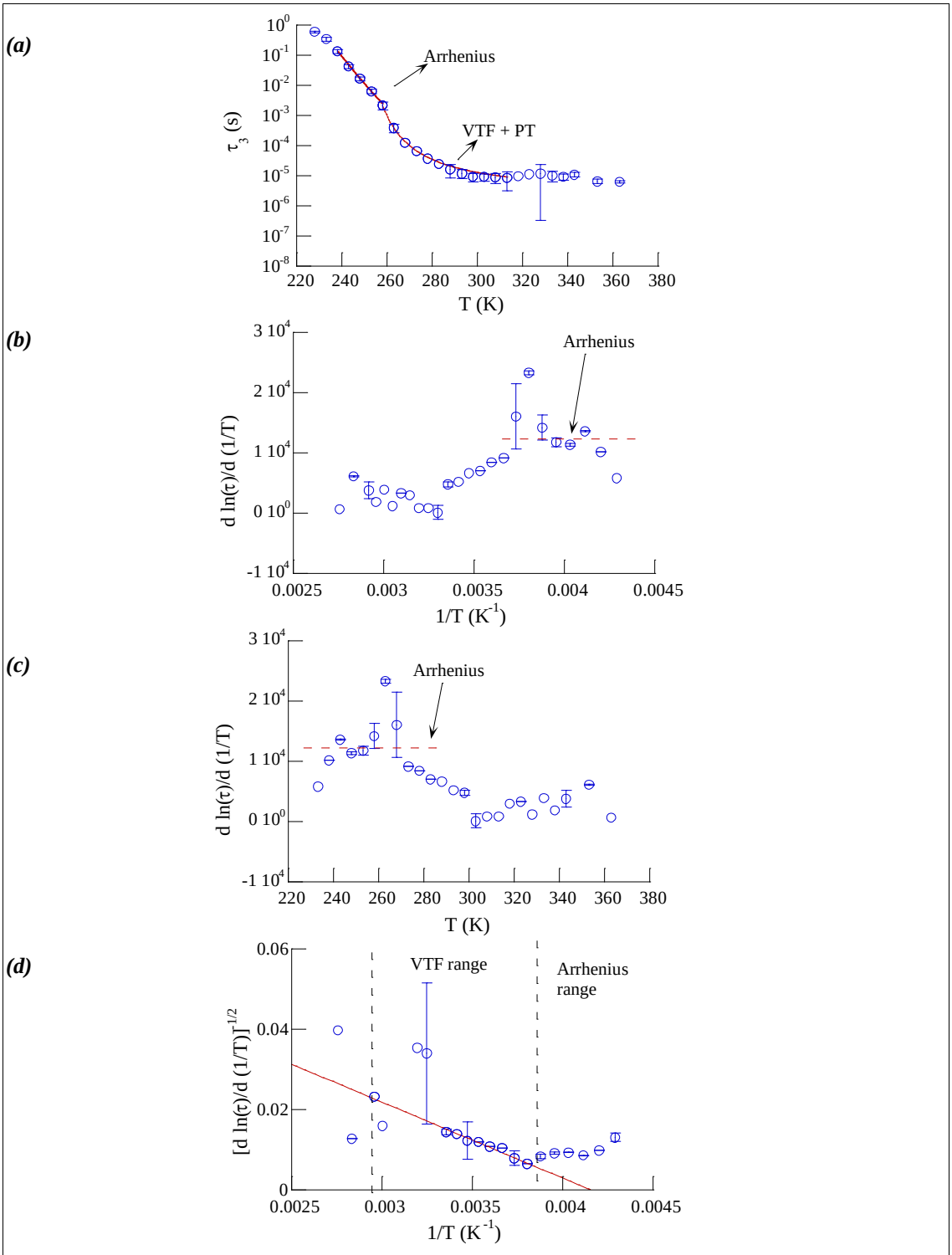

Figure 6.25 *Verification of VTF behaviour on ovalbumin (0.202 g/g): (a) relaxation times versus temperature, (b) derivative for Arrhenius verification, (c) derivative for Eyring verification, (d) derivative for VTF verification. (PT = Percolation Threshold).*

6.4.4.2 Lysozyme

VTF plot and its verification for lysozyme (0.224 g/g) is shown in Figure 6.26. Similar as ovalbumin, the plot of log relaxation times versus temperature shows a mixture of linearity from Arrhenius plot (248 – 308 K) and curvature from VTF behaviour (308 – 348 K) (Figure 6.26 (a)). The curvature of VTF was curling up after reaching temperature ~ 323 K, which was due to the percolation threshold.

Arrhenius plot is verified in the graph of derivative logarithmic of relaxation times over inverse temperature (Figure 6.26 (b)). The temperature independence of the graph in the range of inverse temperature 0.0033 - 0.004 K^{-1} confirmed the Arrhenius plot in the range of 248 – 308 K. Figure 6.26 (c) shows the VTF verification for lysozyme (0.224 g/g). The VTF range was verified by a straight line in the range of inverse temperature ~ 0.0029 – 0.0033 K^{-1}. This line has a gradient of approximately –50.55 and intersects in the ordinate axis at 0.175. Table 6.2 shows the value of VTF characteristic temperature determined from Figure 6.26 (c) using Equation (6.20).

Table 6.2 *Fitting result and verification from derivative function of Arrhenius and VTF behaviours from hydrated lysozyme (0.224 g/g).*

	Arrhenius	VTF		
	ΔH (kJ mol^{-1})	A_{VTF}	T_{VTF} (K)	T_g (K)
Fitting	77.30 ± 1.75	3.56 ± 1.95	307.77 ± 2.25	338 - 388
Derrivative	69.28	32.63 ± 6.8	288.78 ± 3.18	320 - 360

(a)

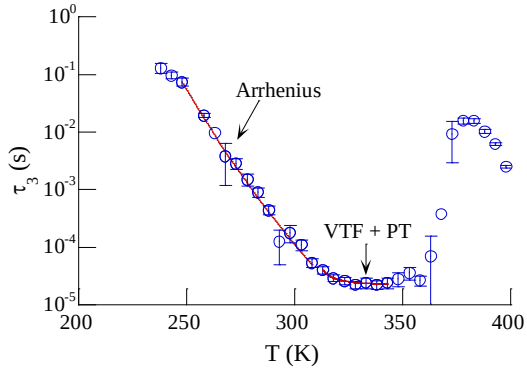

(b)

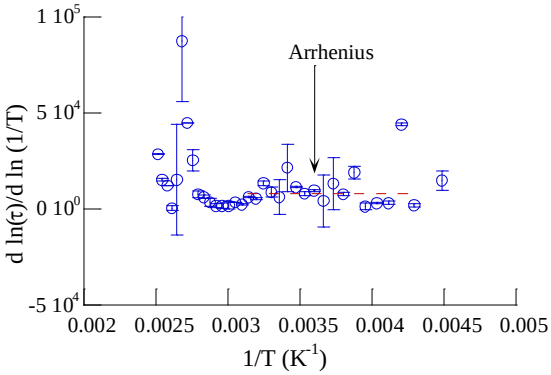

(c)

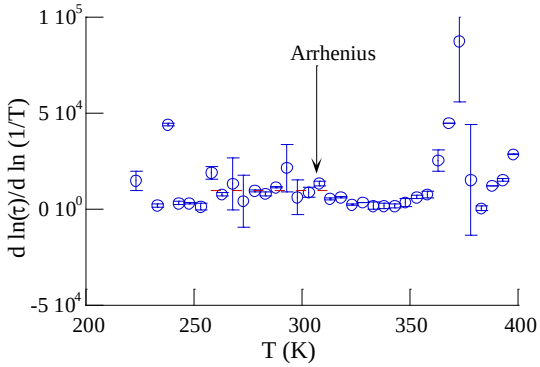

(d)

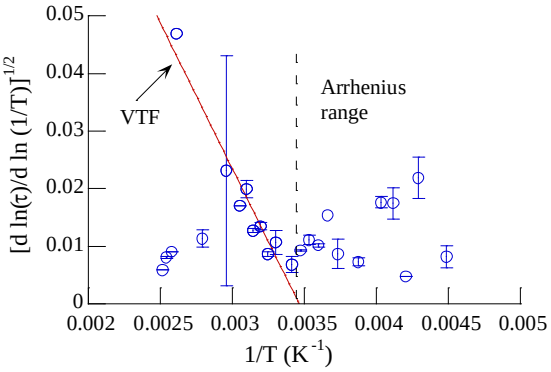

Figure 6.26 *Verification of VTF behaviour on lysozyme (0.224 g/g): (a) relaxation times versus temperature, (b) derivative for Arrhenius verification, (c) derivative for Eyring verification, (d) derivative for VTF verification. (PT = Percolation Threshold).*

6.4.4.1 Pepsin

Unlike ovalbumin and lysozyme, the mixture of Arrhenius and VTF behaviours in pepsin were observed at low hydration level. Figure 6.27 (a) shows the graph of relaxation times versus temperature for pepsin (0.034 g/g). Two Arrhenius plots were observed for pepsin (0.034 g/g). Low temperature (LT) Arrhenius plot was observed below ~ 293 K, while high temperature (HT) Arrhenius was observed after temperature reaching 373 K. Figure 6.27 (b) presents the verification of Arrhenius behaviour. Arrhenius plots are verified by short straight lines, independent on temperature, in the range of inverse temperature 0.00347 – 0.00366 K^{-1} and 0.0025 – 0.00268 K^{-1} for low and high temperature, respectively.

The VTF curvature was observed between 293 – 333 K. The peak of relaxation times started increasing after 323 K, which is due to the percolation threshold. The VTF plots were verified in Figure 6.27 (c) by a straight line in the range of inverse temperature between 0.003 – 0.0035 K^{-1}, with gradient –62.67 and intersection with ordinate axis at 0.22. The value for VTF characteristic temperature T_{VTF} and constant parameter A_{VTF} is shown in Table 6.3. Table 6.3 also displays the comparison between fitting and derivative for Arrhenius and VTF confirmation.

Table 6.3 *Fitting result and verification from derivative function of Arrhenius and VTF behaviours from hydrated pepsin (0.034 g/g).*

	Arrhenius ΔH (kJ mol-1)		VTF		
	Low Temp.	High Temp.	A_{VTF}	T_{VTF} (K)	T_g (K)
Fitting	88.08 ± 4.47	108.52 ± 3.65	19.56 ± 3.40	276.27 ± 1.47	306 - 346
Derrivative	84.8	114.73	19.9 ± 5.02	279 ± 3.01	309 - 349

(a)

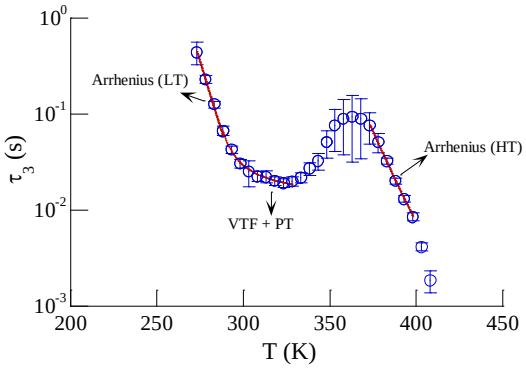

(b)

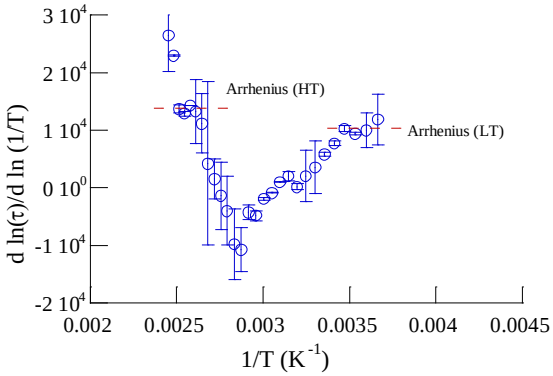

(c)

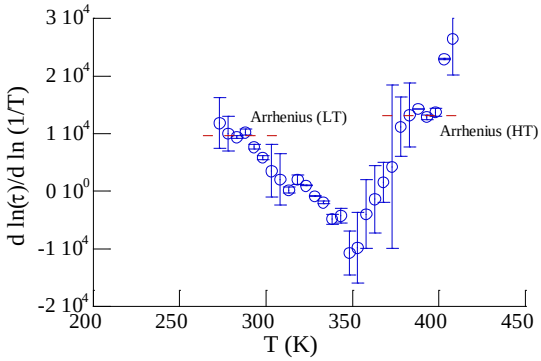

(d)

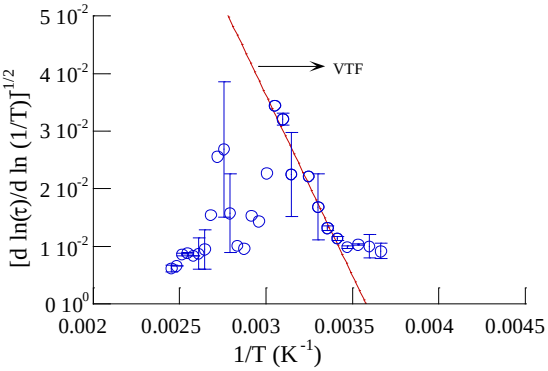

Figure 6.27 *Verification of VTF behaviour on pepsin (0.034g/g): (a) relaxation times versus temperature, (b) derivative for Arrhenius verification, (c) derivative for Eyring verification, (d) derivative for VTF verification. (PT = Percolation Threshold).*

6.5 Fractal Dimension

It has been shown earlier in this section and Section 5.2.3, that the dielectric permittivity of hydrated proteins can be fitted using a model involving a constant phase element for the LFD response. The constant phase element, which involves a power-law function of frequency, has also been used to characterise the dielectric response of many biological systems (animal tissues[60], rabbit liver[99], mouse skeletal muscle), engineering systems and physical systems[70].

The origin of this power-law behaviour can be attributed to a presumed self-similarity (or fractality) in the polarisation by charge in each system[79]. In the case of bulk dielectric relaxation, the constant phase element has been attributed to a self-similar hierarchy of microscopic relaxation processes and fractal based polarisation clusters[76]. Since the system of hydrated protein powder analysed in this work was well characterised by a constant phase element (for the LFD response), it follows that the system may be considered to have a self-similarity or fractal structure. The assumption of a fractal polarisation in hydrated proteins can be illustrated by the cluster model described in Figure 8.3. The fractal polarisation of hydrated protein powder is also inferred by the observation of percolation thresholds in the temperature studies, discussed in Section 6.3. It is also known that percolation clusters are self-similar and can be modelled by fractal structures. All these arguments verified the existence of self-similar phenomenon (or fractality) in the polarisation of hydrated protein powders.

One of the parameters that can be used to describe fractality, in terms of the physical state of the system, is the fractal dimension D. The fractal dimension is not a *Euclidean dimension,* as such, and has a non-integer value that originates from an exponent of the simple power law of distance L for scaling mass M : [100]

$$M \propto L^D \tag{6.21}$$

M can also be related to the number of self similarities and L can be related to a magnification factor. For a dimensionality D_w of a random walk on a fractal, Equation (6.21) may also be expressed as[121]:

$$n \propto r^{D_w} \tag{6.21a}$$

where n is the total number of steps of the random walk, and r is the displacement/distance of the walker. The fractal dimension D_w of the random walk is approximately equal to $3D/2$ [124].

Table 6.4 shows the relationship between structural fractal dimension D, fractal dimension of a random walk D_w, and Euclidean dimension[101]. In a 2-dimensional system, for example, the structural fractal dimension D at percolation threshold will have a value of $D = 91/48$, while the fractal dimension D_w of a random walk is 2.871.

Table 6.4 *Structural and random walk fractal dimensions corresponding to the Euclidean dimension.*

Exponent	**d = 2**	**d = 3**
D (p = pc)	91/48	2.53
D (p < pc)	1.56	2
D (p > pc)	2	3
D_w (p = pc)	2.871	3.8

Fractal dimensionality may also be described as the arrangement of various clusters in the percolation region. The magnitude of fractal dimension depends on the degree of disorder present in the system[102]. In a dielectric relaxation system, if the percolation clusters are considered to have a spherical symmetry and the fractal is assumed to be isotropic, then the fractal dimension D_f in a 3-dimension Euclidean geometry may be determined using the expression[103]:

$$D_f = 3\nu \tag{6.22}$$

where:

ν = stretching exponential from Kohlrausch-Williams-Watts equation for the dielectric response in time domain (Equation (6.23))

$$\phi(t) = \exp\left[-\left(\frac{t}{\tau_{WW}}\right)^{\nu}\right] \tag{6.23}$$

where:

$\phi(t)$ = dipole correlation function

τ_{WW} = average characteristic relaxation time

ν = stretching exponential

This study employed a frequency domain dielectric measurement rather than a time-based measurement (as described in Equation (6.23)). In order to obtain information about fractal dimension of the system, the data from frequency domain has to be first transformed to the time-domain, from which the value of stretching exponential ν is derived. An alternative approach is to adopt the analytical relation between the shape parameters (α, β) from frequency domain and stretching exponential ν from time domain, as suggested by Alvarez, et al (1991)[104] i.e.:

$$\alpha\beta = \nu^{1.23} \tag{6.24}$$

Figure 6.28 shows the fractal dimension D_f determined from Equations (6.22) and (6.24) for various hydration level of ovalbumin, lysozyme, and pepsin. This fractal dimension was determined at the conditions for the observation of a percolation threshold (i.e. $p = p_c$).

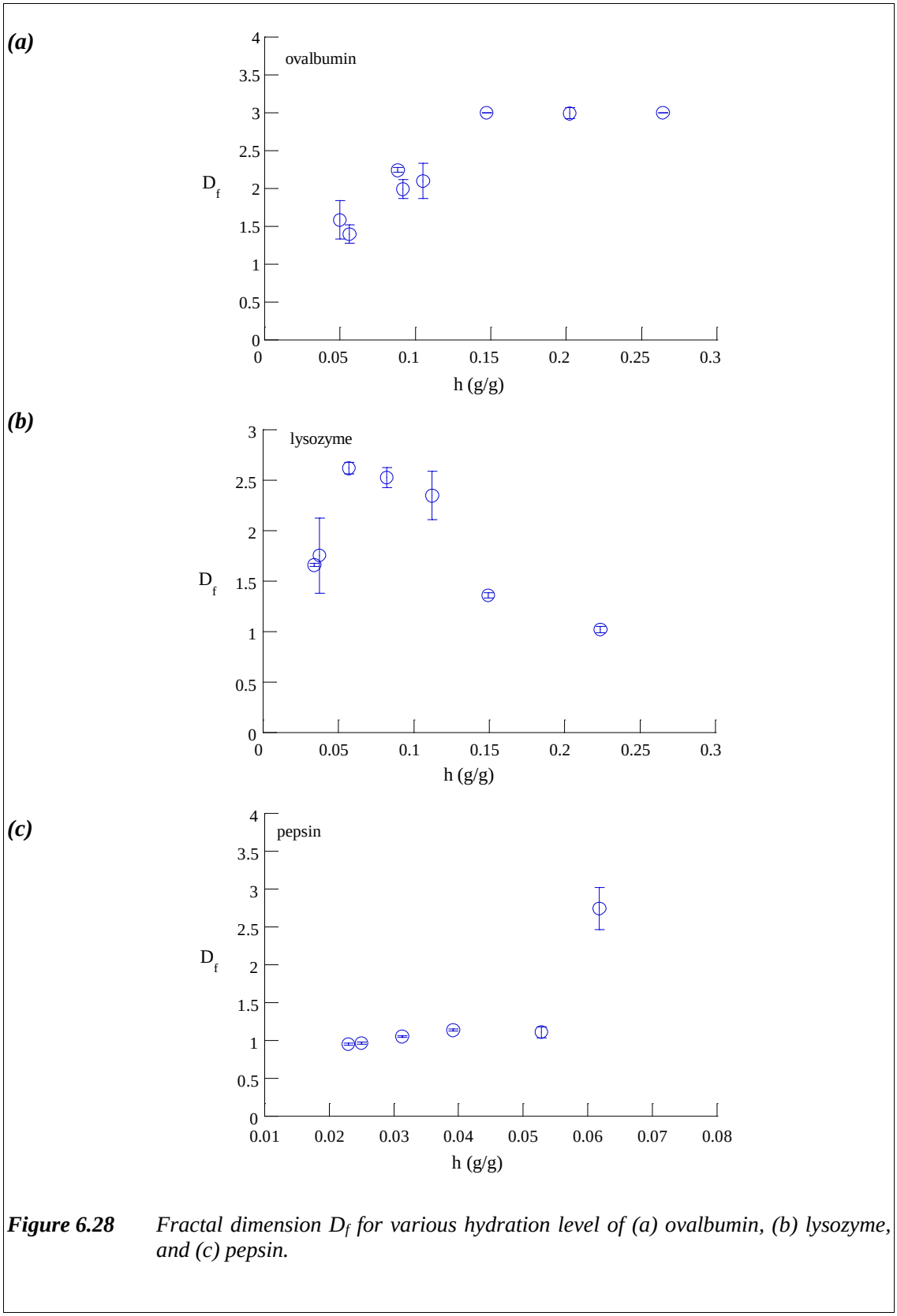

Figure 6.28 *Fractal dimension D_f for various hydration level of (a) ovalbumin, (b) lysozyme, and (c) pepsin.*

6.6 ε_4 dispersion

For lysozyme at low hydration level (0.034 and 0.037 g/g), there is another weak dispersion that is observed (besides ε_3 dispersion) at high frequency (see the isothermal study described in Chapter 5, Figure 5.7). This weak dispersion is called the ε_4 dispersion. The ε_4 dispersion was more clearly observed at lower temperatures (Figure 6.29 (a)).

Figure 6.29 (b) shows the relaxation times, τ_3 and τ_4, from both the ε_3 and ε_4 dispersions, respectively. Since the ε_4 dispersion was present at higher frequency than the ε_3 dispersion, then it follows that the ε_4 dispersion was observed in a different range of temperatures, for any particular hydration level of protein. For low hydration level of lysozyme (0.034 g/g and 0.037 g/g), the ε_4 dispersion could be observed up to ~328 K. The ε_4 dispersion was not observed at higher hydration level (> 0.04 g/g), but would be observed at temperatures lower, or at frequencies higher than the experimental window

This ε_4 dispersion was also found in ovalbumin. This ε_4 dispersion was vaguely observed at ovalbumin 0.202 g/g at low temperature (Figure 6.30 (a)). Figure 6.30 also verified the existence of ε_3 dispersion for higher hydration level ovalbumin, which is often not observed at room temperature for it is overlapped with LFD or Maxwell-Wagner effect. As shown in Figure 6.30, ε_3 dispersion was clearly observed at 233 K and slowly disappeared after 253 K. A slight hump mixed with LFD process at temperature higher than 253 K may originate from both ε_3 dispersion and Maxwell-Wagner effect.

Relaxation time τ_4 for both lysozyme and ovalbumin did not have a regular pattern (Figure 6.29 and Figure 6.30). Unlike ε_3 dispersion, it was difficult to consider if the relaxation time τ_4 for ε_4 dispersion showed any Arrhenius or VTF behaviour. Therefore, the activation energy for ε_4 dispersion is hard to obtain. Unlike hydrated lysozyme and ovalbumin, hydrated pepsin did not show any ε_4 dispersion.

(a)

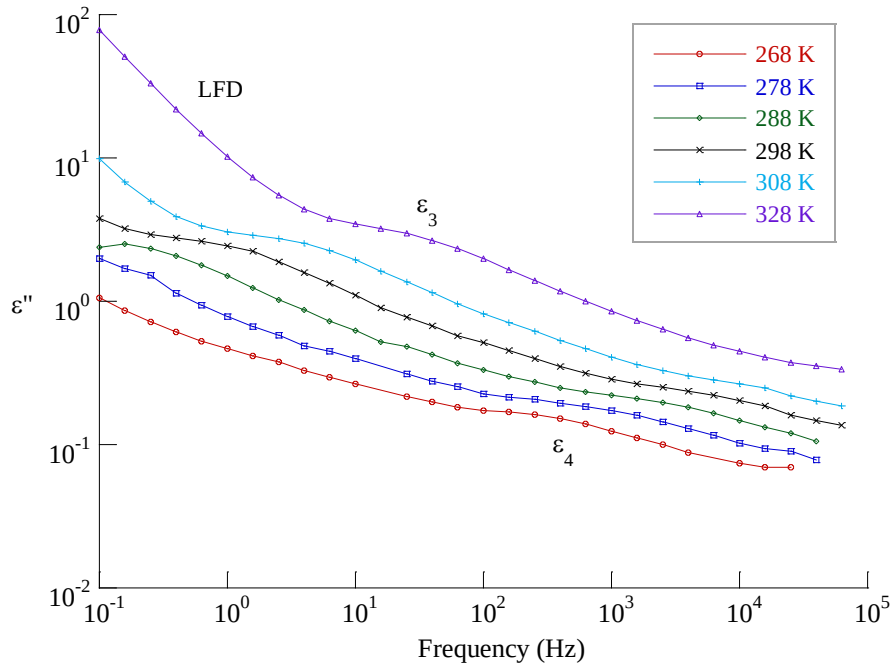

(b)

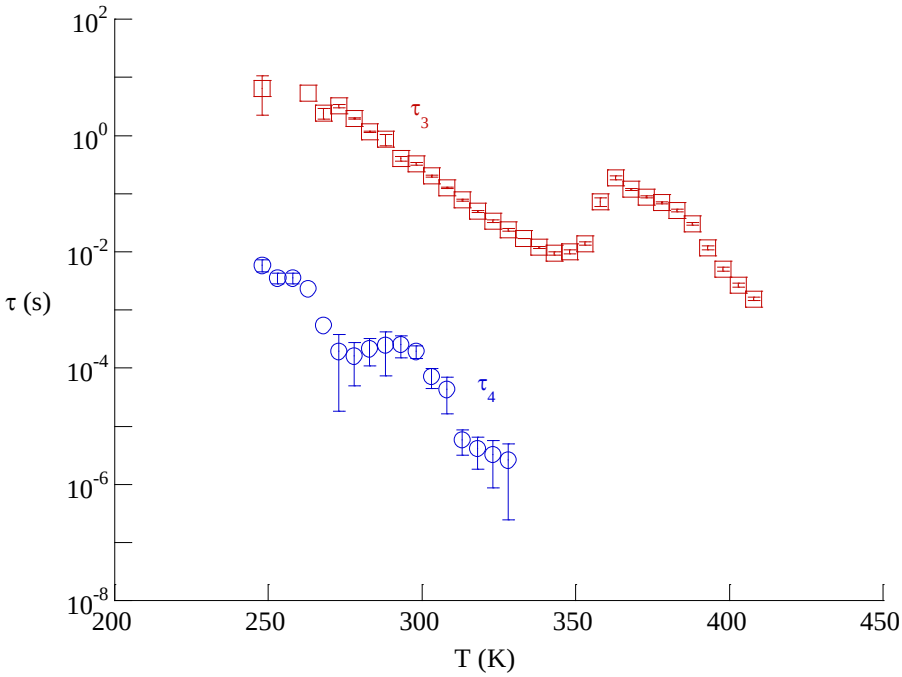

Figure 6.29 *(a) Imaginary permittivity of hydrated lysozyme (0.037 g/g) showing ε_4 dispersion at lower temperature; (b) Relaxation times τ_3 and τ_4 for lysozyme (0.037 g/g) from ε_3 and ε_4 dispersions, respectively.*

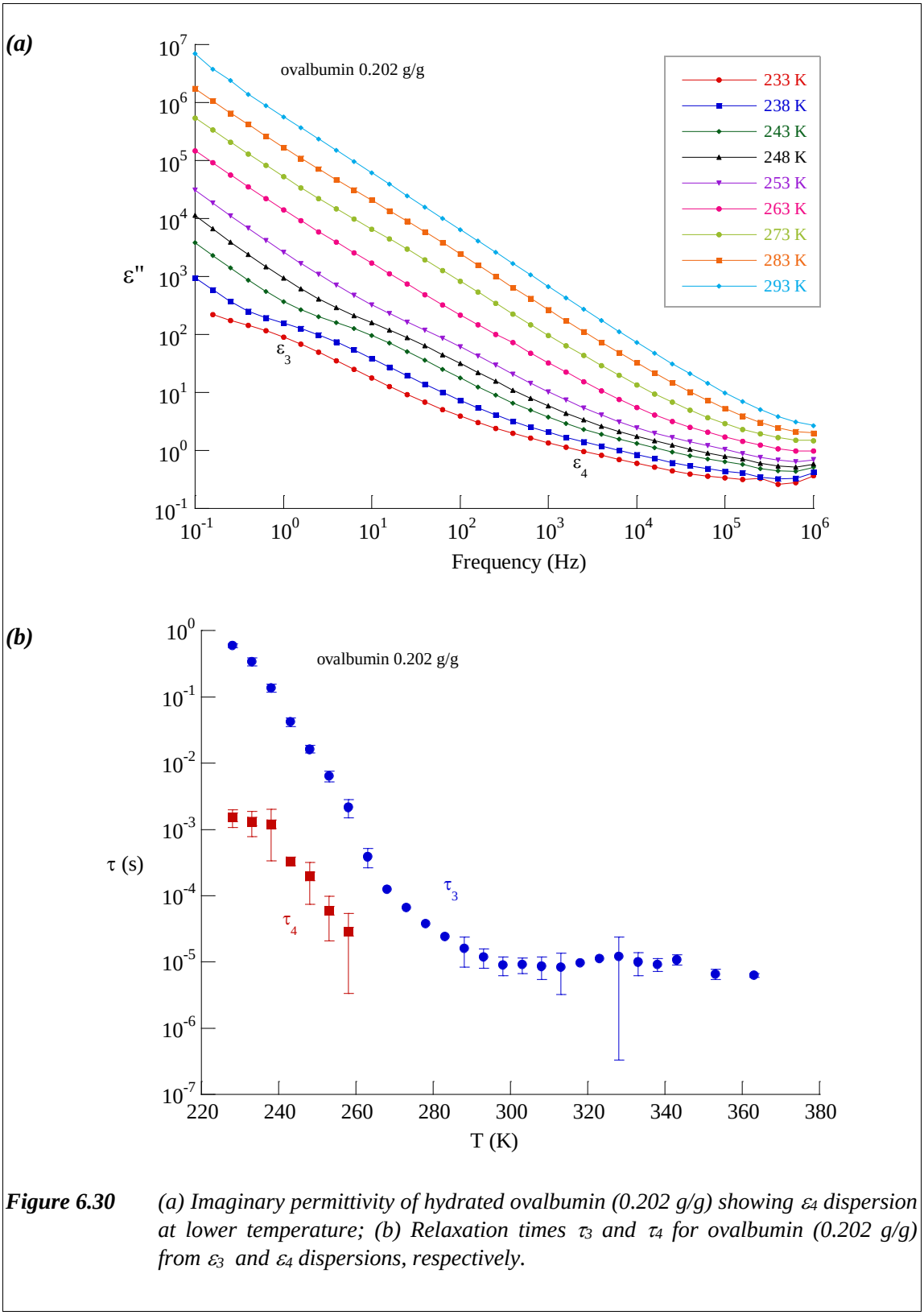

Figure 6.30 *(a) Imaginary permittivity of hydrated ovalbumin (0.202 g/g) showing ε_4 dispersion at lower temperature; (b) Relaxation times τ_3 and τ_4 for ovalbumin (0.202 g/g) from ε_3 and ε_4 dispersions, respectively.*

6.7 Discussion

6.7.1 Percolation Threshold

It has been shown in Section 6.3 that both the LFD and the ε_3 dispersion shifted towards a higher frequency with increased temperature, until the percolation threshold was reached. Furthermore, this percolation threshold temperature shifted to lower temperatures as the hydration level was increased.

For each hydrated protein, the percolation threshold is manifest as a peak in the complex permittivity of each material. Based on the cluster model, this phenomena may be explained as follows. The scaling power law for fractal systems ($\xi \sim (T - T_p)^{\nu}$) (Equation A3.13) describes the increase in cluster size with increasing temperature and hence kinetic energy of the system. This increased kinetic energy results in increased vibrations of water molecules, of which in turn promotes the number of nearest neighbour interactions for proton transport. In essence the increase in dynamic actually translates as an increase in the size and numbers of charge transport clusters. The vibration of the water molecules itself was not detected in the dielectric spectroscopy in this study, as it was out of the experimental frequency window for detecting the vibrational motion. This study, however, detected the change in cluster size of water molecules from the change in the permittivity values.

The increase in cluster size gives rise to an increase in the average dipole moment μ, since the dipole moment is linearly related to the distance r between the charges e (i.e. $\mu = er$). From dielectric theory (Section 3.3), an increase in dipole moment and number of dipoles leads to a rise in permittivity. Thus, as observed in this study, the permittivity values went up with the increase of temperature. Figure 6.31 gives an illustration of increasing cluster size due to the increased number of sites/water molecules, which were closer to each other with the increase of temperature.

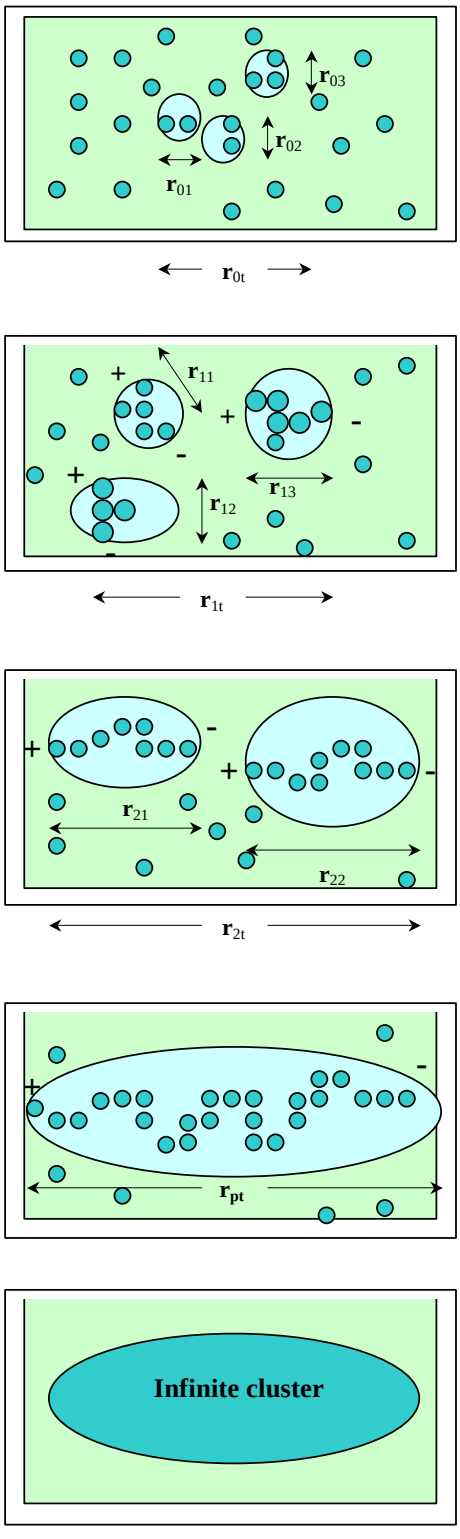

$\mathbf{T_0 < T_1 < T_2 < \ldots\ldots < T_p}$

ε_3 dispersion:

$\bar{r}_0 < \bar{r}_1 < \bar{r}_2 < \ldots\ldots < \bar{r}_p$

$\bar{\mu}_0 < \bar{\mu}_1 < \bar{\mu}_2 < \ldots\ldots < \bar{\mu}_p$

$\bar{\varepsilon}_0 < \bar{\varepsilon}_1 < \bar{\varepsilon}_2 < \ldots\ldots < \bar{\varepsilon}_p$

$\bar{\tau}_0 > \bar{\tau}_1 > \bar{\tau}_2 > \ldots\ldots > \bar{\tau}_p$

LFD:

$r_{ot} < r_{1t} < r_{2t} < \ldots\ldots < r_{pt}$

$A_{ot} < A_{1t} < A_{2t} < \ldots\ldots < A_{pt}$

Figure 6.31 *Illustration of increasing cluster size with the increase of temperature.*

Illustration in Figure 6.31 can be used to describe the mechanism either for the LFD, ε_3 dispersion or the ε_4 dispersion. For illustration of the ε_3 and ε_4 dispersion, the small dark-blue circle is considered as unit cluster polarisation , and the big light-blue circle is considered as a distribution of cluster polarisation. The system for the ε_3 and ε_4 dispersions is considered as unit domain and single macromolecule, respectively. For the LFD response, the small dark-blue circle is considered as a water molecule, and the big light-blue circle is considered as a unit cluster polarisation, which consists of a group of water molecules. The system itself is considered as the whole bulk of sample.

At certain temperature T_p at which the percolation threshold occurred, an infinite cluster was formed (Figure 6.31). The charges were both separated in the furthest possible distance in infinite cluster and thus permittivity reached the highest value. At this percolation threshold temperature, the mobility of proton is also assumed to reach maximum/saturation. For the ε_3 dispersion, the infinite cluster is formed throughout a single macromolecule, while for the LFD response, the infinite cluster is formed throughout the sample. This infinite cluster represents the maximum range of proton transport through the hydrogen bonding of water molecules.

As temperature was increased further beyond the percolation threshold temperature, the permittivity of the sample decrease. This may be explained as follows. At percolation threshold, the cluster polarisation may reach saturation. The saturation of cluster polarisation may be due to the formation of infinite cluster, which creates an open channel for proton transport. The proton may percolate freely through this open channel/infinite cluster, and thus no more cluster polarisation is generated. Since there is no more cluster percolation, the number of charges in the system is constant. On the other hand, the energy of the system increases since the temperature is kept rising. As a result, the capacitance (or permittivity) of the system decreases.

Another possibility that may occur after the percolation threshold was that the water in the sample evaporated. The loss of water therefore caused the decrease in the permittivity and

LFD response after reaching the percolation threshold temperature. However, the TGA measurement did not contribute this assumption (Figure 2.7). The percentage of weight loss from TGA measurement for each hydrated protein show that the total water loss occurred at ~ 100 °C. It is expected, therefore, that the percolation threshold temperature should occur at ~ 100 °C, if it is due to the water loss. Moreover, if the peak of percolation threshold was due to the water loss, each hydrated protein should experience the same percolation threshold temperature (i.e. ~ 100 °C).

The calculation of the mass loss of the samples after temperature measurement also does not contribute the assumption of water loss. Each hydrated ovalbumin and lysozyme still contained water after temperature measurement (Table 6.5). The exception was found for pepsin, where the sample mass after temperature measurement was higher than that before temperature measurement. It is not clear whether pepsin sample has decomposed through the temperature measurement, since the colour of pepsin sample after temperature measurement changed to brown colour.

Table 6.5 *Mass fraction of remain water (g/g) in the samples after once temperature measurement (up to ~ 100 °C).*

	Hydration (g/g)	Remain water (g/g)
ovalbumin	0.047	0.007
	0.088	0.036
	0.092	0.023
	0.099	0.024
	0.105	0.034
	0.111	0.026
	0.202	0.086
	0.264	0.087
lysozyme	0.034	0.017
	0.057	0.048
	0.149	0.071
	0.224	0.076
	0.255	0.086

Additional temperature study was also carried out to investigate whether the decrease in permittivity after reaching the percolation threshold was due to the water loss.

Figure 6.32 shows the relaxation times τ_3 and pre-exponential factor A for three consecutive measurements of ovalbumin 0.1 g/g, i.e.

- 1st measurement: temperature range 228 K – 363 K, with remain water 0.0224 g/g after measurement.
- 2nd measurement: temperature range 298 K – 363 K, and no remain water after measurement.
- 3rd measurement: temperature range 298 K – 408 K.

As expected, the percolation threshold temperature shifted to higher temperature, from the 1st measurement to the 3rd measurement, owing to the fact that the hydration level was lower with the later measurements. It is interesting that the percolation threshold was still present in the 3rd measurement, even though there was no remain water after the 2nd measurement. From this result, it may be inferred that percolation of charge could occur in a 'dry' protein, as the protein itself can contribute charges from ionisable groups.

The activation energy (ΔH) and the entropy (ΔS) for these three consecutive measurements are listed in Table 6.6. The activation energy (ΔH) is higher with the later measurement, whereas the entropy (ΔS) is lower. The decrease in entropy with the later measurement is expected since the water content was lower. However, the result for ΔH is opposite than expectation. Since the later experiment has lower water content (or even no more water content as in the 3rd measurement), the ΔH should decrease, instead of increasing as seen in Table 6.6. This may be explained that the dispersion observed for the 2nd and 3rd measurements was due to the proton transport from cluster of water molecules that originated from bound water/structured water, that was still present after temperature study.

(a)

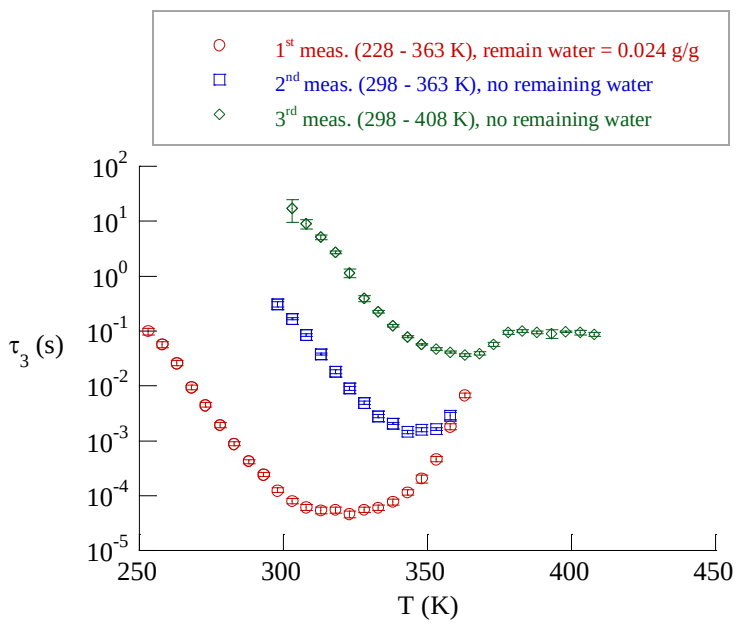

(b)

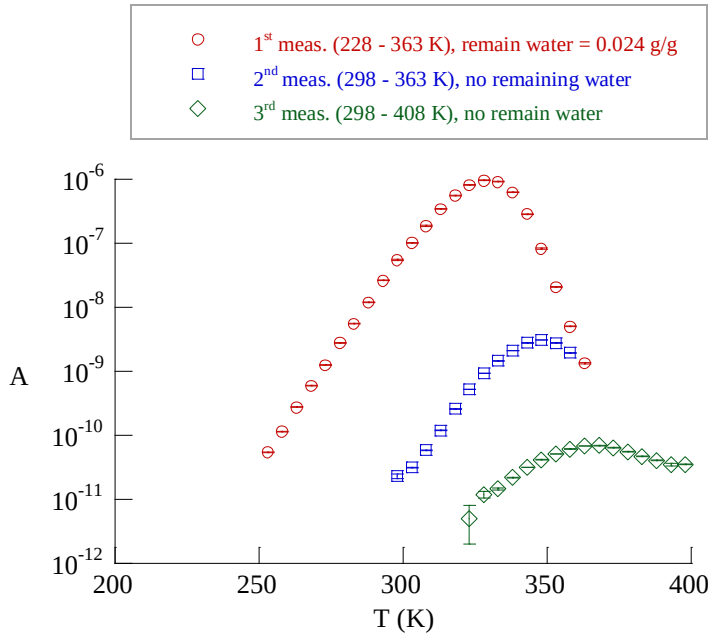

Figure 6.32 *(a) Relaxation time τ_3 and (b) pre-exponential factor A for ovalbumin (0.1 g/g), from three consecutive measurements.*

Table 6.6 *Activation energy (ΔH) and entropy change (ΔS) for ovalbumin 0.1 g/g.*

	ΔH (kJ mol^{-1})	ΔS (kJ mol^{-1} T^{-1})
1st measurement	98.93 ± 1.35	276.69 ± 2.12
2 nd measurement	114 ± 1.03	269.82 ± 2.52
3 rd measurement	122.66 ± 4.14	264.65 ± 5.58

After reaching percolation threshold, the relaxation is getting slower as temperature increases. This might be due to the thermal energy is used to change system that cause proton jump more difficult. The hydrogen bonding between water molecules may stretch, so creating bigger barriers for proton transport. This change of the protein system may then cause the proton refolding that is indicated by the sharp point at the onset of high temperature Arrhenius. The possibility of the refolding of the proteins at elevated temperature results in the re-formation of clusters. The assumption of protein refolding at elevated temperature may also be evidenced from the similarity of the FTIR spectra before and after temperature measurement (Figure 6.33).

At the refolding stage, the bound water or structured water may be revealed and polarised by the applied electrical field. This structured water may then be responsible for the formation of new clusters. These new clusters (high temperature clusters) may have bigger size than the previous ones (at below percolation threshold temperature), and thus results in higher relaxation times. The assumption of bigger size of 'new clusters' was also supported by the higher activation energy after percolation threshold temperature as found in lysozyme and pepsin (see Section 6.4.1.2). The idea of 'new clusters' also verifies the

presence of new LFD and ε_3 dispersion after percolation threshold as observed in Figure 6.7 (a) and Figure 6.8 (c).

With the higher hydration level, the percolation threshold moved to lower temperature. When the hydration level increased, the number of water molecule in a system increased. The formation of infinite cluster was therefore able to form at lower temperature compared to the one with lower hydration level.

Compared with ovalbumin and pepsin, lysozyme showed a distinguishing property during the percolation threshold, i.e. the presence of transition process briefly after percolation threshold (Figure 6.6 (b)). The origin of this transition process is still not clear. It may correspond to a typical structure existing in lysozyme, but not present in ovalbumin and pepsin. More studies should be carried out related to this matter.

(a)

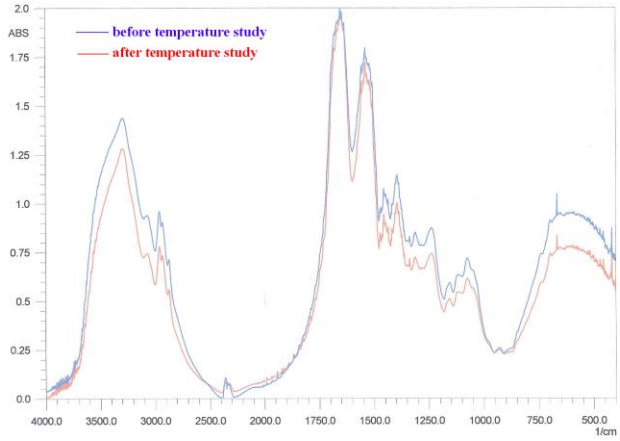

(b)

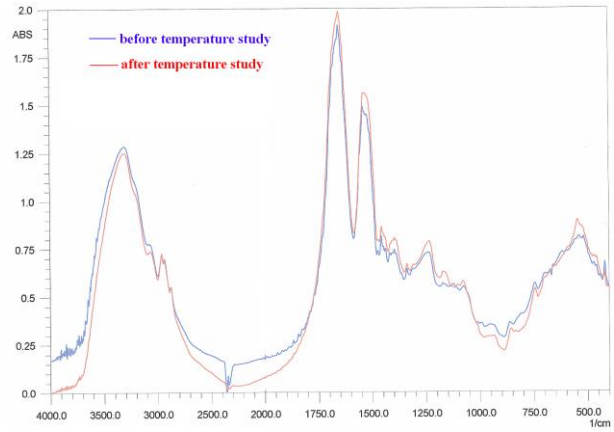

(c)

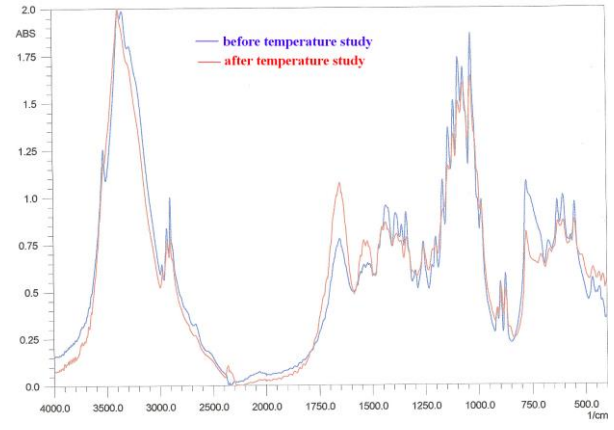

Figure 6.33 *Comparison of FTIR spectra before and after temperature measurement for (a) ovalbumin, (b) lysozyme, and (c) pepsin,*

6.7.2 Arrhenius, VTF, and glass transition

Arrhenius behaviour in a certain temperature range for ovalbumin, lysozyme, and pepsin has been shown and verified in Section 6.3.5. It is clearly demonstrated that when Arrhenius plot is observed, the derivative function of log relaxation times over inverse temperature gave a straight line, independent on temperature; while non-Arrhenius behaviour gave a straight line dependent on temperature.

The non-Arrhenius behaviour is mostly detected at relatively higher hydration level. This is shown clearly in 3-dimensional graph of permittivity versus temperature, and from the graph of relaxation times dependent on temperature. It has been shown that as hydration level is getting higher, the percolation threshold was less sharp and tend to be flattened, except for pepsin which experienced oppositely as describe in Section 6.3.4.

The flattened peak of percolation threshold may be due to the onset of glass transition mixed with percolation threshold. There was a probability that at higher hydration the glass transition and percolation threshold occurred simultaneously. The VTF fit to the flattened curve confirmed the formation of glass transition.

Glass transition temperature T_g decreased with the increase of hydration level. For relatively low hydration level, the glass transition T_g of the sample occurred at higher temperature above the percolation temperature. The percolation threshold was therefore not affected by the glass transition for low hydration level.

When hydration level increased, the percolation temperature decreased. Similarly, glass transition temperature T_g also decreased with the increase of hydration level. In one point, the percolation threshold may occur simultaneously with the onset of glass transition, resulting in a flattened peak of percolation threshold.

Table 6.7 shows the glass transition temperature T_g from representative hydrated proteins obtained from DSC measurement (Figure 6.34). The temperature at which percolation

threshold occurred was also displayed for comparison. This temperature for percolation threshold was obtained from the peak observed at 3-dimensional graph in Figures 6.9 – 6.13. Another alternative, it can also be obtained from the peak observed at the fitting result of relaxation time τ and pre-exponential parameter A over various temperatures as shown in Figure 6.14, Figure 6.15, and Figure 6.16.

Table 6.7 *Glass transition temperature (T_g) and temperature for percolation threshold (T_p) for some hydrated proteins*

	Hydration (g/g)	Tg (°C)	Tp (°C)
Ovalbumin	0.047	100*	~ 70
	0.105	90	~ 60**
	0.202	80	30 - 50
Lysozyme	0.037	90	~ 75
	0.224	80	50 - 70
Pepsin	0.034	-	40 - 60
	0.053	-	~ 70

* DSC graph was not shown for 0.047 g/g.

** The 3D-graph was not shown for 0.105 g/g.

The glass transition temperature T_g for lysozyme and ovalbumin was approximately 30 °C higher than temperature for percolation threshold, irrespective of hydration level (Table 6.7). The exception was for pepsin. The temperature range of glass transition was about ± 20 °C, from the exact point of glass transition (Figure 6.34). Therefore, it was possible that for ovalbumin and lysozyme the onset of glass transition is coincident with the percolation threshold, which then caused a flattened peak of percolation threshold.

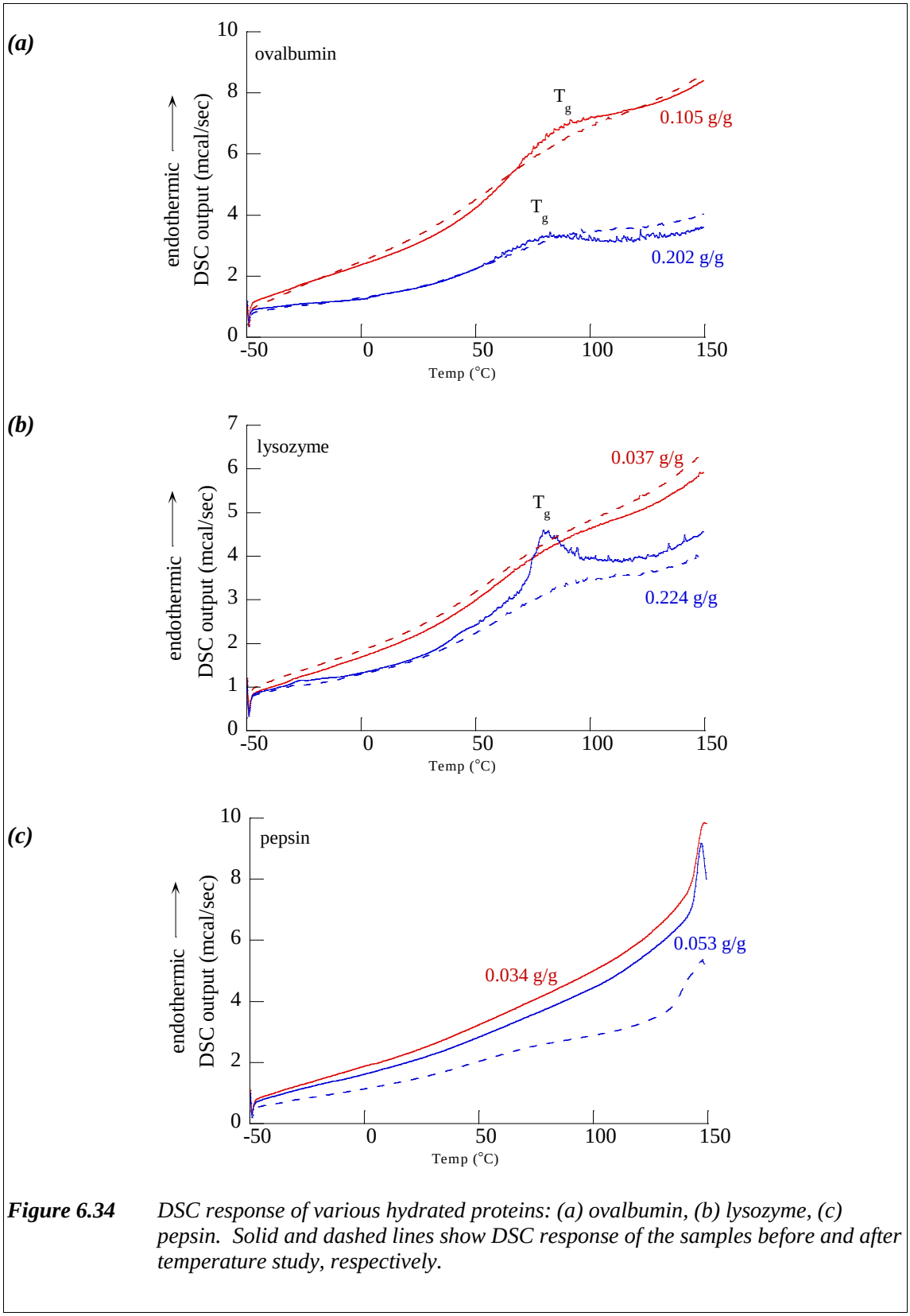

Figure 6.34 *DSC response of various hydrated proteins: (a) ovalbumin, (b) lysozyme, (c) pepsin. Solid and dashed lines show DSC response of the samples before and after temperature study, respectively.*

DSC plot for pepsin did not show a clear indication of glass transition. It was probably present at higher temperature than the experimental window (Figure 6.34 (c)). The higher temperature of glass transition for pepsin seemed reasonable since the XRD pattern for pepsin showed a higher degree of crystalline state compared with ovalbumin and lysozyme (Figure 5.35). The sharp peak observed at about 145 – 150 °C on DSC plot of pepsin may refer to the melting point of the sample (Figure 6.34 (c)).

The VTF response observed showed the presence of cooperative motion in the proteins at the onset of percolation threshold at higher hydration level. This cooperative motion may originate from the interaction between water-water and water-interior protein structure.

The percolation temperature obtained in this study was still below denaturation temperature for the studied hydration range. The hydration dependence of the denaturation temperature of ovalbumin and lysozyme from calorimetric study was found about 350 – 400 K for hydration level up to 0.2 g/g. Hence, the percolation temperature observed was unlikely to correspond with denaturation state of the protein.

The temperature response of pepsin was slightly different compared with ovalbumin and lysozyme. Unlike ovalbumin and lysozyme, the temperature range for Arrhenius and VTF behaviours in pepsin is narrower. Moreover, there were two Arrhenius plots observed in pepsin, i.e. at low temperature range (below percolation temperature - Figure 6.16 (a)) and at high temperature range (Figure 6.20).

The high temperature Arrhenius response probably corresponds to a new LFD and ε_3 dispersion observed after percolation threshold. As have been discussed earlier, these new dispersions originated from the bigger size of cluster (see Section 6.7.1). This explanation is consistent with the observation that activation energy of high temperature Arrhenius response was higher than that from low temperature Arrhenius.

It is possible that high temperature Arrhenius response for ovalbumin may occur at higher temperature range than that for lysozyme and pepsin, and as such is beyond the

experimental window in this work. Certainly in the case of lysozyme, the trend in the data above transition process gives some suggestion of an Arrhenius response (Figure 6.15 (a)).

6.7.3 Proton glass

The presence of a proton glass has been mentioned in Section 6.3.4 in relation to the observed small shoulder at about 270 – 280 K. The idea of a proton glass in hydrated protein powders originated from the consideration of the similar behaviour of ferroelectric proton glasses and magnetic spin glasses[105]. By analogy, the proton glass in hydrated protein powder may originate from the progressive quenching of the random interactions between protons migrating among the ionised side-chains of protein surface. The ordering process at low temperature/freezing temperature T_f was perturbed due to the competing interactions between electrostatic forces on the protein surface [106,107].

The temperature at which proton glass was observed was in the range of freezing temperature of water (i.e. 273 K). However, it was considered that the hump observed at temperature ~ 270 – 280 K was not due to the bulk ice. Some studies have shown that water in hydrated proteins in a hydration range up to ~ 0.3 – 0.4 g/g is unfreezeable and remains mobile at very low temperature[50,108]. This unfreezable water does not experience crystallisation even with long periods of slow cooling or heating rate. The formation of ice on cooling therefore does not occur at this level of hydration range.

6.7.4 Enthalpy, Entropy, and Fractal Dimension

It has been shown in Figure 6.21 and Figure 6.28 that the enthalpy, entropy, and fractal dimension for ovalbumin, lysozyme, and pepsin as a function of hydration, all reached saturation after a particular hydration level. This particular hydration level is different for each protein. It is interesting that this particular hydration level is similar with the critical hydration level (h_{c1}) obtained from dielectric parameters in the isothermal hydration study (Section 5.2.3.3). Table 6.8 shows the value of critical hydration level and saturated value

of activation energy, entropy, and fractal dimension for each protein. It also displays an approximate number of water molecules and unit cluster polarisation per single macromolecule.

Table 6.8 *Critical hydration (h_c) and saturated value of activation energy (ΔH), entropy (ΔS), fractal dimension (D_f) for ovalbumin, lysozyme, and pepsin.*

		Ovalbumin	Lysozyme	Pepsin
ΔH_{sat} (kJ mol^{-1})		100	70	40
ΔS_{sat} (kJ mol^{-1} T^{-1})		300	220	200
$(D_f)_{sat}$		3	2.5	1
h_{c1} (g/g)		0.08	0.06	0.023
h_{c2} (g/g)		-	0.1	0.037
No. of H-bond/unit cluster polarisation		~ 5	~ 4	~ 2
No. H_2O/macromolecule	**h_{c1}**	200	50	43
	h_{c2}	-	83	70
No. unit cluster polarisation / macromolecule	**h_{c1}**	~ 40	~ 12	~ 21
	h_{c2}	-	~ 20	~ 35

Based on the assumption that the dielectric response observed in hydrated proteins involve a process of water-assisted proton transport, then it follows that the activation energy (ΔH) obtained in this study may be related to the dissipation of hydrogen bonding. Considering that proton transport necessarily involves the cooperative involvement of number of water molecules, then the activation energy must correspond to breaking and formation of several hydrogen bonds.

Based on the activation energy (ΔH), the number of hydrogen bonding involved in the proton transport are 5, 4, and 2, for ovalbumin, lysozyme, and pepsin, respectively. It is assumed that these are the average numbers responsible for one unit cluster polarisation.

Pepsin has the lowest number of hydrogen bonding in its unit cluster polarisation. This may be due to the fact of different crystallinity state of pepsin and also the possibility of denaturation of the pepsin sample itself. The pepsin sample was mostly crystalline (as shown in the XRD pattern in Section 5.4.6), while ovalbumin and lysozyme were mainly amorphous. The interaction of water molecules with the main chain protein or the backbone protein in crystalline materials may be different with the amorphous materials. In crystalline materials, the structure is well ordered. Water molecules may bind stronger when added to a crystalline materials and less number of water molecules which are loosely bound on the interior of protein surface. As a result, less hydrogen bonding need to be broken. Less water molecules in the protein surface also suggested less water molecules cluster, and hence, less proton transport in the cluster. This explained the obscure ε_3 dispersion in pepsin compared with ovalbumin and lysozyme. When the hydration level increased, the system became more amorphous. This explained that pepsin started to perform similarly as ovalbumin and lysozyme when the hydration level was higher.

Figure 6.19 shows that the entropy ΔS increased with the increase in hydration level. The entropy (ΔS) may be explained as the ratio of the number of available sites between the activated states and inactivated states (Section 6.4.1). The increase in hydration level creates more available sites for protons. Therefore the entropy ΔS increased with the higher hydration level. It also may be assumed that the local ordering of water molecules that is responsible for the dispersion, increase with more water molecules.

Below the critical hydration level, the fractal dimension at percolation threshold for ovalbumin and lysozyme is ~1.5, whereas above the critical hydration level the fractal dimension is saturated at ~ 3 for ovalbumin and ~ 2.5 for lysozyme. Based on Table 6.4, it can be seen that the fractal dimension obtained for ovalbumin and lysozyme below the

critical hydration level referred to 2 dimensional system, whereas above critical hydration level referred to 3 dimensional systems. It may be assumed that below the critical hydration level, the proton may percolate along the surface of macromolecules, while above the critical hydration level, the protons may move within the matrix of protein structure. The formation of various 'layers' of water molecules covering each macromolecules may also explain the form of the three dimensional system at above critical hydration level. So, above critical hydration level, the proton may move through the water molecule layers, creating 3 dimensional system.

Again, pepsin showed differences compared with ovalbumin and lysozyme. The fractal dimension for pepsin increased continuously from 1 to ~ 1.2 up to ~ 0.055 g/g which referred to the continuous change from one dimensional to two-dimensional system. The abrupt change to 3-dimensional system occurred after ~ 0.055 g/g. It is not clear how to explain the interaction of water molecules in the protein for one-dimensional system. It is probably that at low hydration level of pepsin, the percolation phenomenon had not emerged yet. This may explain the flattened peak at 3-dimensional graph for low hydrated pepsin 0.025 g/g (Figure 6.12 (a)). This may also be connected to condition of crystalline state for pepsin 0.025 g/g as shown in the XRD pattern in Figure 5.36. In the crystalline state, the system is in order condition so the percolation phenomenon may not occur since percolation is a phenomena of stochastic and disordered systems. However, when the hydration level of pepsin was increased the system started to become amorphous. In the amorphous hydrated system, percolation took place and the mechanism was comparable with that for ovalbumin and lysozyme (as explained above).

6.7.5 ε_4 dispersion

The ε_4 dispersion was routinely observed at frequencies higher than the ε_3 dispersion, but only at relatively low temperature.

The frequency difference between the ε_3 and ε_4 dispersion of lysozyme was smaller than ovalbumin. As a consequence, the ε_3 and ε_4 dispersions were observed more clearly for lysozyme, whereas the ε_4 dispersion for ovalbumin was most likely found at frequencies beyond the experimental window.

In the limit of the experimental frequency range, it is difficult to obtain a complete dispersion processes (LFD, ε_3, and ε_4 dispersions) in one plot. However, this dispersion can be detected by analysing a wide range of hydrations and temperature. For example, the LFD process could be mistaken for the tail of another dispersion at low frequency. However, by looking at the pattern obtained from higher hydration levels and various temperature ranges (see Section 6.2.2), it was then possible to confirm that the LFD was not a tail of another dispersion.

Similar possibilities exist for the ε_3 and ε_4 dispersions. The ε_4 dispersion, for low hydrated lysozyme, was vaguely observed at ambient temperature (Figure 5.7 (b)). However at low temperature, the existence of ε_4 dispersion would be more readily realised (Figure 6.29). The ε_3 dispersion, for example, was hardly observed at high hydration levels and ambient temperature, since it was buried under LFD (Figure 5.6 (a)). Again, the existence of the ε_3 dispersion was revealed at low temperature (Figure 6.30).

Since the ε_4 dispersion existed at higher frequency than the ε_3 dispersion, the ε_4 dispersion was suggested to originate from less size cluster than that of the ε_3 dispersion. Based on the cluster model as has been described before, the ε_4 dispersion may originate from distribution of cluster polarisation within the domain unit in protein.

Hawkes and Pethig also mentioned briefly about another weak dispersion for lysozyme at higher frequency than the loss peak of ε_3 dispersion[34]. This weak dispersion was considered as similar as ε_4 dispersion found in this work. Hawkes and Pethig suggested that this weak dispersion was due to vibrational motions of the polypeptide backbones and the plasticising action of bound water[34].

6.8 Summary

All proteins studied (ovalbumin, lysozyme, and pepsin) showed an LFD and ε_3 dispersion that shifted toward higher frequency with an increase in temperature. The percolation threshold observed, confirmed the proposed cluster model to describe the mechanism of water-protein interaction in the proteins.

Simple Arrhenius behaviour was observed at temperatures below percolation threshold temperature but above the 'freezing' temperature (thought to be due to the formation of a proton glass). This Arrhenius behaviour changed to the VTF behaviour (for ovalbumin and lysozyme) as the hydration level was increased above 0.2 g/g. This was probably due to the coincidence between the percolation threshold and the onset of glass transition. Another Arrhenius behaviour at high temperature was observed afterwards, which may be due to the cluster polarisation from the structure/bound water in the protein.

The dielectric response of pepsin was different to ovalbumin and lysozyme. The ε_3 dispersion was not observed clearly for pepsin. The onset of VTF behaviour occurred at lower hydration levels for pepsin, compared with ovalbumin and lysozyme. Pepsin also did not show any ε_4 dispersion, nor proton glass. It is not clear whether differences observed in pepsin was simply due to different hydration level or due to different physicochemical state in pepsin. As has been shown, there were some physical differences in the starting material of pepsin compared with ovalbumin and lysozyme. The starting material pepsin was predominantly in the crystalline state. The morphology of pepsin powder, from SEM images, revealed a disordered bulky shape, instead of nice sphere typical spray-dried particles as shown for ovalbumin and lysozyme. And most of all, the FTIR spectrum for pepsin showed the probability of pepsin having significant different structure compared with ovalbumin and lysozyme (Section 5.4.6). It was probable that the starting material for pepsin has undergone denaturation or other structural changes, which

then created differences in the measurement results compared with ovalbumin and lysozyme.

7 IN-SITU DIELECTRIC MEASUREMENT ON FREEZE DRYING PROTEINS

7.1 Introduction

This chapter involves a novel technique for *in situ* dielectric measurement of a sample inside a freeze drying glass vial. The purpose of this study was to determine whether the end point of lyophilisation process could be detected by dielectric measurements, and thereby provide a measurement for establishing the residual water content of the sample inside a freeze drying glass vial*.

It has been described in Section 1.4 that most previous attempts to use electrical measurements for process control during freeze-drying were based on the placement of electrodes inside the glass vials, within the freeze-drying chamber. These approaches were therefore destructive to the sample and could not be used for routine analysis of an entire cycle.

In order to obtain non-invasive measurements of a material inside a freeze-drying vial, it is necessary to develop a remote-electrode system specifically for this purpose. In the context of this work, a remote electrode system is defined as electrodes that are separated from the sample by non-conductive and non-dispersive medium. In Section 5.3, the remote electrode system was formed by placing polyethylene films between the parallel plate electrodes and the sample. For the purpose of monitoring the freeze-drying process, a remote electrode system was established using custom-made electrodes, attached externally to the freeze-drying glass vial.

* This part of the work has now been accepted for publication in the Pharmaceutical Research journal (see Appendix A7.1).

With insight into the frequency response of such composite dielectric systems[109] (in this case a sample contained inside a glass container), it should be possible to carefully select a frequency range over which the sample characteristics dominate the dielectric response of the composite system. It will then be possible to undertake measurements of sample properties without introducing probes into the system.

In order to establish the validity of the remote electrode approach, it was first necessary to characterize the intrinsic dielectric properties of the samples, over the frequency range 10^{-1} – 10^{6} Hz, using conventional parallel plate electrodes (see Chapter 5). The second stage was to simulate a remote electrode measurement by placing non-conductive, non-dispersive polymer films between the sample and electrodes (see Section 5.3). Finally a study on the dielectric measurement of protein contained in a 10 ml freeze-drying vial was undertaken with the electrodes external to the glass vial. Measurements, in each of the three stages, were taken as a function of water content of commercial spray dried proteins, since spray dried protein is readily available and inexpensive. A freeze-dried proteins was used for a final test to investigate whether the end product of lyophilisation could be measured using remote electrodes.

7.2 Electrode Design for *in situ* Dielectric Measurement inside a Glass Vial

7.2.1 Introduction

The dielectric measurement for *in situ* monitoring of water content inside a glass vial, was initiated by designing the electrodes that attached externally to the freeze drying glass vial. Two types of electrode design were made, i.e. coated-type electrodes and custom-made electrodes.

7.2.2 Coated electrodes

The coated electrodes were designed by coating the glass vial surface with a good conducting material, such as gold and silver. Gold is considered not economical for research purpose, so this work used silver as the conducting element.

Conducting silver paint (Radio Spares) was chosen to form the remote electrodes on the external surface of the glass vial. Based on the smallest stray capacitance, obtained from the investigation on custom-made electrodes, an area of 250 mm^2 silver was used to form each electrodes (see Section 7.2.3). Figure 7.1 illustrates a typical coated vial.

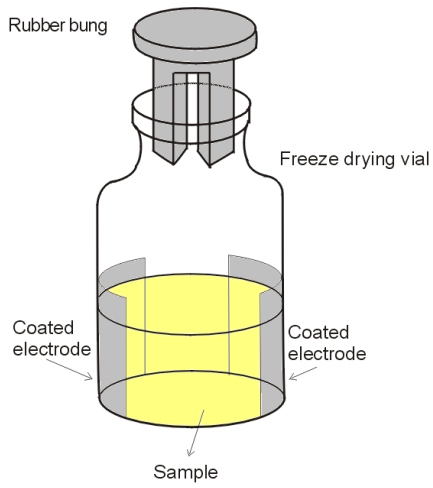

Figure 7.1 *Schematic of freeze-drying glass vial with coated electrodes.*

Figure 7.2 shows the measurements of hydrated ovalbumin (0.06 g/g) in a silver coated vial, compared with a measurement on the same material using conventional parallel plate electrodes. As shown in the figure, the ε_3 dispersion was found in the same frequency range. The relaxation time obtained from the fitting result was also comparable (see key in Figure 7.2).

Fitting to spectra obtained from the measurement using coated electrode vials, employed the circuit model shown in the Figure 5.2 (c). Since the empty glass vial itself showed LFD behaviour then it may be assumed that the LFD element in this case came from both the sample and glass vial. Fitting for the empty vial was based on the sum of two power law functions, which was represented as a parallel circuit of two constant phase angle elements (see the circuit model in the inset of Figure 7.2).

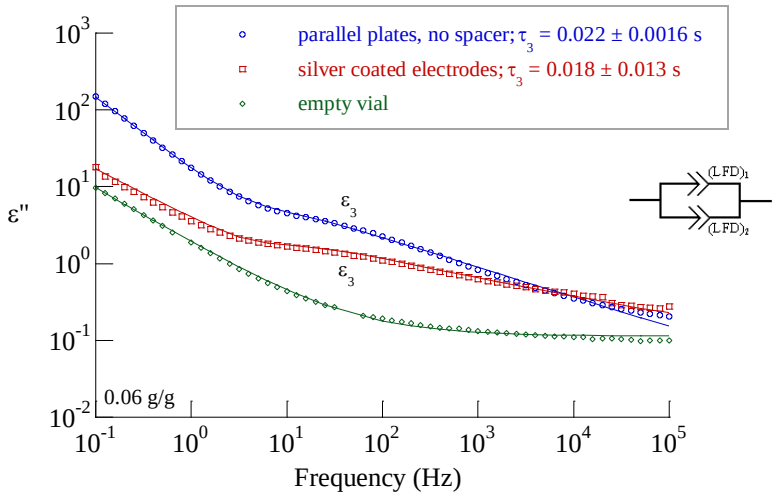

Figure 7.2 *Hydrated ovalbumin (0.06 g/g) inside a glass vial with silver coated electrodes, compared with the measurement using parallel plate electrodes without any spacer. Symbols represent measurement data, lines represent fitting. Circuit model in the inset was employed to fit the empty vial.*

The comparison of measurements on ovalbumin, with a higher hydration level, is shown in Figure 7.3. With the higher hydration level, the new dispersion (i.e. ε_2 dispersion) was observed. It has been discussed in Section 5.3, that the ε_2 dispersion (observed from the measurement using parallel plate electrodes with spacer) was due to the composite impedance of polyethylene films and the LFD of the sample. In Figure 7.3, the ε_2 dispersion observed was due to the composite formation from both the sample and glass

vial. This ε_2 dispersion was fitted with another Davidson-Cole element. Therefore, the whole fitting for higher hydration level employed two Davidson-Cole elements, as shown in Figure 7.3 (b). Unlike the circuit model shown in Figure 5.26, the LFD element is still present for this kind of remote electrodes, since as has been mentioned earlier, the glass vial itself has LFD behaviour. Therefore, the LFD element from the circuit in Figure 7.3 (b) originated from both the sample and glass vial.

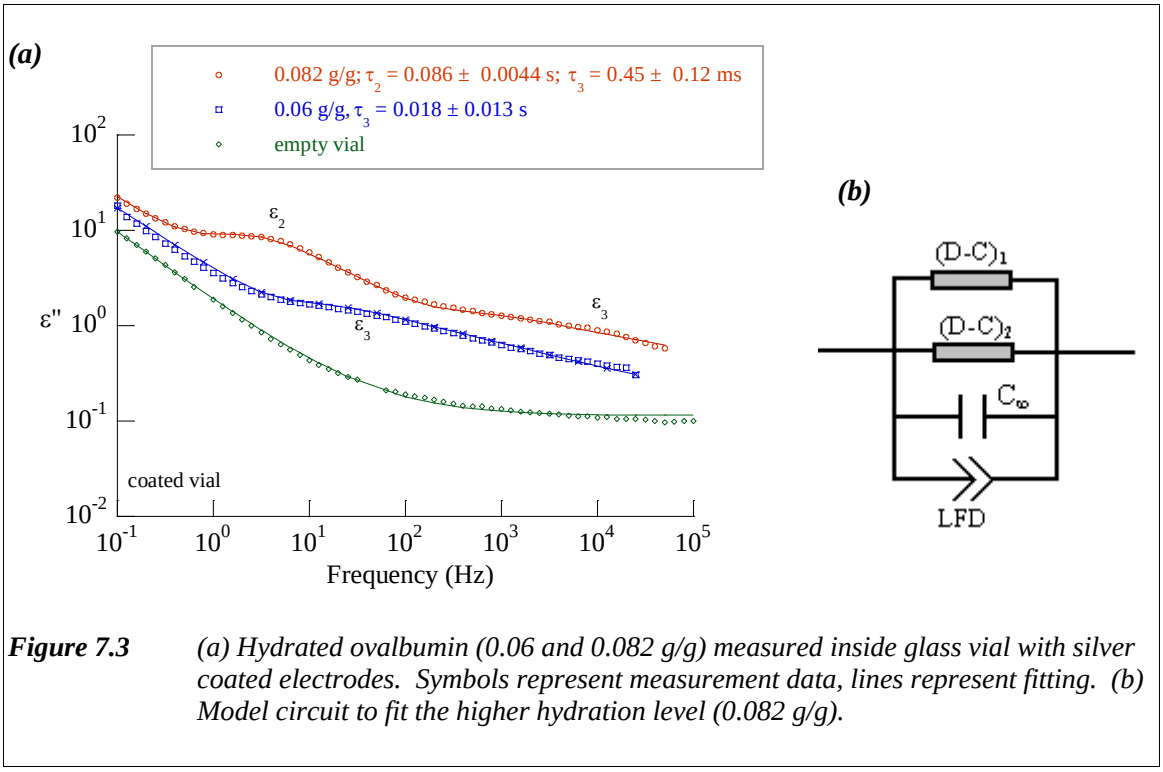

Figure 7.3 *(a) Hydrated ovalbumin (0.06 and 0.082 g/g) measured inside glass vial with silver coated electrodes. Symbols represent measurement data, lines represent fitting. (b) Model circuit to fit the higher hydration level (0.082 g/g).*

The results shown in Figure 7.2 and Figure 7.3 suggested that the method of dielectric measurement of the sample inside glass vial using silver coated electrodes for *in situ* freeze drying purposes is sensitive to the water content in the sample. However, these coated electrodes are not desirable for practical freeze-drying procedures. The coating material may interfere with the samples during the lyophilisation process which may further create

unwanted results. The coating method on the glass vial is also not efficient for the mass-industrial production.

7.2.3 Custom-made electrodes

Another alternative, for designing a remote electrode system for the purpose of *in situ* freeze drying process, is to use free standing electrodes that were custom-made to the shape and dimensions of the vials used. Various sizes (i.e. 10 x 10 mm^2, 25 x 10 mm^2, 579.6 mm^2, and 672.5 mm^2) of brass electrodes were examined in order to minimise the effect of measurement residual, especially stray capacitance. Besides the size, the shape/dimension of the electrodes is also considered for the use during freeze drying process to avoid any unwanted effect, especially heating transfer.

The stray capacitance was determined by measuring at ambient temperature various solutions with known dielectric constant, i.e. water, ethanol, methanol, and the mixtures of 50 % water + 50 % ethanol, and 50 % water + 50 % methanol . The permittivity of the mixture solutions was examined using a high frequency dielectric measurement (50 MHz – 20 GHz) at ambient temperature. Dielectric constant of the mixture solutions was obtained from fitting to Debye model (Figure 7.4).

The capacitance of the various mixture solutions, measured inside glass vial using various size of custom-made electrodes, are shown in Figure 7.5 and Figure 7.6. The intersection from the plot of capacitance (C) versus permittivity (ε) produces a stray capacitance, with the gradient as empty cell capacitance.

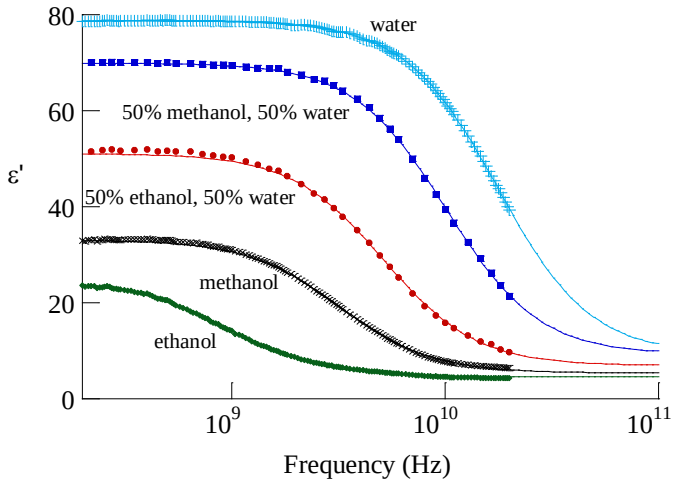

Figure 7.4 *Real permittivities for various solutions at frequency range 100 MHz - 20 GHz. Symbols represent the experimental data, lines represent the curve fitting using a Debye expression (Equation 3.28).*

(a)

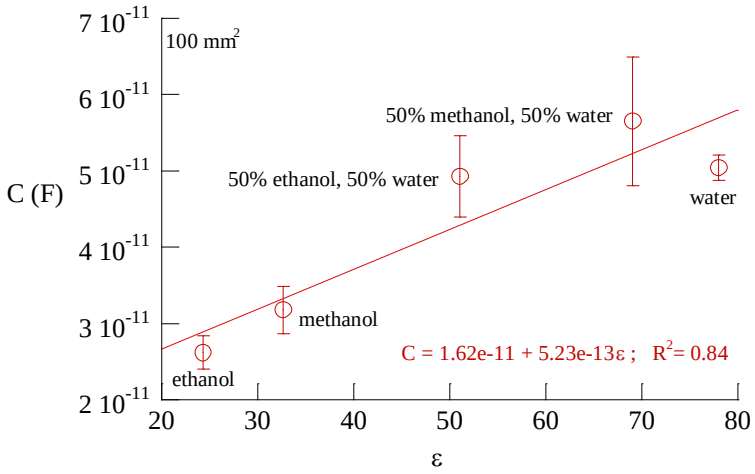

(b)

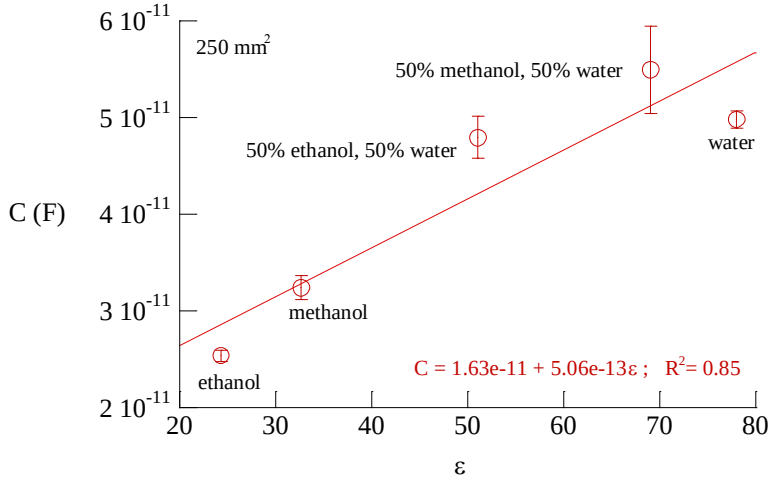

Figure 7.5 *Capacitance versus permittivities for electrode sizes (a) 10 x 10 mm^2, (b) 25 x 10 mm^2. Symbols represent the experimental data, lines represent the linear curve fitting.*

(a)

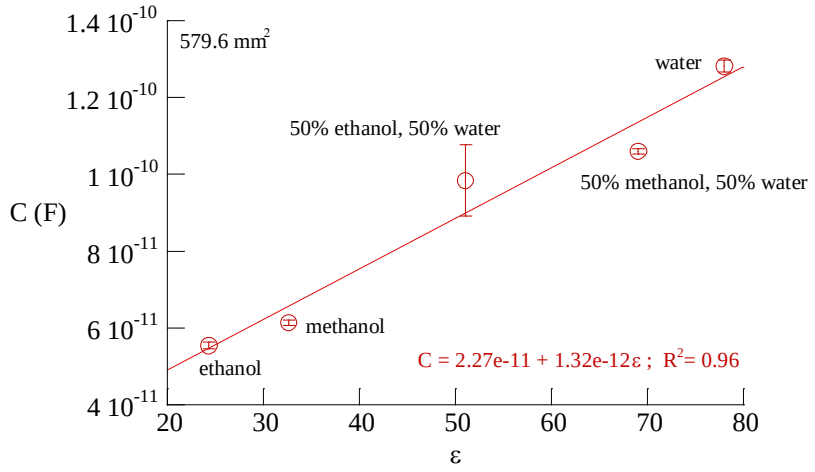

(b)

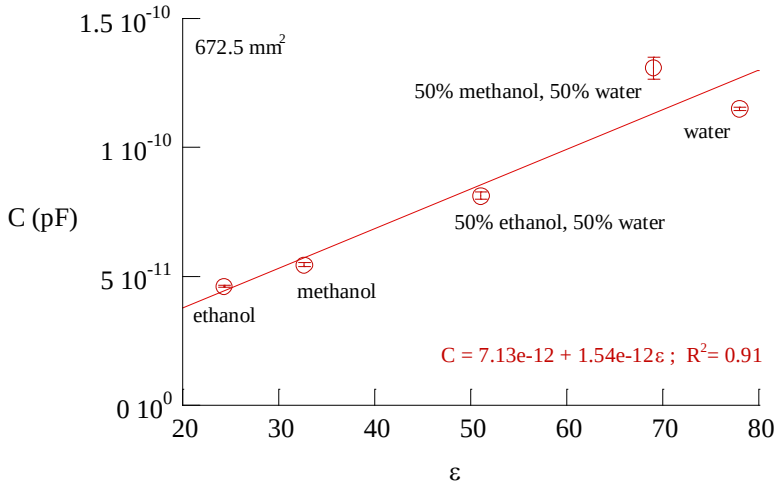

Figure 7.6 *Capacitance versus permittivities for electrode sizes (a) 579.6 mm^2, (b) 672.5 mm^2. Symbols represent the experimental data, lines represent the curve fitting.*

Table 7.1 shows the stray capacitance obtained from various electrode sizes as calculated from Figure 7.5 and Figure 7.6. It can be seen from Table 7.1 that custom-made electrode of 672.5 mm^2 had the smallest stray capacitance. However, it had the biggest empty cell, and also the geometry for electrode size 672.5 mm^2 is not ideal for the freeze-drying process, compared with other electrode sizes, since large mass of electrode may affect the heat transfer to the sample during the freeze-drying process. The stray capacitances for the 100 mm^2 and 250 mm^2 custom-made electrodes are almost comparable. However, of these two options, 250 mm^2 electrodes are preferable, since the height of the freeze dried sample in the vial may be more than 10 mm. Therefore, an electrode size of 250 mm^2 was chosen as a representative custom-made electrode system for this work.

Table 7.1 *Stray capacitance obtained from various electrode size.*

Electrode size (mm^2)	Stray Capacitance (pF)	Empty Cell Capacitance (pF)
100	16.2	0.523
250	16.3	0.506
579.6	22.7	1.32
672.5	7.13	1.54

Figure 7.7 shows the set-up of the custom-made electrodes attached externally to the glass vial. The sample was placed in the 10 ml freeze drying glass vial, with a rubber bung on the top of the vial. The vial was placed on a metal base, sandwiched between the custom-made electrodes, and the sample was packed routinely to a height of ~ 10 mm. This set-up was designed to imitate the real conditions of the freeze drying process. For the freeze dried samples, the glass vial containing the sample 'cake' (obtained from the lyophilisation process) was placed directly between the custom-made electrodes.

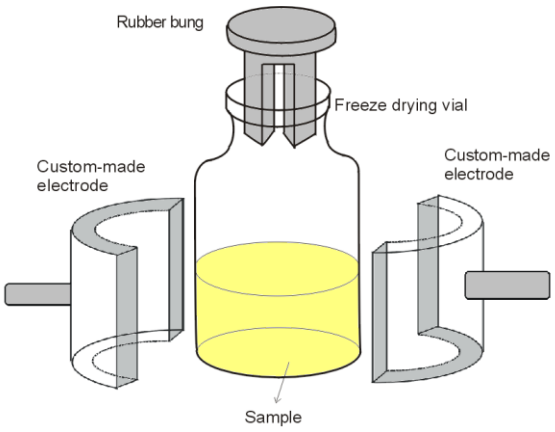

Figure 7.7 *Set-up of custom-made electrodes attached externally to the glass vial*

Figure 7.8 (a) shows the comparison between a measurement for ovalbumin 0.06 g/g using parallel plate electrodes, without any spacer, with a measurement using remote electrodes (i.e. custom-made electrodes attached externally to the glass vial). Again, the dielectric response using custom-made electrodes attached to the glass vial is comparable with the one measured by parallel plate electrodes (Figure 7.2).

An ε_2 dispersion was also observed in the measurement of a higher hydration level of ovalbumin (0.08 g/g) (Figure 7.8 (b)). All fitting models were the same as those described for coated electrodes (Section 7.2.2.)

Pronounced changes in the dielectric spectra with water content indicated that the technique of using custom-made electrodes attached to the glass vial was also sensitive to water content (Figure 7.8).

(a)

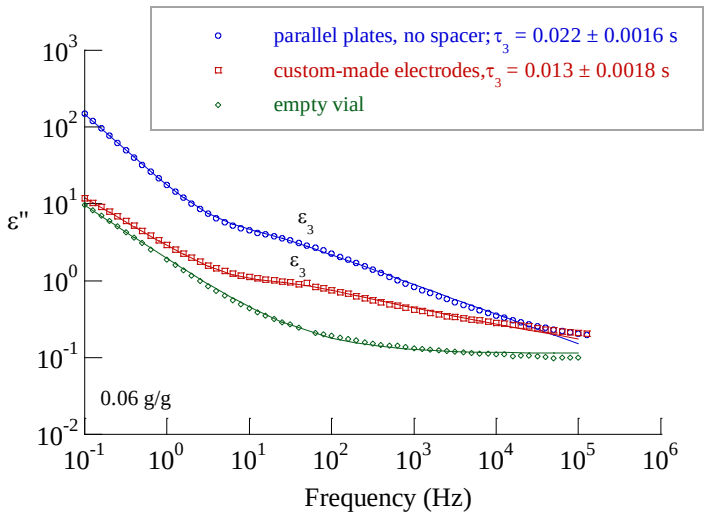

(b)

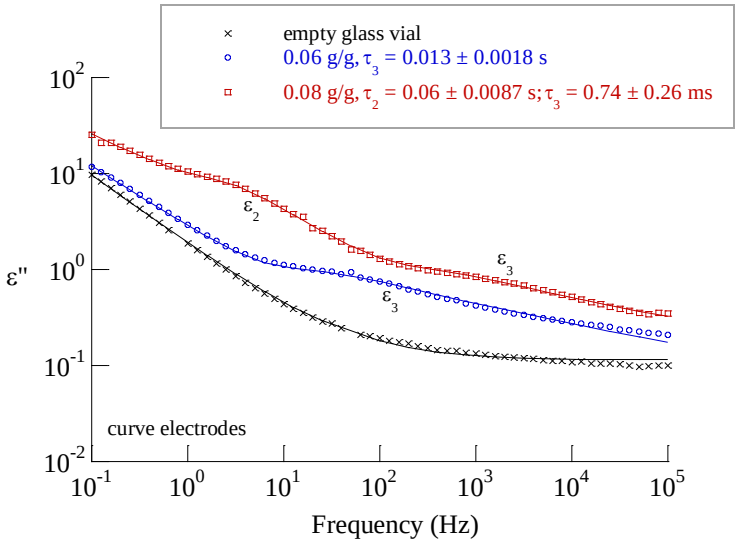

Figure 7.8 *(a) Hydrated ovalbumin (0.06 g/g) inside a glass vial with custom-made electrodes, compared with the measurement using parallel plate electrodes without any spacer. (b) Hydrated ovalbumin (0.06 and 0.08 g/g) measured inside glass vial with custom-made electrodes. Symbols represent measurement data, lines represent fitting.*

7.2.4 Comparison between silver coated and custom-made electrodes

The use of custom-made electrodes is preferred, over coated electrodes, for a number of reasons. The experimental set-up using custom-made electrodes was more convenient and relatively more repeatable, as the electrode system could be reused for any standard vial. For this reason, also, the electrode system was standardised between vials. This is not possible with the hand-painted silver coated electrodes (although a method for routine and repeatable manufacture could have been configured).

The design for freeze-drying purpose using custom-made electrodes is better than coated electrodes. The physical properties of conductive material for coating probably changes during the lyophilisation process, since the freeze drying process involves a very wide range of temperatures (i.e. about - 40 °C – + 20 °C) and pressure (up to ~ 10^{-2} mbar). It is also possible that any chemical degradation may create impurities for the samples being freeze-dried. The coating to the glass vial is also not efficient for the mass production of freeze-drying samples.

A comparison between the use of coated electrodes and custom-made electrodes is shown in Figure 7.9, for hydrated ovalbumin 0.06 g/g and 0.08 g/g. The dielectric response of empty glass vial is also shown. The parameter that can be used as a variable for monitoring the water content of the sample inside the glass vial is relaxation time τ_3 from the ε_3 dispersion. As shown in Figure 7.9, the dielectric response from both the coated electrodes and custom-made electrodes are comparable. The relaxation time τ_3 was also comparable within the error range.

(a)

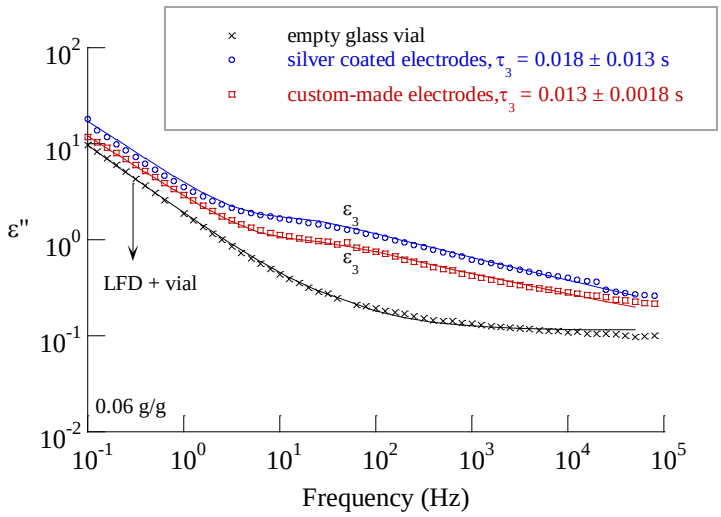

(b)

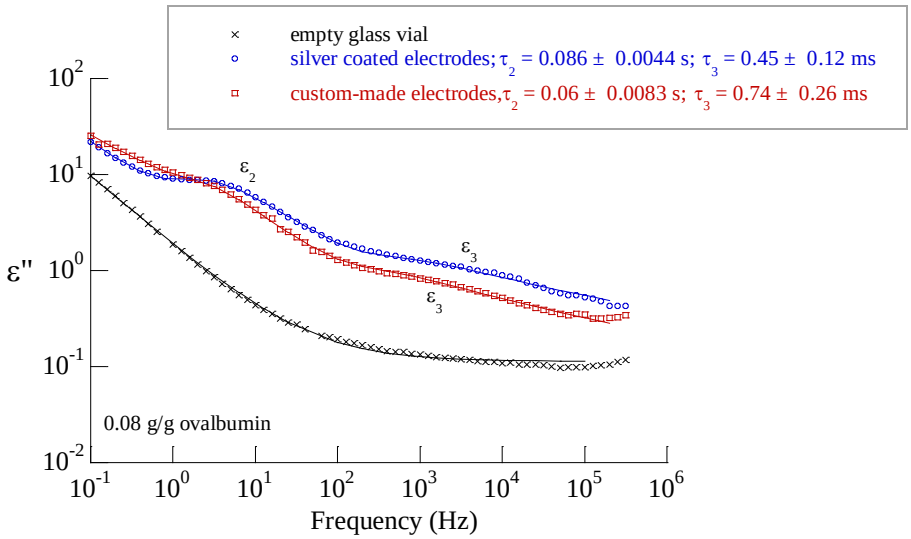

Figure 7.9 *Comparison between coated electrodes and custom-made electrodes on measurement of hydrated ovalbumin (a) 0.06 g/g, (b) 0.08 g/g.*

Figure 7.10 show all dielectric measurement techniques employed in this work for hydrated ovalbumin 0.08 g/g, i.e. the comparison between the use of conventional parallel plate electrodes, the use of remote electrodes from parallel plate electrodes with polyethylene films, and the use of remote electrodes from the use of coated electrodes and custom-made electrodes attached externally to the glass vial.

With all the measurement techniques, an ε_3 dispersion was observed. The ε_2 dispersion was observed for all remote electrode measurements, and was due to the composite structure of the sample/spacer arrangement. For the use of polyethylene films, ε_2 dispersion was observed as a clear dielectric loss peak, originated from the composite of polyethylene films and LFD from the sample. For the use of glass vial, ε_2 dispersion was more vague, since the response was followed with the LFD behaviour which came from both the sample and the glass vial itself.

The significant point from the comparison of all these techniques is that the results from the new technique of using remote electrodes are comparable with the one using the conventional technique. All the techniques show the sensitivity for monitoring water content based on the measurement of the relaxation time τ_3 of the ε_3 dispersion.

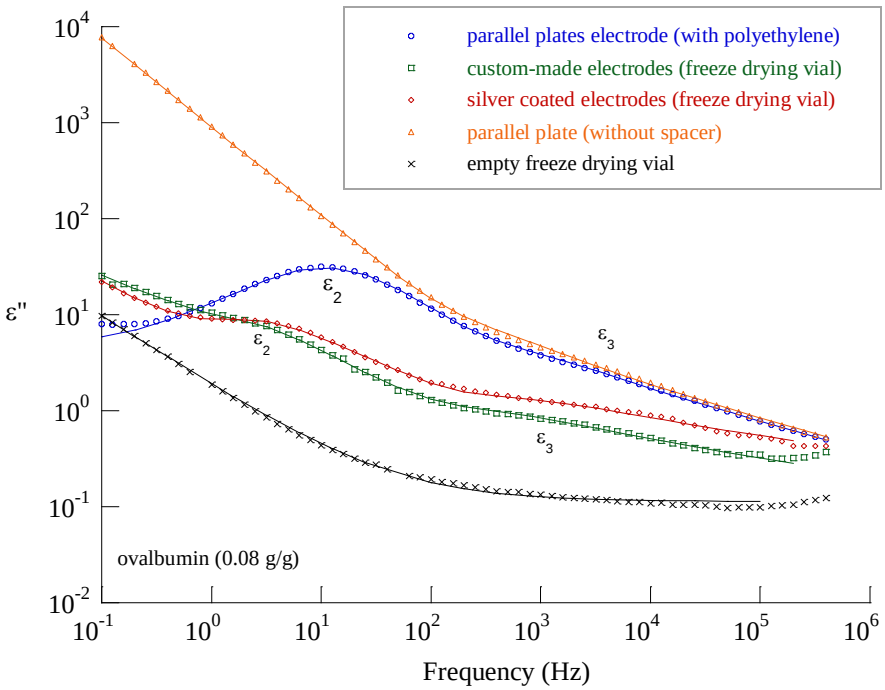

Figure 7.10 *Comparison between dielectric measurement using conventional parallel plate electrodes and remote electrodes (coated electrodes, custom-made electrodes, and parallel plate electrodes with polyethylene films) on measurement of hydrated ovalbumin (0.08 g/g).*

7.3 Measurement of hydrated proteins inside a glass vial

The previous section has shown that the technique of dielectric measurements on samples inside a glass vial, is sensitive to water content and that the results obtained are comparable to those from the conventional technique. The study showed that the use of custom-made electrodes was favoured over the use of coated electrodes. The following sections therefore deal with the experiments using custom-made electrodes. All the experimental work mentioned in previous section was conducted on hydrated ovalbumin. For general validation of the technique, the experiment was then conducted on other selected proteins, i.e. hydrated lysozyme and pepsin.

Figure 7.11 shows the comparison of dielectric measurement with and without remote electrodes for hydrated lysozyme and pepsin. As found for ovalbumin, the dielectric response (mainly the ε_3 dispersion) measured using conventional parallel plate electrodes was comparable with the response measured using remote electrodes (i.e. parallel plate electrodes with the insertion of polyethylene films and custom-made electrodes attached to the glass vial).

The comparison of relaxation times τ_3 from the ε_3 dispersion between measurement with and without remote electrodes, for various hydration levels of the selected proteins (ovalbumin, lysozyme, and pepsin), is shown in Figure 7.12.

(a)

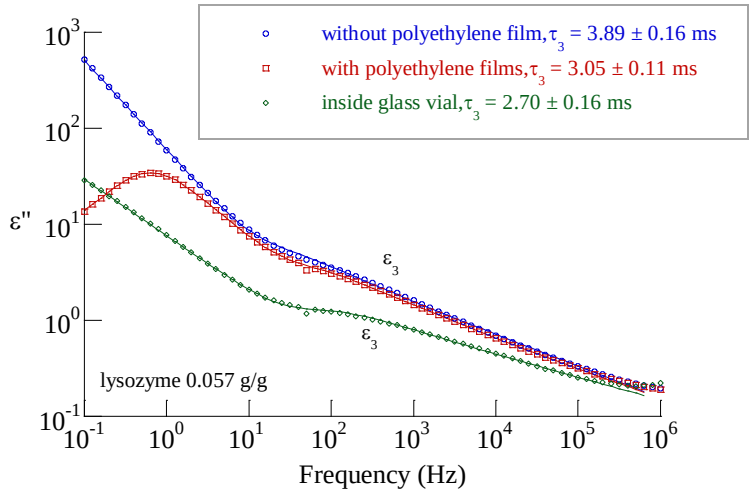

(b)

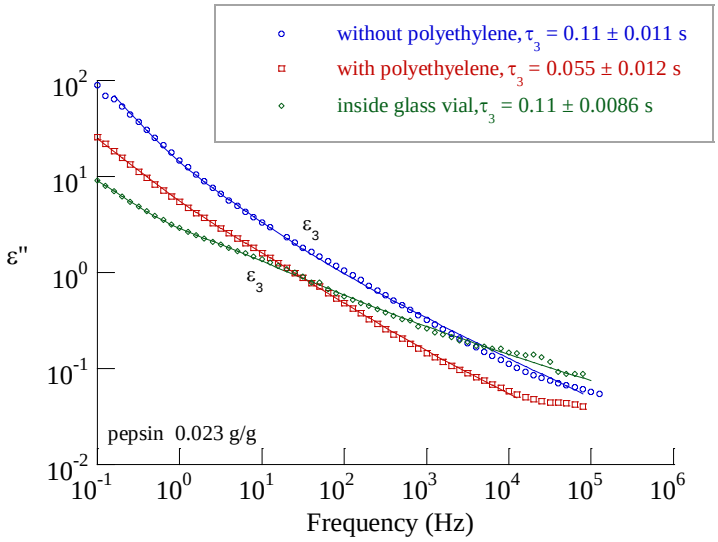

Figure 7.11 *Comparison between dielectric measurement using conventional parallel plate electrodes and remote electrodes (custom-made electrodes, and parallel plate electrodes with polyethylene films) on measurement of hydrated (a) lysozyme (0.057 g/g), (b) pepsin (0.023 g/g). Symbols represent experimental data, lines represent fitting.*

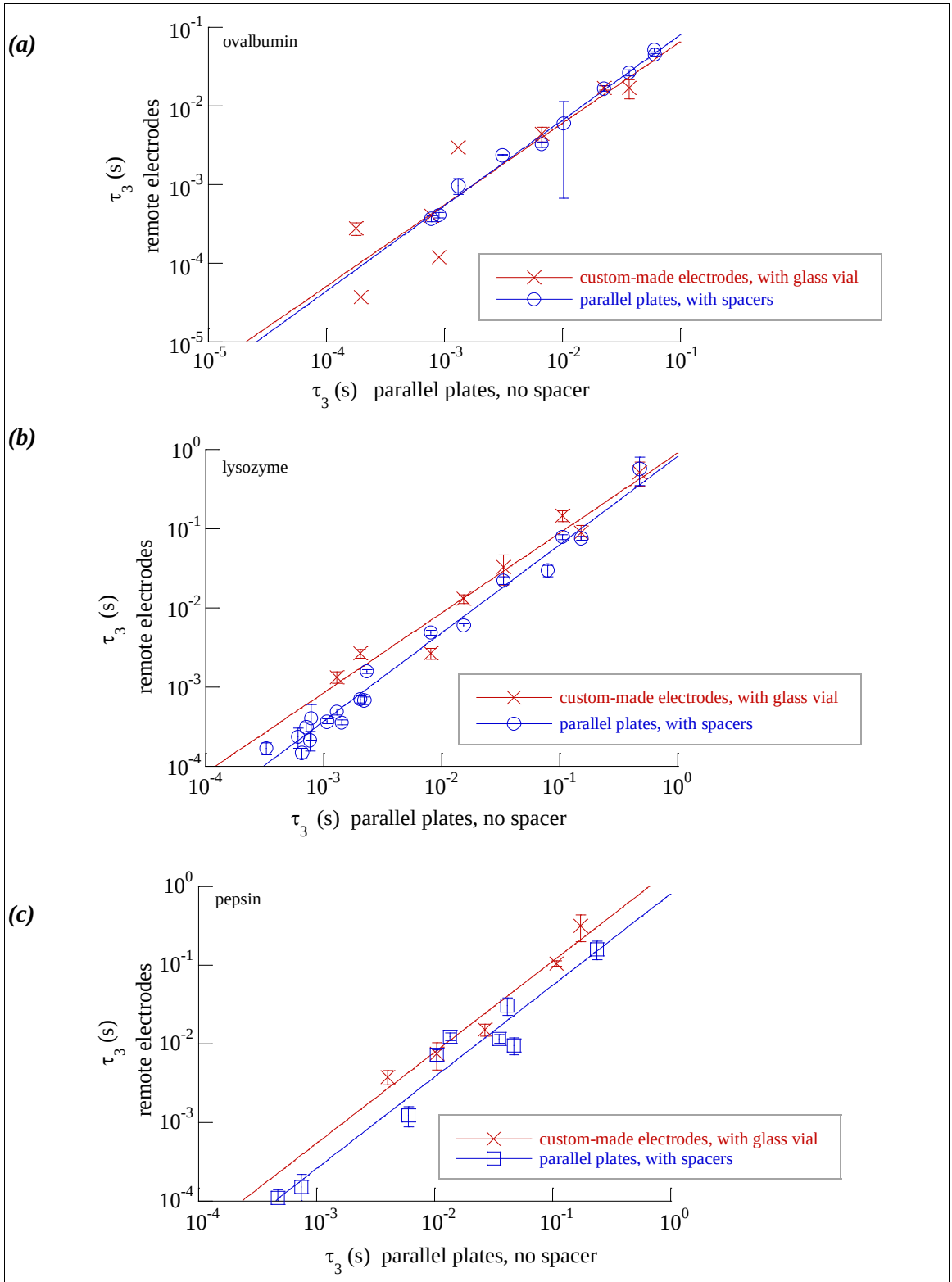

Figure 7.12 *Comparison between measurement with and without remote electrodes for various hydration level of (a) ovalbumin, (b) lysozyme, and (c) pepsin. Symbols represent experimental data, lines represent fitting.*

The data in Figure 7.12 was fitted with the following power function:

$$\tau_{remote-electrodes} = A * \tau_{no-remote-electrodes}^{m} \tag{7.1}$$

The logarithmic function of Equation (7.1) gives a linear function for log-log curve:

$$\log \tau_{remote-electrodes} = \log A + m \log \tau_{no-remote-electrodes} \tag{7.2}$$

with a gradient m and intersection point (0, $\log A$).

The relaxation times, obtained from measurements with and without remote electrodes, are equivalent when the gradient m makes an angle of 45° (i.e. $m = 1$), $\log A \to 0$, and correlation $R^2 = 100\%$. Table 7.2 shows value of intersection point ($\log A$), the gradient (m), and the correlation coefficient (R^2) that describe the relationship between the electrodes for each selected protein. In all cases, the values for intersection point and gradient deviated less than 10% from the required values (i.e. $m = 1$ and $\log A \to 0$), which indicates good agreement between the measurements with and without remote electrodes.

Table 7.2 *Fitting results from Equation (7.2) for measurements using parallel plate with spacers and custom-made electrodes with glass vial.*

Proteins	**Parallel plates, with spacers**			**Curved electrodes, with glass vial**		
	Intersection Point, log A	Gradient m	Correlation R^2 (%)	Intersection Point, log A	Gradient m	Correlation R^2 (%)
Ovalbumin	-0.004	1.09	99	-0.143	1.03	91
Lysozyme	-0.081	1.11	97	-0.041	1.01	97
Pepsin	-0.086	1.16	98	0.212	1.16	94

7.4 Dielectric measurement of freeze-dried proteins inside a glass vial

7.4.1 Introduction

The previous section has shown the dielectric study of hydrated proteins inside glass vial. The result has shown that the technique is capable of monitoring the water content of a sample inside glass vial, based on the observation of the ε_3 dispersion. With the purpose of *in situ* monitoring of water content during freeze drying process, the study now continues with the dielectric investigation of a freeze dried sample inside the glass vial. This section involves freeze dried sample preparation, the dielectric measurement of a freeze-dried protein inside glass vial, and the characterisation of freeze dried samples using other complementary techniques. Due to the frame time of the study and the inferior condition of freeze dryer itself, only ovalbumin was chosen as a model protein for this freeze drying study.

7.4.2 Method

7.4.2.1 Freeze drying experimental

2.5 ml aliquots of ovalbumin solution of various concentrations: 1%, 2.5%, 5%, and 10% w/v were placed in 10 ml glass vials and lyophilised in a Secfroid Lyolab G freeze-drier. Several cycles of freeze drying ovalbumin were carried out. Each cycle has different period of primary and secondary drying (Table 7.3). The different cycles were designed to achieve different water contents, while the different formulations (i.e. different use of buffer, excipients, pH) were investigated for the purpose of establishing a stable product (Table 7.4).

Table 7.3 *Various cycles for freeze drying ovalbumin*

Cycles	Primary Drying	Secondary Drying
I	-20 °C for 24 hours -10 °C step wise to 10 °C	+15 °C for 24 hours
II	-30 °C for 24 hours -20 °C for 24 hours -10 °C for 5 hours	+10 °C for 24 hours (vacuum failed!, start freezing and drying again for a short period) +20 °C for 2 hours
III	-30 °C for 24 hours -20 °C for ~ 7 hours, step wise to 0 °C	0 °C for 24 hours +10 °C for 9 hours
IV	-30 °C for 24 hours -20 °C for 24 hours -10 °C for 3 hours, step wise to 0 °C	0 °C for 24 hours +10 °C for 6 hours

Table 7.4 *Various formulation for freeze drying ovalbumin*

Ovalbumin	Solutions	Excipients	Cycles
1%	H_2O	Sucrose	(see Table 7.3)
2.5%	Phosphate buffer pH 7		
5%	Tris buffer pH 9		
10%			

7.4.2.2 Characterisation of freeze drying sample

Freeze drying ovalbumin was characterised by other complementary methods (i.e. SEM, DSC, XRD, and FTIR), in order to investigate that the in-house freeze dried ovalbumin has the right properties compared to commercial freeze dried ovalbumin, and is therefore suitable for dielectric analysis.

SEM photographs are useful for displaying the macroscopic morphology of the freeze-dried samples. The morphology or shape of the powder may affect the type of dielectric response. DSC was carried out to determine the glass transition of the sample. Different glass transition may cause a different dielectric response, since the glass transition depends on the water content in the sample. FTIR spectra may be able to investigate the structure of freeze-dried samples, such as changes in secondary structure, aggregation, conformation etc. Changes in protein conformation may affect the dielectric response. XRD data is useful to investigate the crystalline state of the sample. The amorphous or crystalline state may give rise to a different dielectric spectra. The experimental of using SEM, DSC, FTIR, and XRD have been described in Section 5.2.2.3.

7.4.2.3 Dielectric measurement of material inside a glass vial

The purpose of these measurements was to establish the use of custom-made electrodes attached to a glass vial, as a technique for *in situ* monitoring of water content during lyophilisation. In order to validate the measurement from the new technique (i.e. using custom-made electrodes), the dielectric spectra were also compared with measurements using conventional parallel plate electrodes.

The method used for *in situ* dielectric measurement is similar to that described in the previous section (see Section 7.2). For this study, the sample in the glass vial was obtained directly from freeze drying process. The freeze dried 'cake' obtained from lyophilisation process was placed directly between the custom-made electrodes (Figure 7.13).

(a) ***(b)***

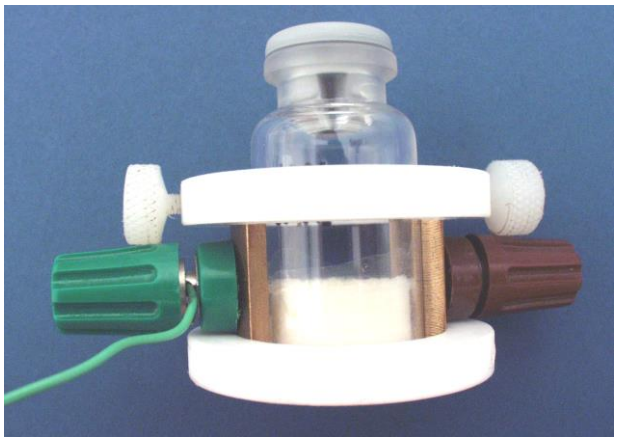

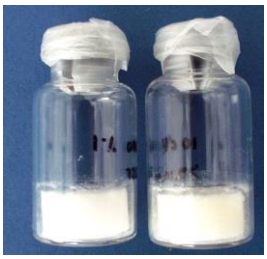

Figure 7.13 *(a) Set up of custom-made electrodes attached to the freeze drying ovalbumin in a glass vial, obtained directly from the lyophilisation process, (b) typical features of freeze-dried ovalbumin inside a glass vial.*

7.5 Results

7.5.1 Freeze Drying characterisation

7.5.1.1 FTIR

Samples from all cycles show similar FTIR spectra to that obtained for commercial freeze dried samples from Sigma. Figure 7.14 (a) shows the FTIR spectra from one of the in-house freeze dried ovalbumin compared with the commercial freeze dried ovalbumin from Sigma.

The FTIR spectra for freeze dried proteins showed a majority of the OH bonds in water, and the amide I ($RCONH_2$) and amide II $(RCO)_2NH$ groups in the protein. A significant part of the study of protein FTIR spectra focused on the amide I vibrational mode (~ 1700 – 1600 cm^{-1})[110]. This amide I vibrational mode is sensitive to the conformational structure of protein backbone, since it originates from the peptide carbonyl stretching mode[18,111]. Changes in conformation, are usually observed in terms of shifting or broadening of the amide I or amide II peak. As shown in Figure 7.14 (a), there is no difference in the position or width of the amide I or amide II peaks, between the commercial and in-house freeze dried ovalbumin. This showed that the structure of the in-house freeze dried ovalbumin was comparable with the commercial one, and the prepared samples thus were suitable for further analysis.

Figure 7.14 (b) shows the FTIR spectra of freeze dried ovalbumin, prepared with the addition of 2.5 wt% sucrose as stabilizer. Several studies have shown the effect of the various additives on freeze dried samples[18,110]. Polyols and sugars, such as sucrose can stabilise proteins against denaturation in solution. These additives also protect lyophilised proteins from denaturation[112 113]. Lyophilised proteins with these additives have similar FTIR spectra to the spectra observed in proteins solutions. It was suggested that the

addition of these additives maintain the protein structure during dehydration. It was predicted that these additives may function as water substitutes in the proteins, in which the additives such as sucrose interact directly with the hydroxyl groups of the protein[18].

If the addition of additives affects the protein structure, the difference is observed via a shift in the peak of amide band or the peak broadening. In this study, the addition of an optimum amount of sucrose does not affect the IR spectrum. However, the addition of high concentration of sucrose gave an additional peak in IR spectrum (see Figure 7.14 (b)). The additional peak observed with the addition sucrose was identified as a primary OH group which is probably mixed with the aromatic OH-ring, which all originate from sucrose.

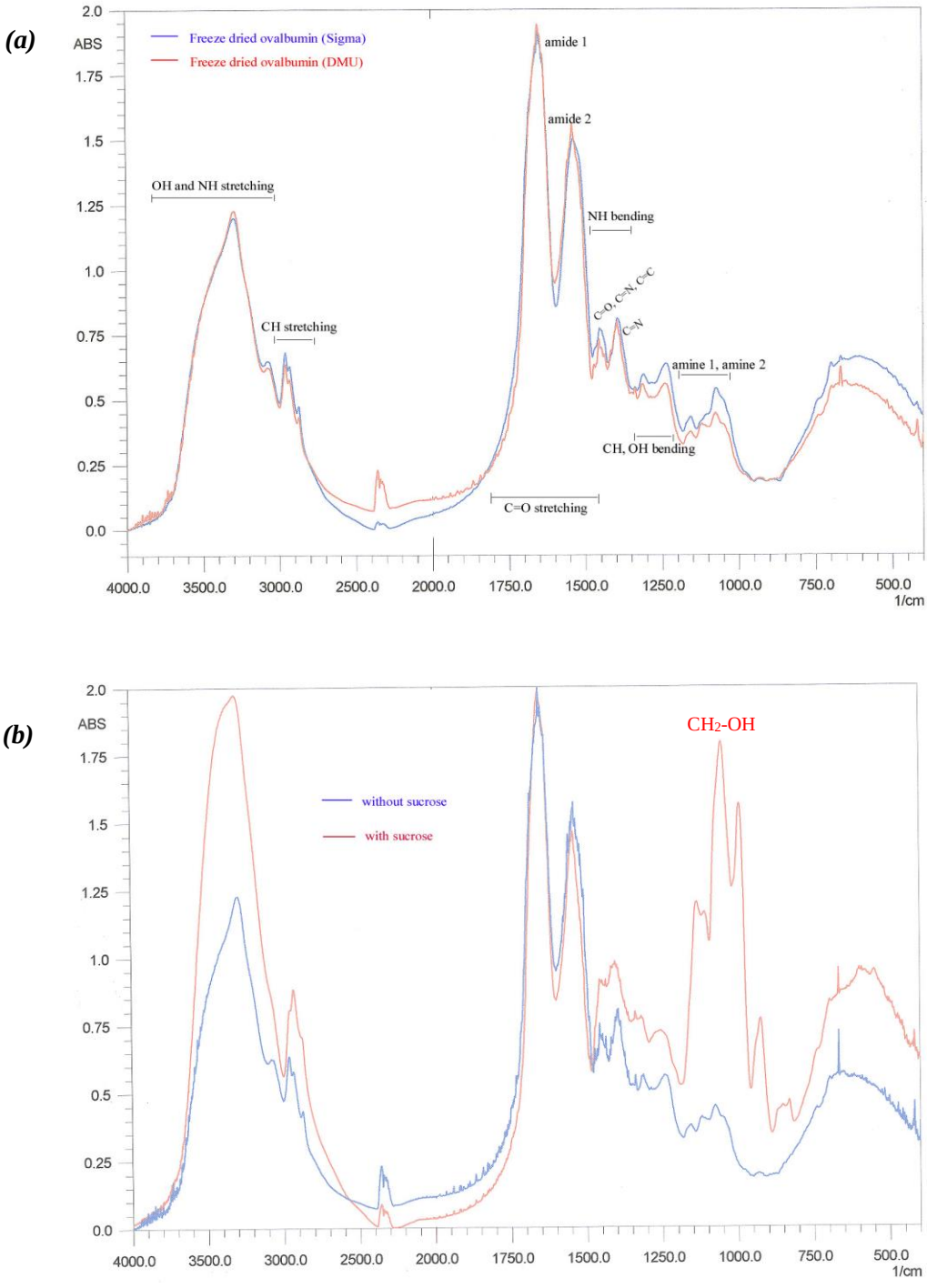

Figure 7.14 *Comparison of FTIR spectra of freeze dried ovalbumin (a) between commercial production (Sigma) and in-house preparation (DMU), (b) between the use of with and without sucrose.*

7.5.1.2 XRD

Figure 7.15 shows the XRD pattern for commercial freeze dried ovalbumin (Sigma) and in house freeze dried ovalbumin (DMU). The spectra confirm that both of the samples were in a highly amorphous state. In terms of stability, the form of crystalline of the freeze-dried sample is more preferable than the amorphous form. However, the crystalline state of macromolecule substance is difficult to achieve. The process of crystallising macromolecules, like proteins, is a complex and time consuming task, and so freeze-dried proteins are usually found in the amorphous state. This is due to the high-energy processing in the freeze-drying process and also due to the large molecular size of proteins[114].

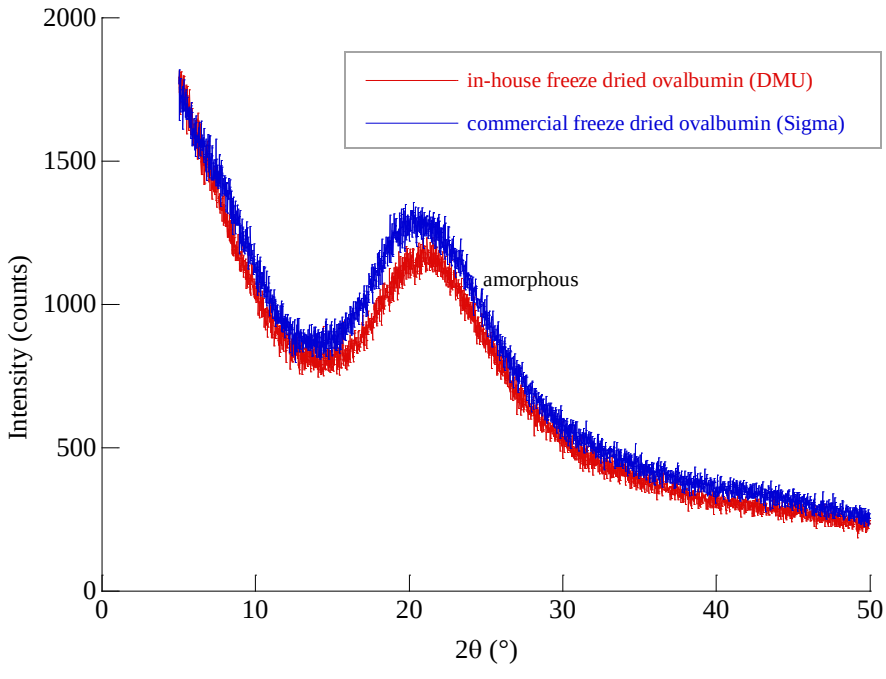

Figure 7.15 *XRD pattern of commercial and in-house freeze dried ovalbumin.*

7.5.1.3 DSC

DSC thermograms for commercial freeze dried ovalbumin (Sigma) and in-house freeze dried ovalbumin (Sigma) are shown in Figure 7.16. These thermograms show that both the commercial and in-house freeze dried ovalbumin have similar glass transitions (T_g) at ~ 85 °C. Differences in the intensity of the DSC output are just due to the different amount of measured samples.

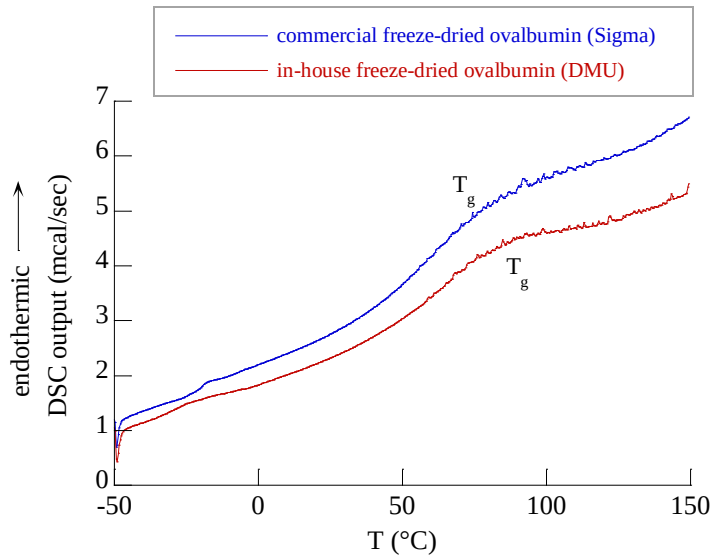

Figure 7.16 *DSC plots of commercial and in-house freeze dried ovalbumin.*

7.5.1.4 SEM

Figure 7.17 shows the SEM micrographs comparing the micro-structure of the commercial freeze dried ovalbumin (Sigma) to the in-house freeze dried ovalbumin (DMU). Both of the SEM pictures from commercial and in-house freeze dried ovalbumin show a typical shape of freeze dried product, i.e. sharp flake morphology.

The excessive addition of sucrose may change the morphology of freeze dried samples. When a small number of sucrose was increased, the flake particles contained some holes (see Figure 7.18 (a)). These holes increased in size when more sucrose was added, and the particle shape changed probably because of surface tension. The morphology of freeze-dried ovalbumin with sucrose is no longer flake-shape anymore, but has a rounded edges (Figure 7.18(b) and Figure 7.18 (c)).

(a)

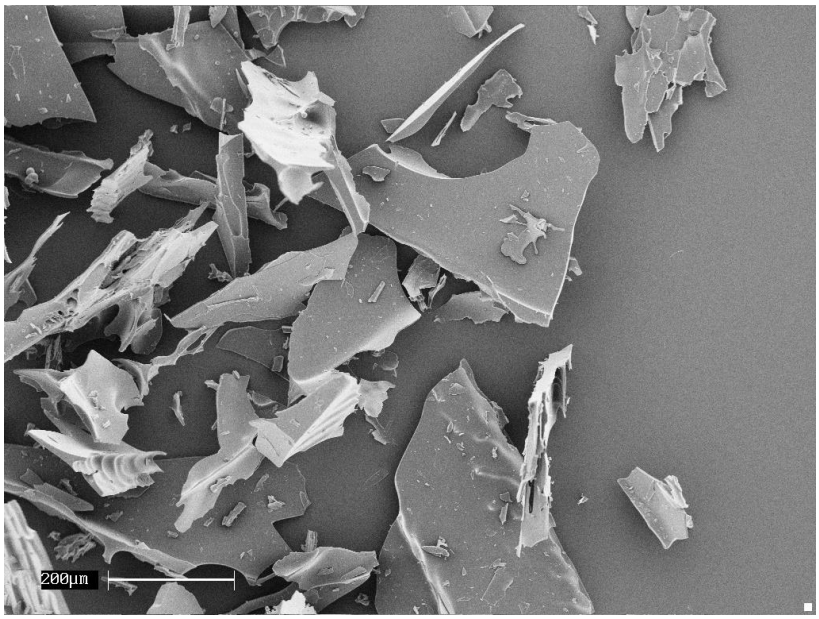

(b)

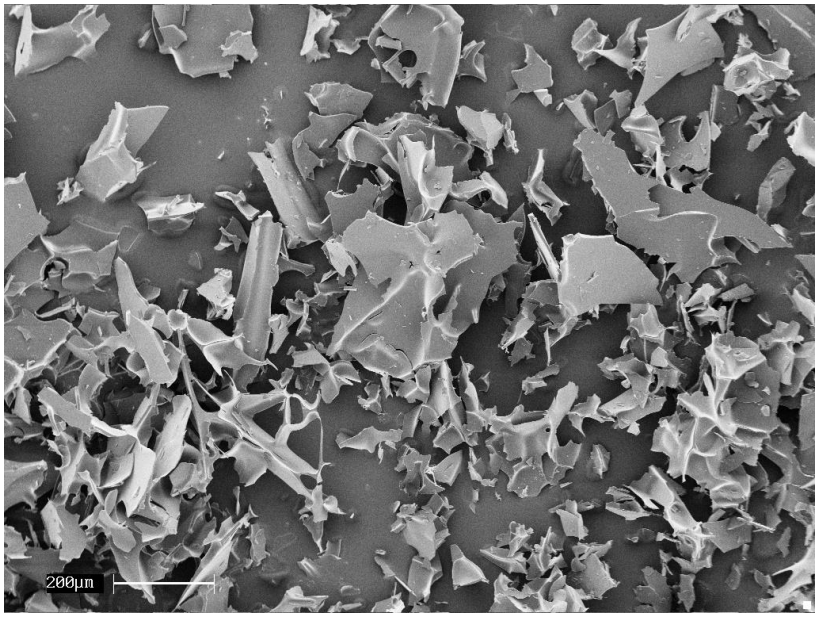

Figure 7.17 *SEM images for (a) commercial and (b) in-house freeze dried ovalbumin.*

(a)

10 wt% ovalbumin,
5 wt% sucrose

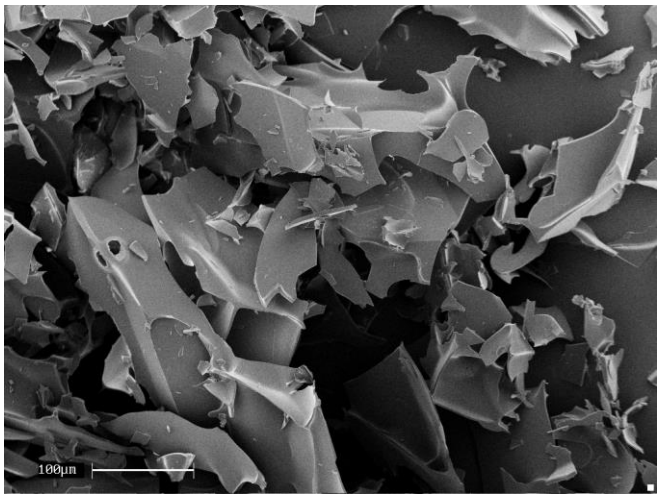

(b)

5 wt% ovalbumin,
5 wt% sucrose

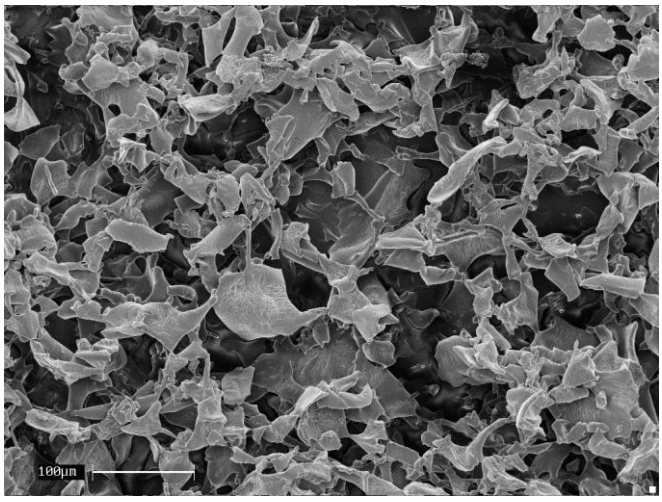

(c)

2.5 wt% ovalbumin,
5 wt% sucrose

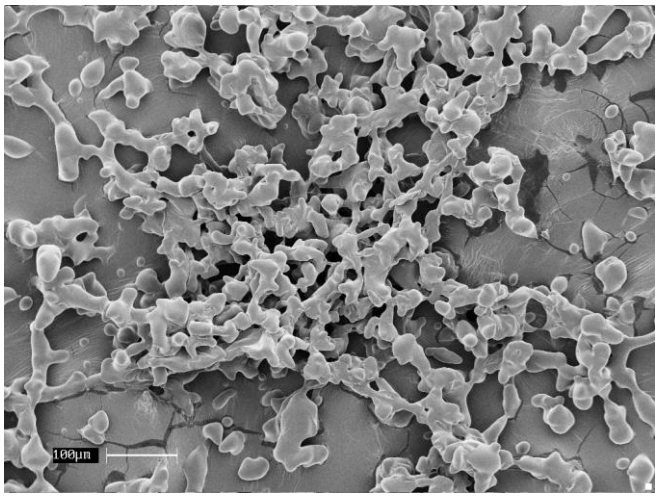

Figure 7.18 *SEM images of in-house freeze dried ovalbumin from different formulations*

7.5.2 DRS of Freeze Drying

7.5.2.1 Freeze dried ovalbumin

Figure 7.19 shows a typical dielectric response for ovalbumin, obtained directly from the freeze drying process and measured using custom-made electrodes attached to a glass vial. As shown in the figure, there is no obvious dispersion observed in the dielectric response for freeze dried ovalbumin measured inside glass vial. Previous sections, however, have shown that this technique is able to reveal ε_3 dispersion for hydrated ovalbumin (0.04 – 0.1 g/g). The reasons of why the dispersion is obscured is probably because the freeze dried ovalbumin prepared in this study contained very low concentration of residual water content. As a result, the ε_3 dispersion probably occurred at frequencies lower than 0.1 Hz which is beyond the experimental window.

The determination of residual water content in the freeze dried ovalbumin by the drying method gave a value of ~ 0.01 – 0.02 g/g. However, this value is a rough approximation, since the drying method should be carried out in a temperature and humidity controlled, which is not fulfilled in this study. The estimate of residual water content was probably higher than the true value because of water uptake from the ambient humidity or the absorbed water on the glass vial wall and the rubber bung cover.

The dielectric response from the measurement of freeze dried ovalbumin inside the glass vial was fitted with a parallel circuit of quasi-dc and Davidson-Cole elements. Although no visible dispersion was observed in the spectrum, the fitting parameter of relaxation time for dielectric spectrum in Figure 7.19 revealed a dispersion at frequency ~ 0.7 Hz with a very small distribution parameter ($\beta = 0.158$). It is therefore possible that there may be a weak dispersion from the freeze dried sample, which buried under low frequency process (i.e. LFD + glass vial)

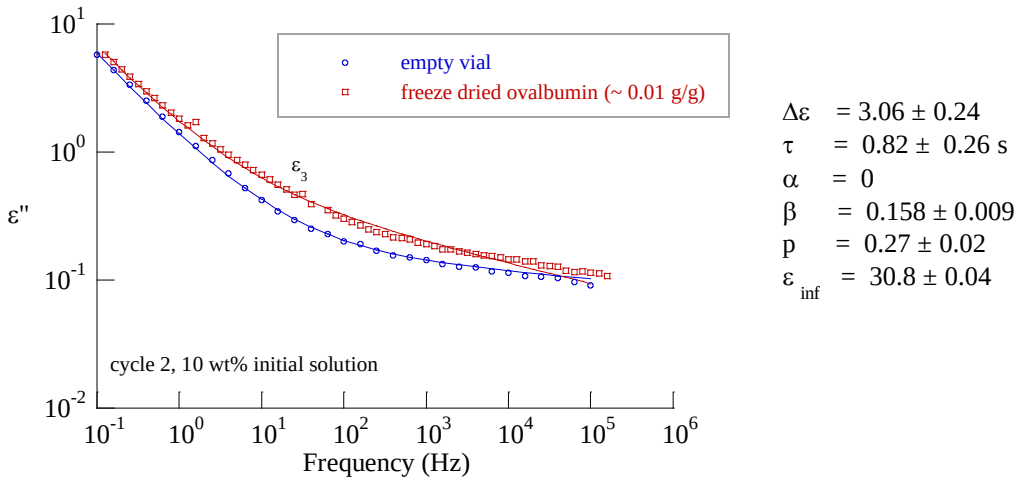

Figure 7.19 *Imaginary permittivity of freeze dried ovalbumin measured inside glass vial, using custom-made electrodes attaching to the vial. Symbols represent experimental data, solid line represents the fitting. The inset show dielectric parameters obtained from the fitting results to freeze dried ovalbumin.*

7.5.2.2 Comparison of freeze dried ovalbumin from different initial concentration

The concentration of protein in the initial solution for freeze-drying, may affect the final water content of each freeze-dried sample. Figure 7.20 shows the relaxation time τ_3 of freeze dried ovalbumin, obtained from different concentration of the initial solution. The comparison was revealed for cycles 1, 2, and 4. Cycle 3 only consisted of freeze-dried samples from initial concentrations of 1 wt% and 2.5 wt%, so the graph of various concentration from cycle 3 is not displayed. All the measurements were carried out using the custom-made electrodes attached to a glass vial.

Figure 7.20 shows that, on average, freeze-dried ovalbumin from 5 wt% initial concentration has lower relaxation time compared to the samples from initial concentration of 1 wt%, 2.5 wt%, and 10 wt%. The exception is for samples from cycle 1 (with 1 wt% initial concentration) and cycle 4 (with 10 wt% initial concentration). The errors for relaxation time as shown in Figure 7.20 are quite high (~ 30 – 50%). This is probably due to the obscure dispersion which yields a vague result.

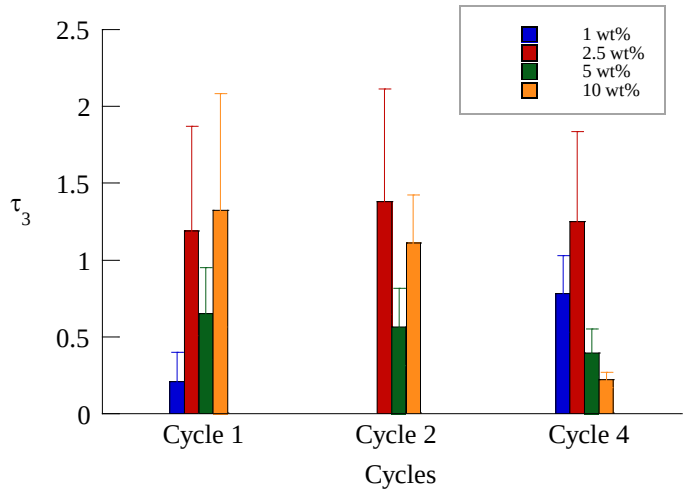

Figure 7.20 *Relaxation time τ_3 of freeze drying ovalbumin obtained from various initial concentration of ovalbumin solution from cycles 1, 2, and 4; measured using remote electrodes attached to a glass vial.*

7.5.2.3 Comparison of freeze dried ovalbumin from different cycles

Since each cycle has different formulation varying in the time and temperature profile for primary and secondary drying, the residual moisture content from different cycle is expected to be different. Figure 7.21 shows the relaxation time τ_3 of freeze dried ovalbumin for various cycles, obtained from initial concentration of 2.5 wt%, 5 wt%, and 10 wt%. Relaxation time for cycle 3 was not shown in the initial concentration of 5 wt% and 10 wt%, since those concentration were not carried out in cycle 3.

In average, cycle 4 has the lowest relaxation time compared with other cycles, which indicates more moisture content in the sample from cycle 4. This is consistent with the fact of the shortest cycles for secondary drying in cycle 4. The duration of heating for secondary drying on cycle 4, for example, is longer than cycle 2, but the temperature for secondary drying for cycle 4 is half than cycle 2. The water content in cycle 4 is therefore expected to be higher than samples from cycle 2. Relaxation times from cycles 1 and 2 were almost comparable in the error range, since the cycles were not significantly different. Cycle 3 has almost similar cycles with cycle 4. As can be observed, the relaxation time for cycle 3 is almost comparable with cycle 4. Unfortunately, the initial concentration of 5 wt% and 10 wt% were not employed for cycle 3, so no further inference can be drawn. However, it may be expected that the relaxation time for cycle 3 for these formulation will reveal comparable result with cycle 4.

Figure 7.20 and Figure 7.21 have shown that different cycle and different formulation gave different relaxation time τ_3 which indicate different moisture level. This shows that formulation involving the time and temperature profile in freeze drying process, played an important role in determining the moisture level of freeze-drying proteins, and that the technique is sensitive for monitoring moisture level.

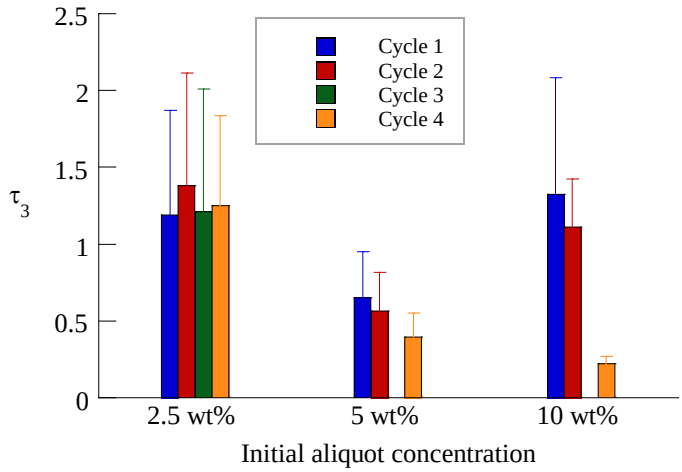

Figure 7.21 *Relaxation time τ_3 of freeze drying ovalbumin for different cycles, obtained from initial concentration of 2.5 wt%, 5 wt%, and 10 wt%; measured using remote electrodes attached to a glass vial.*

7.5.2.4 Rehydration

It has been mentioned previously that the freeze dried ovalbumin obtained in this study contained less moisture (~ 0.01 – 0.02 g/g) compared to the commercial freeze dried ovalbumin, which contained ~ 0.04 g/g moisture. The over-drying of the freeze drying sample prepared in this study was probably due to the cycle design for freeze drying or due to the formulation of the initial solution/aliquot.

Hence, to simulate the situation in which the freeze dried sample contained more residual moisture, the in-house freeze dried ovalbumin was rehydrated in a similar way as hydration method for spray dried samples as described in Section 2.4.1.

Figure 7.22 shows imaginary permittivities obtained from cycles 2 and 3, measured inside glass vial and compares the samples, directly from the freeze-drying process and those after rehydration. The dielectric spectra from all cycles showed that there was no visual indication of a dispersion for those sample obtained directly from freeze drying process. When the freeze dried sample was rehydrated, ε_3 dispersion was clearly observed. The ε_2 dispersion was also observed, which is due to the composite response from the use of remote electrodes, i.e. LFD process from the sample properties and the properties from the glass vial.

(a)

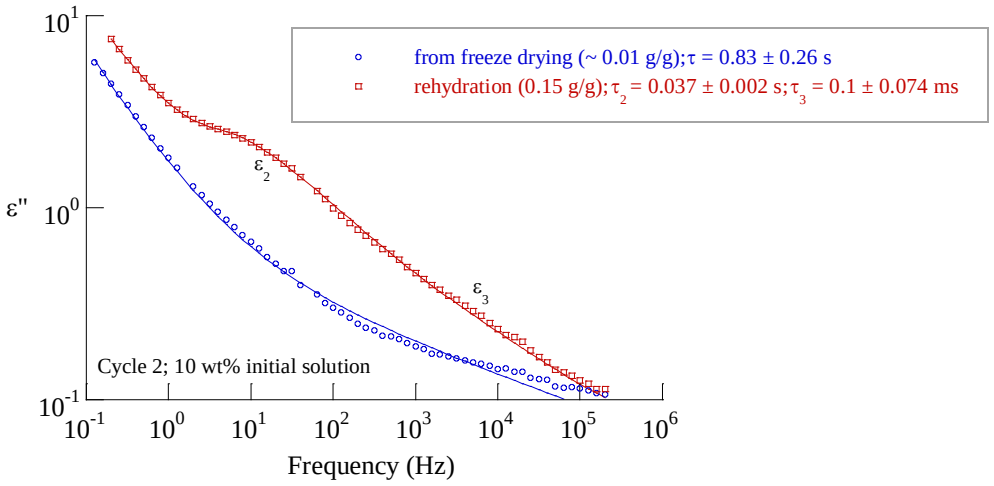

(b)

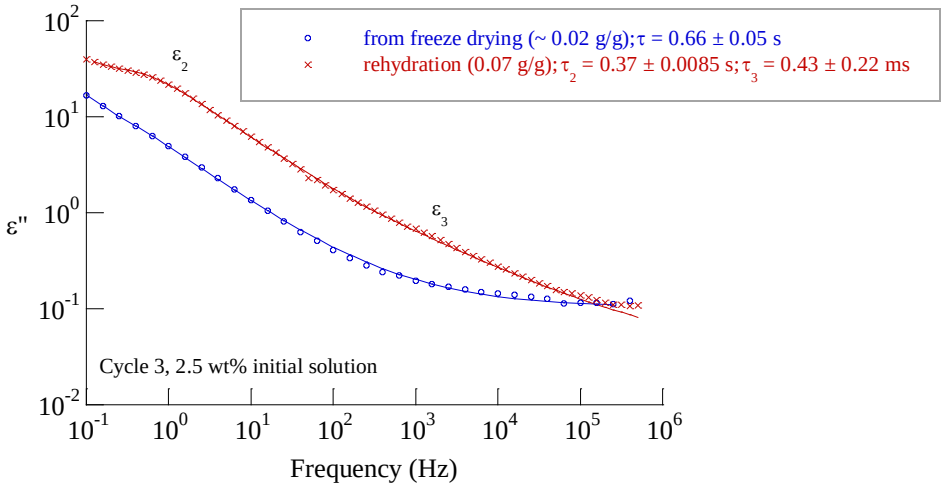

Figure 7.22 *Imaginary permittivity of freeze dried ovalbumin from different cycles obtained from different concentration of initial solution: (a) cycle 2, (b) cycle 3; measured using remote electrodes attached to a glass vial.*

To verify the validity of this novel technique in revealing the ε_3 dispersion, the rehydrated samples were also measured using parallel plate, with and without polyethylene films. Figure 7.23 shows the measurement using parallel plate electrodes with and without polyethylene films for rehydrated freeze dried samples compared with the measurement using glass vial with custom-made electrodes. The measurement using remote electrodes (i.e. parallel plate electrodes with polyethylene films and custom-made electrodes attached to a glass vial) produced an ε_2 dispersion which originated from the composite system of spacers from remote electrodes and LFD of the sample property. Moreover, the spectra showed that ε_3 dispersion was observed in all dielectric spectra from measurement using parallel plate (with and without polyethylene films) and the measurement inside glass vial using remote electrodes.

(a)

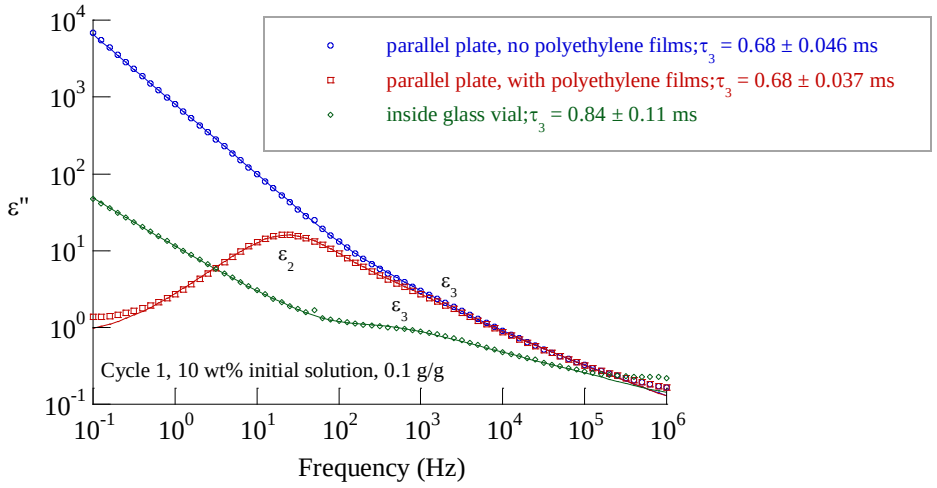

(b)

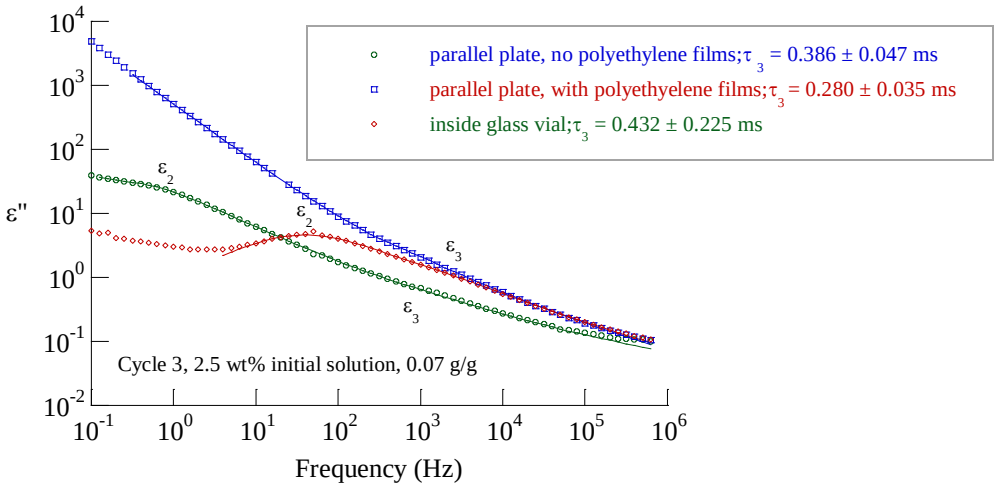

Figure 7.23 *Imaginary permittivity of rehydrated freeze dried ovalbumin from different cycles obtained from measurements with and without remote electrodes : (a) cycle 1 and (b) cycle 3. Symbols represent experimental data, lines represent the fitting.*

Unlike other cycles, freeze dried samples from cycle 4 showed a degree of instability on atmosphere exposure, i.e. the freeze dried samples from cycle 4 seemed to adsorb moisture from environment more readily than samples from other cycles.

Figure 7.24 shows dielectric spectroscopy of freeze dried ovalbumin (prepared in-house) before and after contact with the atmosphere. The figure shows that the first measurement of the sample from cycle 4 (straight from freeze dryer) did not show any indication of an ε_3 dispersion. This suggests that the sample is almost dry or contained only trace amount of water (~ 0.01 g/g). After several measurements using different electrode types (in which the samples has to contact with environment), the next measurement showed a clear ε_3 dispersion.

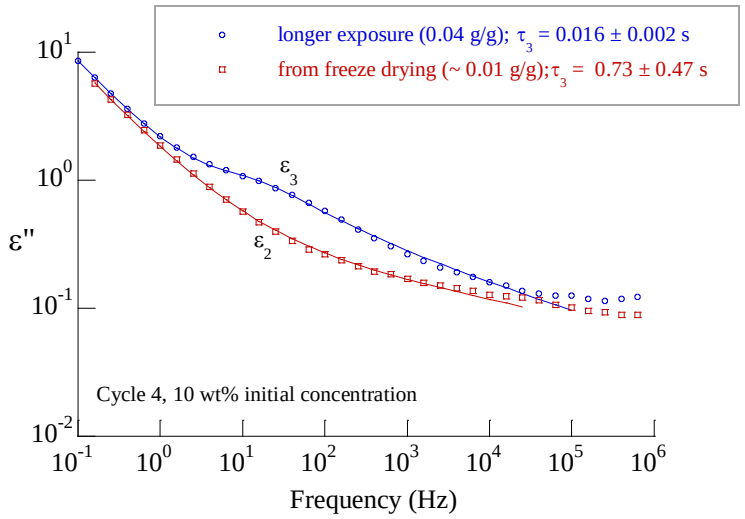

Figure 7.24 *Imaginary permittivity of freeze dried ovalbumin from cycle 4, measured using custom-made electrodes attached to a glass vial, comparing the dielectric response before and after contact with environment.*

Again, to validate the presence of ε_3 dispersion, the measurement of the sample inside glass vial was compared with the measurement using parallel plate electrodes with and without polyethylene films. The comparison of the dielectric responses is shown in Figure 7.25.

The result shows that relaxation times τ_3 from the ε_3 dispersion observed from all types of electrode are comparable. Once more, this shows that this novel technique of using custom-made electrodes attached to the glass vial is able to detect the water content of the end product of freeze dried sample.

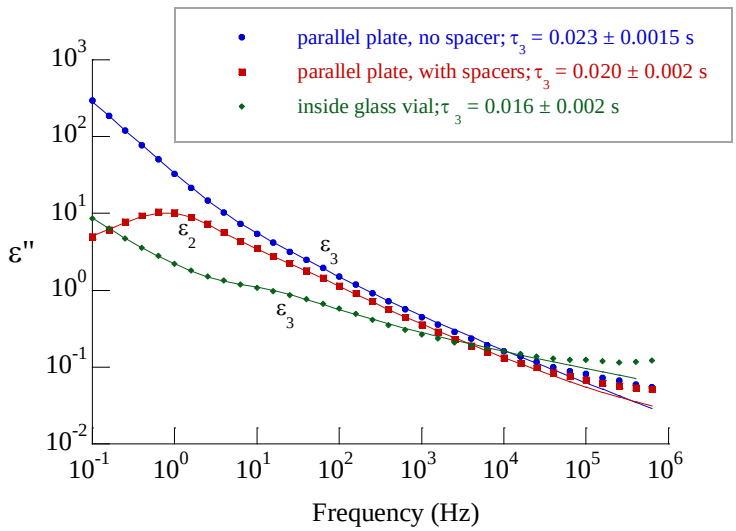

Figure 7.25 *Imaginary permittivity of freeze dried ovalbumin(0.04 g/g) from cycle 4 after contact with environment, measured with and without remote electrodes.*

For all freeze dried samples prepared in-house, only freeze dried samples from cycle 4 has a similar DRS plot with the commercial freeze dried sample. The DRS spectra for the sample from cycle 4 after contact with environment gave a similar response to the commercial freeze-dried ovalbumin from Sigma (Figure 7.26). It was thought that the process parameters of cycle 4 may be responsible for the comparable results with the commercial product. However, the formulation of freeze-dried sample still has to be improved in order to optimise the stability to environmental moisture.

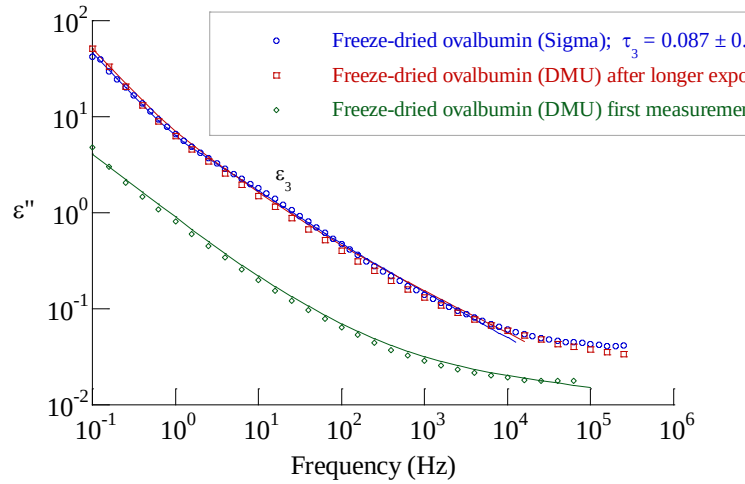

Figure 7.26 *Dielectric relaxation spectroscopy using conventional parallel plate electrodes without spacer for ovalbumin from commercial freeze dried ovalbumin (Sigma) and in-house freeze dried ovalbumin (DMU).*

7.5.2.5 Effect of formulation/Effect of sucrose

Figure 7.27 shows relaxation time τ_3 of freeze dried ovalbumin (formulated with and without sucrose), measured inside the glass vial using custom-made electrodes. The addition of sucrose was to protect the freeze-dried proteins from denaturation and improve the stabilisation. As shown in Figure 7.27, the relaxation time τ_3 was slightly higher for sample formulated with sucrose, compared with the ones without sucrose, but the values were considered equivalent within the error.

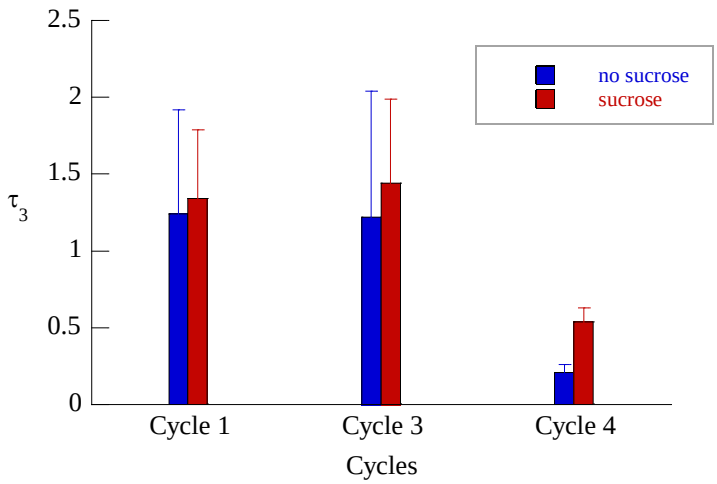

Figure 7.27 *Relaxation time τ_3 of freeze drying ovalbumin obtained from formulation with and without sucrose: (a) cycle 1, (b) cycle 3, (c) cycle 4; measured using remote electrodes attached to a glass vial.*

7.5.2.6 Sensitivity of the technique

Dielectric measurements using remote electrodes attached to a glass vial are not only sensitive to water content, but also sensitive to the macro-physical condition of the freeze dried 'cake'. Because of several causes (e.g. poor formulation and incomplete freezing), the freeze dried sample sometimes shrinks and moves away from the inner surface of the glass vial. This creates a relatively wide air gap between the freeze dried cake and the wall of glass vial[115].

Unlike samples from cycle 2 and cycle 3, the ε_2 dispersion from cycle 1 was found very close to the ε_3 dispersion. This resulted in a broad peak dispersion (Figure 7.28). The reason of this difference is probably due to the macro-physical state of the final product of freeze-dried sample from cycle 1. The ovalbumin 'cake' from cycle 1 was separated further from glass wall, which created a relatively wide gap between the glass wall and sample (Figure 7.29). In some vials from cycle 1, the gap was also filled with the soft skeleton (soft web) from the sample. This appearance may cause a complex dielectric response and may cause the ε_2 dispersion to overlap with ε_3 dispersion.

The cause of shrinkage for freeze-dried sample from cycle 1 was probably due to the incomplete freezing of the sample. The first stage of primary drying in cycle 1 started at –20 °C, while the drying temperature for the other cycles started at –30 °C, thereby allowing longer time for freezing before the onset of primary drying.

Further investigation of the impact of all these faults during freeze drying on the *in situ* measurement using dielectric spectroscopy has to be undertaken.

(a)

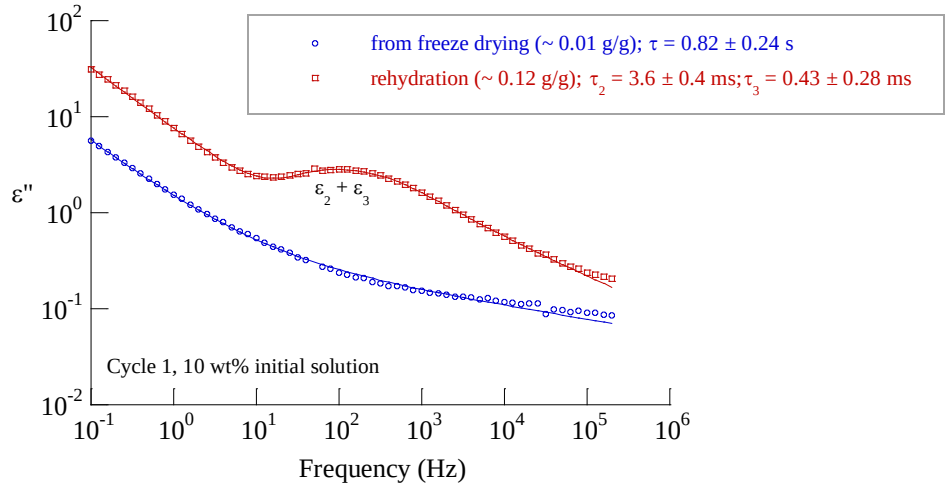

(b)

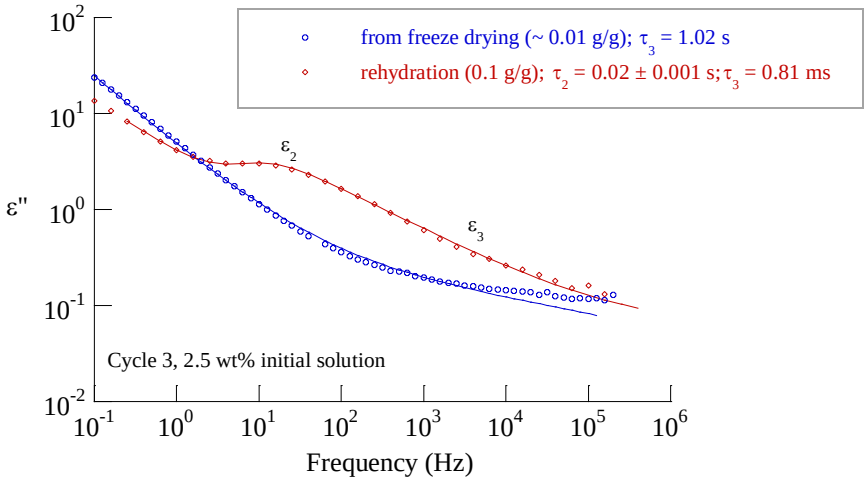

Figure 7.28 *Imaginary permittivity of freeze-dried ovalbumin before and after rehydration (a) cycle 1, (b) cycle 3; measured using remote electrodes attached to a glass vial.*

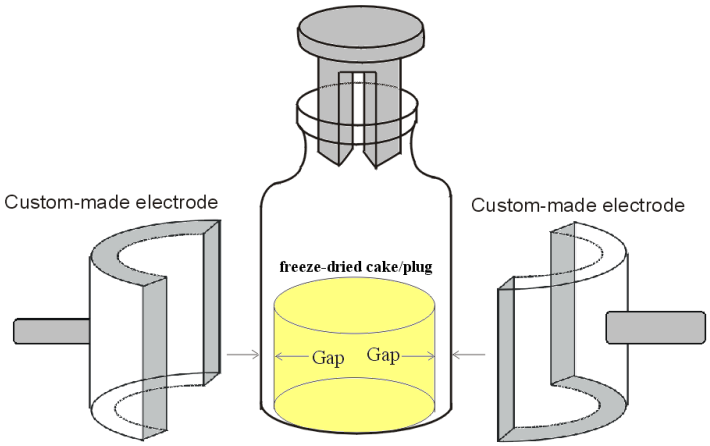

Figure 7.29 *Formation of gap between the freeze-dried cake/plug with glass wall due to the shrinkage during drying.*

7.6 Discussion

7.6.1 Dielectric measurement of hydrated proteins inside glass vial

The study has shown that the dielectric technique of measuring hydrated proteins inside the glass vial, using custom-made electrodes, is sensitive to water content through the impact on the ε_3 dispersion. Marginal deviation from the measurement using conventional parallel plate electrodes (as shown in Table 7.2) was mostly due to the geometrical properties of the glass vial in addition to the dielectric property of the glass vial itself. Nevertheless, with the careful choice of frequency range and familiarity with the properties of the sample, the technique shows promise as a new method for *in situ* monitoring water content for freeze dried proteins.

The moisture content from commercial spray dried ovalbumin (Sigma) is ~ 0.045 g/g, with relaxation time ~ 0.2 s (Section 5.2.3), whereas the moisture content of commercial freeze dried ovalbumin (Sigma) is ~ 0.03 g/g, with relaxation time ~ 0.1 s (Figure 7.26). The relaxation time, τ_3, obtained from the in-house freeze dried ovalbumin is ~ 0.7 – 1.5 s, depending on the formulation and cycles of the samples. The relaxation time, τ_3, of the in-house freeze dried ovalbumin was therefore higher than commercial ovalbumin (Sigma), which indicates that the residual moisture content in the in-house freeze dried sample is lower. With the lower moisture content, the ε_3 dispersion occurred at lower frequency range which may not be observed clearly since it was buried by the LFD process or beyond the experimental window.

The relaxation times (τ_2) of the ε_2 dispersion, derived from measurement inside the glass vial, were considerably different from those obtained from measurements using the 'remote' parallel plate electrodes. The ε_2 dispersion, as mentioned before, was due to the composite capacitor characteristics of spacer and sample. The glass vial has significantly different permittivity and thickness to the polyethylene spacer ($\varepsilon_{PET} \approx 2$, $\varepsilon_{glass} \approx 5$, $d_{PET} \approx$

0.1 mm, $d_{glass} \approx 3$ mm). It would therefore be expected that the relaxation times (τ_2) of the ε_2 dispersion, using glass vial measurements, would be considerably different from those determined using parallel plate and polyethylene as remote electrodes.

7.6.2 Effect of formulation and cycles

Figure 7.20, Figure 7.21, and Figure 7.27 have shown that different formulation and cycles (i.e. varieties in initial concentration of solution, addition of sucrose, varieties in time and temperature profile) gave different values of relaxation time, τ_3, which indicates different moisture level. The technique therefore showed the sensitivity of measuring moisture level of materials inside a glass vial. The technique, however, still needs improvement for the errors found in the relaxation times are quite high (~ 30 – 50%), which may be due to the obscure dispersion, especially at very low hydration ($\leq$ 0.01 g/g).

When the freeze-dried samples were prepared using sucrose, the FTIR spectra show additional IR-peaks, ascribed to the aliphatic and aromatic ring hydroxyls of the sucrose. The effect of sucrose on the properties of ovalbumin was also observed clearly in the SEM images. However the addition of sucrose did not have a significant effect on the dielectric spectrograms. There is only a slight difference in the relaxation time τ_3 between the freeze dried samples prepared with and without sucrose, and the values may be considered equivalent within the error range (Figure 7.27). It means that there were insignificant differences in the moisture content of the freeze-dried sample investigated. It may be possible to infer that the majority of the residual water in the product is preferentially adsorbed onto the protein itself, rather than sucrose. Therefore, addition of sucrose in the formulation was not clearly detected in the dielectric spectroscopy.

7.6.3 Significance of the technique

In this *in situ* study, the comparison was investigated only through the relaxation times from ε_3 dispersion. It has been demonstrated (Chapter 5 and Chapter 6) that the relaxation

time τ_3 from the ε_3 dispersion is a bulk property of the material. In principle, the use of remote electrodes is therefore unlikely to affect the relaxation time, unless of course the impedance of the remote electrodes dominate the measured impedance over the frequency band. Other dielectric parameters such as the pre-exponential factor *A*, the exponential parameter *p*, the relaxation strength $\Delta\varepsilon_3$, the distribution parameter β, and the infinite permittivity ε_∞ are also bulk properties of the sample.

This new technique is not only able to investigate the residual moisture from the sample inside glass vial, but it may also be employed to determine other physical-macroscopic properties of the freeze-dried sample, such as the porosity and shrinkage of the 'cake'. This is shown in the section where the shrinkage of the freeze-dried cake was expressed in the different dielectric responses of the ε_2 dispersion.

In the case of freeze-dried samples containing very low hydration ($\leq$ 0.01 g/g), the ε_3 dispersion was not observed. An alternative indicator is therefore required as the sample approaches low water contents. In this case, it may be appropriate to determine the moisture level from the characteristic of the ε_2 dispersion, or it may be possible to use the cross-over frequency (ω_c). When the cross over frequency (ω_c) was also outside of the experimental frequency window, it could be obtained simply by the extrapolation of the real and imaginary permittivities to the low frequency. In this study, estimates for ω_c of 0.078 Hz, 0.11 Hz, and 3.2 Hz were obtained for moisture contents of ~ 0.01 g/g, 0.04 g/g, and 0.07 g/g, respectively.

Another novel strategy could be employed, which involves a method called 'Eigen-coordinates' procedure, to reveal the hidden ε_3 dispersion at very low hydration level[116]. All this techniques are not discussed in this thesis but will be the subject of continued study.

7.6.4 Difficulties/Barriers

The main problem in this work was the difficulties in freeze-dried sample preparation, since the freeze dryer available did not work properly. The adjustment of the freeze drying cycle, in attempt to reach different hydration level at the end product, was sometimes not possible. The planned hydration level in different cycles was therefore difficult to achieve. Sometimes in the middle of secondary drying, the freeze dryer would stop automatically, thus ruining the planned cycles. Some of the freeze drying samples in this work were therefore rehydrated, for the purpose of investigating the sensitivity of the technique to water content.

Although the difficulties as mentioned above, the results showed that this novel technique is encouraging for the application of *in situ* monitoring of water content during freeze drying process using dielectric measurement to determine the end point of lyophilisation.

7.7 Lab scale design for in situ freeze drying measurement

It has been shown that the technique of dielectric measurements on hydrated samples inside glass vial using custom-made electrodes is sensitive for monitoring water content. Since the idea is to apply the technique for the freeze-drying process, the next step was then to place the previously designed apparatus (i.e. custom-made electrodes) inside a small freeze-drying unit.

Figure 7.30 shows a sketch of the design for using custom-made electrodes, attached to a glass vial, inside a small freeze dryer. This experimental set-up is designed to measure *in situ* of the whole process of lyophilisation, from prefreezing, primary drying, and secondary drying.

There are a number of important considerations when performing the *in situ* dielectric measurement during freeze-drying process. These are:

- positioning of the cables and connectors to reduce the stray capacitance
- grounding
- the base of glass vial should be clean and dry to avoid unwanted dielectric response

The limited time frame and the amount of work that has already been carried out, precluded the development of this design, and it is therefore reserved for future work.

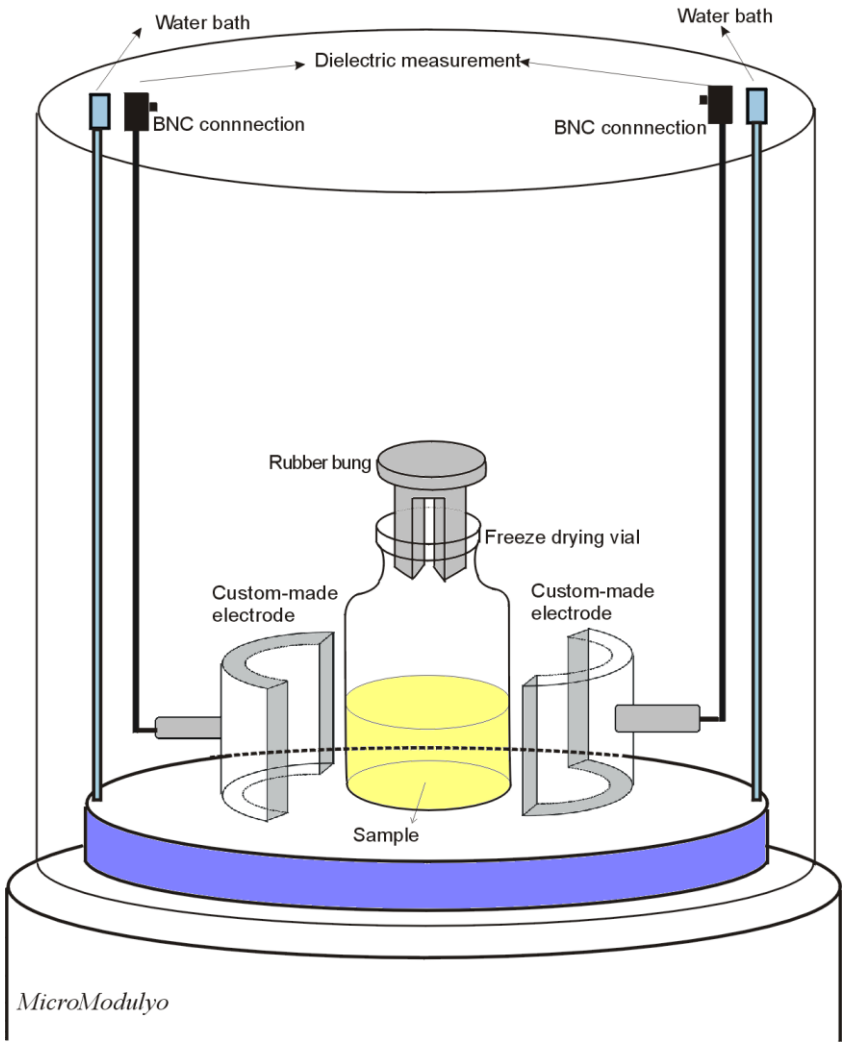

Figure 7.30 *Lab scale design for in situ determination of water content during freeze drying process using custom-made electrodes attached to the glass vial.*

7.8 Summary

This study has shown that the technique of measuring hydrated samples inside a glass vial, using custom-made remote electrodes, was sensitive to water content. This approach may be therefore applicable for monitoring the water content of the final product from the freeze-drying process. Due to several problems (mainly originating from the freeze dryer), it was not possible to obtain samples with variable water content, approaching that normally achieved by the end of the process. Thus, the dielectric spectra did not reveal the response as expected. The problem was addressed by re-hydrating the freeze-dried sample to achieve the required range of hydration level.

Sample characterisation using FTIR, SEM, DSC, and XRD shows that freeze dried samples from all cycles, have similar morphology, structure, and crystalline state with commercial freeze dried samples from Sigma. However, the dielectric measurement showed that only samples from cycle 4 showed comparable water content with commercial freeze dried sample from Sigma. Dielectric spectroscopy showed that freeze dried samples from other cycles only contained a trace amount of water.

8 GENERAL DISCUSSION

8.1 Summary and extended discussion

8.1.1 Cluster Model

This study clearly showed that low frequency dielectric measurements (0.1 Hz - 10 MHz) on hydrated globular proteins, displayed two major dispersions, i.e. the LFD and the ε_3 dispersion, which originate from the bulk properties of the material. In some cases (at low hydration or low temperature), another weak dispersion at higher frequency than that of ε_3 dispersion was observed, which is named as ε_4 dispersion.

The broad dielectric spectrum of hydrated globular proteins obtained in this study may be illustrated as in Figure 8.1, which shows the response of low frequency ($\omega < \omega_c$) and high frequency ($\omega > \omega_c$) parts of the LFD. The low frequency part of LFD fulfilled a power law dependence of frequency (Equation 3.44a). The high frequency part of LFD involved: ε_3 dispersion, ε_4 dispersion, and tail of high frequency part of LFD fulfilling Equation (3.45a).

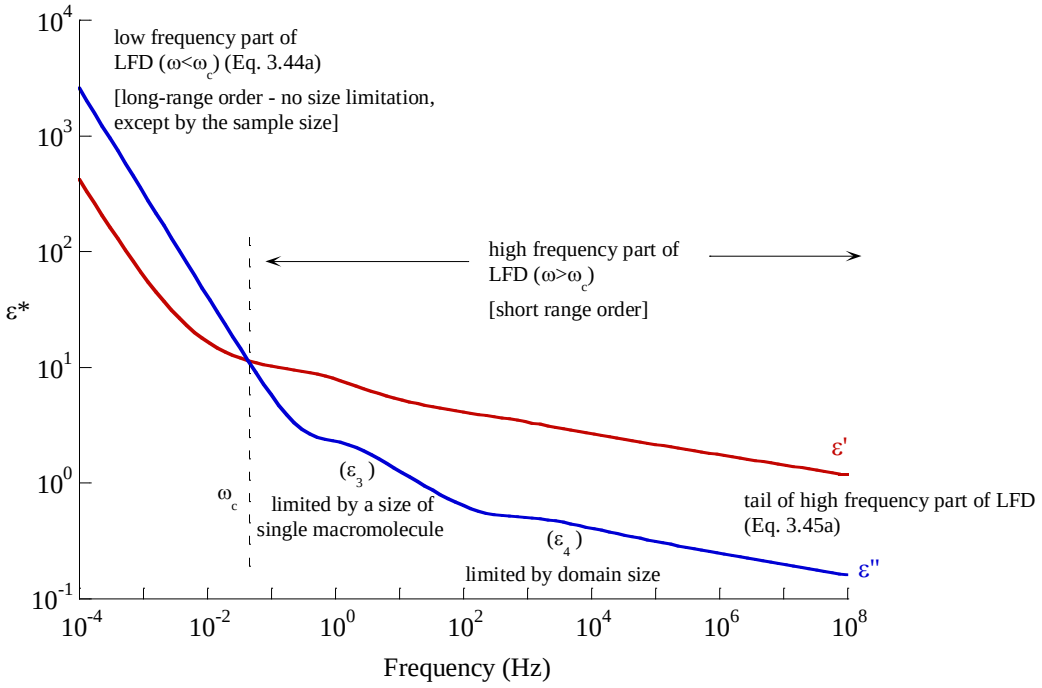

Figure 8.1 *Global dielectric spectra of real and imaginary permittivities showing long range and short range order of LFD response of hydrated globular proteins.*

The mechanism of proton transport, that is responsible for the dielectric response, can be illustrated using the cluster model described in Figure 8.2. Small dark-blue circles in Figure 8.2 represent water molecules. These water molecules form a network, in which water molecules are hydrogen bonded to each other and to the protein structure (i.e. main chain and side chains - see Figure 5.28).

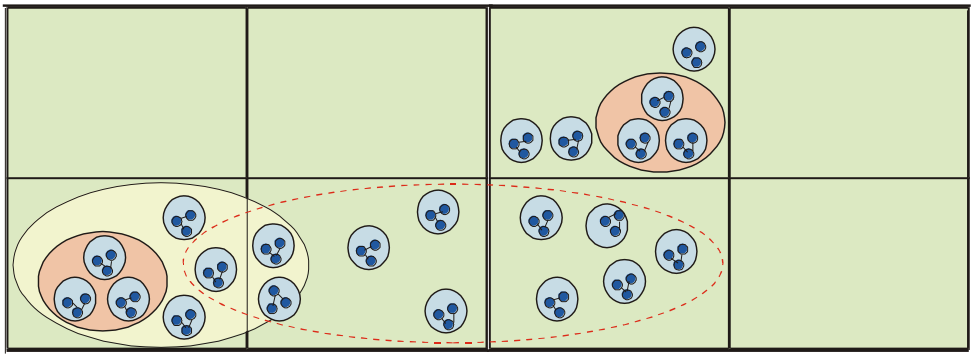

= water molecule

= cluster of water molecules, connected in H-Bond
= cluster polarisation unit
= tail of high frequency part of LFD
= size and number depends on protein structure, temperature, frequency, and hydration level

= group of clusters
= distribution of cluster polarisations within domain size, results in the ε_4 dispersion
= size and number depends on protein structure, temperature, frequency, and hydration level

= distribution of cluster polarisation within a single macromolecule
= results in ε_3 dispersion
= size and number depends on protein structure, temperature, frequency, and hydration level

= single domain

= single macromolecule, consists of 4 domains

= distribution of cluster polarisation within a whole range of bulk material
= results in low frequency part of LFD

Figure 8.2 *Model illustrating the cluster polarisation responsible for the dielectric dispersions shown in Figure 8.1.*

In the presence of an alternating electric field (in the frequency range of 0.1 Hz – 10 MHz), the water molecules dissociate, forming H_3O^+ at one end and OH^- at the other end. This is due to the proton transport along the thread of water molecules network, that occurs due to the breaking and formation of hydrogen bonding. When proton transport occurs between nearest neighbours of water molecules, then a group of nearest neighbour water molecules can be considered as a 'cluster polarisation unit'. The size of a 'cluster polarisation unit' is therefore dependent on the number of breaking/formation of hydrogen bonding, which can be determined from the activation energy (see Sections 6.4.1 and 6.7.4). The consequence of proton transport within the cluster (intra-cluster transport) of water molecules, which generates H_3O^+ at one end and OH^- at the other end, creates a cluster polarisation, and is responsible for the tail at high frequency LFD (which fulfil Equation (3.45a)).

These cluster polarisations distribute through the entire surface of hydrated proteins. The specific geometrical structure of globular proteins (or even the macroscopic aggregates of protein) may create a limited size of fluctuation in the distribution of cluster polarisations. These structural features therefore lead to the distinct ε_3 and ε_4 dispersions. For example, when the distribution of cluster polarisation is limited to the domain size of proteins, the ε_4 dispersion is observed. The ε_3 dispersion on the other hand, may be due to the defined size of a single macromolecule (which may consists of more than one domain). The size of distribution of cluster polarisation of the ε_3 dispersion is therefore larger than that of the ε_4 dispersion. This is the reason of the appearance of the ε_3 dispersion at lower frequency compared with the ε_4 dispersion. The limited size of distribution in cluster polarisation also resulted in the appearance of loss peak for the ε_3 and ε_4 dispersions.

It is also possible that the ε_3 and ε_4 dispersions that are observed distinctly in ovalbumin and lysozyme (but less so in pepsin – see Figure 5.32 for comparison) is due to the polarisation of domains, that are defined by the 'regular' spherical particle geometries of these spray dried materials (see Figure 5.33). This would explain why the ε_3 dispersion is

not so obvious for pepsin (with its irregular morphology) and why the ε_3 dispersion is barely observed for freeze-dried ovalbumin, which is flaky in structure (Figure 7.17)

The loss peak of the ε_3 and ε_4 dispersions was not simply due to the relaxation from dipolar water molecules sorbed in the protein samples. The relaxation of dipolar water molecules is a fast process, and therefore should be present in the higher frequency, which is far beyond the experimental window in this study. Moreover, being present in the solid powder form, the water molecules sorbed in the protein samples would not have enough degrees of freedom to experience relaxation. Free charge carriers such as electrons may one of the possibilities causing the dielectric behaviour. But again, dielectric response of these free charge carriers is only observed at high frequency range of 10 – 100 GHz. Across the low frequency range used in this work, the most possible mechanism for dielectric behaviour came from hopping of localised charge carriers, in the frame work of the cluster model. The deuteration study verified that protons were the charge carriers responsible for the observed dispersion.

At low frequency, i.e. where $\omega < \omega_c$, the protons have enough time to move to other neighbouring clusters (inter-cluster charge transport). This proton transports occur in the distance larger than cluster size, and may occur throughout the sample. Therefore a 'giant dipole' is generated, which is evidenced from the enormous real and imaginary permittivities of LFD response at low frequency ($\omega < \omega_c$). These proton transports only occur within the hydrogen-bonded network, and therefore there is no dc-conductivity observed. Table 8.1 shows the summary and description of the cluster model, which is used to explain the dielectric response in this study.

Table 8.1 *Summary and description of the cluster model of hydrated globular proteins.*

Model	**Description**	**Frequency dependent dielectric response**	**Mechanism**
Cluster (Intra-cluster transport)	• Polarisation unit • group of water molecules • number of water molecules in a cluster may be determined from ΔH • the size of cluster is defined by the range over which proton still can correlate	• Tail from high frequency part ($\omega > \omega_c$) of LFD, fulfilling power law (Equation 3.45a)	Charge carrier (i.e. protons) transport within a distance d, where: H - bond length < d < cluster size
Group of cluster within domain size	• cluster size is limited to the size of domain • only observed at low hydration or low temperature, since at low hydration or low temperature, the frequency of cooperative proton transport is less, resulting in higher relaxation time, and thus still observable in the experimental frequency window	• ε_4 dispersion • appearance as a loss peak at: $\omega_C < \omega < (\omega)_{\text{high frequency LFD}}$	Fluctuation in distribution of cluster polarisation within the domain size of protein. The domain size may involve the protein subunit.
Group of cluster within single macro-molecule	• cluster size is limited to the size of single macromolecule • observed as a major dispersion in hydrated proteins, besides the LFD process	• ε_3 dispersion • appearance as a loss peak at: $\omega_C < \omega < (\omega)_{\varepsilon_4 \text{ dispersion}}$	Fluctuation in distribution of cluster polarisation within the larger domain (i.e. single macromolecule.
Inter-cluster transport	• proton transport is only limited in the hydrogen bonded network, but there is no limited polarisation size • observed as a major dispersion in hydrated proteins	• low frequency dispersion (LFD) at $\omega < \omega_c$, in which real and imaginary permittivities are parallel • no loss peak	Proton transport from one cluster to another cluster from different domains across the bulk sample. This creates a giant dipole, since there is no limited size of polarisation

The cluster model (Figure 8.2) that is used to explain the dielectric responses observed in hydrated proteins, can also be used to confirm the existence of fractality. Figure 8.3 shows the cluster model in purpose to explain the fractality in the hydrated proteins. The existence of self-similarity of cluster polarisation on different scale (due to the surface topography and geometrical macromolecules), which is responsible for dielectric responses observed in hydrated protein, is illustrated clearly in Figure 8.3

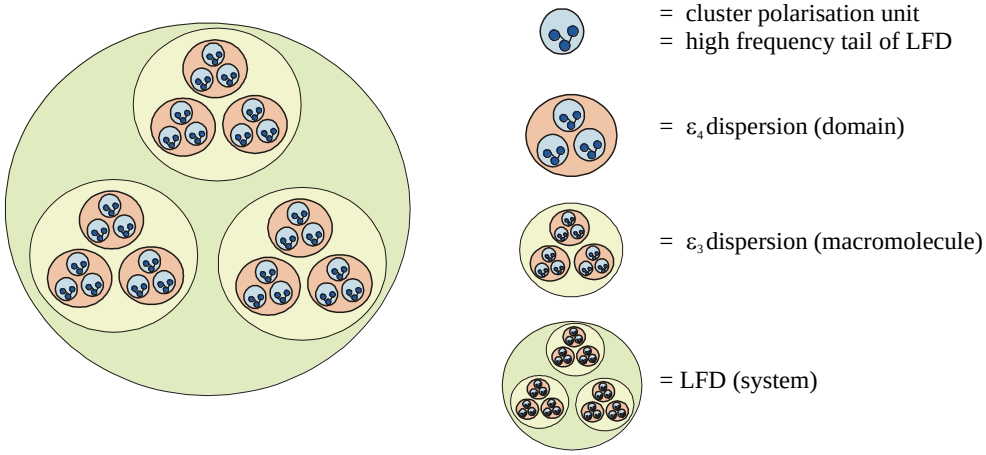

Figure 8.3 *Cluster model illustrating the fractality in the system of hydrated proteins.*

8.1.2 Water-protein interaction

Since the experimental results showed that both the LFD and the ε_3 dispersion were sensitive to the water content, it was considered that the protons involved in charge transport, originate primarily from the sorbed water molecules. The proton was transported from the breaking and formation of hydrogen bonds in the network of water molecules, that were bound to protein surface.

From the fractal dimensions calculated in this study, it was possible to infer that below the first critical hydration level (h_{c_1}), proton charge transport was believed to occur in the plane of the surface of the protein. Above the critical hydration level (h_{c_1} - for ovalbumin, and h_{c_2} - for lysozyme and pepsin), it was possible to infer from the fractal dimension that the water exist in a three dimensional system. Proton migration at this level, not only occurs on the surface but also expanded out of the surface. It is then possible to conclude that this critical hydration relates to the formation of first hydration layer of water molecules in a single macromolecule, or to the saturation of binding sites on the surface of a single macromolecule.

Above the critical hydration level, protons may migrate to another layer of water molecules from different single macromolecule. This may explain the onset of connection to another single macromolecule by water molecules, and the significant increase in $\Delta\varepsilon_3$ at water contents above h_{c_1} for ovalbumin and above h_{c_2} for lysozyme and pepsin. The difference between h_{c_1} and h_{c_2} has been explained in Section 5.4.3.

The characterisation of the LFD response supports this transition from surface bound water associated within an infinite cluster (that is possibly defined by an individual macromolecule) to more diffuse water associated within a 3-dimensional network. The characteristic and mechanism of the LFD can be defined in some way by the parameter p. As p approaches one, the charge transport process becomes more akin to dc-conductivity (i.e. unrestricted charge transport through the 3-dimensional matrix). In the case of

lysozyme and pepsin, the value of p increased dramatically from ~ 0.8 at low water content to ~ 0.95 at the h_{c1}, after which it is more or less constant. This is consistent with the suggestion that the threshold water content is associated with the transition from a 2-dimensional to a 3-dimensional water network. At water contents below h_{c_1}, charge transport is localised within a 2-dimensional area, whereas above h_{c_1} or h_{c_2}, the charge transport extends throughout the 3-dimensional matrix. This interpretation is consistent with the fact that the low frequency part of LFD begins at frequencies immediately below the ε_3 dispersion, and supports the idea that size of infinite cluster is somehow defined by the geometry and structure of the underlying matrix. This maximum limiting size to cluster polarisation could be associated with the size of macromolecule or size of the protein aggregates/particles that are formed on spray drying. The latter is more likely, given the spherical morphology of the spray-dried material, compared with the freeze dried material.

The exponential parameter p may also be related to the distribution of cluster size.[117] Big p values (for example $p \approx 0.9$), indicate a narrow distribution of cluster size, whereas, small p values (for example $p \approx 0.1$) indicate a wide distribution. The p values for each hydrated protein increase dramatically up to h_{c_1}, and then almost constant. This shows that as the hydration increases, the variety of cluster sizes becomes more homogeneous. The parameter p approaches unity when the infinite cluster is formed due to the saturation of the surface binding sites on a single macromolecule. At this point the cluster size distribution reflects the homogeneity of the geometric domains in the system. Again, as stated earlier, these geometric domains could be associated with the level of scale of individual macromolecules or the scale of the spray dried particles of protein.

The suggestion that water-protein interactions occur on the protein surface is also supported by another study investigating water structure in crystalline proteins. The study using single crystal X-ray diffraction data proposed the presence of large voids in the packing of protein molecules crystal which was occupied by water molecules[118]. These

water molecules existed in four environments, i.e. three types in the net form and one in the bulk form. In the first net form, water molecules surrounded a single protein molecule and formed chains that connected charged or dipolar atoms on the surface. In the second form, water molecules formed extensive hydrogen-bonded networks which bound two or more proteins together. These networks were responsible for maintaining the crystal structure of protein. The third net of water consisted of internal water which was buried below the protein surface and tightly held in the protein structure. This third net is considered to be similar to the internal water described in Section 1.6.1. Finally, the bulk water present in the core of the void is structurally disordered. The first and third water nets may play an important role for freeze drying process, while the second water net was the one responsible for the protein hydration, since it related to the hydrogen-bonded network.

Employing the model of water structure in proteins (as explained above), it can be explained that at low hydration (i.e. below the first critical hydration level) the water network may only be formed in a single protein molecule (i.e. only the first form of water network and a small part of the second water network were present). With the increase of hydration (i.e. above the first critical hydration level), the second form of water network starts to grow and form connections to water molecules in other macromolecule, or form another water molecule layer on the top of the first water molecule layer. This explains why $\Delta\varepsilon_3$ increases significantly above h_{c_1} or h_{c_2}.

If proton migration depends on the breaking and formation of hydrogen bonded water molecule within a network, then the activation energy obtained may be related to the number of hydrogen bonding that are involved cooperatively in proton migration. Values of ΔH that are approximation multiples of the single hydrogen bond strength of about 20 kJ mol^{-1} suggest that polarisation (i.e. proton transport) occurs within a cluster polarisation unit that comprises between 3 – 6 water molecules (i.e. 2 – 5 H-bonds) (see Table 6.8). This cluster polarisation unit defines the minimum fractal structure. The size and number of cluster polarisation units depend on water content, temperature, and frequency.

Table 6.8 shows the approximate number of hydrogen bonding involved in the dielectric behaviour of hydrated proteins at the critical hydration level of h_c. It can be seen from Table 6.8 that ovalbumin had the highest number of hydrogen bonding involved in the proton transport at the first critical hydration level. This correlates with the highest molecular weight and number of residues in ovalbumin (Table 2.1).

At below the first critical hydration level, pepsin has lower number of hydrogen bonding involved compared with lysozyme, even though pepsin has higher molecular weight and number of residues. This can be explained from the fact that the starting material for pepsin has very small amount of water content (basal water content for pepsin is only 0.023 g/g). Therefore at below the first critical hydration level, less water molecules were present in the pepsin molecules. The fact of different crystalline state, different particle shapes as has been described before may also contribute to this case. When the hydration was getting higher, pepsin had similar amorphous condition as ovalbumin and lysozyme, and therefore the dielectric properties observed were considerably similar as ovalbumin and lysozyme. Thus at $h > h_{c_1}$, pepsin has approximately higher number of breaking/formation hydrogen bonds compared with lysozyme, considering a higher molecular weight and number of residues of pepsin.

As shown and discussed earlier in Section 6.4.4.1 (Figure 6.15(a), Figure 6.16 (a), and Figure 6.20), lysozyme and pepsin has another Arrhenius behaviour observed at high temperature (above percolation threshold temperature). The activation energy obtained for the high temperature Arrhenius was higher almost 2 – 3 times than the low temperature activation energy. Average number of hydrogen bonds involved in the proton transport at temperature above percolation threshold was approximately 6 – 10, which shows that the cluster size at above percolation threshold is bigger than at below percolation threshold.

8.1.3 Pathway of proton transport

Arrhenius behaviour was observed for all proteins at above the 'freezing' temperature, up to temperature about percolation threshold. The 'freezing' temperature here is defined as the temperature at which the proton glass was formed. The manifestation of Arrhenius behaviour supported the idea that proton transport originated from water molecules in the network bound to the protein. It showed that the process of migrating protons (in this temperature range) may not involve the cooperative rearrangement with the protein structure. This suggests that only water molecules network are involved in the proton transport and that a cooperative polarisation with the protein backbone may be neglected.

When percolation threshold was reached, the stochastic condition may occur in the system. At this stage, the dispersion observed was not only simply due to the proton transport along the water molecules network. At percolation threshold, there was a formation of water molecule network bridging another macromolecule (i.e. the formation of the second form of water network based on the modelling from XRD data – see Section 8.1.1 above). In this stage, the breaking and formation of hydrogen bonding may not only occur in the water-water molecules network, but also occur in the water-protein network (i.e. water – ionised side chains or water – main-chain). Thus, there was a cooperative activity observed at the onset and during the percolation threshold. Since the process were stochastic, it was almost impossible to employ the exact formulation during the percolation threshold. When this percolation threshold coincident with the occurrence of glass transition as observed at the higher hydration level, the process was able to be formulated by the VTF behaviour – although in the very limited temperature range (see Section 6.4.2 and 6.4.4).

During the elevated temperature, the structure in the protein itself may experience a change or decomposition, such as denaturation, aggregation, folding, deamidation, cross-linking, etc. These changes, however, may not be detected by dielectric spectroscopy as employed in this study, if the dielectric response observed was simply due to the proton transport

along the hydrogen-bonding of water molecules network. However, it can be argued that the water molecules network not only consist of water-water H-bonds but the water molecules also bound to the main-chain protein through the C=O groups, N-H groups, or ionised side chain protein. Consequently, any change in the main-chain or side-chain protein may affect the state of hydrogen bond of water molecules network and thus the proton transport. Therefore, it is possible that the percolation threshold observed in this study has a relation with a certain physical change in the proteins. More studies using other methods are necessary to investigate whether there is a correlation between percolation threshold and physical state of protein structure. The calorimetric study – for example - showed that denaturation temperature for both ovalbumin and lysozyme was about 80 – 130 °C for hydration up to 0.2 g/g[119]. It can be seen therefore that the percolation threshold observed in this study was not due denaturation, since it was still below denaturation temperature.

It should be noted as well that the hydration level employed in this study was still below the hydration level where most changes or decomposition reactions may occur[50, 120]. Therefore, it is expected that at below percolation threshold, decomposition may not occur in the protein, and thus there may be no cooperative motion.

In short conclusion from this section, the cooperative motion with the protein structure, only occurred at the onset and during the percolation threshold. Below the percolation threshold the interaction mainly concerned with the water – water molecules network. The cooperative motion may also occur at below freezing temperature which was not the scope in this study.

8.1.4 Percolation clusters model

Another thing that was ignored in the discussion in this study was the negligence of time function during the process. The percolation phenomenon that has been explained in this study is related to a spatial fractal structure only. It may be necessary to consider a further

explanation related to the fractal time since the fractal time may also contribute to the dispersions observed in this study, as has been discussed in earlier studies that the dielectric response observed may originated from a combination of both fractal time and fractal structure[121].

Another point is the question about the interaction between the charge carriers (i.e. protons) in the system. The cluster model presented in this study neglected the Coulomb interaction that may be present due to the interaction between the charge carriers. The cluster model used in this study assumed that specific Coulomb interactions do not impact the mechanism behind the dielectric dispersion. Previous study by Amitrano, et. al. (1985) suggested that long-range interaction may considerably affect the dynamics of fractal structures, which means that it may significantly have an effect on the LFD process[122]. This is probably one of the reasons of the appearance of 'bulge' LFD with the higher hydration level. Besides the effect from interfacial polarisation that was more prominent as water content increased, the Coulomb interaction may be also more essential which then gave a disturbance in the LFD process.

Apart from all the assumption and concerning issue, it has been shown that the percolation clusters model is nevertheless capable of explaining the mechanisms of dielectric dispersion observed for hydrated proteins.

8.1.5 Differences between selected proteins

In general the results from this study showed that all the selected proteins had a similar dielectric behaviour, in terms of the LFD and ε_3 dispersion, which both shifted toward higher frequency with the higher hydration or higher temperature. Detailed analysis, however, showed that some differences were present between the selected proteins (Table 8.2).

Differences in dielectric properties as shown in Table 8.2 may be due several reasons. The differences in the physical properties (e.g. particle size, particle shape) of the starting

material itself may contribute the difference in dielectric properties. Different structures and chemical composition of each protein may be also the reason of differences observed in dielectric properties.

Hen egg white lysozyme as used in this study, for example, contained residues Glu, Trp, Asp, and Gln which are critical to catalytic function. It is known that glutamic acid (Glu) and aspartic acid (Asp) are charged side chains and readily ionisable[39]. Protons may be released from these charged side chains under certain condition (temperature, ionic strength, and hydration). Therefore, besides the protons released from water molecule network bound to protein, other protons originated from the ionisable side chain may contribute to the dielectric response. This may create a more prominent ε_4 dispersion in lysozyme. This suggestion should be evaluated by other complementary techniques.

Table 8.2 *Summary of differences between ovalbumin, lysozyme, and pepsin.*

Ovalbumin	**Lysozyme**	**Pepsin**
Differences in dielectric properties		
Peak frequency between ε_3 and ε_4 dispersions was far apart. Therefore, ε_4 dispersion was only observed in a short temperature range (see Figure 6.30)	Peak frequency between ε_3 and ε_4 dispersions was closer compared with ovalbumin. Therefore, ε_4 dispersion may be observed at longer temperature range (see Figure 6.29)	Vague ε_3 dispersion. No ε_4 dispersion
ΔH_{sat} = 100 kJ mol^{-1}	ΔH_{sat} = 70 kJ mol^{-1}	ΔH_{sat} = 40 kJ mol^{-1}
$h_{c_1} = 0.08$ g/g	$h_{c_1} = 0.06$ g/g	$h_{c_1} = 0.023$ g/g
no h_{c_2}	$h_{c_2} = 0.1$ g/g	$h_{c_2} = 0.037$ g/g
No high temperature Arrhenius, probably beyond the experimental window	High temperature Arrhenius was observed slightly, since it was limited by experimental window (see Figure 6.15)	High temperature Arrhenius was observed.
No transition process	Transition process was observed between percolation temperature and the new LFD/ε_3 dispersion (see Figure 6.6(b)).	No transition process
Proton glass $T_f \approx 275$ K (0.047 g/g)	Proton glass $T_f \approx 280$ K (0.037 g/g)	No proton glass
Differences in starting materials		
Highly amorphous	Partly amorphous and crystalline	Highly crystalline
Nice round shape of typical spray dried particles	Nice round shape of typical spray dried particles	Irregular bulk shape
Good FTIR spectrum	Good FTIR spectrum	Poor FTIR spectrum. Probably the sample has been denatured.

8.2 Significance for Pharmaceutics

8.2.1 Direct Application

The understanding of water-protein interactions developed in this thesis, provides a convenient basis on which the applications for the pharmaceutical industry can be developed. The principle idea is based on the sensitivity of the dielectric response to water content. The final moisture content of freeze dried samples, especially lyophilised protein drugs, is very important for long-term stability. The final moisture content is determined from the end point of the secondary drying stage of the lyophilisation process. However, the technique for *in situ* monitoring water content during lyophilisation is not fully developed yet.

The new technique developed in this study provides the basis for *in* situ monitoring water content by low frequency dielectric spectroscopy. Most of the techniques developed earlier for *in situ* monitoring of water content required a direct contact of the probe measurement to the sample being freeze-dried. These techniques are not preferred since the direct contact of the probe measurement to the freeze-dried sample may cause an alteration in the sample property itself. The technique used in this study employed remote electrodes that were not placed in a direct contact with the sample. The hydrated proteins, used as model samples, were placed in the glass vial with a measurement set up to mimic one which could be applied to a freeze-drying system. The ε_3 dispersion of hydrated proteins was similar to that observed using conventional method, and also sensitive to water content. It follows that the approach may be used to determine the end point of lyophilisation by monitoring the behaviour of ε_3 dispersion.

8.2.2 Implicit Application

The study of the dielectric properties of hydrated protein itself, contributes to our understanding of the role of moisture content in nearly dry proteins. It is well known that

the stability of solid-state protein drugs is strongly dependent on the moisture level, temperature, and powder composition[3]. The development of acceptable dosage forms for protein drug solid will therefore be enhanced, with the understanding of the impact of moisture level and temperature on proteins stability. An understanding of water-protein interaction in terms of hydration level and temperature is also significant in the lyophilised formulation, storage and processing of protein solid drug, and controlled release formulation.

9 CONCLUSION

The low frequency dielectric analysis of hydrated globular proteins that was carried out in this study, has revealed two significant aspects, i.e. the basic understanding of protein-water interactions and an application that may contribute to a novel technique of *in situ* determination of moisture content during lyophilisation.

The study revealed two main dispersions observed in the hydrated globular proteins, i.e. LFD and ε_3 dispersion, which shifted to higher frequency with the increase of either hydration or temperature. Although the dielectric investigations of hydrated proteins have been the subject of study for a number of decades, the detailed characterisation of these two dispersions is considerably new, since most of the earlier studies considered LFD as interfacial electrode polarisation, and the ε_3 dispersion to be an artefact from sample manipulation[59].

The contribution to the knowledge of protein-water interactions mainly arose from the percolation threshold obtained from the temperature study. This percolation phenomenon agreed with the isothermal hydration study which was revealed by the presence of critical hydration. Therefore, in the temperature study, the percolation threshold was shown by the percolation threshold temperature T_p, while in isothermal hydration study, the percolation threshold was shown by the critical hydration h_c. The critical hydration level may be related to the formation of infinite cluster and the formation of first hydration layer on a single macromolecule protein.

The idea of percolation phenomenon in the hydrated proteins combined nicely with the cluster model that has been proposed earlier by Dissado and Hill[71]. This also led to the fractality concept in hydrated protein revealing the feature of water dynamic in hydrated protein. The fractality study proposed that below a critical hydration level, the sorbed water only moved along in the interior of protein surface by breaking and formation of hydrogen bonds. Above the critical hydration level, sorbed water had more degree of

freedom by the possibility of movement through the protein matrix. The fact of the presence of LFD behaviour with its power function of frequency also supported the idea of fractality. The results from fractality study showed that the topology of water-protein interaction is universal for globular proteins.

With the knowledge of water-proteins interaction, the study was extended successfully to the new application of using dielectric spectroscopy to investigate moisture content for the sample inside glass vial, by utilising remote electrodes attached externally to the vial. The study revealed that ε_3 dispersion was sensitive to the moisture content and was still detectable - even with the use of remote electrodes. This idea was then expected to give a contribution to a novel technique of *in situ* monitoring moisture content during lyophilisation.

10 FURTHER WORK

10.1 Continuation set up for *in situ* freeze drying process

The study has clearly shown that low frequency dielectric measurement using custom-made electrodes attached externally to the glass vial was sensitive to determine water content in hydrated globular proteins (ovalbumin, lysozyme, and pepsin). This technique has also been applied for the freeze-drying ovalbumin. The technique has been designed to imitate the set up of freeze-drying process.

A continuation work of applying this technique to the actual process of *in situ* monitoring of water content during freeze-drying process will be very interesting. It may be able to develop a novel technique for industrial application in determining the end point of water content.

Another advantage of this technique is that the measurement is not only usable during the secondary drying to determine the final water content, but it can also be applied during the whole process of freeze drying, i.e. pre-freezing and primary drying. Dielectric measurement of the initial solution during pre-freezing and primary drying may be able to detect the glass transition or unwanted conformational changes during the process.

10.1.1 Other freeze dried materials

Other freeze-dried materials besides proteins should also be investigated. This further work is necessary to find out whether the technique may be applied as general for freeze-drying process.

10.1.2 ε_2 dispersion

The monitoring of water content employed in this study was based on the ε_3 dispersion observed in hydrated samples. Some materials, however, may not reveal ε_3 dispersion, but only LFD process, which involve two power laws (low and high frequency parts – see Equation 3.36). In this case, the monitoring of water content may be employed based on ε_2 dispersion, since ε_2 dispersion was also sensitive to the water content. Further studies regarding this type of samples are required, so the water content can be determined from the representation of ε_2 dispersion.

Other alternatives which have been mentioned in the last part of Section 7.6.3, may also be applied to determine the water content of material, in the case of the absence of the ε_3 dispersion. These involve the determination of the cross over frequency or characteristic frequency (ω_c) and 'Eigen-coordinates' procedure.

10.1.3 Determination of moisture content

Method of determination of moisture content should be extended using other techniques, such as Karl-Fischer method. The results may then be confirmed with the ones from oven drying method.

10.2 Continuation study of water-protein interaction

Dielectric spectroscopy alone is not enough to investigate the protein-water interaction. Other methods that can evidence clearly the role of water molecules in the protein is required. These may include the NMR solid state to investigate the mobility of water molecules in the protein, electron density pattern from X-ray diffraction data to investigate the position of water molecules in the proteins structure, and more rigorous analysis using FTIR such as quantitative amount of water in the protein, quantitative frequency shift from amide bond.

APPENDIX A1 STRAY CAPACITANCES

Stray capacitance occurs due to the stray field effects between the conductor and its surroundings, e.g. the ground, cables, anything metallic, or people. The stray field effect component can be represented by the capacitors as shown in Figure A1.0.1.

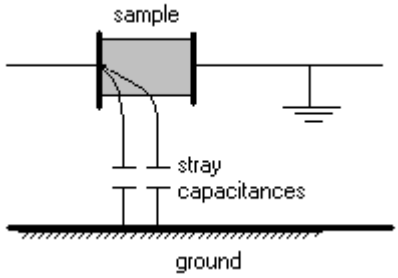

Figure A1.0.1 *Illustration showing the stray fields between the sample and ground. The stray fields are represented as capacitances.*

Therefore, the stray capacitances (C_{stray}) for the measurement system can be performed as a parallel circuit with the sample capacitance C_s and resistance R_s, as illustrated in Figure A1.0.1.

The stray capacitances can be determined in two ways: (a) using capacitance of air and additional material with known permittivity, and (b) using the relation of C vs $1/d$.

The determination of stray capacitances in this work was employed using the second method. The stray capacitance is determined by using an inverse linear relation between capacitance and the spacing between the electrodes:

$$C_s = \frac{\varepsilon\varepsilon_0 A}{d} \qquad \text{(A1.1)}$$

where:

C_s = the capacitance of sample

ε = relative permittivity of sample

ε_0 = permittivity of free space = 8.854 x 10^{-12} $F.m^{-1}$

A = surface area of electrodes

d = spacing between the electrodes

Due to the stray capacitance, the capacitance of air in the sample can be expressed as:

$$(C_s)_{air} = (C_m)_{air} - (C_{stray})_{air} \tag{A1.2}$$

or:

$$(C_m)_{air} = (C_s)_{air} + (C_{stray})_{air} \tag{A1.3}$$

$$(C_m)_{air} = \frac{\varepsilon_{air}\varepsilon_0 A}{d} + (C_{stray})_{air} \tag{A1.4}$$

By plotting the graph of $(C_m)_{air}$ against $\frac{1}{d}$, a straight line should result with a gradient of $\varepsilon_{air}\varepsilon_0 A$ and an intercept on the y-axis of $(C_{stray})_{air}$. Figure A1.2 shows the curve of $(C_m)_{air}$ against $\frac{1}{d}$ to determine the stray capacitance. As shown in Figure A1.2, the stray capacitance measured from this study is almost negligible ($(C_{stray})_{air} \approx 0.08pF$) and $\varepsilon_{air} \approx 1.18$.

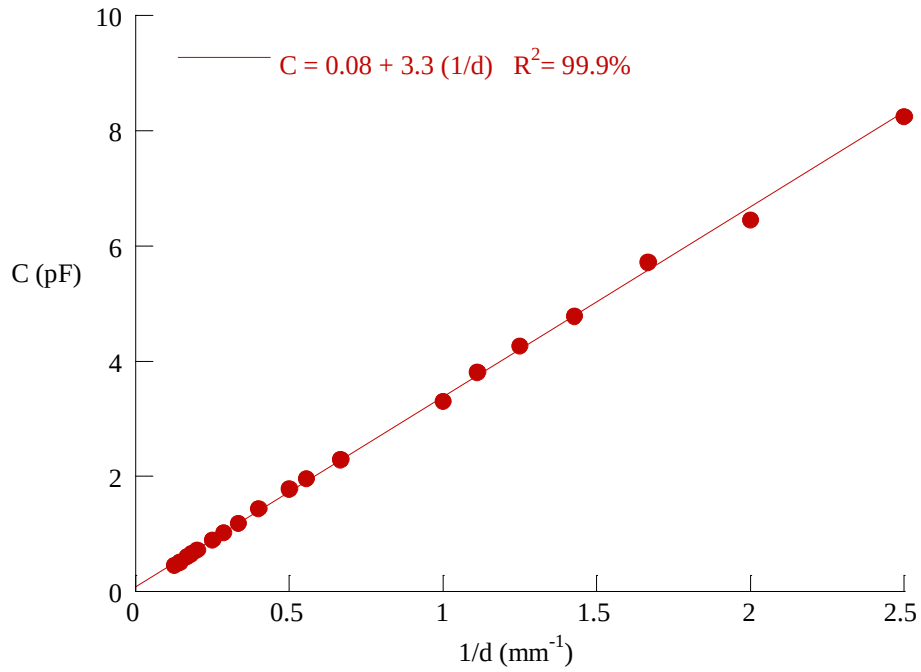

Figure A1.0.2 *Determination of stray capacitance from measurement of capacitance with various distance.*

APPENDIX A2 CONSTANT PHASE ELEMENT

This section involved mathematical derivation to describe the analogy between low frequency dispersion as expressed in Equation (3.44a) with the expression used in the Z-View software.

From Equations (3.36), (3.44), and (3.44 (a)) for low frequency part of LFD expression:

$$\varepsilon^* = A_2\left(\frac{\mathrm{i}\omega}{\omega_c}\right)^{-p} \tag{A2.1}$$

$$\varepsilon^* = \frac{A_2}{\omega_c^{-p}}(\mathrm{i}\omega)^{-p} \tag{A2.2}$$

$$\varepsilon^* = A_2\omega_c^p(\mathrm{i}\omega)^{-p} \tag{A2.3}$$

By substituting Equation (A2.3) to the capacitance in Equation (A2.4):

$$C^* = \varepsilon^* \frac{\varepsilon_0 A_0}{d} \tag{A2.4}$$

$$C^* = A_2\omega_c^p(\mathrm{i}\omega)^{-p}\,\frac{\varepsilon_0 A_0}{d} \tag{A2.5}$$

From Equation (A2.5), the complex impedance may then be expressed as:

$$Z^* = \frac{1}{\mathrm{i}\omega C} \tag{A2.6}$$

$$Z^* = \frac{1}{\mathrm{i}\omega A_2\omega_c^p(\mathrm{i}\omega)^{-p}\,\frac{\varepsilon_0 A_0}{d}} \tag{A2.7}$$

$$Z^* = \frac{1}{(\mathrm{i}\omega)^{1-p}A_2(\omega_c^p)\frac{\varepsilon_0 A_0}{d}} \tag{A2.8}$$

In Z-View software, the constant phase element is used to model the LFD since the constant phase element in Z-View software employ the power function of frequency:

$$Z^*_{Z-View} = \frac{1}{A_{Z-View}(\mathrm{i}\omega)^{n_z}} \tag{A2.9}$$

From equations (A2.8) and (A2.9), it is obtained that:

$$A_{Z-View} = A_2 \frac{\varepsilon_0 A_0}{d}(\omega_c^p) \tag{A2.10}$$

$$p = 1 - n_z \tag{A2.11}$$

The pre-exponential factor A from Equation (3.44a) is equivalent to the pre-exponential factor A_{Z-View}, and may be expressed as:

$$A = A_{Z-View} = A_2 \frac{\varepsilon_0 A_0}{d}(\omega_c)^p \tag{A2.12}$$

The pre-exponential factor A from Equation (3.44a), shown in the results of this study involves the multiplication of cell capacitance. At the same time, the A value itself also involves, the intersection frequency between real and imaginary permittivity (ω_c), and the A_2 value from Equation (3.36).

APPENDIX A3 PERCOLATION THEORY

A3.1 Introduction

This section gives a general review of percolation theory related to the experimental observations of this study, involving fractality, a percolation threshold, and percolation quantities.

A3.2 Percolation

Percolation is a standard model for a system with a structurally disordered medium which is partially connected. The percolation model has been widely applied in many areas of spatially random phenomena, both macroscopic and microscopic, such as porous and amorphous materials, sol-gel materials, polymers, resistor network, galactic structures, etc[123].

In general, percolation model may be characterised as site percolation, bond percolation, and site-bond percolation.[101,124,125]

Site Percolation. Site percolation implies the system consisting of group of sites which are randomly occupied, without considering the bonds between the sites. If the sites are considered occupied randomly by a probability/concentration of p, then the empty sites will have a probability/concentration of $1-p$. A group of nearest neighbour occupied sites is defined as a cluster. The occupied and empty sites may represent different physical properties for different systems. For example, in a conductor-insulator composite material, the occupied sites may represent the electrical conductors, while the empty sites represent insulators.

The system experiences percolation if the occupied sites form a continuous path from one side of the system to another side of the system. A continuous path is one that goes from

an occupied site to a neighbouring occupied site. The smallest probability/concentration p that results in percolation within the system is called a *percolation threshold/percolation transition* (p_c)[126].

The percolation threshold in the site percolation is described as a *geometrical phase transition*, in which the system consists of occupied site clusters with different size at below and above the percolation transition. At below percolation transition ($p < p_c$), only small-occupied sites-clusters are present, and called as *finite clusters*. At above percolation transition ($p > p_c$), the average size of the occupied site-clusters increases and becomes larger than those at below the percolation threshold. The cluster then extends from one side of the system to the other, and is called *infinite cluster*. When the probability/concentration increases further, more sites become part of the infinite cluster, while the finite cluster decreases. At $p = 1$, all sites are belonging to the infinite cluster.

Bond Percolation. In bond percolation, all the sites are considered to be fully occupied, but the bonds from one site connected to its nearest neighbour sites take place with probability q. The unconnected bonds/missing bonds have a probability of $1 - q$. The percolation in the system means a connected path of bonds through the system. In bond percolation, a group of nearest neighbour of connected bonds is called cluster. One example of bond percolation is the polymerisation process, in which small branching molecules can form large molecules by activating more and more bonds between them. If the activation probability p is above the percolation threshold p_c, a network of chemical bonds may extend over the whole system. Below the percolation threshold p_c, only macromolecules of finite size can be generalised. This process is called sol-gel transition. The example for this sol-gel transition is a gelatine process in the boiling egg. At room temperature, the egg is liquid. After heating, the egg becomes more solid-like gel[123].

Site-Bond Percolation. In site-bond percolation, the sites are not are fully occupied and the bonds are not fully connected. Instead, the sites are occupied with concentration/probability p, while the bonds are connected with probability q. The

percolation threshold for site-bond percolation is a critical line (p,q). In this case, a cluster is defined as groups of nearest neighbours of occupied sites connected by bonds.

A3.3 Percolation as a Critical Phenomenon

The percolation threshold/percolation transition p_c as mentioned above is a simple example of a phase transition phenomenon. A most common example of phase transition is thermal phase transition, such as the solid/liquid transition, where an ordered phase (solid) changes into a disordered phase (liquid) at some critical temperature t_c.

The important quantity for percolation threshold is the probability P_∞ that a site (bond) belongs to the infinite cluster. As mentioned previously, at $p < p_c$, only finite clusters are present, so $P_\infty = 0$. At $p > p_c$, the probability P_∞ increases as:

$$P_\infty \sim (p - p_c)^\beta \tag{A3.1}$$

The linear size of the *finite clusters*, below and above p_c, is characterised by the *correlation length*, ξ. The correlation length is defined as the average separation of two sites belonging to the same finite cluster and represents the characteristic length scale in percolation. When p approaches p_c, ξ increases as:

$$\xi \sim |p - p_c|^{-\nu} \tag{A3.2}$$

The exponent ν is the same value below and above the percolation threshold.

The mean number of sites (mass) of a finite cluster S also diverges as:

$$S \sim |p - p_c|^{-\gamma} \tag{A3.3}$$

The exponent γ is also the same below and above the percolation threshold.

All the exponents β, ν, and γ describe the critical behaviour of typical quantities associated with the percolation threshold, and are called the *critical exponents.* These

exponents are universal and independent of the structural details of the systems or the type of percolation. These universal exponents depend only on the dimension d of the system.

For the length scale above ξ, the infinite percolation cluster is a compact structure and homogenous system composed of many unit cells of size ξ, but below ξ, cluster is *fractal and self-similar*.[124] At below ξ, the cluster is characterised by a *fractal dimension* d_f, which may be written mathematically as:

$$M(r) \sim \begin{cases} r^{d_f}, & r << \xi \\ r^{d}, & r >> \xi \end{cases} \tag{A3.4}$$

$M(r)$ is defined as the mean mass of the cluster within a circle of radius r.

Above the percolation threshold, the mass $M(r)$ of the infinite system of size L^d is proportional to $L^d P_\infty$. It is also proportional to the number of unit cells of size ξ, i.e. $\left(\frac{L}{\xi}\right)^d$ multiplied by the mass of each cell which is proportional to ξ^{d_f}. Mathematically, it can be summarised as:

$$M_\infty \sim L^d P_\infty \sim L^d (p - p_c)^\beta \tag{A3.5}$$

$$M_\infty \sim \left(\frac{L}{\xi}\right)^d \xi^{d_f} \sim L^d \xi^{(d_f - d)} \sim L^d (p - p_c)^{-\nu(d_f - d)} \tag{A3.6}$$

therefore,

$$d_f = d - \frac{\beta}{\nu} \tag{A3.7}$$

A3.4 Dynamical Properties of Percolation Systems

The dynamical properties of percolation systems mean that there are transport properties in the percolation system. For example, if the occupied sites are conductors, and the empty sites are insulators, it is assumed that there is a current flow between the nearest neighbour conductor sites.

This section presents briefly the frequency-dependent (ac) electrical properties associated with the percolation model, which is related to this study. The model employs the microscopic lattice-gas model, where N mobile particles perform hops between available nearest-neighbour sites.

A small time-dependent field of frequency ω is applied along one axis (x-axis):

$$E_x(t) = E_0 \sin(\omega t) \tag{A3.8}$$

For non-interacting particles, the frequency-dependent conductivity $\sigma(\omega)$ can be expressed as:

$$\sigma(\omega) \sim \begin{cases} (-i\omega)^n \equiv \exp(-i\frac{\pi}{2}n)\omega^n & \omega >> \tilde{\omega}_\xi \equiv 1/t_\xi \\ D' & \omega << \tilde{\omega}_\xi \end{cases} \tag{A3.9}$$

where

D' = diffusion constant

$$D' \sim (p - p_c)^{\mu-\beta} \tag{A3.10}$$

$$n = 1 - \frac{2}{d'_w} \tag{A3.11}$$

$d'(\omega)$ = diffusion exponent of the random walk on a fractal.

Further mathematical derivation produced the real part of dielectric permittivity at low frequency which can be described as[127]:

$$\varepsilon'(0) \sim \left| p - p_c \right|^{-2\nu+\beta} \tag{A3.12}$$

In the application of percolation theory, the percolation threshold p_c may represent concentration, temperature, etc. For example, Equation (A3.2) may be expressed as:

$$\xi \sim \left| T - T_p \right|^{-\nu} \tag{A3.13}$$

where:

T = temperature

T_p = percolation threshold temperature

APPENDIX A4 VERIFICATION OF ARRHENIUS, EYRING, AND VTF BEHAVIOURS

This section involves mathematical derivation for verification of Eyring, Arrhenius and VTF behaviours. The relationship between relaxation times and temperature may be expressed through Eyring, Arrhenius or VTF behaviour, which may reflect the mechanism behind the observed relaxation times. However, in the limited temperature range, the plot of Eyring, Arrhenius and VTF behaviours may be indistinguishable. This is shown clearly in Figure A4.0.1 and Figure A4.0.2. The following are mathematical derivations for verification of Eyring, Arrhenius and VTF behaviours.

A4.1 Arrhenius and Eyring Verification

As expressed in Equation (6.1), the general empirical expression for relaxation times related to the absolute temperature is:

$$\tau \propto T^{-n} \exp(\Delta H / RT) \tag{A4.1}$$

For Arrhenius behaviour, $n = 0$, so the Arrhenius equation may be expressed as:

$$\tau = \tau_0 \exp(\frac{\Delta H}{RT}) \tag{A4.2}$$

where:

τ = relaxation times (s)

τ_0 = pre-exponential constant for Arrhenius equation (s)

ΔH = activation energy/enthalpy (J mol^{-1})

T = temperature (K)

R = gas constant (8.314 J mol^{-1} K^{-1})

Arrhenius behaviour as expressed in Equation (A4.2), is an empirical model that relates the chemical process (e.g. chemical reaction, viscosity, diffusion, corrosion, electrochemical processes, dielectric polarisation, etc) with temperature.

The logarithmic of relaxation time from Arrhenius equation above is expressed as:

$$\ln(\tau) = \ln \tau_0 + \frac{\Delta H}{RT} \tag{A4.3}$$

The derivative of logarithmic relaxation times from Arrhenius equation over the inverse absolute temperature, produces a constant value, independent of temperature:

$$\frac{d \ln(\tau)}{d(1/T)} = \frac{\Delta H}{R} \tag{A4.4}$$

Since relaxtion time is the inverse of frequency jump between two activated states, Arrhenius equation may also be approximated from the theory of activated states that has been derived by Eyring. For Eyring equation, $n = 1$, so Equation (A4.1) may be expressed as:

$$\tau = \frac{h}{kT} \exp\left(\frac{-\Delta S^*}{R}\right) \exp\left(\frac{\Delta H^*}{RT}\right) \tag{A4.5}$$

where:

k = Boltzmann constant (1.38×10^{-23} J.K^{-1})

h = Planck constant (6.626×10^{-34} J.s)

R = gas constant (8.314 J mol^{-1} K^{-1})

ΔS^* = entropy of activation (J. mol^{-1}. K^{-1}), related to the ratio of the number of available sites between the activated and inactivated states.

ΔH^* = enthalpy of activation (J. mol^{-1}), related to the barrier height between two activated states.

The equivalence between Arrhenius and Eyring behaviours may be expressed as:

$$\Delta S^* = R\ln T - R\ln\tau_0 - 205.85 \tag{A4.6}$$

$$\Delta H^* = \Delta H + RT \tag{A4.7}$$

The logarithmic from the product of relaxation times and the absolute temperature from Eyring equation (A4.5) gives:

$$\ln(\tau T) = \ln\left(\frac{h}{k}\right) - \frac{\Delta S^*}{R} + \frac{\Delta H^*}{RT} \tag{A4.8}$$

Derivative of Equation (A4.8) over the inverse temperature gives a constant value:

$$\frac{d\ln(\tau T)}{d(1/T)} = \frac{\Delta H^*}{R} \tag{A4.9}$$

The logarithmic of relaxation time itself from Equation (A4.5) is expressed as:

$$\ln(\tau) = \ln\left(\frac{h}{kT}\right) - \frac{\Delta S^*}{R} + \frac{\Delta H^*}{RT} \tag{A4.10}$$

The derivative of logarithmic of relaxation times over the inverse absolute temperature gives a linear dependence of the absolute temperature, as expressed in Equation (A4.9):

$$\frac{d\ln(\tau)}{d(1/T)} = \left[\ln(h/k)\right]T + \frac{\Delta H^*}{R} \tag{A4.11}$$

The comparison between Arrhenius and Eyring behaviours is presented in Figure A4.1, which is obtained from the simulation of Equations (A4.2) – (A4.11). Figure A4.0.1(a) shows the simulation plot for relaxation times obtained from Arrhenius and Eyring behaviours, from Equations (A4.2) and (A4.5), respectively. The plot of logarithmic relaxation time from Arrhenius versus inverse absolute temperature (Equation (A4.3)), and the plot of logarithmic of product relaxation times from Eyring with the absolute temperature, versus inverse absolute temperature (Equation (A4.8)), produces a straight line (Figure A4.0.1 (b)).

As shown both in Figure A4.0.1 (a) and (b), it is difficult to distinguish the difference between Arrhenius and Eyring behaviours. However, the derivative procedure as expressed in Equation (A4.4) and (A4.11) for Arrhenius and Eyring, respectively, show an obvious difference between these equations. Figure A4.0.1 (c) shows the difference between Arrhenius and Eyring behaviours as obtained from the Equation (A4.4) and (A4.11). Arrhenius behaviour gives an independent plot of temperature, while the Eyring behaviour gives a linear dependent of absolute temperature. If the derivative is produced from the product of relaxation time and absolute temperature, then the Eyring behaviour gives a constant value as expressed in Equation (A4.4) and shown in Figure A4.0.1 (d).

(a)

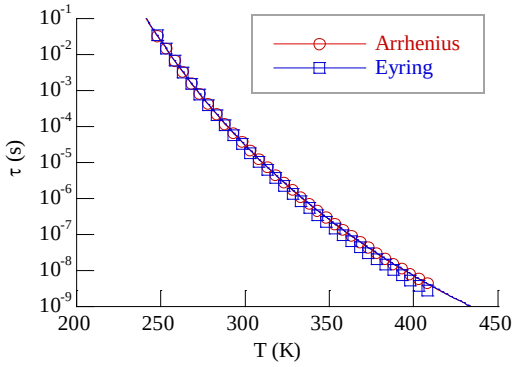

(b)

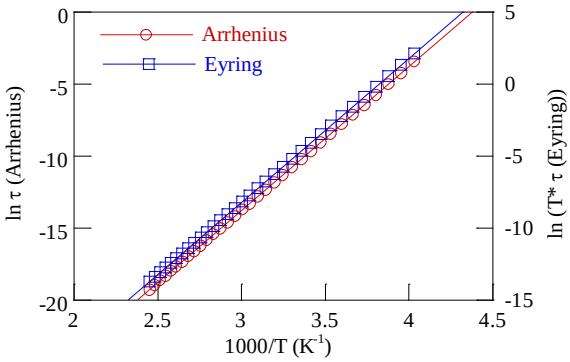

(c)

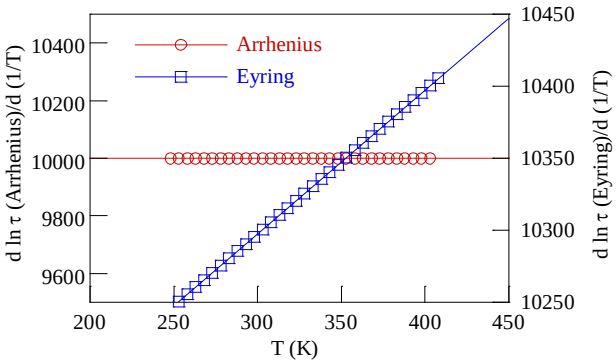

(d)

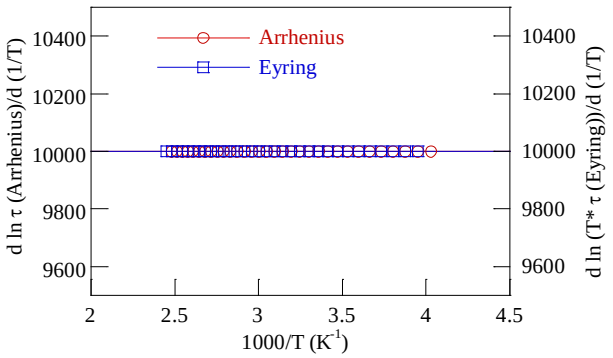

Figure A4.0.1 *Comparison simulation between Arrhenius (ΔH = 10 kJ mol^{-1}, τ_0 = 1x10^{-19} s) and Eyring (ΔH^* = 10 kJ mol^{-1}, ΔS^* = 120 J mol^{-1}K^{-1}).*

A4.2 VTF behaviour

VTF behaviour may be expressed as [94,95]:

$$\tau = \tau_0 \exp\left(\frac{A_{VTF}}{T - T_{VTF}}\right) \tag{A4.12}$$

The logarithmic of relaxation times from VTF equation is found as:

$$\ln \tau = \ln \tau_0 + A_{VTF}(T - T_{VTF})^{-1} \tag{A4.13}$$

if:

$$x = T - T_{VTF} \tag{A4.14}$$

$$dx = dT \tag{A4.15}$$

$$d(\frac{1}{T}) = -T^{-2}dT = -T^{-2}dx \tag{A4.16}$$

$$dx = -T^2 d(\frac{1}{T}) \tag{A4.17}$$

$$\ln \tau = \ln \tau_0 + A_{VTF} x^{-1} \tag{A4.18}$$

$$\frac{d \ln \tau}{dx} = -A_{VTF} x^{-2} \tag{A4.19}$$

$$\frac{d \ln \tau}{-T^2 d(\frac{1}{T})} = -A_{VTF}(T - T_{VTF})^{-2} \tag{A4.20}$$

$$\frac{d \ln \tau}{d(\frac{1}{T})} = A_{VTF} \frac{T^2}{(T - T_{VTF})^2} \tag{A4.21}$$

$$\left(\frac{d\ln\tau}{d(\frac{1}{T})}\right)^{-1/2} = (A_{VTF})^{-1/2}\frac{T - T_{VTF}}{T} \tag{A4.22}$$

$$\left(\frac{d\ln\tau}{d(\frac{1}{T})}\right)^{-1/2} = (A_{VTF})^{-1/2} - (A_{VTF})^{-1/2}T_{VTF}\left(\frac{1}{T}\right) \tag{A4.23}$$

Equation (A4.23) shows that the derivative function of logarithmic relaxation time upon inverse temperature is dependent with temperature.

Figure A4.0.2 (a) and (b) show the simulation plot for Arrhenius and VTF behaviour for broad temperature range (250 – 450 K), obtained from Equations (A4.2) and (A4.12), respectively. The logarithmic plot of relaxation time versus inverse temperature, from Equation (A4.3) and (A4.13), shows a clear difference between Arrhenius and VTF behaviour (Figure A4.0.2 (c) and (d)). The logarithmic relaxation time for Arrhenius behaviour has a linear correlation with the inverse temperature, while VTF behaviour shows a curvature. However, when the temperature range was limited only from 330 – 450K, both Arrhenius and VTF behaviour show linearity (Figure A4.0.2 (e) and (f)). Therefore, in the limited temperature range, the determination of either Arrhenius or VTF behaviour is elusive.

The feature of Arrhenius and VTF behaviour in the limited range may be distinguished by employing a derivative function of logarithmic relaxation time over inverse temperature. Figure A4.0.2 (g) and (h) shows respectively the derivation function for Arrhenius (obtained from Equation (A4.4)) and VTF behaviours (obtained from Equation (A4.23)). It is shown clearly that the derivative function for Arrhenius behaviour is independent of temperature. The VTF behaviour, on the other hand, shows linear dependence with inverse temperature. Therefore, in the limited range of temperature, it is useful to re-examine the Arrhenius and VTF behaviours by employing the derivative function as described in Equations (A4.4) and (A4.23), respectively.

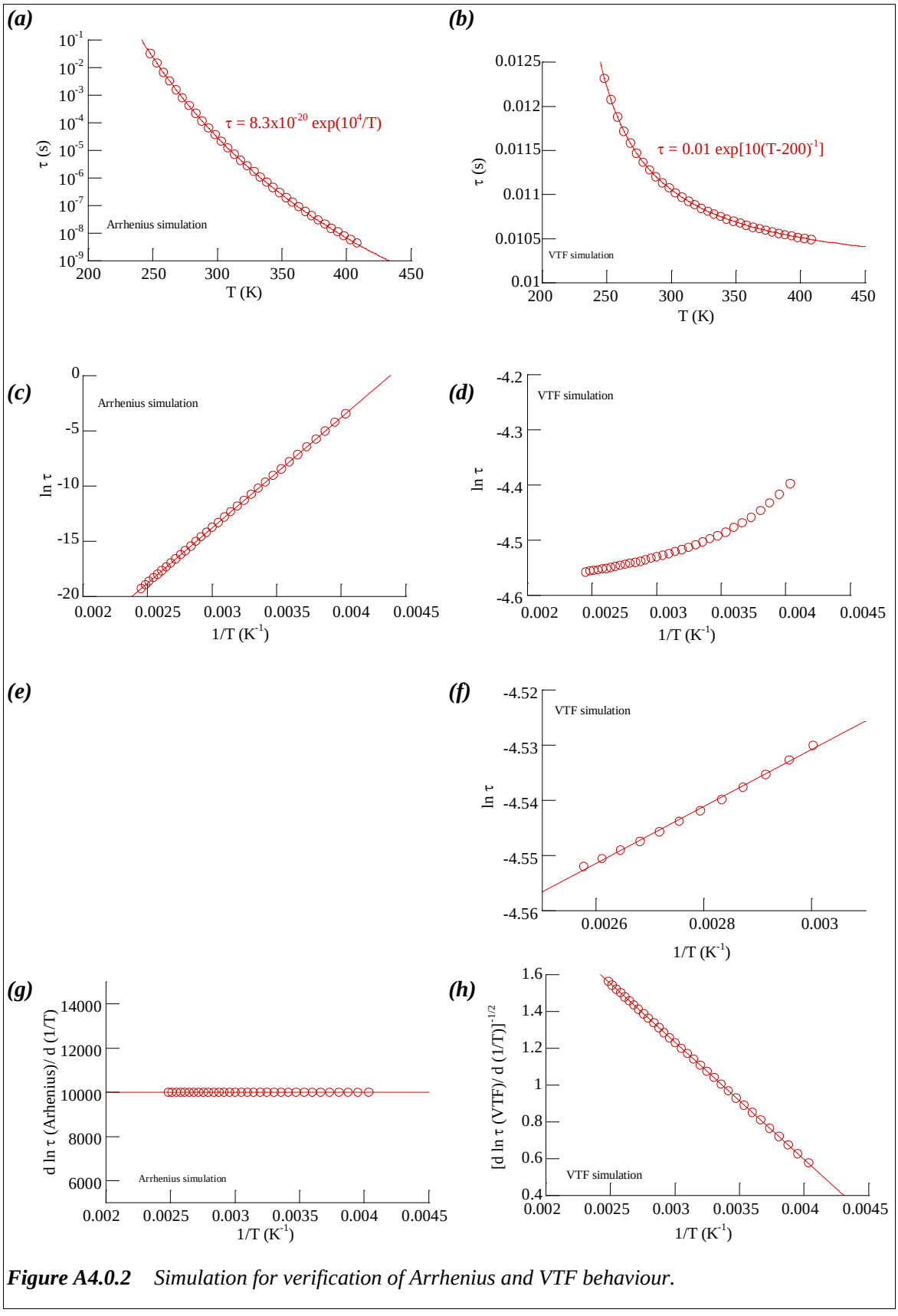

Figure A4.0.2 *Simulation for verification of Arrhenius and VTF behaviour.*

APPENDIX A5 LINEARITY IN MEASUREMENT

As mentioned in Section 5.2.2.1, the voltage applied in this measurement was 3 V_{rms}. The use of this value of voltage is still showing the linearity of the measurement as shown in Figure A5.0.1 below.

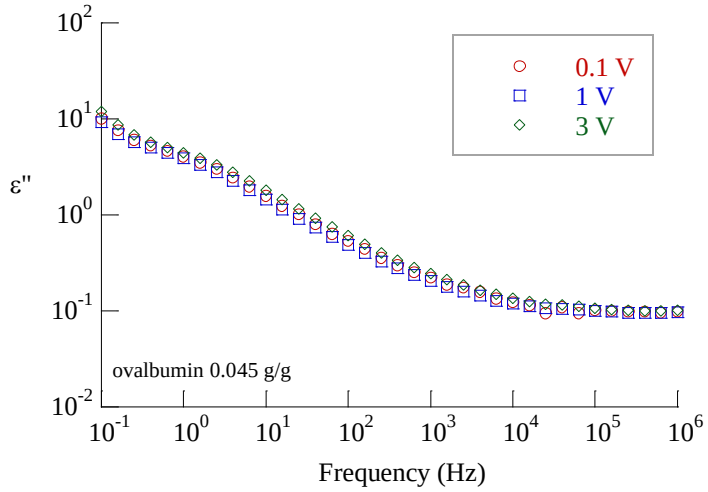

Figure A5.0.1 *Imaginary permittivity of ovalbumin 0.045 g/g for various voltages*

The reason of using 3 V_{rms} voltage is that the applied voltage below 3V usually gives a lot of noises, especially for measurement of air, which is needed for calibration and stray capacitance calculation. Figure A5.0.2 shows the comparison of air measurement using different voltages. It is shown clearly in the figure that the low applied voltage gave more noise than the high applied voltage.

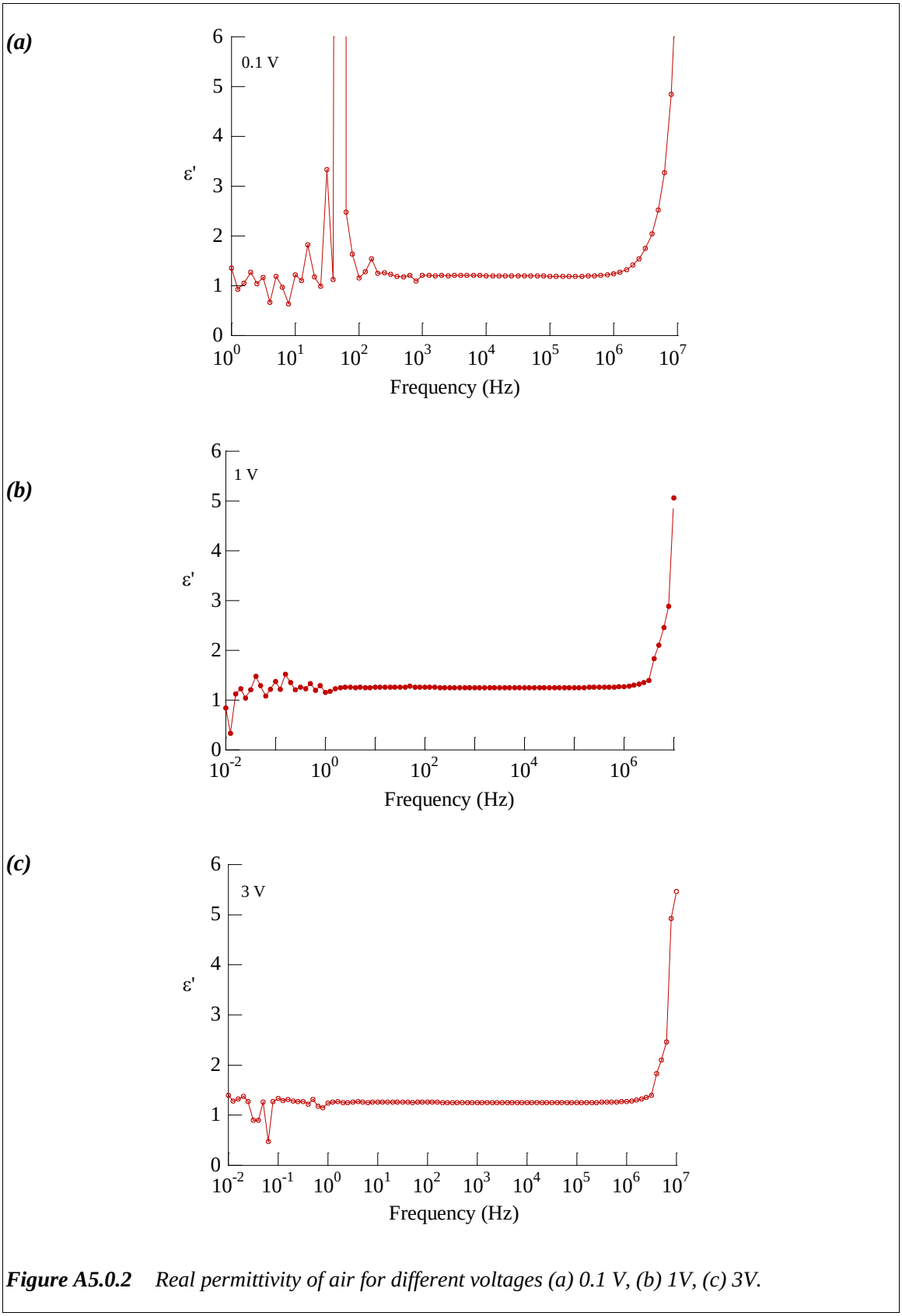

Figure A5.0.2 *Real permittivity of air for different voltages (a) 0.1 V, (b) 1V, (c) 3V.*

APPENDIX A6 TERMINOLOGY

Terminologies/abbreviations frequently used in this thesis:

Cluster	=	a group of nearest neighbour of water molecules where the proton transport occurs
Critical hydration	=	hydration level where the transition in dielectric properties over various hydration level was observed
DSC	=	Differential Scanning Calorimetry
DRS	=	Dielectric Relaxation Spectroscopy
ε_2 dispersion	=	dispersion due to the impedance composite of sample and spacer from remote electrodes
ε_3 dispersion	=	a weak loss peak, observed in hydrated protein at $\omega > \omega_c$
ε_4 dispersion	=	a weak loss peak, observed in hydrated protein at higher frequency than ε_3 dispersion
Finite cluster	=	a group of cluster with a limited size
Fractal dimension	=	representative number in fractal system that may be used to correlate the dimension in fractal system and Euclidean system.
FTIR	=	Fourier Transform Infra Red
Infinite cluster	=	a group of connected clusters forming a divergent cluster size

LFD	=	low frequency dispersion
Lyophilisation	=	freeze drying
Percolation	=	diffusion process in a random/disordered system
Quasi-dc	=	similar to low frequency dispersion
Remote electrodes	=	electrodes that are separated by the spacers from samples
SEM	=	Scanning Electron Microscopy
TGA	=	Thermogravimetry Analysis
VTF	=	Vogel-Tamman-Fulcher
ω_p	=	characteristic frequency for bound dipolar charges
ω_c	=	characteristic frequency for quasi-free charge carriers
XRD	=	x-ray diffraction

APPENDIX A7 PUBLICATIONS

Research publications that have been produced from this work:

A7.1 Refereed Papers

A7.1.1 **Suherman, P.M**., Smith, G., and Taylor, P.M. (2001) *Development of a remote electrode system for monitoring the water content of materials inside a glass vial.* Pharmaceutical Research. (accepted for publication).

A7.1.2 **Suherman, P.M**., Smith G., and Taylor, P.M. (2001) *Low Frequency Dielectric Study on Hydrated Ovalbumin.* Journal of non-crystalline solids. (accepted for publication)

A7.2 Published Conference Papers/Abstracts

A7.2.1 **Suherman, P.M.**, Taylor, P., and Smith G. (2001) *Investigation of low hydrated ovalbumin inside a glass vial – a novel approach of in situ measurement of residual moisture during lyophilisation.* British Pharmaceutical Conference, Science Proceedings 2001, Journal of Pharmacy and Pharmacology, 29.

A7.2.2 **Suherman, P.M.**, Taylor, P., and Smith G. (2001) *An investigation of water/protein interactions from temperature dependent dielectric properties*. British Pharmaceutical Conference, Science Proceedings 2001, Journal of Pharmacy and Pharmacology, 30.

A7.2.3 **Suherman, P.M.** and Smith, G. (2001) *Low frequency dielectric analysis of hydrated ovalbumin using remote electrodes.* Proceedings 1st International Conference on Dielectric Spectroscopy in Physical, Chemical, and Biological Applications, p.182. Jerusalem, 12-15 March 2001.

A7.2.4 **Suherman, P.M.** and Smith, G. (2000) *Characterisation of hydrated proteins from anomalous low frequency dispersion.* Journal of Pharmacy and Pharmacology (supplement). **52**. 250

A7.2.5 **Suherman, P.M.,** Smith, G., and Taylor P.M. (1999) *Macroscopic and microscopic characterisation of hydrated ovalbumin by low frequency dielectric analysis*. Pharmaceutical Sciences **1** (4): 362.

A7.3 Conference Proceedings - unpublished

A7.3.1 **Suherman, P.M** and Smith, G. (2000). Investigation of hydrated proteins by low frequency dielectric spectroscopy. *World Millenium Pharmaceutical Congress.* 15 –18 April 2000, San Francisco, USA.

A7.3.2 **Suherman P.M.**, Smith G., and Taylor, P.M. (1999) *The role of blocking electrode materials in the low-frequency dielectric analysis of hydrated ovalbumin.* UKAPS (United Kingdom Association of Pharmaceutical Sciences) Annual Conference: *New Frontiers in Pharmaceutical Sciences*; 28 May - 30 June 1999, Manchester, England.

A71.1

A7.1.2

Low Frequency Dielectric Study on Hydrated Ovalbumin

Phe Man Suherman, Peter Taylor, Geoff Smith*.

School of Pharmacy and Pharmaceutical Sciences, De Montfort University, Leicester, UK.

* author to whom correspondence should be addressed

CONTACT INFO:

Dr. Geoff Smith
School of Pharmacy and Pharmaceutical Sciences
Faculty of Applied Sciences
De Montfort University
Hawthorn Building
The Gateway
Leicester, LE1 9BH
UK

Tel/Fax: +44 0116 250 6298
Email: geoff@dmu.ac.uk

Abstract

This paper reports the use of low frequency dielectric measurements (0.1 Hz - 1 MHz) in the investigation of low hydrated ovalbumin (< 0.3 g H_2O/g ovalbumin), for the purpose of examining the nature of water-protein interactions.

Dielectric spectra for each hydration of ovalbumin showed two distinct processes at low and high frequency. The low frequency response showed anomalous dielectric behaviour, in which the real and imaginary permittivities are parallel and increased dramatically toward low frequency. This anomalous dielectric response followed a universal fractional power law of permittivity versus frequency and was ascribed to the quasi-dc percolation of protons through the protein matrix. The high frequency response showed a dielectric loss peak which was modeled by the Davidson-Cole expression, and was ascribed to proton hopping at the scale of the protein macromolecule.

A temperature study (253 K - 363 K) on the hydrated ovalbumin revealed that a percolation process was associated with the dielectric response of the hydrated proteins. By calculating fractal dimension from the percolation threshold, it was possible to define a hydration level of 0.08 g/g at which the surface of the protein was saturated by water.

Keywords

Dielectric relaxation spectroscopy, low frequency dispersion, dispersion, ovalbumin, hydration, percolation, fractal dimension

1. Introduction

The interaction of water with biomolecules is one of the significant factors that determines the physical and chemical instability, and hence the biological activity of a protein [1]. Dielectric spectroscopy is particularly suited to the investigation of partially hydrated proteins [2, 3, 4]. The wide frequency range of the dielectric spectrum means that it is possible to characterize the material over broad ranges of both time and scale. Quasi-dc ionic diffusion through a hydrated protein powder [5, 6] provides information at the mesoscopic scale and can be used to characterize the porosity and/or granular properties of a material [7, 8]. Short-range charge hopping between ionisable side chains on a single macromolecule [9], protein backbone flexibility [10, 11] and the reorientation polarization of bound water and surface hydration water [12] can also be used to understand the properties of the system at the molecular scale. All of these processes are dependent to some degree on the residual concentration of water in the protein and the specific interactions between the water of hydration and the protein.

The dielectric behaviour of the majority of hydrated samples show anomalous dielectric properties, in which the permittivity increases dramatically at low frequency [7]. This anomalous dielectric behaviour is known collectively as the low frequency dispersion (LFD) and occurs primarily in dielectric materials with large densities of low-mobility charge carriers. One subcategory of LFD is the quasi-dc process, in which the complex permittivity follows a fractional power law of frequency [7, 8]:

$$\varepsilon^*(\omega) = A * \omega^{-p} \qquad (1)$$

where A* is a complex constant and $0 < p < 1$. If p is in the range $0.8 < p < 1$ then the LFD response may be ascribed to the 'hopping of charge carriers' between localised sites.

Quasi-dc processes are distinguished from dc-conductivity itself by the fact that the real permittivity of LFD is parallel with the imaginary permittivity. For dc-conductivity, p = 1, and the real permittivity is independent of frequency. Quasi-dc processes are also distinguished from electrode polarisation effects (which is due to the interaction of sample with electrode interface). For electrode polarisation effect, $\varepsilon'(\omega) \propto \omega^{-2}$ and $\varepsilon''(\omega) \propto \omega^{-1}$. The fact that quasi-dc follows the power law of frequency also indicates that the LFD behaviour was associated with a percolation process.

Theoretical work by Dissado and Hill showed that quasi-dc response of hydrated proteins may be viewed as proton hopping within clusters of hydrogen bonds [8]. This work aims to employ the quasi-dc processes as a probe for the interactions between water and protein.

2. Materials and Methods

2.1 Hydrated and deuterated ovalbumin.

Spray-dried ovalbumin (crude, dried egg white, grade II, Sigma) was hydrated at 100% RH (25 °C) in a desiccator to give hydration levels between 0 – 0.3 g/g. The hydration level was defined as gram water per gram dry ovalbumin (abbreviated to g/g). The basal water content of the as-received sample was determined by drying the sample in a vacuum oven (80°C, ~ 40 mbar) until no mass reduction was observed. For deuteration, the spray-dried ovalbumin was deuterated in a desiccators containing D_2O at 25 °C.

2.2 Dielectric Measurement

The frequency dependent dielectric response of each sample (at ~ 20 °C) was measured between 0.1 Hz – 10 MHz, using a Solartron 1296 dielectric interface connected to a Solartron 1255 frequency response analyzer. The sample of hydrated ovalbumin (thickness 3 –3.5 mm) was placed between two circular brass electrodes, each with surface area 3.14 x 10^{-4} m^2. A voltage (3 V_{rms}) was applied to the sample. The amplitude and phase shift of the resulting current was then converted to dielectric parameters (e.g. impedances, capacitances, permittivities) using Solartron Impedance Measurement Software version 3.1. Data acquisition and curve fitting to complex functions were undertaken using commercial software (Zplot™ and Zview™). The temperature dependent dielectric response of each hydrated sample was measured using an Oxford temperature controller ITC^{503} and Spectrostat^{DN} cryostat. The measurements were carried out after cooling the samples down to 253 K, followed by heating up to 363 K with a step of 5 K.

3. Results and Discussion

The results showed that each hydrated ovalbumin exhibited an LFD process, which was recognised by a steep rise in permittivity towards low frequency and parallel behaviour in real and imaginary permittivities (Figure 1). At higher frequency, a weak relaxation referred to as ε_3 was observed (Figure 1). With increasing hydration, the ε_3 dispersion became obscured because it was overlapped by the low frequency dispersion and shifted to frequencies above the experimental window (Figure 2).

The LFD process was analysed using a universal form of frequency dependence in complex permittivity (Equation 1), while the higher frequency dispersion was analysed based on the Davidson-Cole model [13].

The p parameter obtained from LFD analysis, has a value ranging from 0.85 to 1, confirming that the mechanism of charge hopping was responsible for this dispersion (Figure 3).

Furthermore, the isotope dependence of ε_3 (Figure 4) showed that protons are the main charge carriers responsible for both processes. These protons may originate from the ionisable carboxylic groups in the protein structure, as has been suggested by Careri [14], or from hydrolytic cleavage of water molecules in the hydration surface of the protein.

A temperature study revealed that both LFD and ε_3 processes were associated with charge percolation through the hydrogen-bonded network of water molecules bound to the protein surface (Figure 5). In this model, the LFD process is assumed to arise from proton hopping between clusters of hydrogen bonded water molecules, and the ε_3 dispersion is due to intracluster of hopping of protons at a local scale. This cluster model has also been suggested by Dissado and Hill [8].

Since these percolation clusters are self-similar over the larger scale then percolation process can be represented by fractal model [15]. The parameters obtained from the fitting of Davidson-Cole model to the ε_3 dispersion were used in the following approximation to determine the fractal dimension [16, 17]:

$$D_f = 3\nu \qquad (2)$$

$$\nu = ((1-\alpha)\beta)^{0.813} \qquad (3)$$

where:

D_f = fractal dimension

ν = stretching parameter from the Kohlrausch-Williams-Watts (KWW) expression.

α, β = empirical constants of Havrilliak-Negami expression

The fractal dimensions (D_f) obtained from this work for various hydration levels are shown in Figure 6. Below hydration level of ~ 0.08 g/g, the fractal dimension is < 2, whereas above hydration level of ~ 0.08 g/g, the fractal dimension is > 2. A fractal dimension of 1.9 corresponds to a 2 dimensional system [15] and therefore it follows that below the hydration level of ~ 0.08 g/g, the proton may percolate along the surface of macromolecules, while above the critical hydration level, the protons may move within the matrix of protein structure. The transition at ~ 0.08 g/g therefore corresponds to the hydration level at which hydrogen bonding sites on the protein surface are saturated by water.

Relaxation times for the high frequency process corresponded to Arhenius behaviour, which enabled the calculation of the activation energy (ΔH) for various hydrated ovalbumin. This activation energy (ΔH) may be related to the ionic self-dissociation of water, and the associated release of protons which can then percolate to another cluster of water molecules.

The transition at hydration level ~ 0.08 g/g was also observed in the activation energy data (Figure 6). Below hydration level of ~0.08 g/g, ΔH < 100 kJ mol^{-1} and at above hydration level of ~ 0.08 g/g, ΔH is almost constant at ~ 100 kJ mol^{-1}.

Furthermore, the *A* parameter from the LFD process also highlighted the transition hydration of ~ 0.08 g/g (Figure 7). The same transition hydration was also observed by Careri [14] on hydrated lysozyme using IR study.

4 Conclusion

Low frequency (< 1 MHz) dielectric behaviour of low hydrated ovalbumin (< 0.3 g/g) showed two dimensional scales for proton hopping in the bulk sample, which are identified as anomalous low frequency dispersion and dielectric loss peak. The dielectric behaviour also showed the transition at ~ 0.08 g/g, which is related to the formation of a saturated hydration layer at the surface of the protein.

Acknowledgements

GlaxoSmithKline and De Montfort University for joint funding this project

References

[1] M.C. Lai and E.M. Topp, J. Pharm. Sci. 88:5 (1999) 489.

[2] G. Smith, A. Duffy, J. Shen, and C.J. Olliff, J. Pharm. Sci. 84:9 (1995) 1029.

[3] D.S. Pearson, and G. Smith, Pharm. Sci. Tech. Today 1:3 (1998) 108.

[4] S. Bone, Phys. Med. Biol. 41 (1996) 1265.

[5] S. Bone, J. Eden, P.R.C. Gascoyne, and R. Pethig, J. Chem. Soc., Faraday Trans. 77 (1981) 1729.

[6] J. Eden, P.R. Gascoyne, and R. Pethig, J. Chem. Soc., Faraday Trans.. 76 (1980) 426.

[7] A.K. Jonscher, Phil. Mag. B 38 :6 (1978) 587.

[8] L.A. Dissado and R.M. Hill, J. Chem. Soc., Faraday Trans 2 80 (1984) 291.

[9] G. Careri, M. Geraci, A. Giansanti, and J. A.Rupley, Proc. Natl. Acad. Sci. 82 (1985) 5342.

[10] S.Bone, J. Eden, and R. Pethig, Int. J. Quant. Chem.: Quant. Biol. Symp. 8: (1981) 307.

[11] J.J. Hawkes, and R. Pethig, Biochim. Biophys. Acta 952 (1988) 27.

[12] E.H. Grant, J. Mol. Biol. 19 (1966) 133.

[13] D.W. Davidson and R.H. Cole, J. Phys. Chem. 18 (1950) 1417.

[14] G. Careri, E. Gratton, P.Yang, and J. Rupley, Nature 284 (1980) 572.

[15] D. Stauffer and A. Aharony, Introduction to Percolation Theory (Taylor and Francis, London, 1998).

[16] F. Alvarez, A. Alegria, J. Colmenero, Phys. Rev. B 44 (1991) 7306.

[17] Y. Feldman, N. Kozlovich, Y. Alexandrov, R. Nigmatullin, and Y. Ryabov, Phys. Rev. E 54 (1996) 5420.

Figure 1

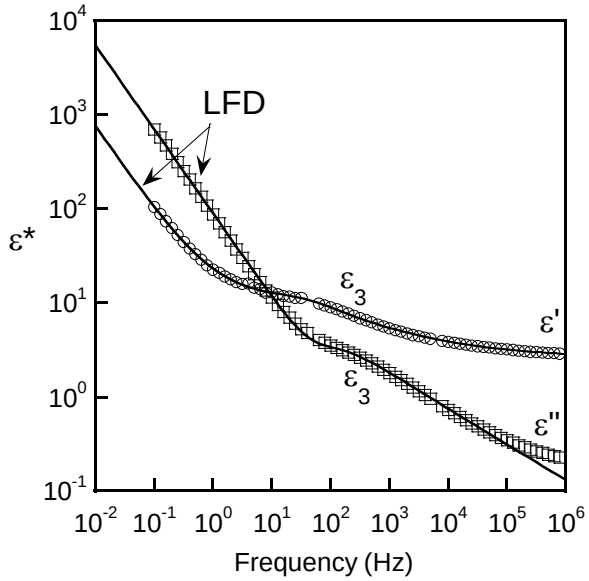

Figure 2

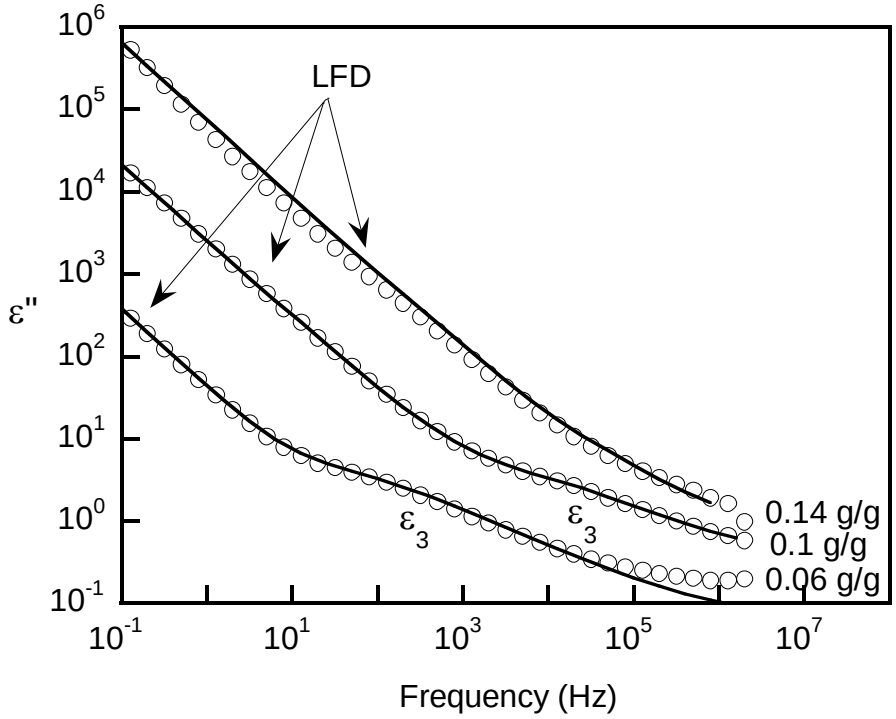

Figure 3

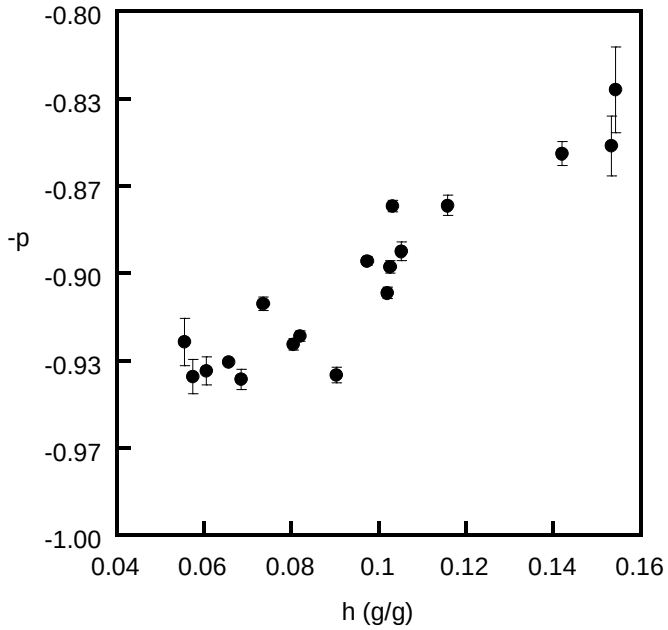

Figure 4

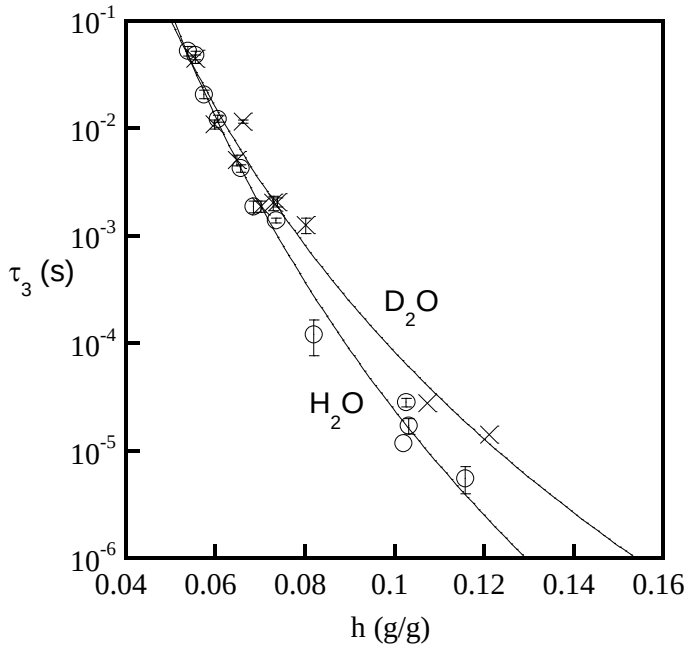

Figure 5

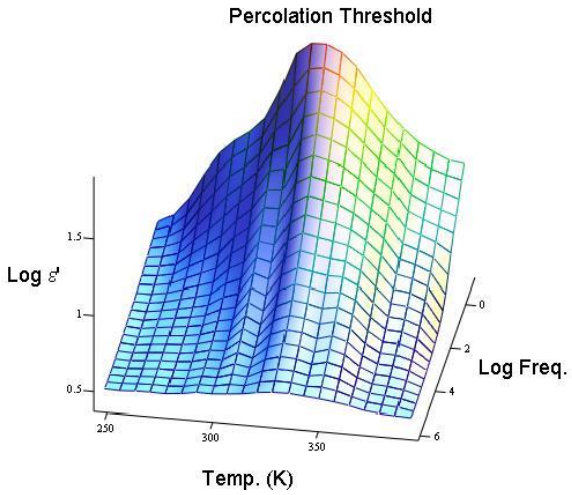

Figure 6

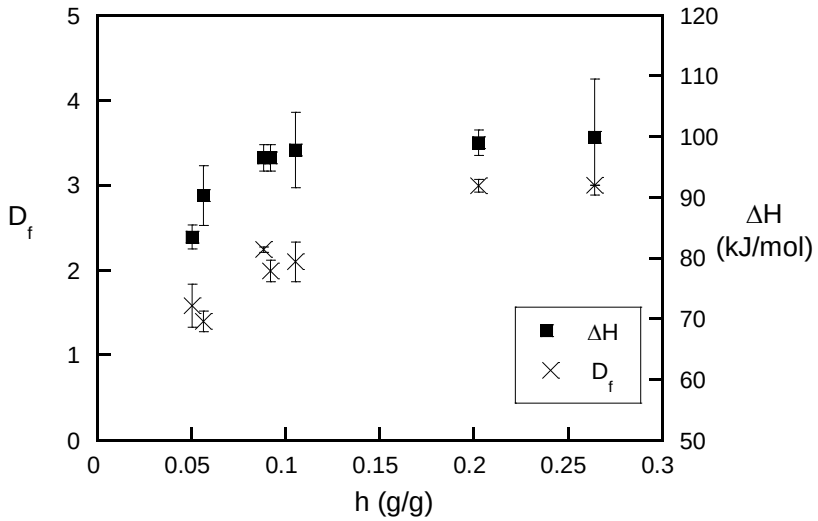

Figure 7

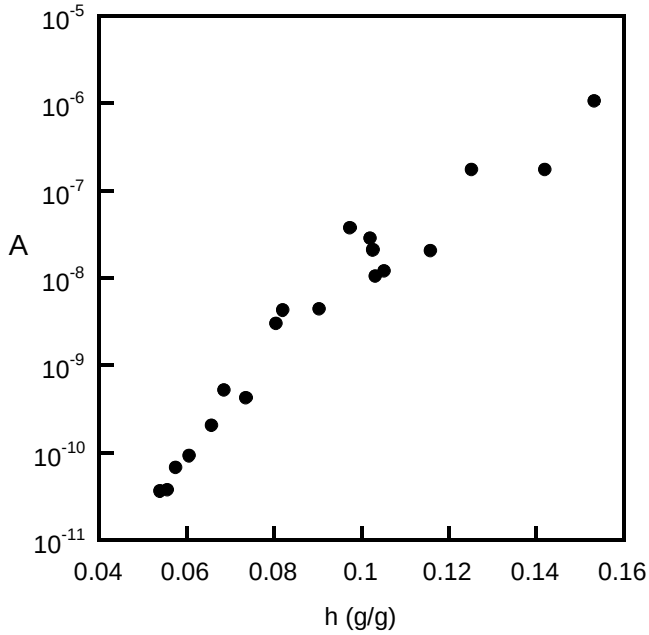

Figure Captions

Figure 1 Real and imaginary permittivity of hydrated ovalbumin (0.07 g/g), showing the LFD and ε_3 dispersion. Solid lines represent the curve fitting, while the symbols represent experimental data.

Figure 2 Imaginary permittivity of various hydrated ovalbumin, showing the shifting toward higher frequency with the higher hydration. Solid lines represent the curve fitting, while the symbols represent experimental data.

Figure 3 The *p* parameter from fitting of the quasi-dc element.

Figure 4 Relaxation times τ_3 from ε_3 dispersion of various hydrated ovalbumin. Solid lines and broken lines represent the curve fitting for hydrated and deuterated samples, respectively. Symbols represent experimental results. Circles represent hydrated samples, crosses represent deuterated samples.

Figure 5 Three-dimension plot of real permittivity of hydrated ovalbumin (0.05 g/g) over various temperature ranges.

Figure 6 Fractal dimension (D_f) and activation energy (ΔH) of various hydrated ovalbumin at percolation threshold.

Figure 7 The constant values *A* from fitting of the quasi-dc element.

A7.2.1

British Pharmaceutical Conference 2001 Abstract Book: 29

Investigation of low hydrated ovalbumin inside a glass vial - a novel approach of in situ measurement of residual moisture during lyophilisation

P.M. SUHERMAN, P. TAYLOR, G. SMITH

School of Pharmacy and Pharmaceutical Sciences, De Montfort University, Leicester, LE1 9BH, UK

The residual moisture content of pharmaceutical materials is an important issue, especially for amorphous freeze-dried and spray-dried products. This study presents the use of dielectric measurements for monitoring the water content of hydrated protein inside the freeze drying glass vial, as an initial stage in the development of a new method for *in situ* measurement of residual moisture during lyophilisation.

Low hydrated ovalbumin (0.05 - 0.2 g water/g dry protein) was chosen as a model protein. A remote-electrode system was developed in order to obtain non-invasive measurement of the protein inside a glass vial. In the context of this work, a remote electrode system is defined as electrodes that are separated from the sample by non-conductive and non dispersive medium, i.e. the glass vial used for the freeze drying process. Dielectric measurements (0.1 Hz - 1 MHz) were carried out using a Solartron 1296 dielectric interface connected to a Solartron 1255 frequency response analyser.

The aim of this study was to compare the dielectric response of ovalbumin as a function of electrode configuration and water content. The three electrode systems studied were: (1) parallel plate electrodes, (2) parallel plate electrodes with polyethylene films between the electrodes and sample, and (3) custom-made electrodes attached outside the freeze drying glass vial.

Figure 1 shows the imaginary permittivity of hydrated ovalbumin (0.08 g/g) measured using the three electrode systems. As reported in a previous paper (Suherman & Smith 2000), the dielectric response of hydrated ovalbumin using conventional parallel plate electrodes shows two processes, i.e. a quasi-dc dispersion and high frequency response (termed ε_3 dispersion). The use of remote electrodes introduced another distinct dielectric response (i.e. ε_2 dispersion), which originated from the superposition of the polyethylene films impedance and the impedance of the quasi-dc process. The high frequency response (ε_3 dispersion) was unaffected by the use of remote electrodes.

The lack of dependence of the high frequency response (ε_3 dispersion) on the choice of electrode system confirmed that this response is due to the internal structure of the bulk sample itself. This inference is then applied to the use of glass vial in a remote electrode configuration.

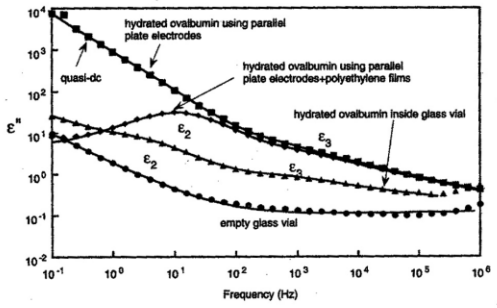

Figure 1. Imaginary permittivity of hydrated ovalbumin (0.08 g/g). Solid lines represent the fitting, symbols represent experimental data.

The results for various low hydrated ovalbumin (0.05 - 0.2 g/g) demonstrate that the relaxation times for the ε_3 dispersion for measurement inside the glass vial are comparable with the measurement using conventional parallel plate electrodes. Since ε_3 dispersion is very sensitive to water content, this study has shown that it is possible to use remote electrodes to monitor moisture content during lyophilisation process.

Suherman. P.M. and Smith G. (2000) *J. Pharm. Pharmacol.* 52 (Suppl.): 250

Acknowledgement: Glaxo SmithKline and De Monfort University for funding of this study.

A7.2.2

British Pharmaceutical Conference 2001 Abstract Book: 30

An investigation of water/protein interactions from temperature dependent dielectric properties

P.M. SUHERMAN, P. TAYLOR, G. SMITH

School of Pharmacy and Pharmaceutical Sciences, De Montfort University, Leicester, LE1 9BH, UK

The interaction of water with proteins is one of the significant factors that determines the properties of biopharmaceutical materials, since it may cause physical and chemical instability that could ultimately lead to loss of activity of protein. This study revealed the percolation behaviour of hydrated protein which can be related to the interaction/mechanism of water molecules in proteins.

Ovalbumin was chosen as a model protein and hydrated to between 0.05 - 0.2 g water/g dry protein. Each sample was placed between two circular brass electrodes and experienced a stepwise increase in temperatures from 253 - 363 K. Low frequency dielectric measurements (0.1 Hz - 1 MHz) were carried out using a Solartron 1296 dielectric interface connected to a Solartron 1255 frequency response analyser and Oxford temperature controller ITC[503].

Previous work has shown that at ambient temperature there were two processes observed in hydrated ovalbumin, i.e. quasi-dc dispersion and high frequency response (Suherman & Smith 2000). With the increase in temperature (253 K - 363 K), both of the processes experienced a threshold at certain temperature. Figure 1 shows clearly the threshold of low frequency response at ~343 K. This is referred to as the percolation threshold, since the dielectric response observed in this work is associated with the percolation process of proton between hydrogen-bonded water molecules.

The low frequency response satisfied Jonscher's power law, while the high frequency response followed a Davidson-Cole model[1]. Below the percolation temperature, the relaxation times from high frequency process conformed to Arrhenius behaviour, which enabled the calculation of the activation energy (ΔH) for variously hydrated ovalbumin. This activation energy (ΔH) may be related to the ionic self-dissociation of water to release a proton which then percolates to another cluster of water molecules.

Cluster percolation is associated with the phenomenon of self-similarity within a framework of a fractal scale. An approximation of fractal dimension in this work is calculated from the empirical distribution parameters obtained from the fitting of Davidson-Cole model for high frequency response (Alvarez et al 1991; Feldman 1996)

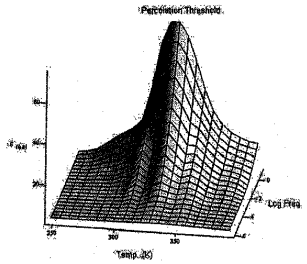

Figure 1. Real permittivity (ε') of hydrated ovalbumin (0.05 g/g) for various range of temperature.

Both the fractal dimension (D_f) and ΔH obtained from this work highlighted a critical hydration level at ~ 0.1 g/g). Below the hydration level of 0.1 g/g, the fractal dimension is ~1.5 and ΔH<100 kJ mol^{-1}, whereas above the critical hydration level the fractal dimension is saturated at ~ 3 and ΔH is almost constant at ~ 100 kJ mol^{-1}. These fractal dimensions refer to 2 and 3 dimensional systems, respectively. Therefore, below the critical hydration level, the proton may percolate along the surface of macromolecules, while above the critical hydration level, the protons may move within the matrix of protein structure. The formation of various layers of water molecules covering each macromolecules may explain the form of the three dimensional system at above critical hydration level. The activation energy itself may be associated with the stability of hydrated proteins, and therefore, this study may lead further understanding of the thermostability of enzymes and proteins.

Suherman. P.M. and Smith G. (2000) *J. Pharm. Pharmacol.* 52 (Suppl.): 250

Alvarez, et. al. (1991) *Phys. Rev. B*, 44: 7306

Feldman, Y. (1996) *Phys. Rev. E*, 54: 5420

Acknowledgement: Smithkline Beecham Pharmaceutical and De Monfort University for funding of this study

A7.2.3

LOW FREQUENCY DIELECTRIC ANALYSIS OF HYDRATED OVALBUMIN USING REMOTE ELECTRODES

Phe Suherman and Geoff Smith

Faculty of Applied Sciences, De Montfort University, Leicester, LE1 9BH, UK
http://www.dmu.ac.uk/ln/Pharmacy/smith.html

Low frequency dielectric measurements often give rise to anomalous dielectric behaviour, in which the permittivity/capacitance increases dramatically at low frequency. This anomalous dielectric response is especially evident for biopharmaceutical materials, and is known as the low frequency dispersion (LFD) [1]. This study presents the use of the low frequency dispersion to characterise hydrated ovalbumin using remote electrodes, i.e. electrodes that are separated from the sample by non-conductive and non dispersive medium.

Freeze dried ovalbumin was hydrated in a standardised environment (100% relative humidity and 25 °C) to water contents of 0 - 0.25 g H_2O/g dry ovalbumin. The sample was placed between two circular brass electrodes. Thin sheets of polymer films (<0.1mm) were placed between the electrodes and the sample, creating remote electrodes. Low frequency dielectric measurements (0.1 Hz - 1 MHz) were carried out using a Solartron 1296 dielectric interface connected to a Solartron 1255 frequency response analyser.

The results show that each hydrated ovalbumin exhibited a steep rise in permittivity towards low frequency. This was recognised as a low frequency dispersion (LFD). This LFD effect is not simply due to DC conductivity since the real permittivity is parallel with the imaginary permittivity.

At higher frequency, a weak relaxation, referred to as ε_3, was observed. With increasing hydration, ε_3 dispersion becomes more obscure since it was overlapped by the low frequency dispersion. When remote electrodes were used, the LFD effect was replaced by a Maxwell-Wagner relaxation, which is referred to as the ε_2 dispersion. The existence of ε_3 is not affected by the use of remote electrodes, affirming that ε_3 dispersion is a bulk property of the sample. It is considered that ε_3 may be associated with vibrational motions of the polypeptide backbone. ε_2 is due to the composite capacitor characteristics of the LFD/remote electrodes. The isotope effect on ε_2 showed that ε_2 from the sample part is probably due to the localised proton hopping between the ionisable carboxylic groups in the protein structure, as has been suggested by Careri [2].

The LFD effect in this study was analysed using a universal form of frequency dependence of dielectric loss [1], while the higher frequency dispersion was analysed based on the empirical Davidson-Cole model. The dependence of the ε_2 and ε_3 dispersions on water content may be used for quality control purposes, e.g. the analysis of freeze dried biopharmaceuticals, in which the properties of residual water play an important role.

References.

[1] Jonscher, A.K. (1978) *Phil. Mag. B*, **38**, No. 6, 587-601
[2] Careri, G. et al (1985) *Proc. Natl. Acad. Sci.* **82**. 5342-5346

Acknowledgement. SmithKline Beecham Pharmaceutical and De Monfort University.

182

A7.2.4

J. Pharm. Pharmacol. 2000, 52 (Supplement): 250

Characterisation of hydrated proteins from anomalous low-frequency dispersion

P. M. SUHERMAN AND G. SMITH

School of Pharmacy and Pharmaceutical Sciences, De Montfort University, Leicester LE1 9BH, UK

Low-frequency dielectric measurements often give rise to anomalous dielectric behaviour, in which the permittivity/capacitance increases dramatically at low frequency. This anomalous dielectric response is especially evident for biopharmaceutical materials, and is known as the low-frequency dispersion (LFD, Jonscher 1978). This study presents the use of the anomalous low-frequency dispersion to characterise hydrated proteins.

Freeze-dried proteins (ovalbumin, lysozyme, and pepsin) were hydrated in a standardised environment (100% relative humidity and 25°C) to water contents of 0-0.25 g H_2O/g dry protein. Each sample was placed between two circular brass electrodes. Thin sheets of polymer films (< 0.1 mm), used as blocking electrodes, were placed between the electrodes and the sample. Low-frequency dielectric measurements (0.1 Hz-1 MHz) were carried out using a Solartron 1296 dielectric interface connected to a Solartron 1255 frequency response analyser.

The results show that each of the hydrated proteins exhibited a steep rise in permittivity towards low frequency (Figure 1). This was recognised as a low frequency dispersion (LFD). This LFD effect is not simply due to DC conductivity since the real permittivity is parallel with the imaginary permittivity.

At higher frequency, a weak relaxation, referred to as ε_3, was observed (Figure 1). In this study, ε_3 was only observed for ovalbumin and lysozyme at low hydration. With increasing hydration, ε_3 dispersion becomes more obscure since it was overlapped by the low frequency dispersion. When polymer films were used as blocking electrodes, the LFD effect was eliminated by a distinct relaxation, which is referred to as the ε_2 dispersion (Figure 1). The existence of ε_3 is not affected by the use of blocking electrode, affirming that ε_3 dispersion is a bulk property of the sample. It is considered that ε_3 may be associated with vibrational motions of the polypeptide backbone. ε_2 is probably due to the composite capacitor characteristics of the sample/blocking electrode. The isotope effect on ε_2 showed that ε_2 from the sample part is probably due to the localised proton hopping between the ionisable carboxylic groups in the protein structure, as has been suggested by Carreri et al (1985).

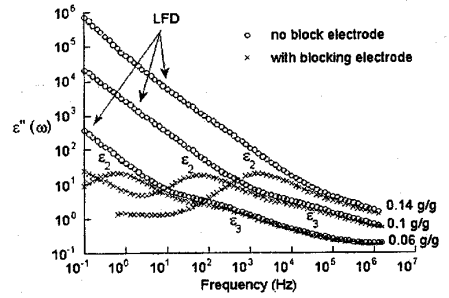

Figure 1. Imaginary permittivity (ε") of various hydrated ovalbumin (0.06-0.14 g/g).

The LFD effect in this study was analysed using a universal form of frequency-dependence of dielectric loss (Jonscher 1978), while the higher frequency dispersion was analysed based on the empirical Davidson-Cole model. The dielectric parameters extracted from both analyses performed the transitions at hydration levels which are consistent with IR study on hydrated lysozyme (Carreri et al 1983). This information could be usefully employed to determine hydration-dependent changes in the properties of each protein, such as enzymatic activity, ionisation state, and conformational change (Carreri et al 1983; Bone 1996).

The dependence of the ε_2 and ε_3 dispersions on water content may be used for quality control purposes, e.g. the analysis of freeze-dried biopharmaceuticals, in which the properties of residual water play an important role.

We acknowledge SmithKline Beecham Pharmaceutical and De Montfort University for funding of this study.

Jonscher, A. K. (1978) Phil. Mag. B 38: 587-601

Carreri, G. et al (1985) Proc. Natl Acad. Sci. 82: 5342-5346

Carreri, G. et al (1983) Nature 284: 572-573

Bone, S. (1996) Phys. Med. Biol. 41: 1265-1275

A7.2.5

INVESTIGATION OF HYDRATED PROTEINS BY LOW FREQUENCY DIELECTRIC SPECTROSCOPY.

Purpose. To characterise hydrated proteins using low frequency dielectric measurements. **Methods.** The low frequency dielectric response of various hydrated proteins (ovalbumin, lysozyme, and pepsin) were analysed using a Solartron 1296 dielectric interface connected to a Solartron 1255 frequency response analyser (frequency range: 0.1 Hz - 10 MHz). The protein samples were hydrated at 100% relative humidity (25 °C) to water contents of 0 – 0.3 g H_2O/g dry protein. The sample (thickness ~ 3 mm) was sandwiched between two circular brass electrodes. Thin sheets of polymer films (< 0.1 mm), used as blocking electrode, were placed between the electrodes and the sample. The various types of materials used for the blocking electrode were: polypropylene (isotactic), polypropylene (atactic) with an adhesive backing, and polyethylene. The results from each dielectric relaxation were fitted to the Davidson-Cole model to give the following dielectric parameters: relaxation time (τ), relaxation strength ($\Delta\varepsilon$), and distribution parameter (β). **Results.** The dispersive nature of each sample depends not only on the protein itself, but also on the choice of blocking electrode material. A number of dispersions may be observed depending on the choice of blocking electrode material. The material used as a blocking electrode is partly responsible for the dispersion at low frequency. At higher frequency, the dispersion observed was independent of choice of blocking electrode material, suggesting that the relaxation was due to the dielectric response of the sample only. The low frequency process could also be related to the macroscopic structure of material since the results show the dependence of the low frequency process on packing. The high frequency process however could be usefully employed to determine changes in the microscopic structure of material (e.g. protein conformational stability, enzymatic activity, and vibrational motions of polypeptide backbone). The results from relaxation strength ($\Delta\varepsilon$), infinite permittivity (ε_∞), and distribution paramter (β) show the critical hydration which may be related to a conformational change and/or the ionisation state of ovalbumin (especially at the active sites for charge transport). **Conclusions.** The study shows that low frequency dielectric spectroscopy may be able to characterise both macroscopic and microscopic properties of hydrated proteins. This application may be employed to monitor the water state in proteins during biological process, especially for freeze drying process. **Acknowledgement.** SmithKline Beecham Pharmaceuticals.

A7.3.1

1367 cm^{-1}) related to the hydrogen bonding among free water adsorbed, NH3 and COO- of APM molecules disappeared gradually after temperature > 50°J, but the peak at 3338 cm^{-1} assigned to the free NH stretching of amine in APM molecule and the peak at 1627 cm^{-1} due to the OH bending of water were stepwise observed. This evidenced an evaporation process of water adsorbed on APM molecule and a transition state in water evaporation process at 63°J. Moreover, an IR spectral shift from 1662 to 1666 cm^{-1} or from 1549 to 1543 cm^{-1} was found after 110°J, attributable to the change of hydrogen bonded C-O and N-H in amides I and II of APM molecule to the free C = O and free N-H, as well as the dehydration process of hydrate in the molecular packing of APM crystal after >110°J. The appearance of IR peaks at 1362 and 1331 cm^{-1} from 110°J also explained the increase of the free -COOH in APM molecule due to the gradual loss of hydrogen bonding in the dehydration process. In addition, the structural arrangement in APM molecule due to intramolecular cyclization resulted in the formation of 3-carboxy-methyl-6-benzyl-2,5-diketopiperazine (DKP) and the liberation of methanol after temperature > 153 °J. The pathway for the lactam ring formation and the demethoxylation from APM molecule started from 153°J, and a transitional state was markedly observed at 165°J. The dramatic change in IR spectra at 50, 110 or 153°J might be explained as the onset temperature for water evaporation, dehydration and cyclization processes, respectively, as compared to the endothermic peaks at 123 and 181°J in DSC curve. Thus, the IR spectra giving a vital information about structure of organic molecules was more sensitive than the DSC curve from thermal analyzer to understand the pathway of physical transformation and chemical reaction in APM molecules.

1-4002 WATER VAPOR ADSORPTION PROPERTIES OF AMORPHOUS CEFDITOREN PIVOXIL EVALUATED BY ADSORPTION ISOTHERMS AND MICROCALORIMETRY

Masato Ohta[1], Yuichi Tozuka[2], Toshio Oguchi[2], Keiji Yamamoto[2].
[1]Pharmaceutical Research Center, Meiji Seika Kaisha, Ltd., 760 Morooka-cho, Kohoku-ku, Yokohama 222-8567; [2]Faculty of Pharmaceutical Sciences, Chiba University, 1-33 Yayoi-cho, Inage-ku, Chiba 263-8522, Japan

Amorphization has been investigated as means of enhancing solubility and improving bioavailability of insoluble drug. Cefditoren pivoxil is a new oral cephalosporin antibiotic. Water vapor adsorption properties of ground cefditoren pivoxil were evaluated by adsorption isotherms and heat of adsorption. Further, the changes of molecular state through grinding process were considered from infrared spectrum. Cefditoren pivoxil was ground using vibrating mill for a predetermined period. The crystallinity of cefditoren pivoxil was determined according to the Ruland's method from powder X-ray diffractogram. Heat of adsorption of cefditoren pivoxil with different crystallinity was determined by isothermal microcalorimetry. The crystallinity of cefditoren pivoxil gradually decreased through grinding process. The amount of water adsorbed increased with a decrease in the crystallinity of cefditoren pivoxil. It was found from the microcalorimetric measurements that the differential heat of water vapor adsorption at the amount of adsorbed water 1.5% was increased with decreasing crystallinity of cefditoren pivoxil, suggesting that hygroscopicity of cefditoren pivoxil was enhanced by grinding. These results indicated that hydrophilic adsorption sites in cefditoren pivoxil increased through grinding process. The results of infrared spectra suggested that the increment of hydrophilic adsorption sites through grinding process resulted from the change of the environment of the hydrophilic groups such as the carbonyl groups in two esters and amide.

1-4005 INVESTIGATION OF HYDRATED PROTEINS BY LOW FREQUENCY DIELECTRIC SPECTROSCOPY

Phe Man Suherman, Geoff Smith, Peter Taylor, David Merrifield. *School of Pharmacy and Pharmaceutical Sciences, De Montfort University, The Gateway, Leicester, LE1 9BH, United Kingdom*

Purpose: To characterise hydrated proteins using low frequency dielectric measurements.

Methods: The low frequency dielectric response of various hydrated proteins (ovalbumin, lysozyme, and pepsin) were analysed using a Solartron 1296 dielectric interface connected to a Solartron 1255 frequency response analyser (frequency range: 0.1 Hz–10 MHz). The protein samples were hydrated at 100% relative humidity (25°C) to water contents of 0 0.3 g H2O/g dry protein. The sample (thickness ~ 3 mm) was sandwiched between two circular brass electrodes. Thin sheets of polymer films (<0.1 mm), used as blocking electrode, were placed between the electrodes and the sample. The various types of materials used for the blocking electrode were: polypropylene (isotactic), polypropylene (atactic) with an adhesive backing, and polyethylene. The results from each dielectric relaxation were fitted to the Davidson-Cole model to give the following dielectric parameters: relaxation time, relaxation strength, and distribution parameter.

Results: The dispersive nature of each sample depends not only on the protein itself, but also on the choice of blocking electrode material. A number of dispersions may be observed depending on the choice of blocking electrode material. The material used as a blocking electrode is partly responsible for the dispersion at low frequency. At higher frequency, the dispersion observed was independent of choice of blocking electrode material, suggesting that the relaxation was due to the dielectric response of the sample only. The low frequency process could also be related to the macroscopic structure of material since the results show the dependence of the low frequency process on packing. The high frequency process however could be usefully employed to determine changes in the microscopic structure of material (e.g. protein conformational stability, enzymatic activity, and vibrational motions of polypeptide backbone).

The results from relaxation strength, infinite permittivity, and distribution paramter show the critical hydration which may be related to a conformational change and/or the ionisation state of ovalbumin (especially at the active sites for charge transport).

Conclusions: The study shows that low frequency dielectric spectroscopy may be able to characterise both macroscopic and microscopic properties of hydrated proteins. This application may be employed to monitor the water state in proteins during biological process, especially for freeze drying process.

Acknowledgement. SmithKline Beecham Pharmaceuticals.

1-4006 ADHESIVE STRENGTH OF AUTOLOGOUS FIBRIN GLUE

Hisahiro Yoshida, Kiyoshi Hirozane, Akira Kamiya. *Department of Pharmacy, Yamaguchi, Japan University Hospital*

Objective: To establish an easy and speedy method for measuring the adhesive strength of fibrin glue and to clarify the factor(s) most affecting the strength. A study was made on the effect of the concentration of plasma components on the strength of cryoprecipitate (Cryo) prepared from a subject's own autologous plasma to be used as fibrin glue.

Method: The adhesive strength of each prepared Cryo was measured as follows: two pieces of materials (ground flat glass, clear glass, clear plastic, or smooth and flat wood chips) of 4 cm^2, bound to cubic wood with chemical adhesive, were prepared. Ten of Cryo was applied to one piece and 10 of a given concentration mixture of thrombin and $CaCl_2$ to the other. Both applied surfaces were adhered together. The materials adhered through Cryo were fixed in a tension measuring device and maximum tensile adhesive strength was measured.

Results: (1) The strength of Cryo applied to ground flat glass was significantly greater than that applied to clear glass, clear plastic, or smooth and flat wood chips. (2) The adhesive strength of Cryo depended on the concentration of thrombin with the optimal concentration being 50 units/ml. (3) The concentration of $CaCl_2$ did not affect the adhesive strength of Cryo. (4) The adhesive reaction was dependent on the temperature and the adhesive strength more quickly reached a steady state at 37 than at lower temperature. (5) The adhesive strength was correlated well with the total concentration of fibrinogen and fibronectin.

Conclusions: These results indicate that the adhesive strength of Cryo can be easily and quickly evaluated using a tester and ground glass with thrombin at 50 units/ml, and that the adhesive strength of Cryo can be predicted from the total concentration of fibrinogen and fibronectin.

1-4007 FORMULATION AND IN VITRO-IN VIVO EVALUATION OF PIRIBEDIL SOLID LIPID PARTICLES

Muzeyyen Demirel, Yasemin Yazan, Rainer H. Müller, Fatma Kilic, Berrin Bozan. *Anadolu University, Faculty of Pharmacy, Department of Pharmaceutical Technology, 26470, Eskisehir, Turkey*

Modification of the dissolution rate and thus the enhancement of the bioavailability of a dopaminergic drug, piribedil, which has a low aqueous solubility and short elimination half-life have been aimed in this study. Preparation of micron- and submicron particles using solid lipid carriers has been performed for this purpose.

For the avoidance of solvent residues resulting from the preparation technique, cold and hot homogenization methods have been used to prepare solid lipid particles. Following the obtention of appropriate particle size, piribedil loading and preparation yield by the use of those two methods, various formulations have been prepared with different lipid, drug and surfactant materials. The factors mentioned were found to effect properties of the particles.

When the in vitro releases from all formulations were examined, release rate was found to be the fastest in acidic medium.

Suspensions of intact piribedil and a formulation, selected according to the results obtained from in vitro dissolution and particle size experiments, were compared using tremor tests in mice. The same suspensions were applied perorally to rabbits and bioavailability of the solid lipid particle was found to be 4-fold higher than intact piribedil. This may be due to the adhesion of lipid

A7.3.2

The role of blocking electrode materials in the low-frequency dielectric analysis of hydrated ovalbumin

Phe Man Suherman, Geoff Smith*, Peter M. Taylor.
School of Pharmacy and Pharmaceutical Sciences, Faculty of Applied Sciences,
De Montfort University, Leicester, LE1 9BH, UK.

In recent years, proteins have become a focus for the development of novel therapeutic agents, with numerous unique applications being highlighted for routine medical treatments. It is well known that the interaction of water with a protein can cause physical and chemical instability that could ultimately lead to loss of activity. Dielectric analysis is one of a number of techniques that can be used to investigate partially hydrated proteins.

The most commonly used sample cell for low-frequency dielectric measurement (< 10 MHz) consists of two parallel metal electrodes. However, the contact between metal and sample (especially hydrated biological samples) can result in an electrode polarisation impedance that is wrongly associated with the bulk dielectric properties of the sample. This artifact can be overcome partly by the use of blocking electrodes, i.e. metallic electrodes that are coated with a thin film of insulating material. However, even this type of electrode can produce artifactual responses that have to be carefully screened.

This study involved dielectric measurements (0.1 Hz – 10 MHz) on hydrated ovalbumin (0 – 0.25 g/g) using various polymer films as blocking electrodes. The results from each blocking electrode study were fitted to the Davidson-Cole model to give the following dielectric parameters: relaxation time (τ), relaxation strength ($\Delta\varepsilon$), and distribution parameter (β). The results show that one or two dispersions may be observed depending on the choice of blocking electrode material. The material used as a blocking electrode is partly responsible for the dispersion at low frequency. At higher frequency, the dispersion observed was independent of choice of blocking electrode material, suggesting that the relaxation was due to the dielectric response of the sample only.

The low frequency process could also be related to the macroscopic structure of freeze-dried material since the results show the dependence of the low frequency process on packing. The high frequency process however could be usefully employed to determine changes in the microscopic structure of freeze-dried material (e.g. protein conformational stability). The results from the relaxation strength ($\Delta\varepsilon$) also shows the critical hydration level at about 0.08 – 0.1 g/g which may be related to a conformational change and/or the ionisation state of ovalbumin (especially at the active sites for charge transport).

The study shows that the choice of a suitable material for the blocking electrode is important if interpretation errors from low-frequency dielectric spectroscopy of biological materials are to be prevented. Applications for such measurements in the quality control or on-line monitoring of proteins during freeze-drying are suggested.

Acknowledgement
SmithKline Beecham Pharmaceuticals

REFERENCES

[1] Middaugh, C. (1994). "The analysis of protein pharmaceuticals: Near future advances." *Cryotechnology* **15**: 187-194.

[2] Pikal, M. J. (1999). "Mechanisms of protein stabilisation during freeze-drying and storage: the relative importance of thermodynamic stabilisation and glassy state relaxation dynamics". in "*Freeze-drying/lyophilisation of pharmaceutical and biological products"*. L. Rey and C. J. May. New York, Marcel Dekker, Inc.

[3] Manning, M., Patel, K. and Borchardt, R. (1989). "Stability of Protein Pharmaceuticals." *Pharmaceutical Research* **6** (11): 903-918.

[4] Carpenter, J. F. and Chang, B. S. (1996). "Lyophilization of protein pharmaceuticals". in "*Biotechnology and biopharmaceutical manufacturing, processing and preservation"*. K. E. Avis and V. L. Wu. Buffalo Grove, Interpharm press. **2:** 199-264.

[5] Rudolph, A. S., Crowe, J. H. and Crowe, L. M. (1986). "Effects of three stabilizing agents - proline, betain, and trehalose - on membrane phospholipids." *Arch. Biochem. Biophys.* **245**: 134-143.

[6] Pikal, M. J. (1990). "Freeze-Drying of Proteins Part 1: Process Design." *Biopharm* (September): 18-27.

[7] Deluca, P. P. (1977). "Freeze drying of Pharmaceuticals." *Journal of Scientific Technology* **14** (1): 620-629.

[8] Murgatroyd, K. (1997). "The freeze drying process". in "*Good Pharmaceutical Freeze-Drying Practice"*. P. Cameron. Buffalo Grove, Interpharm press Inc.**:** 1-58.

[9] Murgatroyd, K. (2001). "Freeze-drying - A review." *European Journal of Parental Sciences* **6** (1): 21 - 25.

[10] Rey, L. R. (1990). "*Basic Aspects and Future Trends in the Freeze-Drying of Pharmaceuticals"*. International Symposium on Biological Product Freeze-Drying and Formulation, Bethesda, USA, Karger.

[11] Jennings, T. A. (1999). "*Lyophilisation. Introduction and Basic Principles."*. Denver, Colorado, Interpharm Press.

[12] Pikal, M. J. (1990). "Freeze-Drying of Proteins Part 2: Formulation Selection." *Biopharm* (October): 26-30.

[13] Pikal, J., Dellerman, K. and Roy, M. L. (1991). "Effects of moisture and oxygen on the stability of freeze dried formulations of human growth hormone." *Development Biological Standard* **74**: 21-38.

[14] Hsu, C. C., Ward, C. A., Pearlman, R., Nguyen, H. M., Yeung, D. A. and Curley, J. G. (1990). "*Determining The Optimum Residual Moisture in Lyophilized Protein Pharmaceuticals"*. International Symposium on Biological Product Freeze-Drying and Formulation, Bethesda, USA, Karger.

[15] Prisoupil, T. I., Kramlova, M., Fortova, H. and Ulrych, S. (1985). "Haemoglobin lyophilised with sucrose: the effect of residual moisture on storage." *Haematologia* **18**: 45-52.

[16] Kett, V. L., Craig, D. Q. M., Taylor, K. M. G. and Deutsch, D. (1998). "Thermal analysis of a freeze dried formulation - the effect of drying time." *Journal of Pharmacy and Pharmacology* **50**: 62.

[17] Allison, S. D., Dong, A. C. and Carpenter, J. F. (1996). "Counteracting effects of thiocyanate and sucrose on chymotrypsinogen secondary structure and aggregation during freezing, drying, and rehydration." *Biophysical Journal* **71** (4): 2022-2032.

[18] Prestrelski, S. J., Arakawa, T. and Carpenter, J. F. (1997). "*Structure of Proteins in Lyophilised Formulations Using Fourier Transform Infrared Spectroscopy*, American Chemical Society.

[19] Separovic, F., Lam, Y. H. and Chan, H.-K. (1998). "A solid state NMR study of protein hydration and stability." *Pharmaceutical Research* **15** (12): 1816-1821.

[20] Vemuri, S. (1990). "*Lyophilization Cycle Development for Interleukin-2"*. International Symposium on Biological Product Freeze-Drying and Formulation, Bethesda, USA, Karger.

[21] Dawson, P. J. and Hockley, D. J. (1990). "*Scanning Electron Microscopy of Freeze-Dried Preparations: Relationship of Morphology to Freeze-Drying Parameters"*. International Symposium on Biological Product Freeze-Drying and Formulation, Basel, Karger.

[22] Hatley, R. H. M. (1990). "*The Effective Use of Differential Scanning Calorimetry in the Optimisation of Freeze-Drying Processes and Formulations"*. International Symposium on Biological Product Freeze-Drying and Formulation, Bethesda, USA, Karger.

[23] Elissalde, C. and Ravez, J. (1997). "*Low and High Frequency Dielectric Relaxations in a Tetragonal Tungsten Bronze Type Ceramics"*. 9th International Meeting on Ferroelectricity (IMF-9), Seoul, South Korea, CNRS, INST CHIM MAT CONDENSEE BORDEAUX, F-33608 PESSAC, FRANCE.

[24] Williamson, W., Chen, H. D., Cross, L. E. and Gilber, B. K. (1997). "*High Frequency Dielectric Properties of PLZT Thin Films"*. 9th International Symposium on Integrated Ferroelectrics, Santa FE, NM.

[25] Arjavalingam, G. (1990). "*High-Frequency Dielectric Properties of Polymers"*. 48th Annual Technical Conference of the Society of Plastics Engineers - Plastics in the Environment: Yesterday, Today, and Tomorrow (ANTEC 90), Dallas, Texas, IBM Corp.

[26] Sliva, P., Leffler, M., Bliss, M., Cross, L. E. and Scheetz, B. E. (1987). "*High Frequency Dielectric Response of Calcium Aluminate Cements - Potential Packaging Substrate Materials"*. 3rd Symposium on Electronic Packaging Materials Science at the Fall Meeting of the Materials Research Society, Boston, M.A.

[27] GarciaMoreno, B., Dwyer, J. J., Gittis, A. G., Lattman, E. E., Spencer, D. S. and Stites, W. E. (1997). "Experimental Measurement of the Effective Dielectric in the Hydrophobic Core of a Protein." *Biophysical Chemistry* **64** (no. 1-3): 211-224.

[28] Pethig, R. (1988). "Dielectric studies of proton transport in proteins." *Ferroelectrics* **86**: 31-39.

[29] Takashima, S. and Minakata, A. (1973). "Dielectric behavior of biological molecules." *Dig. of Dielectr. Literature* **37**: 602-653.

[30] Bone, S., Eden, J., Gascoyne, P. R. C. and Pethig, R. (1981). "Conduction and Dielectric Polarisation in Proteins and Molecular Complexes." *Journal of Chemical Society, Faraday Transaction* **77**: 1729-1732.

[31] Consolini, G. (1996). "*Glassy Dielectric Relaxation of Protons in Hydrated Protein Powders"*. International School of Physics Enrico Fermi, Villa Monastero, Varenna, Italy.

[32] Bone, S., Eden, J. and Pethig, R. (1981). "Electrical Properties of Proteins as a Function of Hydration and NaCl Content." *International Journal of Quantum Chemistry: Quantum Biology Symposium* **8**: 307-316.

[33] Bone, S. and Pethig, R. (1985). "Dielectric studies of protein hydration and hydration-induced flexibility." *Journal of Molecular Biology* **181**: 323-326.

[34] Hawkes, J. J. and Pethig, R. (1988). "Low-frequency dielectric properties of lysozyme as a function of hydration and pH of lyophilisation." *Biochimica et Biophysica Acta* **952**: 27-36.

[35] Pethig, R. (1987). "Dielectric properties of body tissues." *Clin. Phys. Physiol. Meas.* **8**: 5-12.

[36] Saenger, W. (1987). "Structure and dynamics of water surrounding biomolecules." *Ann. Rev. Biophys. Chem.* **1987**: 93-114.

[37] Takashima, S. (1989). "*Electrical Properties of Biopolymers and Membranes"*. Bristol, Adam Hilger.

[38] Wong, D. and Parasrampuria, J. (1997). "Pharmaceutical Excipients for the stabilization of Proteins." *BioPharm* **10** (11): 52-61.

[39] Stryer, L. (1995). "*Biochemistry"*. New York, W.H. Freeman and Company.

[40] Jakubke, H. D. and Jeschkeit, H. (1977). "*Amino Acids, Peptides and Proteins - An Introduction"*. London, Macmillan.

[41] http://www.cryst.bbk.ac.uk/PPS2/course. 18 October 2001.

[42] Stein, P. E., Leslie, A. G. W., Finch, J. T. and Carrell, R. W. (1991). "Crystal Structure of Uncleaved Ovalbumin at 1.95 A Resolution." *Journal of Molecular Biology* **221**: 941-959.

[43] http://jsdnt.claremont.edu/biochem98/ovalbumin. April 1999.

[44] http://jsdnt.claremont.edu/biochem98/lysozyme. April 1999.

[45] http://jsdnt.claremont.edu/biochem98/pepsin. April 1999.

[46] Creighton, T. E. (1997). "*Protein Structure: A practical approach"*. Oxford.

[47] Gregory, R. B. . in "*Protein-Solvent Interaction",* Marcel Dekker, Inc.

[48] Poole, P. L. and Finney, J. L. (1986). "Solid-phase protein hydration studies." *Methods Enzymology* **127**: 284-293.

[49] Sartor, G., Mayer, E. and Johari, G. (1994). "Calorimetric studies of the kinetic unfreezing of molecular motions in hydrated lysozyme, hemoglobin, and myoglobin." *Biophysical Journal* **66** (1): 249-258.

[50] Rupley, J. A. and Careri, G. (1991). "Protein Hydration and Function." *Advances in Protein Chemisty* **41**: 37-172.

[51] Levy, R. A. (1968). "*Principles of Solid State Physics"*. New York and London, Academic Press.

[52] Packard, H. (1992). "Basics of measuring the dielectric properties of materials. Application Note 1217-1", Hewlett Packard Co.

[53] Debye, P. (1929). "*Polar Molecules"*. New York, Dover Publications.

[54] Cole, K. S. and Cole, R. H. (1941). "Dispersion and absorption in dielectrics. I. Alternating current characteristics." *J. Chem. Phys.* **9**: 341-351.

[55] Davidson, D. W. and Cole, R. H. (1950). "Dielectric relaxation in glycerine." *J. Phys. Chem.* **18**: 1417.

[56] Havriliak, S. and Nagami, S. (1966). "A complex plane analysis of alpha-dispersions in some polymer systems." *Journal of Polymer Sciences* **Part C** (14): 99-117.

[57] Jonscher, A. K. (1978). "Low frequency dispersion in carrier dominated dielectrics." *Philosophical Magazine B* **38** (6): 587-601.

[58] Jonscher, A. K. (1998). “"Universal" response of hopping carriers.” *Journal of Materials Science Letters* (17): 1975 - 1977.

[59] Shablakh, M. and Dissado, L. A. (1984). “Nonconductive long range charge transport in hydrated biopolymers.” *Journal of Biological Physics* **12**: 63 - 78.

[60] Dissado, L. A. (1990). “A fractal interpretation of the dielectric response of animal tissues.” *Phys. Med. Biol.* **35** (11): 1487-1503.

[61] Saraidov, T., Axelrod, E., Feldman, Y. and Reisfeld, R. (2000). “Dielectric behaviour and percolation phenomena in porous silica gels.” *Chemical Physics Letter* **324**: 7-14.

[62] Jonscher, A. K. (1980). “A many-body universal approach to dielectric relaxation in solids”. in “*Physics of Dielectric Solids”*. C. H. L. Goodman. Bristol, London, Institute of Physics**:** 22-45.

[63] Bak, G. W. and Jonscher, A. K. (1999). “Low-frequency dispersion in hopping electronic systems.” *Journal of Materials Science* **34**: 5505 - 5508.

[64] Jeevanandam, P. and Vasudevan, P. (1997). “Anomalous low frequency dispersion and dielectric relaxation in the layer intercalated compounds Cd0.75PS3A0.5(H2O) [A=K,Cs].” *Journal of Chemical Physics* **108** (3): 1206 - 1215.

[65] Jonscher, A. K. and Husain, A. (1996). “Dynamic transport on humid silica surface I.” *Physica B* **217**: 29 - 34.

[66] Husain, A. and Jonscher, A. K. (1996). “Dynamic transport on humid silica surface II.” *Physica B* **222**: 123 - 130.

[67] Bak, G. W. and Kryszewski, M. (1997). “Low frequency dielectric properties of some organic compounds.” *Proceedings SPIE - International Society Optical Engineering* **3181**: 2 - 10.

[68] Lunkenheimer, P., Rall, H., Alkemper, J., Fuess, H., Bohmer, R. and Loidl, A. (1995). “Ionic motion in bioactive ceramics investigated by dielectric spectroscopy.” *Solid State Ionics* **81**: 129-134.

[69] Jonscher, A. K. (1991). “Low-frequency dispersion in volume and interfacial situations.” *Journal of Materials Science* **16**: 1618-1626.

[70] Jonscher, A. K. (1999). “Dielectric relaxation in solids.” *Journal of Physics D-Applied Physics* **32** (14): R57-R70.

[71] Dissado, L. A. and Hill, R. M. (1984). “Anomalous Low-frequency Dispersion: Near direct current conductivity in disordered low-dimensional materials.” *Journal of the Chemical Society, Faraday Transactions 2* **80**: 291-319.

[72] Jonscher, A. (1996). “*Universal Relaxation Law”*. London, Chelsea Dielectrics.

[73] Jonscher, A. K. (1983). “*Dielectric Relaxation in Solids”*. London, Chelsea Dielectrics.

[74] Hill, R. M. and Dissado, L. A. (1988). “Constant phase angle response with fractal electrodes.” *Solid State Ionics* **26**: 295-297.

[75] Scribner Associates, I. (1999). “Zplot for Windows. Electrochemical Impedance Software. Operating Manual. Version 2.1”. Southern Pines.

[76] Dissado, L. A. and Hill, R. M. (1988). “Constant-phase-angle and power law regimes in the frequency response of general determinate fractal circuit.” *Physical Review B* **37**: 3434-3439.

[77] Mandelbrot, B. (1982). "*The fractal geometry of nature"*. New York (Oxford), Freeman.

[78] Liu, S. H. (1986). "Fractals and their application in condensed matter physics." *Solid state physics* **39**: 207-273.

[79] Dissado, L. A. and Hill, R. M. (1989). "The fractal nature of the cluster model dielectric response functions." *Journal of Applied Physics* **66** (6): 2511-2524.

[80] de Gennes, P. G. (1982). "Kinetics of diffusion-controlled processes in dense polymer systems. I. Nonentangled regimes." *Journal of Chemical Physics* **76**: 3316-3321.

[81] Kremer, F. (1994). "Dielectric Spectroscopy: Old spectroscopic technique gains new actuality." *Novocontrol GmbH Dielectrics Newsletter* **March**: 3-4.

[82] Kremer, F. and Arndt, M. (1997). "Broadband dielectric measurement techniques". in "*Dielectric spectroscopy of polymeric materials. Fundamentals and Applications."*. J. P. Runt and J. J. Fitzgerald. Washington, DC., American Chemical Society**:** 461.

[83] Schaumburg, G. (1994). "Overview: Modern measurement techniques in broadband dielectric spectroscopy." *Novocontrol GmbH Dielectrics Newsletter* **March**: 4-7.

[84] Wellstead, P. E. "Frequency Response Analysis".

[85] Prestrelski, S., Tedeschi, N., Arakawa, T. and Carpenter, J. (1993). "Dehydration-induced Conformational Transitions in Proteins and Their Inhibition by Stabilizers." *Biophysical Journal* **65**: 661-671.

[86] Jonscher, A. K. (1978). "Low frequency dispersion in carrier dominated dielectrics." *Philosophical Magazine B* **38** (6): 587-601.

[87] Careri, G. (1999). "*Protein-solvent interaction and biological functions. Models from statistical physics."*. Biological Physics: 3rd international symposium.

[88] Careri, G. (1998). "Cooperative charge fluctuations by migrating protons in globular proteins." *Progress in Biophysics and Molecular Biology* **70**: 223-249.

[89] Rupley, J. A., Gratton, E. and Careri, G. (1983). "Water and globular proteins." *Trends in Biochemical Sciences* **8**: 18-22.

[90] Careri, G., Gratton, E., Yang, P.-H. and Rupley, J. (1980). "Correlation of IR spectroscopic, heat capacity, diamagnetic susceptibility and enzymatic measurements on lysozyme powder." *Nature* **284**: 572-573.

[91] Zallen, R. (1983). "*The Physics of Amorphous Solids"*. New York, Chichester, Wiley.

[92] Careri, G., Consolini, G. and Bruni, F. (1999). "Dielectric relaxation of a proton glass in hydrated protein powders." *Solid State Ionics* **125**: 257-261.

[93] Grant, E. H., Sheppard, R. J. and South, G. P. (1978). "*Dielectric Behaviour of Biological Molecules in Solution"*. Oxford, Clarendon Press.

[94] Tamman, G. and Hesse, G. (1926). "Die abhängigkeit der viskosität der temperatur bei unterkülten flüssigkeiten." *Z. Anorg. Allegem. Chem.* **156**: 245-257.

[95] Vogel, H. (1921). "Das temperaturabhängigkeitsgsetz der viskosität von flüssigkeiten." *Physikalishe Zeitschrift* **22**: 645-646.

[96] Adam, G. and Gibbs, J. H. (1965). "On the temperature dependence of cooperative relaxation properties in glass-forming liquids." *Journal of Chemical Physics* **43** (1): 139-146.

[97] Schonhals, A. (1997). "Dielectric Properties of Amorphous Polymers". in "*Dielectric Spectroscopy of Polymeric Materials"*. J. P. Runt and J. J. Fitzgerald. Washington DC., American Chemical Society**:** 81 - 106.

[98] Stickel, F., Fischer, E. W. and Richert, R. (1995). "Dynamics of glass-forming liquids. I. Temperature-derivative analysis of dielectric relaxation data." *Journal of Chemical Physics* **102** (15): 6251 - 6257.

[99] Ludt, H. and Herrman, H. D. (1973). "In vitro measurement of tissue impedance over a wide frequency range." *Biophysik* **10**: 337 - 345.

[100] Mandelbrot, B. B. (1982). "*The fractal geometry of nature. Updated and augmented"*. New York (Oxford), Freeman.

[101] Stauffer, D. and Aharony, S. (1998). "*Introduction to Percolation Theory"*. London, Taylor and Francis.

[102] Feldman, Y. and Kozlovich, N. (1995). "Time-domain dielectric spectroscopy studies of macromolecular solutions." *Trends in Polymer Science* **3** (2): 53-60.

[103] Feldman, Y., Kozlovich, N. and Alexandrov, Y. (1996). "Mechanism of the cooperative relaxation in microemulsions near the percolation threshold." *Physical Review E* **54** (5): 5420-5427.

[104] Alvarez, F., Alegría, A. and Colmenero, J. (1991). "Relationship between the time-domain Kohlrausch-Williams-Watts and frequency-domain Havriliak-Negami relaxation functions." *Physical Reviews: Part B: Condensed Matter* **44** (14): 7306-7312.

[105] Courtens, E. (1986). "Scaling Dielectric Data On Rb1-X(Nh4)Xh2po4 Structural Glasses and Their Deuterated Isomorphs." *Physical Review B* **33** (4): 2975-2978.

[106] Howell, F. L., Pinto, N. J. and Schmidt, V. H. (1992). "Complex Permittivity of the Deuterated and Undeuterated Proton Glass Rb1-X(Nh4)Xh2aso4." *Physical Review B* **46** (21): 13762-13766.

[107] Pirc, R., Tadic, B. and Blinc, R. (1992). "Proton and Deuteron Glasses." *Physica a* **185** (1-4): 322-330.

[108] Sartor, G., Hallbrucker, A. and Mayer, E. (1995). "Characterizing the secondary hydration shell on hydrated myoglobin, hemoglobin, and lysozyme powders by its vitrification behavior on cooling and its calorimetric glass ∅ liquid transition and crystallization behavior on reheating." *Biophysical Journal* **69** (6): 2679-2694.

[109] van Bede, L. K. H. (1967). "Dielectric behaviour of heterogenous systems." *Prog. Dielectr.* **7**: 71-114.

[110] Carpenter, J. F., Arakawa, T. and Crowe, J. H. (1991). "Interactions of stabilizing additives with proteins during freeze-thawing and freeze-drying." *Development of Biological Standard* **74**: 225-239.

[111] Prestrelski, S. J., Arakawa, T. and Carpenter, J. F. (1997). "*Structure of Proteins in Lyophilised Formulations Using Fourier Transform Infrared Spectroscopy*, American Chemical Society.

[112] Prestrelski, S. J., Arakawa, T. and Carpenter, J. F. (1993). "Separation of freezing- and drying-induced denaturation of lyophilised proteins using stress-specific stabilisation. II. Structural studies using infrared spectroscopy." *Archives of Biochemistry and Biophysics* **303** (2): 465-473.

[113] Carpenter, J. F. and Crowe, J. H. (1989). "An infrared spectroscopic study of the interactions of carbohydrates with dried proteins." *Biochemistry* **28** (9): 3916-3922.

[114] Hancock, B. C. and Zografi, G. (1994). "The relationship between the glass transition temperature and the water content of amorphous pharmaceutical solids." *Pharmaceutical Research* **11** (4): 471-477.

[115] Rowe, T. W. G. and Snowman, J. W. (1976). "Edwards Freeze-drying Handbook". Crawley, Sussex, Edwards High Vacuum.

[116] Nigmatullin, R. R. (1998). "New method of analytical function identification experimental measurements." *Applied Magnetic Resonance* **14**: 601.

[117] Hill, R. M. (1985). "Characterization of the Dielectric-Properties of Thin-Films." *Thin Solid Films* **125** (3-4): 277-289.

[118] Jensen, L. H. (1990). "*the Structure of Water in Protein Crystals"*. International Symposium on Biological Product Freeze-Drying and Formulation, Bethesda, USA, Karger.

[119] Hageman, M. J. (1992). "Water sorption and solid state stability of proteins". in "*Stability of Protein Pharmaceutical, Part A"*. New York, Plenum**:** 273-309.

[120] Hageman, M. J. (1988). "The role of moisture in protein stability." *Drug Development and Industrial Pharmacy* **14** (14): 2047-2070.

[121] Niklasson, G. A. (1987). "Fractal Aspects of the Dielectric Response of Charge-Carriers in Disordered Materials." *Journal of Applied Physics* **62** (7): R1-R13.

[122] Amitrano, C., Bunde, A. and Stanley, H. E. (1985). "Diffusion of Interacting Particles On Fractal Aggregates." *Journal of Physics a-Mathematical and General* **18** (15): L923-L929.

[123] Sahimi, M. (1994). "*Applications of Percolation Theory"*. London, Taylor and Francis.

[124] Bunde, A. and Dieterich, W. (2000). "Percolation in composites." *Journal of Electroceramics* **5** (2): 81-92.

[125] Stauffer, D. and Aharony, S. (1998). "*Introduction to Percolation Theory"*. London, Taylor and Francis.

[126] Schroeder, M. R. (1991). "*Fractals, chaos, power law: minutes from an infinite paradise"*. New York, W.H. Freeman.

[127] Clerc, J. P., Giraud, G., Laugier, J. M. and Luck, J. M. (1985). "Electrical-Properties of Percolation Clusters - Exact Results On a Deterministic Fractal." *Journal of Physics a-Mathematical and General* **18** (13): 2565-2582.